ISTANBUL TECHNICAL UNIVERSITY ★ GRADUATE SCHOOL

DEVELOPMENT OF LATERAL LOAD RESISTANCE-DEFLECTION CURVES FOR PILES IN COHESIONLESS SOILS UNDER EARTHQUAKE EXCITATION

Ph.D. THESIS

Ozan ALVER

Department of Civil Engineering

Soil Mechanics and Geotechnical Engineering Programme

FEBRUARY 2023

ISTANBUL TECHNICAL UNIVERSITY ★ GRADUATE SCHOOL

DEVELOPMENT OF LATERAL LOAD RESISTANCE-DEFLECTION CURVES FOR PILES IN COHESIONLESS SOILS UNDER EARTHQUAKE EXCITATION

Ph.D. THESIS

Ozan ALVER
(501152305)

Department of Civil Engineering

Soil Mechanics and Geotechnical Engineering Programme

Thesis Advisor: Assoc. Prof. Dr. E. Ece BAYAT

FEBRUARY 2023

ISTANBUL TEKNİK ÜNİVERSİTESİ ★ LİSANSÜSTÜ EĞİTİM ENSTİTÜSÜ

KOHEZYONSUZ ZEMİNLERDE GÖMÜLÜ KAZIKLAR İÇİN DEPREM YÜKLERİ ALTINDA YATAY YÜK-YERDEĞİŞTİRME BAĞINTILARININ GELİŞTİRİLMESİ

DOKTORA TEZİ

Ozan ALVER
(501152305)

İnşaat Mühendisliği Anabilim Dalı

Zemin Mekaniği ve Geoteknik Mühendisliği Programı

Tez Danışmanı: Doç. Dr. E. Ece BAYAT

ŞUBAT 2023

Ozan Alver, a Ph.D. student of ITU Graduate School student ID 501152305, successfully defended the thesis/dissertation entitled “DEVELOPMENT OF LATERAL LOAD RESISTANCE-DEFLECTION CURVES FOR PILES IN COHESIONLESS SOILS UNDER EARTHQUAKE EXCITATION”, which he prepared after fulfilling the requirements specified in the associated legislations, before the jury whose signatures are below.

Thesis Advisor : **Assoc. Prof. Dr. E. Ece BAYAT** ....
İstanbul Technical University

Jury Members : **Prof. Dr. Recep İYİSAN** ....
İstanbul Technical University

Prof. Dr. Özer ÇİNİCİOĞLU ....
Boğaziçi University

Assoc. Prof. Dr. Pelin TOHUMCU ÖZENER ....
Yildiz Technical University

Assis. Prof. Dr. Berrak TEYMÜR ....
İstanbul Technical University

Date of Submission : 27 December 2022
Date of Defense : 16 February 2023

To my parents,

FOREWORD

This thesis focus on the pile behavior under earthquake loading in the soil-pile-structure interaction problems. 3-dimensional numerical analyses were performed to understand the problem better. The thesis presents the numerical analysis results and proposes mathematical models to characterize pile-soil behavior using load-displacement relationships. The main conclusions are summarized in the last chapter of the thesis, and the recommendations are presented for future research.

I would like to thank my thesis supervisor, Assoc. Prof. Dr. E. Ece BAYAT for the guidance and support throughout the research. The long and valuable discussions during the thesis have taught me how academic research is carried out. I appreciate her curiosity and encouragement, which have inspired me much.

I am grateful to the steering committee members Prof. Dr. Recep İYİSAN and Prof. Dr. Özer ÇİNİCİOĞLU for their helpful comments and support during the progress presentations.

The author would like to thank Dr. Amin RAHMANI and Prof. Dr. Mahdi TAIEBAT for providing the centrifuge test data in the verification analyses.

Special thanks to Prof. Dr. Gürkan ÖZDEN, who encourages me to use the Bouc-Wen model.

I would like to acknowledge the financial support of The Scientific and Technological Research Council of Turkey, TÜBİTAK (Grant No. 119M624).

I wish to thank the Tubitak Project team; Prof. Dr. Akihiro TAKAHASHI, Dr. Dan GHIOCEL, Dr. Yalçın BULUT, Dr. Yavuz DURGUN, Prof. Dr. Ercan YÜKSEL, Omid BAGHERI, Mehmet Şamil GÜNDÜZ, Onur DENIZ, Emre GÖNÜLCÜ, Elvin GURBANOV for their help and support.

December 2022

Ozan ALVER
(Civil Engineer, M.Sc.)

TABLE OF CONTENTS

Page

ABBREVIATIONS

AFAD	**:** Afet ve Acil Durum Yönetimi Başkanlığı
API	**:** American Petroleum Institute
BNWF	**:** Beam on Nonlinear Winkler Foundation
DIN	**:** Deutsches Institut für Normung
GQ/H	**:** General Quadratic and Hyperbolic model
FLAC^{3D}	**:** Fast Lagrangian Analysis of Continua in Three-Dimensions
PEER	**:** Pacific Earthquake Engineering Research Center
SAP2000	**:** Software for Structural Analysis and Design

SYMBOLS

a_o	: Dimensionless frequency factor
c	: Cohesion
c_r	: Radiation damping coefficient
D	: Pile diameter
D_R	: Relative density
E_0	: Small-strain stiffness
E_{50}	: Secant stiffness
E_p	: Elastic modulus of pile
E_{ur}	: Unloading/reloading stiffness
EI	: Flexural stiffness
E_{py}	: Modulus of p-y curve
f_{max}	: Maximum frequency
G_{max}	: Initial shear modulus
h	: Height
H	: Lateral load
I_p	: Moment of inertia of pile
k	: Stiffness
k_h	: Lateral subgrade reaction modulus
k_n	: Interface stiffness in normal direction
k_s	: Interface stiffness in shear direction
K	: Bulk modulus
K_0	: Lateral earth pressure coefficient at rest
K_p	: Passive lateral earth pressure coefficient
L	: Pile length
m	: Mass; power for stress dependency
M	: Bending moment
n	: Nonlinearity parameter
p	: Lateral soil resistance
p_a	: Atmospheric pressure
p_u	: Ultimate lateral soil resistance

$\mathbf{R_f}$	: Hyperbolic model parameter
r	: Pile radius
s	: Nonlinearity parameter
t	: Time
T	: Period
$\mathbf{V_s}$	: Shear wave velocity
$\mathbf{V_{s,30}}$	: Average shear wave velocity in 30 m depth
y	: Pile deflection
$\mathbf{y_{ref}}$	: Reference displacement
z	: Depth
$\boldsymbol{\eta_h}$	: Soil modulus constant
γ	: Unit weight of soil
ϕ	: Angle of friction
ω	: Angular frequency
$\Delta \mathbf{l}$	: Vertical dimension of the zone
λ	: Wavelength
τ	: Shear stress
γ_{ref}	: Reference strain
σ'_m	: Effective confining stress
σ'_v	: Vertical effective stress
σ'_h	: Horizontal effective stress
ψ	: Dilation angle
ρ_s	: Mass density
ν	: Poisson's ratio
β	: Nonlinearity parameter
ζ	: Degradation parameter

LIST OF TABLES

Page

LIST OF FIGURES

Page

DEVELOPMENT of LATERAL LOAD RESISTANCE-DEFLECTION CURVES for PILES in COHESIONLESS SOILS UNDER EARTHQUAKE EXCITATION

SUMMARY

Pile foundations must be designed safely to withstand the lateral loads such as wave loads and seismic loads in offshore/onshore structures, seismic loads in bridges, buildings, port structures etc. The most common analysis method for the design is the Winkler spring approach. Researchers have suggested nonlinear formulations for the lateral load resistance-deflection (p-y) curves, but the contribution of the degree of soil nonlinearity was not studied thoroughly. The main drawback of the current approach is the use of a single stiffness in considering the soil nonlinearity. This study investigates the laterally loaded pile problem using the pressure-dependent hardening soil model with small-strain stiffness (HS-Small Model), where the degree of soil nonlinearity is better integrated. The numerical model was created, and parametric analyses were carried out on the verified model for various pile and soil properties. A modified hyperbolic model was proposed for static p-y relation, including the initial stiffness, ultimate soil resistance, and degree of nonlinearity parameters based on the numerical analysis results. The validity of the model was shown by simulating the field and centrifuge tests from the literature. The proposed model agrees with the test results in the variation of bending moment along the pile. Besides, a significant enhancement was provided in the estimation of pile deflections. Therefore, the proposed model with four parameters can more precisely consider the soil nonlinearity from very small to large displacements. The proposed p-y curves can be utilized in the design of piles subject to static lateral loading.

The analysis of dynamic soil-pile interaction problems requires the relation of soil resistance to lateral loading that is represented by nonlinear p-y curves in the beam on the nonlinear Winkler foundation (BNWF) approach. Current methods for p-y curves are either based on static load tests or cannot accurately consider the dynamic soil nonlinearity. This study investigates the dynamic soil-pile interaction in cohesionless

soils by numerical analyses to better characterize the p-y curves considering the nonlinear soil behavior under dynamic loading. A numerical pile-soil-structure model was created in FLAC^{3D} and verified by two centrifuge tests published in the literature. The parametric analyses were performed to obtain the p-y curves for various pile diameters, soil relative densities, and degrees of nonlinearities. Based on the parametric analyses, a mathematical model was proposed for the dynamic p-y curves for cohesionless soils. The proposed model characterizes the backbone of dynamic p-y curves based on the three leading parameters (initial stiffness K_{py}, ultimate resistance p_u, and degree of nonlinearity n). The numerical analyses showed that the p-y curve nonlinearity mainly depends on the employed modulus reduction curves of soils. In the model, the degree of nonlinearity parameter (n) was directly related to the soil parameter "reference strain" (γ_r), which solely represents the modulus reduction curve of soils. In this regard, the dependence on various dynamic soil parameters was diminished by correlating the dynamic p-y curves to the reference strain. The validation analyses performed in structural analysis software demonstrated that the proposed dynamic p-y model could accurately estimate the pile and structure response under earthquake loading by incorporating the hysteretic nonlinear soil behavior. Superstructure accelerations and bending moments along the single pile obtained using the proposed model under different earthquake records were closer to the 3-dimensional numerical analysis results when compared with the results calculated by API. Finally, the proposed static and dynamic p-y models will contribute to the design of piles by improving the initial stiffness, ultimate resistance and nonlinearity of the static load-displacement behavior and by integrating the dynamic soil nonlinearity and hysteretic behavior under directly applied seismic loads.

KOHEZYONSUZ ZEMİNLERDE GÖMÜLÜ KAZIKLAR İÇİN DEPREM YÜKLERİ ALTINDA YATAY YÜK-YERDEĞİŞTİRME BAĞINTILARININ GELİŞTİRİLMESİ

ÖZET

Kazıklı temellerin ön tasarımı statik yükler kullanılarak yapılabilir, ancak sismik olarak aktif bölgelerdeki kazıkların nihai tasarımı dinamik yükleri de içermelidir. Kazıkların deprem yüklemesi altındaki davranışı, yanal yüklemeli bir kazık problemi olarak kabul edilebilir. Yanal yüklü kazık problemlerinde yaygın olarak iki yöntem kullanılmaktadır: Sürekli ortam yaklaşımı ve Winkler yay yaklaşımı. Her iki yöntemde de kazık yapısal bir kiriş elemanı olarak düşünülebilir ancak temel fark zeminin modellenmesidir. Sürekli ortam yaklaşımında zemin ortamı iki veya üç boyutlu sonlu elemanlar kullanılarak modellenebilirken, yay yönteminde zeminin yanal yüklemeye direnci kazık boyunca yerleştirilen bir dizi yay ile idealleştirilmektedir. Yay yöntemi, lineer olmayan Winkler yöntemi olarak adlandırılmakta ve zemin-kazık sisteminin yanal yüke tepkisi, yanal yük-yer değiştirme (p-y) eğrileri ile dikkate alınmaktadır. Tarihsel olarak kazık ve üst yapı, doğrusal davranışa uygun modellenmiş ve doğrusal zemin-kazık-yapı etkileşimi birçok araştırmacı tarafından yeterince çalışılmıştır. Ancak zeminler, düşük deformasyonlar altında bile yüksek oranda doğrusal olmayan davranış sergilemektedir ve analizlerdeki temel zorluk, bu doğrusal olmama durumunu hesaba katan modelleme yaklaşımından kaynaklanmaktadır.

Kazıklı temeller, açık deniz veya karada bulunan yapılarda yanal yüklere dayanacak şekilde tasarlanmalıdır. En yaygın analiz yöntemi bir önceki paragrafta özetlenen Winkler yay yaklaşımıdır. Araştırmacılar, Winkler yay yönteminde kullanılmak üzere yanal yük direnci-deformasyon (p-y) eğrileri için doğrusal olmayan formülasyonlar önermişler, ancak zemin nonlineeritesinin etkisi tam olarak incelenmemiştir. Literatürde en yaygın kullanılan yaklaşımın yüksek başlangıç rijitliğe sahip olduğu birçok araştırmacı tarafından vurgulanmıştır. Son zamanlarda yapılan bazı çalışmalarda, hiperbolik modelin kullanılması önerilmiştir. Bununla birlikte,

hiperbolik modelin dezavantajı, p-y eğrilerinin doğrusal olmama durumunu temsil etmek için tek bir rijitlik parametresini kullanmasıdır. Buna göre kullanılan rijitlik parametresi, çoğu durumda p-y eğrilerini tanımlamak için yetersizdir. Bu nedenle, kazık yer değiştirmelerini ve iç kuvvetleri doğru bir şekilde tahmin etmek için analiz öncesi seçilecek rijitlik parametresi çok önemli olabilmektedir.

Bu tezde yanal yüklü kazıkların davranışı 3-boyutlu sonlu farklar analizleri ile incelenmiştir. Analizlerde statik ve dinamik yükleme durumu ayrı olarak dikkate alınmıştır. Statik analizlerde HS-Small zemin modeli kullanılmıştır ve zeminin nonlineeritesi uygun bir şekilde tanımlanarak analizlere entegre edilmiştir. 3-boyutlu analizlerin doğrulanması amacıyla literatürde detayları bulunan gerçek ölçekli bir saha deneyi seçilerek sayısal modeli oluşturulmuştur. Oluşturulan modelde kazık ve zemin parametreleri belirlenerek yanal yük kazık başlığından uygulanmıştır. Kazık-zemin sistemi yanal yük altında analiz edilerek yanal yük-yerdeğiştirme ilişkisi elde edilmiştir. Ayrıca belirli derinliklerde yanal yük-yerdeğiştirme eğrileri bulunmuştur. Elde edilen bu eğriler literatürde verilen saha deneyi sonuçlarıyla karşılaştırılarak oluşturuan sayısal modelin doğruluğu irdelenmiştir.

Sayısal modelin geçerliliği bir saha deneyi ile gösterildikten sonra parametrik analizler için ayrıca bir model kurulmuştur. Belirli kazık ve zemin özellikleri seçilerek bu parametrelerin yanal yük-yer değiştirme eğrilerine olan etkileri sayısal analizler ile incelenmiştir. Statik p-y ilişkisi için, sayısal analiz sonuçlarına dayalı olarak başlangıç rijitliği, nihai zemin direnci ve nonlineerite parametrelerini içeren dört parametreli modifiye hiperbolik model önerilmiştir. p-y eğrisinin başlangıç rijitliği zeminin başlangıç modülüne, kazık çapına ve derinliğe bağlı olarak verilmiştir. Nihai zemin direnci ise; kazık çapına, düşey efektif gerilmeye, yanal zemin basıncı katsayısına ve derinliğe bağlı olarak verilmiştir. p-y eğrilerinin nonlineeritesi zemin nonlineer davranışına bağlı olarak sunulmuştur. Zemin nonlineeritesi ise başlangıç modülünün sekant modülüne oranı olarak tanımlanmıştır. Bu oran büyüdükçe (sekant modülü küçüldükçe) nonlineerite artmaktadır. Önerilen p-y eğrilerinin 3-boyutlu sayısal analiz sonuçlarına yakınlığı gösterilmiştir. Daha sonra modelin geçerliliği literatürden bir saha deneyi ve ve santrifüj testi simüle edilerek gösterilmiştir. Buna göre önerilen model, kazık boyunca eğilme momentinin değişimi konusunda test sonuçlarıyla uyumludur. Ayrıca kazık yerdeğiştirme tahmininde önemli bir iyileştirme sağlanmıştır. Bu nedenle, önerilen model dört parametreli, çok küçükten büyük yer değiştirme seviyeleri için, zeminin nonlineeritesini daha iyi bir şekilde dikkate alabilmektedir. Önerilen p-y eğrileri, statik yanal yüklemeye maruz kalan kazıkların tasarımında kullanılabilir. Ayrıca deprem yükü altında üstyapı ivmelenmesi yönetmeliklerde verilen tasarım spektrumları ile tahmin edilebilir. Üstyapı ivmelenmesinden kaynaklanan yanal yük kazıklara statik olarak uygulanarak analiz edilebilir. Önerilen statik p-y eğrileri, deprem yüklemesini artımsal itme yöntemiyle dikkate alan bu yaklaşımlarda da kullanılabilir.

Deprem yüklemesine maruz kalan kazıklı temellerde dinamik zemin-kazık-yapı etkileşimi analizleri gerçekleştirilmelidir. Winkler yay yaklaşımı ile yapılan dinamik analizlerde zemin davranışı doğrusal olmayan p-y eğrileri ile temsil edilmektedir. p-y eğrileri için mevcut yöntemler ya statik yükleme testlerine dayalıdır ya da dinamik yük altındaki zeminin nonlineeritesi doğru bir şekilde dikkate alınamamaktadır. Bu tezin amacı, kohezyonsuz zeminlerde bulunan kazıkların dinamik zemin-kazık-yapı etkileşimi analizlerinde davranışının daha doğru temsil edilebilmesi için sayısal analizler ile dinamik yükleme altındaki nonlineer zemin davranışını göz önünde bulundurabilen p-y eğrilerini geliştirmektir. Bu amaçla kazık-zemin-yapı etkileşimi analizleri $FLAC^{3D}$ programında 3-boyutlu olarak yapılmıştır. Öncelikle literatürde sunulan iki santrifüj deneyi modellenmiş ve sayısal model sonuçları ile test sonuçları karşılaştırılarak oluşturulan sayısal model doğrulanmıştır. Analizlerde zeminin nonlineer davranışı modül azalım eğrileri ile dikkate alınmıştır. Bu eğriler zeminin dinamik özelliği olup referans birim şekil değiştirme (reference strain) parametresi ile oluşturulmaktadır. Doğrulama analizleri sonrasında, parametrik analizler için bir sayısal model oluşturulmuştur. Farklı kazık çapları, zemin rölatif sıkılıkları ve nonlineer zemin davranışı için referans birim şekil değiştirme parametreleri için p-y eğrileri sayısal analizler sonucunda elde edilmiştir. Parametrik analizlere dayanarak, kohezyonsuz zeminlerdeki kazıkların dinamik p-y eğrileri için Bouc-Wen modeli önerilmiştir. Önerilen model, üç parametreye (başlangıç rijitliği, nihai zemin direnci ve nonlineerite) dayalı olarak dinamik p-y eğrilerinin omurga eğrisini karakterize etmektedir. Sayısal analizler, nonlineer p-y eğrilerinin esas olarak zeminlerin nonlineer davranışına ve kullanılan modül azalım eğrilerine bağlı olduğunu göstermiştir.

Önerilen modelde p-y eğrileri için nonlineer davranış parametresi, zeminlerin modül azalım eğrisini temsil eden ve zemin davranışına bağlı olan referans birim şekil değiştirme parametresi ile doğrudan ilişkilendirilmiştir.

Önerilen dinamik p-y eğrilerinin geçerliliği literatürde yayınlanan santrifüj testleri kullanılarak gösterilmiştir. Buna göre önerilen model ile elde edilen üstyapı ivmeleri ve kazık eğilme momentleri santrifüj deneyi sonuçlarına yakın bulunmuştur. Santrifüj testlerinde kullanılan deprem kayıtlarının sayısı sınırlı olduğu için, FLAC^{3D} programında yeni bir sayısal model oluşturulmuş ve ilave olarak seçilen deprem kayıtları ile ek analizler yapılmıştır. 3-boyutlu analiz ile önerilen model sonuçları karşılaştırılmıştır. Zemin-kazık-yapı etkileşim analizi sonuçları, deprem kayıtlarının seçiminin çıktılarda anahtar rol oynadığını ortaya koymuştur. Doğrulama analizi sonuçları, önerilen dinamik p-y eğrilerinin kazık ve yapı tepkisini doğru bir şekilde tahmin edebildiğini göstermiştir. Zemin-kazık-yapı etkileşimi probleminin karmaşıklığı göz önüne alındığında, önerilen modelin bu analizler için oldukça pratik olduğu söylenebilir.

Önerilen dinamik p-y modelinin en önemli avantajı, zeminin nonlineer davranışını dikkate alabilen histeretik p-y eğrilerini oluşturabilmesidir. Doğrusal olmayan zemin davranışı, referans birim şekildeğiştirme parametresi ile temsil edilebilmektedir. Bu parametrenin laboratuvar testleri ile belirlenerek dinamik p-y eğrilerine dahil edilmesi, dinamik yükleme altında gerçek zemin-kazık etkileşim davranışının dikkate alınabilmesine olanak tanımaktadır. Ayrıca, modül azalım eğrileri kullanılarak kohezyonsuz zeminler için bu model önerilmiş olmasına rağmen, referans şekil değiştirmenin doğru olarak belirlenmesi şartıyla herhangi bir zemine uygulanabilir. Genel olarak, dinamik p-y eğrileri için önerilen model, doğrusal olmayan p-y davranışını önemli ölçüde etkileyen dinamik zemin özelliklerini dikkate alabilmekte ve kazık-zemin-yapı etkileşimlerinde kullanılabilmektedir.

Önerilen model kullanılarak farklı deprem kayıtları altında, tek kazık boyunca elde edilen üst yapı ivmeleri ve kazık eğilme momentleri, API ile hesaplanan sonuçlarla karşılaştırıldığında 3 boyutlu sayısal analiz sonuçlarına daha yakın çıkmıştır. Son olarak, önerilen statik ve dinamik p-y modelleri, statik yük-yer değiştirme davranışını tahmin etmekte ve doğrudan uygulanan sismik yükler altında dinamik davranışı dikkate alabilmekte tasarıma katkıda bulunacaktır.

1. INTRODUCTION

Pile foundations are the structural elements embedded in the ground to transmit the superstructure loads to the suitable soil. The preliminary analysis in pile foundations is often performed considering the vertical loading. However, the piles are subject to lateral loading in most cases. Hence, the final design must also include lateral loading. Soil behavior under lateral loading affects the pile and the structure response, and the structure/pile movement varies the soil behavior simultaneously. Therefore, this phenomenon is defined as the soil-pile-structure interaction problem. Commonly encountered soil-pile-structure interaction problems are shown in Figure 1.1.

The initial design of the pile foundations presented in Figure 1.1 should be performed using the static loads, but the final design must also include the dynamic loads in the earthquake-prone regions. The behavior of piles under earthquake loading can be regarded as a laterally loaded pile problem (Reese & Van Impe, 2000). Two methods have been used widely for the laterally loaded pile problems: The continuum approach and the spring approach. In both approaches, the pile can be considered as a structural beam element, but the main difference is the modeling of the soil. In the continuum approach, the soil domain is discretized by solid elements, while in the spring method, it is idealized either by a single (lumped) spring and dashpot system at the pile head or a set of springs through the pile. The latter is called the beam on nonlinear Winkler foundation (BNWF) approach, and the reaction of the soil-pile system to the lateral load is taken into account by the lateral load-displacement (*p-y*) curves. Historically, the assumption of linear behavior for the pile and the superstructure is valid in most cases, and various researchers have well studied the linear soil-pile-structure interaction. However, soils exhibit highly nonlinear behavior even under low strains, and the main uncertainty in the analyses arises from the modeling approach taking this nonlinearity into account.

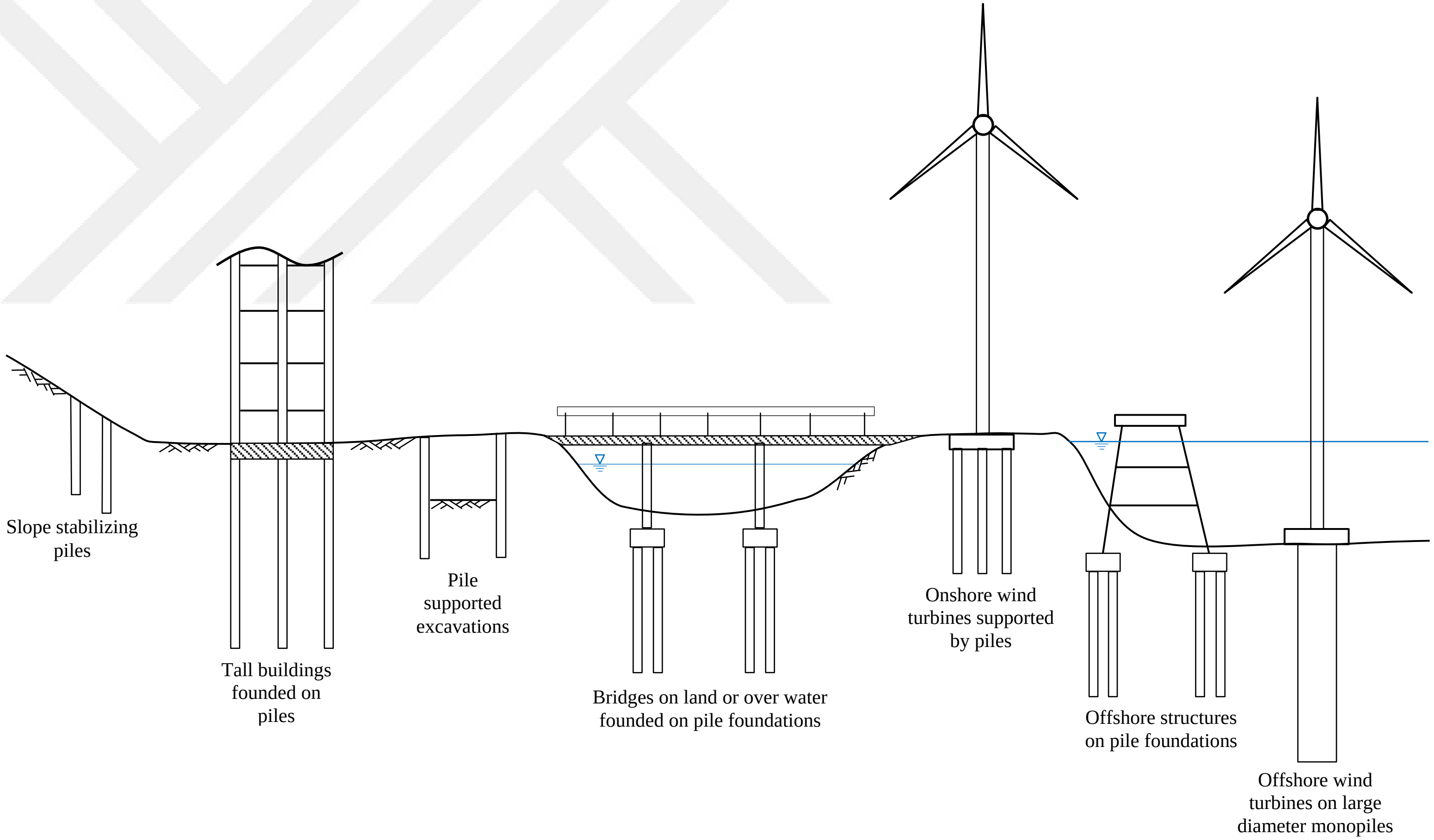

Figure 1.1 : Examples of pile foundations in geotechnical engineering.

The behavior of piles under lateral loads has been studied in the literature extensively. Analytical solutions (Kuhlemeyer, 1979; Poulos, 1971) or finite element analyses (Baguelin et al., 1977; Banerjee & Davies, 1978; Randolph, 1981) were presented using the elastic theory. The early studies were limited to linear analysis, whereas the soil behavior is highly non-linear. Therefore, the 3-dimensional finite element approach has been extended to consider soil nonlinearity (Brown & Shie, 1991), but no proposals have been made for practical design purposes (Reese & Van Impe, 2000). The subgrade reaction method is the more straightforward approach to the laterally loaded pile problem, where the soil is represented by discrete Winkler springs. Although the continuity of the soil is disregarded in this approach, the non-linear behavior can be taken into account by lateral load resistance-deflection (p-y) curves. While the continuum approach is superior, soil modeling using discrete Winkler springs is advantageous, especially for geotechnical/structural engineers dealing with complex soil-pile-structure interaction problems. Although the use of the current approach has been questioned by some researchers for monopiles (rigid) piles (Burd et al., 2020; Murphy et al., 2018; Taborda et al., 2020), a more recent study (Wang et al., 2022) has shown that p-y curves can be employed for rigid piles as well. Therefore, the p-y curve method is widely used in soil-pile-structure interaction analyses.

Several researchers have suggested direct correlations for piles in clays using the rigid disc analogy (Bransby, 1999; Randolph & Houlsby, 1984; Zhang & Andersen, 2017). However, the problem has not been clearly understood for piles in cohesionless soils since the shear strength of sands is not constant but depends upon the effective confining stress, which increases with depth. Several researchers studied the lateral load-displacement behavior of piles in cohesionless soils. The simplest relation was the linear equation suggested by Terzaghi (1955), in which the subgrade reaction modulus depends on the relative density of the soil. Nonlinear *p-y* curves based on the full-scale field tests were presented by Reese et al. (1974). API (2007) proposed a hyperbolic tangent function based on the mentioned field test results. Georgiadis (1992) implemented the hyperbolic model into *p-y* curve relation based on the centrifuge test results. Pender (1993) developed a new form using the finite element analysis results from back-analyzed full-scale field tests. Thieken et al. (2015) developed new equations for *p-y* curves in sands based on the finite element analysis results.

On the one hand, the studies mentioned so far have focused on static *p-y* curves. On the other hand, soil-pile interaction under dynamic loads has been investigated by many researchers (Allotey & El Naggar, 2008; El Naggar & Novak, 1996; Gazetas & Dobry, 1984; Makris & Gazetas, 1992; Nogami et al., 1992; Wang et al., 1998). The lateral load-deflection behavior under dynamic loads was studied by Kagawa and Kraft (1980), and a procedure was proposed based on the free-field site response analysis results. Gohl (1991) adopted the Ramberg and Osgood (1943) model to represent the *p-y* curves under cyclic (dynamic) loading based on the centrifuge test results. Brown et al. Brown et al. (2001) proposed a dynamic *p-y* curve relation based on the statnamic field tests. Lim and Jeong (2018) improve the original hyperbolic function of Kondner (1963) by suggesting initial modulus relations using the shake table test results. Several other experimental studies have been conducted on the dynamic soil-pile structure interaction (Nguyen et al., 2018; Rovithis et al., 2009). However, no practical relation was suggested for dynamic *p-y* curves. Many researchers have studied the topic through numerical analyses (Gerolymos et al., 2009; Gerolymos & Gazetas, 2005; Giannakos et al., 2012; Varun, 2010), and they have suggested the Bouc-Wen model to represent the dynamic *p-y* curves. Choi et al. (2016) have studied the problem using the plasticity theory. However, the effect of the degree of soil nonlinearity on the dynamic *p-y* curves has not been studied thoroughly.

Georgiadis et al. (1992) employed the suggestion of Terzaghi (1955) for the subgrade reaction modulus, although it was 2-3 times lower than the value suggested by Reese et al. (1974). The most commonly used relation for p-y curves, API (2007), has also proposed high values for initial stiffness, as in Reese et al. (1974). Many researchers have indicated the problem of the high initial modulus of API (Choi et al., 2016; Finn, 2005; Murchison & O'Neill, 1984; Rahmani et al., 2018). Several recent studies have employed the hyperbolic model to overcome the mentioned problem (Bouzid, 2021; Lim & Jeong, 2018; Lu et al., 2021; Papadopoulou & Comodromos, 2014; Zhou et al., 2020). However, the drawback of the hyperbolic model is that a single stiffness parameter is required to represent the nonlinearity of p-y curves, which is insufficient to describe the curves from very small to large displacements. Therefore, selecting this stiffness parameter is crucial to predict the pile displacements and internal forces accurately. Moreover, another drawback of the API (2007) is the low ultimate resistances anticipated at shallow depths (Rahmani et al., 2018; L. Zhang et al., 2005).

The most widely used *p-y* relation is the one suggested by API (2007), which can be employed as the backbone for static and dynamic analyses for simplicity. However, Boulanger (1999), Finn et al. (2002), Finn (2005), Allotey and El Naggar (2008), Thavaraj and Finn (2010), Choi et al. (2016), and Rahmani et al. (2018) stated that the main drawback of API (2007) is the high initial modulus which linearly increases with depth. Another drawback of the current relations is that the soil nonlinearity under dynamic loading is disregarded. According to Nist (2012) even the elastodynamic solution methods, in which the pile-soil system is modeled as a single lumped mass, may be superior to the *p-y* curve approach (Correia & Pecker, 2021). They emphasize the need for new-generation curves due to the infinite initial modulus and the inability of API (2007) to consider the degraded soil stiffness under dynamic loading. Although the reliability of the discrete element approach (using *p-y* curves) is questioned (Rahmani et al., 2018), the method is still in practice due to its simplicity since modeling and analyzing particularly complex soil-pile-structure systems in the continuum approach is cumbersome. Therefore, the existing *p-y* curve approach needs to be improved to capture the soil nonlinearity under cyclic loading. Hence, the current *p-y* curve approach must be improved considering the stiffness degradation for very small to large displacements in the soil-pile system.

This thesis investigates the laterally loaded pile problem in FLAC^{3D} numerically (Itasca Consulting Group, 2019). The parametric analyses were performed on the verified numerical models to show the effect of soil and pile properties on the static and dynamic *p-y* curves. The hardening model with small-strain stiffness (HS-Small Model) was used for the static analyses. The Mohr-Coulomb model with the hysteretic damping approach was employed for dynamic analyses. The selected parameters were the pile diameter, the relative density of soil, and the degree of soil nonlinearity. The modified hyperbolic model was proposed to characterize the static *p-y* curves. The proposed model includes the initial stiffness, the ultimate soil resistance, and two additional parameters for the degree of nonlinearity, the last of which allows the *p-y* curves to be efficient from very small to large displacement ranges. The initial stiffness of the p-y curves was estimated using the small-strain modulus of soil, which can be determined precisely by seismic methods.

In addition to the static p-y curves, this thesis suggested a practical approach to dynamic p-y curves using the Bouc-Wen model, which includes the initial stiffness, the ultimate soil resistance, and the nonlinearity parameter. Two centrifuge tests from the literature were simulated numerically by the 3-dimensional analyses performed in FLAC^{3D}, and the results of the verification analysis were presented. The parametric studies were carried out to show the effect of soil and pile properties on the cyclic *p-y* curves. The total-stress approach considered the soil nonlinearity using the small-strain shear modulus and modulus degradation curves. The Bouc-Wen model equations were proposed to represent the *p-y* curves obtained. The validity of the proposed model was shown by implementing the proposed curves in structural analysis software.

The main aim of this thesis is to improve the load-deflection curves of piles under lateral loading to be used in earthquake excitation. The thesis includes the following chapters:

Chapter 2: Literature Review: The developments of the current practice for lateral load-deflection relationships are summarized. Past studies on the subject are given, and crucial conclusions are presented.

Chapter 3: Methods for Dynamic Soil-Pile-Structure Interaction Analyses: The analysis methods are outlined in this chapter. Modeling the soil behavior and analyzing the system under the seismic loading are given.

Chapter 4: Numerical Modelling of Laterally Loaded Pile Problem: Static Pile Head Loading: The numerical analysis results for the laterally loaded pile problem are given for the static loading conditions.

Chapter 5: Numerical Modelling of Laterally Loaded Pile Problem: Dynamic Loading: The numerical analysis results for the laterally loaded pile problem are given for the dynamic loading conditions.

Chapter 6: Proposed Models for Static and Dynamic p-y Curves: The mathematical models to represent the numerically derived p-y curves were presented separately for static and dynamic loading.

Chapter 7: Conclusions and Recommendations: The main outputs of the thesis are summarized, and recommendations for future works are given.

2. LITERATURE REVIEW

In this chapter, past studies related to the lateral load resistance-deflection (p-y) relations for piles in cohesionless soils were presented. First, a brief introduction to the laterally loaded pile problem and the suggestions made by the researchers for constructing p-y relations are given. Then, the studies are summarized related to the parameters required for creating p-y curves, such as the initial stiffness and the ultimate soil resistance. Finally, the drawbacks of the current approaches for p-y curves are highlighted with an emphasis on the literature studies.

2.1 Laterally Loaded Pile Problem

Reese and Van Impe (2000) explain the pile behavior under lateral load as in Figure 2.1. The initial state of the pile and deflection pattern after horizontal loading is applied from the top is shown in Figure 2.1a. Figure 2.1b and 2.1c show the uniform confining pressure distribution at rest and the pressure after the horizontal deflection takes place, respectively.

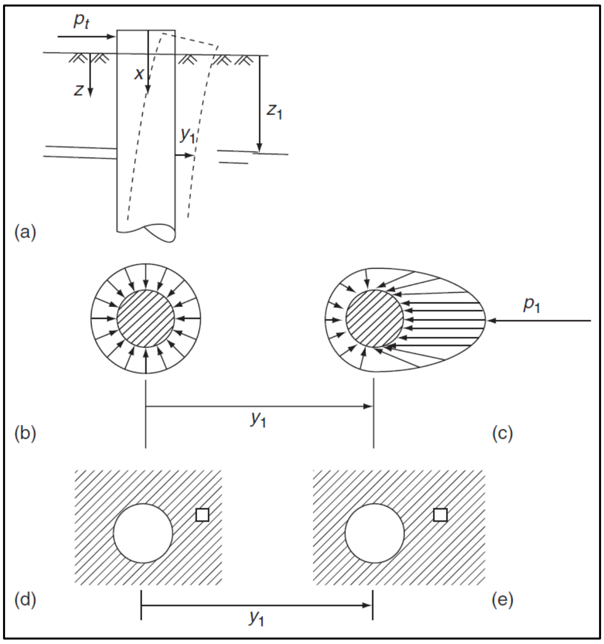

Figure 2.1 : Increasing the horizontal stresses in the soil due to pile movement.

The behavior of piles under lateral loading consists of three stages: The elastic response of the soil and the pile material, the plastic behavior of the soil, and finally, the plastic response of the pile. The governing behavior in the design is not the soil failure but the bending moment capacity of the pile (Scott, 1981). However, in recent years, the design concept has shifted from capacity-based to performance-based, in which the main concern is internal forces and displacements. As the lateral load increases, the soil behavior becomes highly nonlinear. Soil reaction depends on pile displacement, and soil behavior affects pile motion (Pile-Soil-Structure Interaction). Therefore, the pile foundation analysis aims to determine the internal forces (shear force and bending moment) along the pile and the displacement response of the soil-pile-structure system.

The response of piles under lateral loading can be expressed with a differential equation (Equation 2.1) by assuming the pile as a beam resting on nonlinear Winkler springs.

$$E_p I_p \frac{d^4 y}{dx^4} + E_{py} y = 0 \tag{2.1}$$

The analytical solution of equation 2.1 is limited, and the solution highly depends on the boundary conditions. Therefore, the solution is obtained mostly using the p-y curve approach. $E_{py}y=p$ is the soil resistance, and y is pile deflection in the equation. E_p, I_p, and E_{py} represent the elastic modulus of pile material, the moment of inertia of the cross-section, and soil modulus, respectively. The lateral soil resistance vs. pile deflection relation (p-y) is not linear, and the soil modulus (E_{py}) decreases as the pile deflection increases. The relation is given by (Reese & Van Impe, 2000) in Figure 2.2.

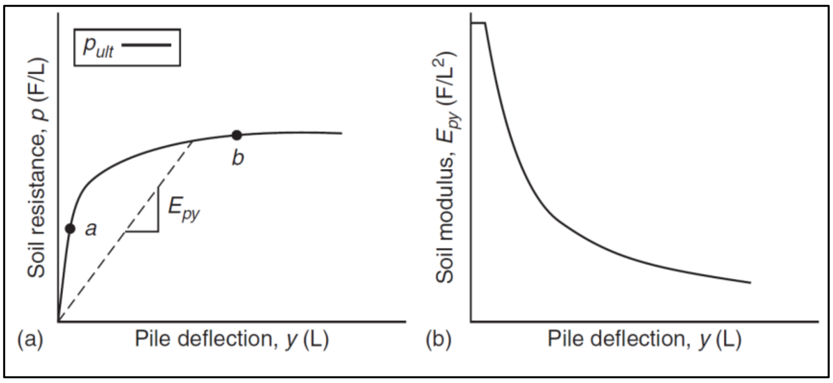

Figure 2.2 : A typical p-y curve and reduction of soil modulus with pile deflection.

2.2 Construction of Lateral Load Resistance-Deflection (p-y) Relations

In this section, the past studies on the construction of lateral load resistance-deflection relations are summarized.

Terzaghi (1955)

Terzaghi (1955) presented the first suggestion for the lateral load resistance-deflection relation for piles in cohesionless soils. The suggested linear relation is given as follows:

$$p = k_h y \tag{2.2}$$

where k_h is the lateral subgrade reaction modulus, and the following equation was given for k_h:

$$k_h = \eta_h \frac{z}{D} \tag{2.3}$$

where η_h was the constant depending on the relative density, z was the depth, and D was the pile diameter. The values in Table 2.1 was suggested for η_h values. According to Finn (2005), the suggestions of Terzaghi (1955) for horizontal subgrade reaction correspond to a lateral displacement of 25 mm.

Table 2.1 : Values of the constant of horizontal subgrade reaction η_h (Terzaghi, 1955).

Relative Density of Sand	Loose	Medium	Dense
Dry or moist sand (MN/m^3)	2.2	6.6	17.6
Submerged sand (MN/m^3)	1.25	4.4	10.7

Reese et al. (1974)

The first thorough study based on full-scale experiments for the development of p-y curves was presented by Reese et al. (1974). The field tests were performed at a site on Mustang Island in Texas. The study aimed to measure the bending moments along the pile to obtain the pile displacement, y, and the soil resistance, p, obtained by double integration and second-order derivative with respect to depth, x, respectively.

$$y = \iint \frac{M(x)}{EI} \; and \; p = \frac{d^2}{dx^2} M(x) \tag{2.4}$$

A nonlinear relation was suggested by Reese et al. (1974) for the p-y curves in cohesionless soils. The initial part of the relation is a straight line representing the elastic region. Next, a parabolic curve was suggested to limit displacement beyond the elastic region. The final part of the p-y relation consists of a straight line with the ultimate soil resistance. A typical curve showing the construction of p-y curves is shown in Figure 2.3.

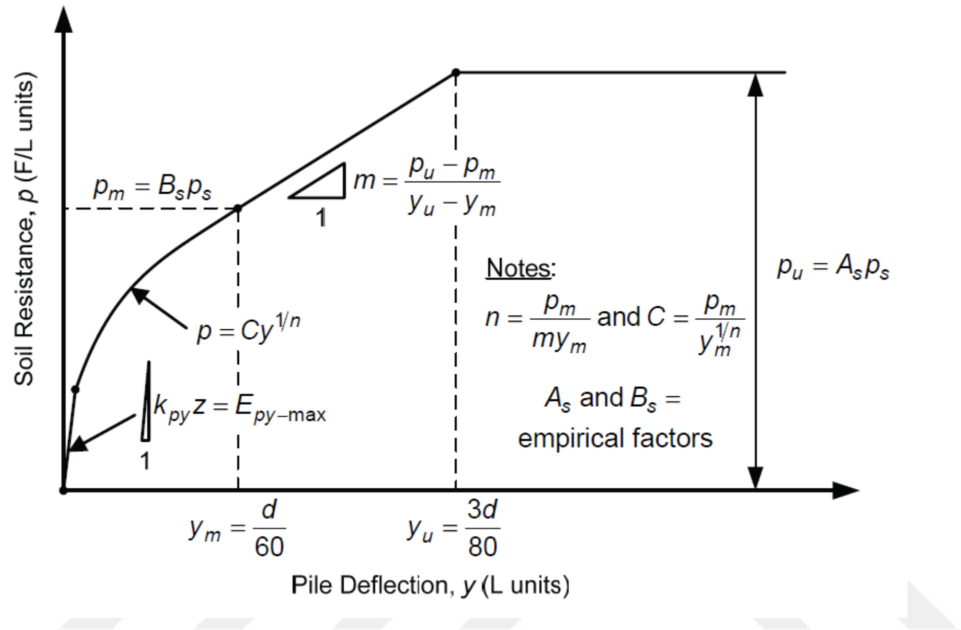

Figure 2.3 : Definition of a typical p-y curve suggested by Reese et al. (1974).

The procedure of constructing the p-y curves for sands, according to Reese et al. (1974), is summarized as follows:

1. The ultimate soil resistance, p_u, is determined. The ultimate soil resistance near the ground surface, p_{ct}, can be calculated as follows:

$$p_{ct} = \gamma H \left[\frac{K_0\, H\, tan\phi\, sin\beta}{\tan(\beta - \phi)\, cos\alpha} + \frac{tan\beta}{\tan(\beta - \phi)}(b + H\, tan\beta\, tan\alpha) + K_0\, H\, tan\beta\, (tan\phi\, sin\beta - tan\alpha) - K_a b\right] \tag{2.5}$$

The ultimate soil resistance at a depth is given as follows:

$$p_{cd} = K_a\, b\, \gamma\, H\, (tan^8\beta - 1) + K_0\, b\, \gamma\, H\, tan\phi\, tan^4\beta \tag{2.6}$$

2. The following values were suggested for computing the ultimate soil resistance:

$$\beta = 45 + \frac{\phi}{2}\ ;\ K_0 = 0.4\ ;\ K_a = tan^2(45 - \frac{\phi}{2}) \tag{2.7}$$

where α=ϕ/3 for static loading, and α =3ϕ/4 for cyclic loading.

3. X_t is the depth at which the ultimate lateral soil resistance near the ground surface and at a depth are equal. p_{ct} and p_{cd} are used when the p-y curve is constructed above and below X_t, respectively.
4. Compute the threshold displacements y_u=3b/80, y_m=b/60, and resistance values p_u=Ap_c, p_m=Bp_c.
5. The initial slope of the p-y curve is determined using k_{py} (Table 2.2).
6. The equation of parabola between the points *k* and *m* is given as

$$p = C\, y^{\frac{1}{n}} \tag{2.8}$$

7. The parameters for the parabola are given below:

$$m = \frac{p_u - p_m}{y_u - y_m}\ , n = \frac{p_m}{m y_m}\ , C = \frac{p_m}{{y_m}^{1/n}} \tag{2.9}$$

and the point *k* is determined as:

$$y_k = \left(\frac{C}{kx}\right)^{\frac{n}{n-1}} \tag{2.10}$$

Table 2.2 : Reese et al. (1974) recommendations for initial stiffness for p-y curves in cohesionless soils.

Relative Density of Sand	Loose	Medium	Dense
Dry or moist sand (MN/m^3)	6.8	24.4	61
Submerged sand (MN/m^3)	5.4	16.3	34

The construction of the p-y curves is completed by finding the point k. The procedure summarized above can be applied to any depth of interest. However, the suggested curves were based on the field test results performed in dense sand. As a result, the initial stiffness values (Table 2.2) were far greater than the suggestion of Terzaghi (1955). Besides, there is no single function to construct the suggested curves, but it consists of three parts.

Desai and Kupsusamy (1980)

The modified Ramberg & Osgood method was suggested by Desai and Kuppusamy (1980) for the construction of p-y curves. They performed finite element analyses for laterally loaded piles and sheet pile problems. The following form was employed in the analyses based on the curves suggested by Reese et al. (1974).

$$p = \frac{(k_0 - k_f)y}{\left[1 + \left\{\frac{(k_0 - k_f)y}{p_u}\right\}^m\right]^{\frac{1}{m}}} + k_f y \tag{2.11}$$

where k_0 and k_f represent the initial and final stiffness, p_u is the ultimate lateral soil resistance, and m is the nonlinearity parameter. For m=1 and k_f=0, the equation reduces to a hyperbola.

API (2007)

American Petroleum Institute (API, 2007) suggested the following form of hyperbolic function for p-y curves in cohesionless soils:

$$p = A\ x\ p_u x \tanh\left[\frac{k\ x\ H}{A\ x\ p_u} x\ y\right] \tag{2.12}$$

where p_u is the ultimate soil resistance, k is the initial stiffness, and A is the factor for the loading condition. The parameter A is constant (0.9) for cyclic loading, but it depends on the depth for static loading, as shown in equation 2.14.

$$A = 0.9\ \ for\ cyclic\ loading \tag{2.13}$$

$$A = \left(3 - 0.8\frac{H}{D}\right) \geq 0.9\ \ for\ static\ loading \tag{2.14}$$

The following equations were suggested for the ultimate soil resistance under lateral loading at shallow and deep depths:

$$p_{us} = (C_1\ x\ H + C_2 x\ D)\ x\ \gamma\ x\ H \tag{2.15}$$

$$p_{ud} = C_1\ x\ D\ x\ \gamma\ x\ H \tag{2.16}$$

where γ is the effective unit weight, H is the depth, D is the pile diameter, and C_1, C_2, *and* C_3 are the coefficients that can be determined using Figure 2.4. The initial stiffness in API can be determined using Figure 2.5.

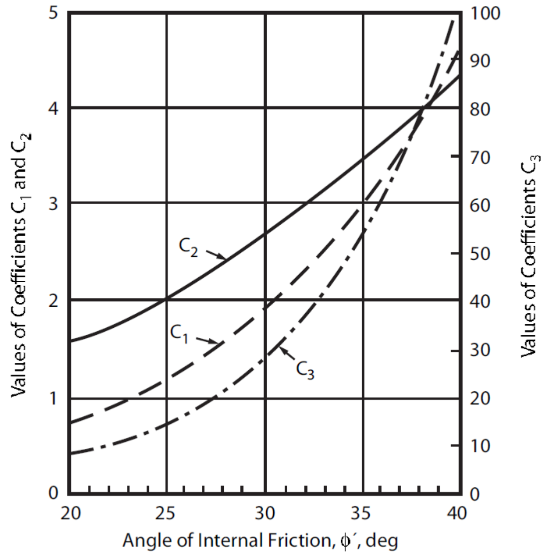

Figure 2.4 : The coefficients required for the ultimate resistance in API.

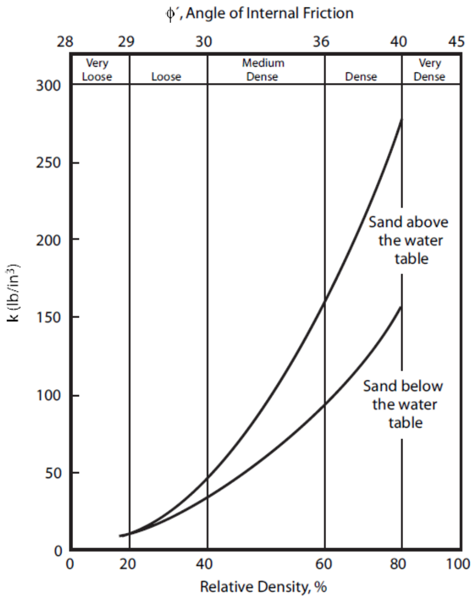

Figure 2.5 : Subgrade reaction modulus for sands in API.

Gohl (1991)

The centrifuge tests were performed by Gohl (1991) in dry sand for steel pipe piles. Harmonic input motion was applied at the base of the shake table, and cyclic p-y loops were obtained. The study showed that the subsequent loading/unloading hysteresis could be represented using the Masing (1926) rule. However, the agreement was poor in the API (2007) for the backbone curves of the pile response. Gohl (1991) suggested the modified form of the Ramberg & Osgood equation for the p-y curves.

$$p = \frac{k_h\, y}{1 + a\left(\frac{p}{p_u}\right)^{r-1}} \tag{2.17}$$

The above form of the Ramberg & Osgood equation was first proposed by Ishihara (2021) for the stress-strain response of soils subject to cyclic loads. Gohl (1991) modified the equation to model the experimentally derived p-y curves. In the equation, k_h and p_u were the initial stiffness and the ultimate soil resistance, respectively. The α and r were the curve fitting parameters. Equation 2.18 was suggested by Gohl (1991) for the parameter r:

$$r \cong \frac{1 + (\pi/2)D_{max}}{1 - (\pi/2)D_{max}} \tag{2.18}$$

where D_{max} is the maximum damping ratio mobilizing at large displacements, the damping ratio value must be lower for small displacements at which the soil strains are lower. However, the study did not suggest a damping ratio considering the displacement level; instead, Gohl (1991) suggested the maximum damping ratio (D_{max}) to estimate the parameter r. Therefore, equation 2.19 is suggested for the parameter α:

$$\alpha = \frac{y_{ult}}{y_r} - 1 \tag{2.19}$$

where y_{ult} was the displacement at which the ultimate soil resistance was mobilized, and Gohl (1991) proposed to set y_{ult} as 5% of the pile diameter (y_{ult}=0.05D). The parameter y_r was the reference deflection which was given as:

$$y_r = \frac{p_{ult}}{k_h} \tag{2.20}$$

Gohl (1991) suggested the Barton et al. (1983) equation for the ultimate soil resistance, p_{ult} as follows:

$$p_{ult} = \beta\, K_p\, \sigma'_v\, D \tag{2.21}$$

where K_p is the passive earth pressure coefficient, σ'_v vertical effective stress, D is the pile diameter, and β is a coefficient. The β values in Gohl (1991) varied from 1.75 to 3.5. In addition, Gohl (1991) employed larger values for β near the ground surface, which decreased as the depth increased, contradicting the findings of Barton (1982), who suggested increasing the β with depth. Lastly, the horizontal stiffness k_h was calculated based on Kagawa and Kraft (1980) as follows:

$$k_h = \bar{\delta} E_{max} \tag{2.22}$$

where E_{max} can be estimated using the low strain shear modulus (G_{max}). The parameter $\bar{\delta}$ in Kagawa and Kraft (1980) depends on pile flexibility; however, a constant value of 1.9 was adopted by Gohl (1991).

<u>*Georgiadis et al. (1992)*</u>

Centrifuge tests were performed by Georgiadis et al. (1992) for piles embedded in dry sand. The tests were carried out by applying the lateral load at the pile head level. The hyperbolic function of Kondner (1963) was employed to fit the p-y curves obtained in the tests. The p-y curve relation was written in the following form of the hyperbolic function:

$$p = \frac{y}{\frac{1}{k_{ini}} + \frac{y}{p_u}} \tag{2.23}$$

where the k_{ini} is the initial stiffness and p_u is the ultimate soil resistance. The study adopted the Reese et al. (1974) equations for ultimate soil resistance (p_u), and the suggestion of Terzaghi (1955) was implemented for initial stiffness (k_{ini}) since a better agreement with the centrifuge test results was observed. The equation was highly efficient compared to Reese et al. (1974). However, the study showed that the selection of initial stiffness is vital. The authors stated that the suggestion of Reese et al. (1974) for initial stiffness was too high, yielding significantly different responses than the test results. Therefore, the main drawback of the hyperbolic function is the sensitivity of the p-y response to the selection of initial stiffness.

Pender (1993)

Pender (1993) suggested equation 2.24 for the nonlinear equation of the p-y curves. The equation includes the initial stiffness (k_{ini}), the ultimate soil resistance to the lateral loading (p_u), and the parameter n for the extent of nonlinearity.

$$y = \frac{p}{k_{ini}}\left(\frac{p_u}{p_u - p}\right)^n \tag{2.24}$$

Pender (1993) proposed the Broms (1964) equation for the ultimate soil resistance (p_u), which is given as follows:

$$p_u = 3\ K_p \sigma'_v D \tag{2.25}$$

The equation of Vesić (1961) was proposed by Pender (1993) for the initial stiffness, which is given as follows:

$$k = \frac{0.65\ E_s}{(1 - v_s{}^2)} \sqrt[12]{\frac{E_s D^4}{E_p I_p}} \tag{2.26}$$

According to Pender (1993), small-strain stiffness of the soil could be employed for E_s in Vesic's equation. Therefore, the nonlinearity parameter, n, could be taken as 1 for sands.

Brown et al. (2000)

Brown et al. (2001) suggested equation 2.27 for p-y curves under dynamic loading based on the static p-y curves:

$$p_d = p_s\left((\alpha + \beta a_0{}^2 + \mathrm{K} a_0\left(\frac{\bar{w}y}{D}\right)^n\right), p_d < p_u \tag{2.27}$$

where p_s is the resistance under static loading, a_o frequency of loading ($a_o = \omega r_o / V_s$), ω angular frequency of loading, r_o is the pile radius, y lateral displacement, D is the pile diameter, α, β, κ and n are the constants from curve fitting.

The p_s in equation 2.27 is the static loading resistance that API was adopted in Brown et al. (2000). Table 2.3 shows the constants in equation 2.27 for the dynamic multiplier parameters.

Table 2.3 : Dynamic p-y parameter constants according to Brown et al. (2001).

Soil Type	Description	α	β		κ	n
			α_o<0.025	α_o>0.025		
Soft clay	c_u< 50 kPa V_s<125 m/s	1	-180	-200	80	0.18
Medium clay	50<cu< 100 kPa 125<Vs<175 m/s	1	-120	-360	84	0.19
Stiff clay	cu>100 kPa Vs>175 m/s	1	-2900	-828	100	0.19
Medium-dense sand (saturated)	50<Dr< 85 125<Vs<175 m/s	1	3320	1640	-100	0.1
Medium-dense sand (unsaturated)	50<Dr< 85 125<Vs<175 m/s	1	1960	960	-20	0.1
Dense sand (saturated)	Dr> 85 Vs>175 m/s	1	6000	1876	-100	0.15

Varun (2010)

Varun (2010) created a 3-dimensional (3D), finite element model to develop a macroelement for piles in liquefiable soils. Multi-yield constitutive soil model with a kinematic hardening rule was employed based on the plasticity theory. Parametric soil-pile interaction analyses were performed, and the Bouc-Wen model was suggested for the p-y formulation. The soil resistance p can be written as:

$$p = p_y \zeta \tag{2.28}$$

where p_y is the ultimate soil resistance, and ζ is a hysteretic parameter controlling the curve nonlinearity. The last parameter could be calculated in an incremental form as:

$$d\zeta = \{A - f_\zeta[\beta + \gamma \; sign \; (du.\zeta]\} \frac{du}{u_y} \tag{2.29}$$

where A is the parameter generally taken as 1, $u_y = p_y/K$ is the yield displacement, K is the initial stiffness, du is the incremental relative displacement, β=1-γ are parameters controlling the unloading and reloading behavior, f_ζ is the monotonically increasing function of ζ.

Varun (2010) suggested an initial stiffness for the p-y curve formulation:

$$K = 1.25\, E_s \tag{2.30}$$

The ultimate resistance of soil to the lateral loading p_u:

$$p_u = 3.25K_p + 0.3{K_p}^2 \tag{2.31}$$

The last parameter for the nonlinear backbone of the dynamic p-y curves was the function of the f (ζ) parameter, which was equal to ζ^n in the original Bouc-Wen model; however, Varun (2010) suggested the following form for the nonlinearity parameter:

$$f(\zeta) = \frac{\tanh(\alpha\zeta)}{\tanh(\alpha)} \tag{2.32}$$

The parameter α in the above equation was suggested as 2.7 for dense sand, 2.8 for medium-dense sand, and 2.9 for loose sands.

Yang et al. (2011)

A series of 1g shaking table tests were performed by Yang et al. (2011) in cohesionless soils to obtain the dynamic p-y curves. The tests were conducted in dense sand with a relative density of D_R=80 %. An aluminum alloy pipe was used to simulate piles, and strain gages were placed along the pile to measure the bending strain. Several loading schemes were applied to the test setup. The dynamic p-y curves were determined using the bending moments as follows:

$$p = \frac{d^2}{dz^2} M(z) \tag{2.33}$$

$$y_{pile} = \iint \frac{M(z)}{EI} dz \tag{2.34}$$

where p is the lateral soil resistance, y_{pile} is pile displacement, $M(z)$ is the bending moment along the pile, EI is the flexural stiffness of the pile, and z is the depth below the ground surface. The bending moments in the above equations were calculated using the measured bending strains as follows:

$$M = \frac{E\,\varepsilon\,I}{y} \tag{2.35}$$

The experimental results obtained by the shake table tests were best fitted by the hyperbolic function of Kondner (1963), expressed in equation 2.21.

The study suggested lower bound and upper bound equations for the ultimate resistance of dynamic p-y curves:

$$\frac{p_u}{D} = 6.32 K_p \gamma' z^{1.22}\ (N/cm^2)\ \ for\ lower\ limit\ backbone \tag{2.36}$$

$$\frac{p_u}{D} = 11.83 K_p \gamma' z^{1.11}\ (N/cm^2)\ \ for\ upper\ limit\ backbone \tag{2.37}$$

The study suggested lower bound and upper bound equations for the initial stiffness of dynamic p-y curves:

$$K = 208.31 p_a \left(\frac{\sigma'}{p_a}\right)^{0.5}\ \ for\ lower\ limit\ backbone \tag{2.38}$$

$$K = 333.48 p_a \left(\frac{\sigma'}{p_a}\right)^{0.5}\ \ for\ upper\ limit\ backbone \tag{2.39}$$

Yoo et al. (2013)

Dynamic centrifuge tests were performed by Yoo et al. (2013) for a pile in dry sand. Pile diameter, the relative density of soil, loading amplitude, and frequency were the variables. Based on the test results, the hyperbolic model was suggested to represent the backbone of p-y curves. The initial stiffness parameter was recommended for loose and dense sand as follows:

$$K = 4.26 D p_a \left(\frac{\sigma'}{p_a}\right)^{0.5}\ \ for\ loose\ sand \tag{2.40}$$

$$K = 7.29 D p_a \left(\frac{\sigma'}{p_a}\right)^{0.5}\ \ for\ dense\ sand \tag{2.41}$$

The ultimate soil resistance to lateral loading equations was given for loose and dense sand as follows:

$$\frac{p_u}{D} = 12.5DK_p\gamma' z^{0.90}\ for\ loose\ sand \tag{2.42}$$

$$\frac{p_u}{D} = 13.3DK_p\gamma' z^{1.02}\ for\ dense\ sand \tag{2.43}$$

Thieken et al. (2015)

Thieken et al. (2015) investigated the large-diameter monopile behavior under lateral loading using the finite element method. They stated that the conventional p-y curves do not accurately represent the foundation stiffness which was overestimated at large loads and underestimated at small loads. Therefore, they created a numerical model in PLAXIS3D using the HSsmall model for constitutive soil behavior. Based on the comprehensive parametric study, they suggested a set of equations for p-y curves in cohesionless soils. The following equations for the resistance values for displacement intervals were given, and the definitions were plotted in detail in Figure 2.6 and Figure 2.7.

$$p = p_B\left(\frac{y}{y_B}\right)^{1/n}\ for\ p < p_B \tag{2.44}$$

$$p = p_B + \left(\frac{p_C - p_B}{y_C - y_B}\right)(y - y_B)\ for\ p_B < p < p_C \tag{2.45}$$

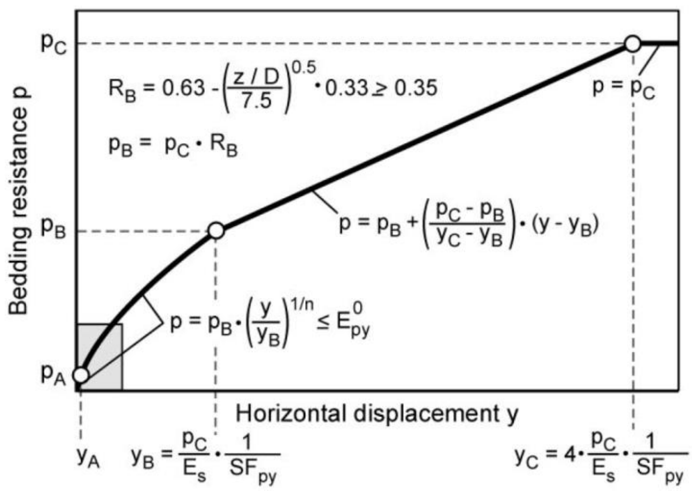

Figure 2.6 : Construction of p-y curves in Thieken et al. (2015).

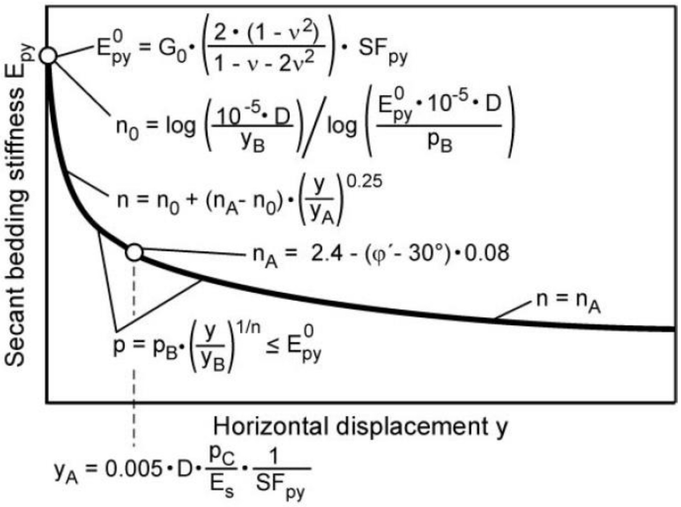

Figure 2.7 : Reduction of secant stiffness with the horizontal displacement in Thieken et al. (2015).

Lim and Jeong (2018)

Shake table tests were performed by Lim and Jeong (2018) for piles in dry sand under dynamic loading. The pile behavior was investigated similarly to the study presented by Yang et al. (2011). The hyperbolic function was suggested for p-y curve formulation. In addition, the initial stiffness and ultimate soil resistance values were presented for the p-y behavior. The proposed p-y curves were employed in pseudo-static analyses, and the results were compared with Reese et al. (1974) and the API results. The authors stated that the proposed curves lead to better agreement with the test results.

Lu et al. (2020)

The centrifuge tests by Lu et al. (2021) showed that the hyperbolic function could represent the p-y curves under static loading. The initial stiffness in the p-y relation is calculated using equation 2.49.

$$k_{ini} = \eta_h Z^{\alpha} \tag{2.49}$$

The experimental study showed that the η_h can be taken as 2000 kN/m^3 and α is taken as 0.5. Therefore, the ultimate soil resistance to lateral loading p_u can be calculated using the API equation of p_u at depth:

$$p_{ud} = C_3 D \gamma Z \tag{2.50}$$

where C_3=100. The suggestions for the p-y curves are summarized in Table 2.4.

Table 2.4 : Summary of the p-y curve suggestions in the literature.

Reference	p-y relation	Explanation
Terzaghi, 1955	$p=k_h y$ $k_h = n_h \frac{z}{B}\ ve\ n_h = \frac{A\gamma}{1.35}$ γ is the unit weight of soil, and A is a factor	A linear relation is suggested based on elasticity theory
Reese et al., 1974	$p_a = k_h y_a \frac{z}{D}\ \ ve\ p_b = p_u \frac{B}{A}$ A and B are empirical factors; $y_a = D(p_b/zk_n)^{n/m-1}(D/y_b)^{1/m-1}$; $y_b = D/60$; $y_u = 3D/80$;	The relation is based on full-scale static and cyclic field tests
Desai and Kupsusamy, 1980	$p = \frac{(k_0 - k_f)y}{\left[1 + \left\{\frac{(k_0 - k_f)y}{p_u}\right\}^m\right]^{\frac{1}{m}}} + k_f y$	A modified form of the Ramberg-Osgood model is suggested
API, 2007	$p = A p_u \tanh(\frac{kz}{A p_u} y)$	Back calculated relation from the full-scale field test is suggested
Gohl, 1991	$p = \frac{k_h\, y}{1 + a\left(\frac{p}{p_u}\right)^{r-1}}$	A modified form of the Ramberg-Osgood model is suggested for the dynamic backbone based on the centrifuge test results
Georgiadis et al. (1992), Yang et al. (2011), Yoo et al. (2013) Lim and Jeong (2018), Lu et al. (2020)	$p = \frac{y}{\frac{1}{k_{ini}} + \frac{y}{p_u}}$	The hyperbolic model of Kondner (1963) was suggested based on shake table experiments.
Pender, 1993	$y = \frac{p}{E_{py-max}}\left(\frac{p_u}{p_u - p}\right)^n$	Developed by finite element model from back-analyzed full-scale field tests
NCHRP, 2001	$p_d = p_s\left((\alpha + \beta {a_0}^2 + \mathrm{K} a_0 \left(\frac{\overline{w} y}{d}\right)^n\right), p_d$	Based on the statnamic, field tests
Varun, 2010	$p = p_y \zeta$ $d\zeta = \{1 - f_\zeta[b + g\ sign\ (du.\zeta]\} \frac{du}{u_y}$ $f(\zeta) = \frac{\tanh(\alpha\zeta)}{\tanh(\alpha)}$	The Bouc-Wen model was proposed based on the finite element analyses results
Thieken et al., 2015	$p = p_B \left(\frac{y}{y_B}\right)^{1/n}\ for\ p < p_B$ $p = p_B + \left(\frac{p_C - p_B}{y_C - y_B}\right)(y - y_B)\ for\ p_B < p < p_C$	The suggested curve has three parts based on the finite element analysis results

2.3 Initial Stiffness of the p-y Curve

The formulations for the construction of p-y curves presented in the previous section showed that the relations require the initial stiffness of the pile under lateral loading. There have been several studies on the stiffness of piles subject to lateral loads, and some of the suggestions, including Broms (1964); Kagawa and Kraft (1980); Poulos (1971); Vesić (1961); Scott (1980); Gerolymos and Gazetas (2006), Augustesen et al. (2009); Sørensen (2012) were presented in this section.

Terzaghi (1955)

The first suggestion for the initial stiffness of piles subject to lateral loading was made by Terzaghi (1955). Then, the following form of the p-y relation was suggested based on the theory of elasticity:

$$k_h = \frac{0.74E_s}{D} \tag{2.51}$$

where E_s is the soil modulus and D is the pile diameter.

Vesic (1961)

Vesić (1961) proposed an equation for the spring stiffness of piles resting on the elastic foundation:

$$k_s = \frac{0.65E_s}{1-\upsilon^2}\sqrt[12]{\frac{E_s D^4}{E_p I_p}} \tag{2.52}$$

Poulos (1971)

The pile response under lateral loading was investigated by Poulos (1971), and a relation was suggested for initial stiffness:

$$k_h = \frac{0.82E_s}{D} \tag{2.53}$$

Kagawa and Kraft (1980)

Kagawa and Kraft (1980) have studied the dynamic lateral load-deflection relationship for piles subject to lateral pile head and seismic loading. The study suggested a simplified approach to dynamic p-y curves by estimating the degraded soil modulus under dynamic loading conditions, which requires site response analyses in the first step of the method. The p-y response was written in the nondimensional form as follows:

$$\frac{p}{E_s y} = \delta_1 + i\delta_2 = \delta \tag{2.54}$$

The δ_1 parameter in the above equation represents the true spring stiffness and δ_2 energy dissipation due to material and radiation dampings.

Several suggestions were made for the real part of the spring stiffness (δ_1). Kagawa and Kraft (1980) presented these suggestions in a plot as given in Figure 2.8. The δ_1 values depend on the relative pile stiffness K_r which is defined as follows:

$$K_r = \frac{EI}{E_s H^4} \tag{2.55}$$

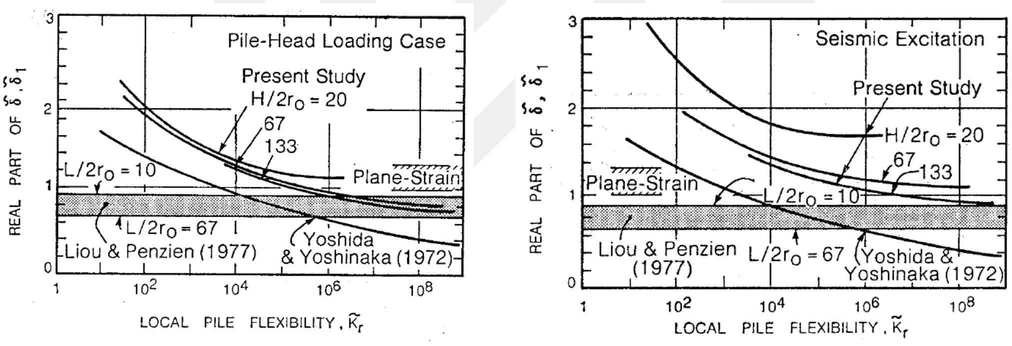

Figure 2.8 : Real part of the initial stiffness parameter in Kagawa and Kraft (1980).

Scott (1980)

Scott (1981)suggested the bilinear function for the p-y relation, stating that using the method proposed by Reese et al. (1974) is too complicated. Instead, he proposed the initial stiffness to be equal to the soil modulus for the sake of simplicity.

Augustensen (2009)

Augustesen et al. (2009) compared the FLAC^{3D} analysis with the Winkler approach results for an offshore monopile subjected to extreme lateral loads. They employed the API approach for the p-y curves, and the following expression was proposed for the initial stiffness to fit the suggestion of API best:

$$k_{sand} = 0.008085\ \phi^{2.45} - 26.09\ \left(\frac{MPa}{m}\right) \tag{2.56}$$

<u>Gerolymos and Gazetas (2006)</u>

The distributed stiffness of a cylindrical-shaped caisson foundation was suggested by Gerolymos and Gazetas (2006):

$$k_x = 1.60 \left(\frac{z}{D}\right)^{-0.13} E_s \tag{2.57}$$

<u>Sorensen (2012)</u>

Sørensen (2012) performed several numerical analyses in $FLAC^{3D}$ for large-diameter monopiles and concluded the following form for the initial stiffness of p-y curves:

$$E_{py} = a \left(\frac{x}{x_{ref}}\right)^b \left(\frac{D}{D_{ref}}\right)^c \left(\frac{E_s}{E_{s,ref}}\right)^d \tag{2.58}$$

where a=1 MPa, b=0.3, c=0.5, and d=0.8

The studies related to the initial stiffness of p-y curves are summarized in Table 2.5.

Table 2.5 : Suggestions in the literature for the initial stiffness of the p-y curve.

Reference	p-y relation
Terzaghi, 1955	$k_h = \frac{E_s}{1.35\ B}$
Vesic, 1961	$k_s = \frac{0.65E_s}{1-\upsilon^2} \sqrt[12]{\frac{E_s B^4}{E_p I_p}}$
Poulos, 1971	$k_h = \frac{0.82E_s}{B}$
Kagawa and Kraft (1980)	$\frac{p}{E_s y} = \delta_1 + i\delta_2 = \delta$ $\delta_1\ depends\ on\ the\ pile\ flexural\ stiffness$ $\delta_2\ depends\ on\ the\ loading\ frequency$
Scott (1980)	$k_h = \frac{E_s}{B}$
Gerolymos (2006)	$k_x = 1.60 \left(\frac{z}{D}\right)^{-0.13} E_s$
Sorensen (2012)	$E_{py} = a \left(\frac{x}{x_{ref}}\right)^b \left(\frac{D}{D_{ref}}\right)^c \left(\frac{E_s}{E_{s,ref}}\right)^d$

2.4 Ultimate Soil Resistance to Lateral Loading

All the p-y curve formulations require the ultimate soil resistance to lateral loading. The studies on the ultimate soil resistance in cohesionless soils are summarized below.

Broms (1964)

Broms (1964) suggested equation 2.59 for the soil reaction to lateral loading per unit length of the pile:

$$p_u = 3K_p D\sigma'_{vo} \qquad (2.59)$$

where *D* is the pile diameter, σ'_{v0} is the vertical effective stress, and K_p is the lateral earth pressure coefficient which can be calculated as:

$$K_p = tan^2(45 + \frac{\phi}{2}) \qquad (2.60)$$

Broms (1964) stated that the lateral earth pressure was independent of the shape of the pile cross-section.

Zhang et al. (2005)

L. Zhang et al. (2005) proposed a method for predicting the ultimate soil resistance to lateral loading. They suggested equation 2.61, which includes the normal frontal reaction and the side friction reaction:

$$p_u = (\eta p_{max} + \xi\tau_{max})D \qquad (2.61)$$

In equation 2.61, *D* is the pile diameter, η and $\xi$the parameters depend on the pile shape in Table 2.6.

Table 2.6 : Parameters required for the ultimate soil resistance of L. Zhang et al. (2005).

Pile shape	η	ξ
Circular	0.8	1.0
Square	1.0	2.0

The frontal soil resistance to lateral loading is defined as follows:

$$p_{max} = K_p{}^2\sigma_{v0}' \qquad (2.62)$$

The shear drag resistance to lateral loading is defined as follows:

$$\tau_{max} = K\sigma_{v0}' \tan\delta \tag{2.63}$$

Fleming (2008)

The centrifuge tests performed by Barton et al. (1983) have shown that the ultimate soil resistance to lateral loading estimated by Broms (1964) was underestimated. Therefore, the equation was modified by Fleming et al. (2008) as follows:

$$p_u = {K_p}^2 D\sigma_{v0}' \tag{2.64}$$

The modified form of the equation allows greater p_u values than Broms' equation since the constant multiplication three was replaced by K_p, which is higher than 3 for the angle of friction values larger than 30°.

Thieken et al. (2015)

Thieken et al. (2015) performed finite element analyses to develop a new static p-y curve approach for piles in cohesionless soils. They concluded that the ultimate soil resistance can be represented by the DIN 4085 approach, for which the following equation is proposed:

$$p_u = \frac{11}{16}\gamma z^{1.5} K_{pgh}(1 + 2\,tan\phi')\sqrt{D} \tag{2.65}$$

The passive earth pressure coefficient K_{pgh} in the above equation depends on the internal angle of friction ϕ' and the passive wall friction; the latter was assumed to be δ_p=-2/3 ϕ'. Therefore, the K_{pgh} equation is given as follows:

$$K_{pgh} = \sqrt{\frac{K_p(1 - 0.53\frac{-2\phi'}{3})^{0.26+5.96\phi'}}{1 + \left(tan\frac{-2\phi'}{3}\right)^2}} \tag{2.66}$$

The ultimate soil resistance equations to lateral loading for piles in cohesionless soils given in the literature are summarized in Table 2.7.

Table 2.7 : Suggestions in the literature for the ultimate soil resistance.

Reference	p_u
Broms, 1964	$p_u = 3K_pB\sigma'_{vo}$
Reese et al., 1974	$p_u = p_{st}A$ At greater depths A=3-0.8(z/D)
Zhang, 2005	$p_u = (\eta p_{max} + \xi\tau_{max})B$
Fleming et al., 2008	$p_u = {K_p}^2B\sigma_{v0}'$
Varun, 2010	$p_u = (3.25K_p + 0.25{K_p}^2)B\sigma_{v0}'$
Thieken et al. (2015) (DIN 4085)	$p_u = \frac{11}{16}\gamma z^{1.5}K_{pgh}(1 + 2\ tan\phi')\sqrt{D}$ $where\ K_{pgh} = \sqrt{\frac{K_p(1 - 0.53\frac{-2\phi'}{3})^{0.26+5.96\phi'}}{1 + \left(tan\frac{-2\phi'}{3}\right)^2}}$

2.5 Limitations of the Current Practice

The first attempt for lateral load-deflection relations was made by Terzaghi (1955) using the theory of elasticity. However, the given relation was linear, and the coefficient of subgrade reaction modulus (k) corresponding to 25 mm lateral displacement was suggested. The nonlinear p-y curve formulation for piles in sands was recommended by Reese et al. (1974). The suggestion was based on the full-scale field tests performed in Mustang Island (Texas). First, bending moments were obtained using the strain gages placed along the pile. The second-order integration of the bending moments gives the pile deflection, y, and the second-order differentiation provides the soil with resistance, p. Then, the soil resistance-pile deflection relations (p-y curves) were obtained for each depth, and the pile deflection was normalized by the pile diameter. However, the relation is not a continuous function but consists of three parts. Besides, the suggested initial stiffness is far greater than the one proposed by Terzaghi (1955).

Murchison and O'Neill (1984) suggested a hyperbolic p-y relation for sand soils based on the field test results. The given relation was adopted by API (2007) and has been commonly used in the industry since then. The initial stiffness of Reese et al. (1974) was adopted by API (2007) depending on the relative density of sand.

The API (2007) relation is used in the offshore industry and is very common to analyze piles under seismic loading conditions. Although several researchers studied the p-y curve approach, the API (2007) is the most common method due to its simplicity. According to Finn (2005) and Rahmani et al. (2018), the suggestion of Terzaghi (1955) is too conservative, and the initial stiffness given by API (2007) is too high that it cannot capture the nonlinear behavior accurately. Moreover, the relation was obtained by applying the static load from the top of the pile for the dense sand and did not consider different soil nonlinearities. Especially the soil behavior under earthquake loading must be properly considered in the soil-pile-structure interaction analyses. For this purpose, researchers have conducted numerical and experimental studies (Allotey & El Naggar, 2008; Brown et al., 2001; Hussein & El Naggar, 2022; Lombardi et al., 2017; Naggar & Bentley, 2000; Rahmani et al., 2018; Wilson, 1998).

McGann et al. (2011) stated that API (2007) relation gives reasonable results at shallow depth, but the results are not realistic as the depth increases since the kinematic effect of seismic loading cannot be taken into account. They analyze the soil-pile interaction problem by modeling the piles as vertical beams. The soil was modeled as 8-noded brick 3D solid elements in OpenSees. They used interface elements to obtain the load transferred from soil to pile. Drucker-Prager soil model considers the nonlinear behavior of soil by McGann et al. (2011). In the study, instead of finding the soil resistance and the pile deflection using the bending moments, they were obtained directly in the 3D model. The pile deflection was determined at the beam nodes, and the soil resistance was obtained at the pile-soil interface elements.

The authors compared the obtained p-y curves with the API (2007) curves and concluded that API (2007) relation was not validated, especially at the deeper soil stratum. This result was presented in Figure 2.9: The p-y curves at 1.0 m and 2.4 m below the ground surface were compatible with the numerical results, but the results at 9.9 m and 14.7 m were significantly different for the two methods. Soil resistance at the deep obtained using the finite element solution is relatively low compared to the API (2007) suggestion. Therefore, the obtained internal forces (shear force and bending moment) and displacements using the API (2007) relation may cause the design to be unsafe.

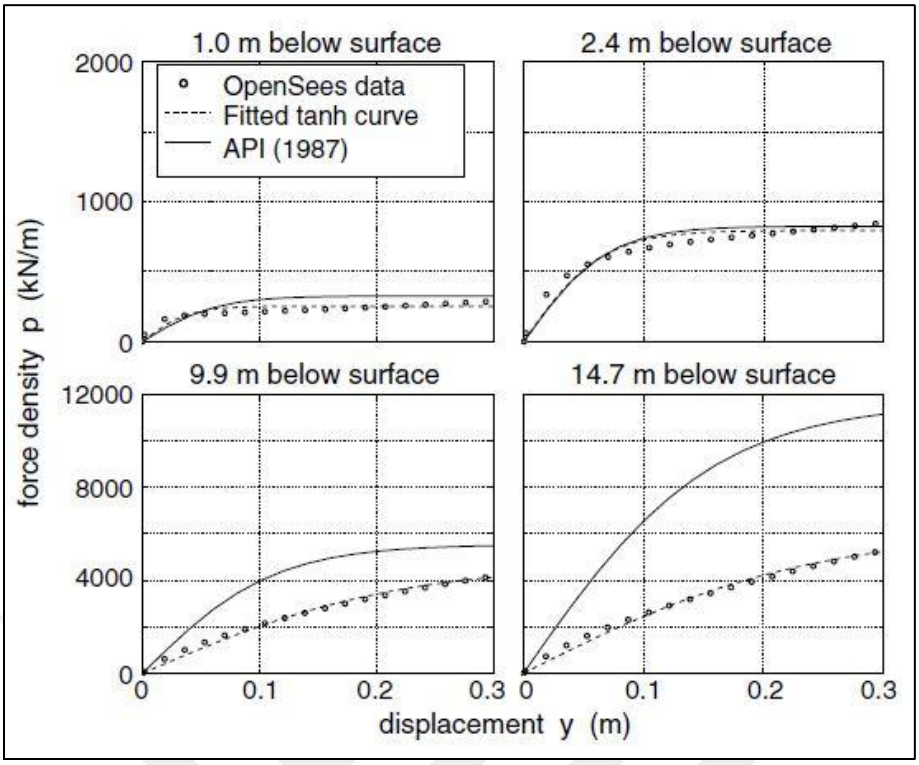

Figure 2.9 : p-y curves for different depths obtained using API (2007) and finite element method McGann et al. (2011).

Choi et al. (2016) stated that API (2007) relation has some drawbacks, such as 1) Ultimate lateral load capacity is low in API (2007) suggestion, 2) Elastic initial stiffness is used instead of compatible deformation modulus and 3) The slope of the curve at low deformations are too high. The authors used plasticity theory and offered a model that considers the mentioned drawbacks. The results of the suggested model was compared with the API (2007) and the centrifuge test results. The experimental p-y backbone, API (2007) curve, and the curve obtained from the suggested model are presented in Figure 2.10. Besides, the dependency of the p-y relation on the earthquake acceleration is shown in Figure 2.10. According to the results, the slope of the p-y curves decreases as the maximum acceleration increase. As a result, the ultimate lateral load capacity was greater than the API (2007) relation. Although the suggested method fills the gap of the API (2007) relation, it is not practical to implement the model in design since it has many input parameters, and determining these parameters is not easy. The soil resistance-pile deflection relations (p-y curves) suggested so far are summarized in Table 2.8.

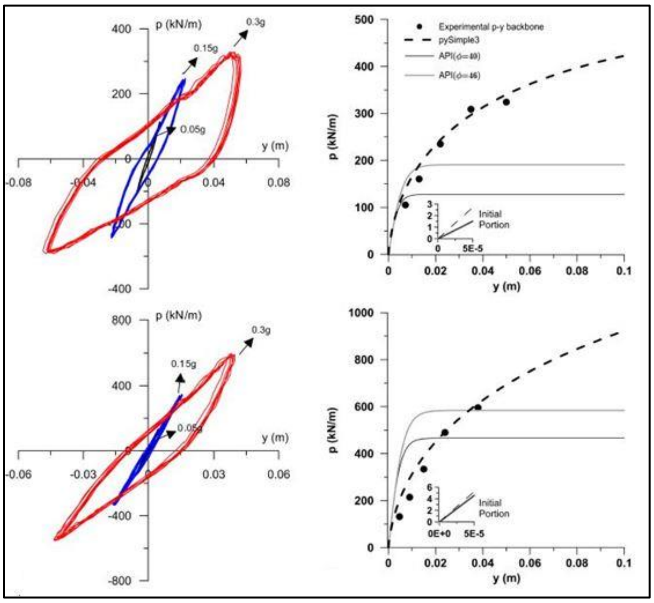

Figure 2.10 : The effect of dynamic load amplitude on p-y curves (Choi et al., 2016).

Table 2.8 : Summary of the studies related to pile behavior under lateral loading.

Reference	Soil Type	Experimental Setup	Numerical Analysis Method	Loading Condition	Suggested (or adopted) p-y Model
Terzaghi, 1955	Sand	-	Elasticity theory	Pile head	Initial stiffness
Reese et al., 1974	Sand	Full-scale field test	-	Pile head	Static and cyclic
Gohl, 1991	Dry Sand	1g-Shake Table and Centrifuge test	1D Site response analysis	Seismic loading	Ramberg&Osgood
Wilson, 1998	Liquefiable Sand	Centrifuge	Dynamic p-y	Seismic loading	-
Brown et al., 2000	Sand	-	Dynamic p-y	Pile head-statnamic	Dynamic (frequency dependent)
Gerolymos, 2006	Sand	-	3D-Finite element analysis	Static	Initial stiffness
API, 2007	Sand-Clay	-	-	Pile head	Hyperbolic relation
Varun, 2010	Liqueafiable sand	-	3D-Finite element analysis	Cyclic loading	Bouc-Wen model
McGann et al., 2011	Liquefiable Sand	-	OpenSees (3D Finite element method)	Seismic acceleration loading	-
Yang et al., 2011	Dense Sand (non liquefied)	1g-Shake Table	Dynamic p-y	Model base (Harmonic)	Empirical (dynamic tests)
Sorensen, 2012	Sand	-	3D-Finite element analysis	Pile head	Initial stiffness
Choi et al., 2015	Sand	Centrifuge	OpenSees (finite element using the p-y)	Seismic displacement loading	Based on plasticity theory
Thieken et. al., 2015	Sand	-	Finite Element-OpenSees	Seismic acceleration loading	A new function is proposed
Lim and Jeong, 2018	Sand	1g-Shake Table	-	Model base (harmonic)	Hyperbolic model

3. METHODS for DYNAMIC SOIL-PILE-STRUCTURE INTERACTION ANALYSES

Pile foundations are the structural elements embedded in the ground to transmit the external loads to the surrounding soil. The pile movement under horizontal loading affects the soil behavior, and increasing soil displacements alter the pile behavior. The pile-soil system behavior is affected by each component, and the resulting phenomenon is called as soil-pile interaction problem. Depending on the use of the piles, the problem includes the superstructure, which becomes the soil-pile-structure interaction problem. This problem is even more complex when the external loading is earthquake excitation. Two approaches exist for soil-structure interaction analyses: Direct analysis and substructure analysis. The direct analysis includes the soil and structure systems in a single model, whereas the superstructure and foundation systems are modeled separately in the substructure approach. In general, the analysis of any foundation includes the following stages, according to Scott (1981):

1. To define the physical problem involving the size, nature, and magnitude of loading related to structure and soil.
2. Idealization of the physical problem: Since the physics of an engineering problem is too complex to handle, the whole system must be idealized to make the problem more manageable. In addition, soil and structure properties must be defined for foundation analysis. Therefore, the most important stage in idealization is to ignore some of the available data for both soil and structure.
3. To set the mathematical relations and define the boundary conditions.
4. To solve the idealized model and obtain the stresses and displacements: The analysis aims to design the structures based on the internal forces (axial and shear force, bending moment) and check the performance in terms of the displacements.
5. To compare the analysis with the full-scale tests in the field or scaled model test results in the lab.

This study focuses on the single pile behavior under earthquake excitation. The analysis of a soil-pile-structure system can be performed with several approaches. These are: (1) Fully nonlinear dynamic analysis in three-dimension (3D), (2) Fully nonlinear dynamic analysis with the beam on nonlinear Winkler foundation (BNWF) method, and (3) Nonlinear static (pushover) analysis with BNWF approach. The most commonly used methods are 3-dimensional (3D) finite element or finite difference methods. The 3D analysis is the most versatile idealization of the real (physical) problem. In this method, the soil domain is discretized with finite volumes. The piles are usually modeled with the beam element. However, analyzing the soil-pile-structure system together (direct approach in soil-structure interaction analysis) in 3D models is highly time-consuming, especially for complex structures. The second approach is the beam on nonlinear Winkler foundation (BNWF) method, where the continuum of the soil domain is disregarded, and nonlinear springs are used to simulate the soil behavior. The later approach takes more attention due to its simplicity. However, the springs used in the BNWF method must represent the true nonlinear behavior of soil. This study aims to enhance the nonlinear load-displacement relations using the 3-dimensional analysis results so that the relations can be used in the BNWF method to better estimate the pile and structure response. Detailed explanations about these methods are given in this chapter.

3.1 Fully Nonlinear 3-Dimensional (3D) Analysis

The physical problem of a single pile-soil-structure system subjected to earthquake excitation is idealized, as shown in Figure 3.1a. The numerical model of the problem includes the beam elements for the pile and structure system. The linear material behavior is often adopted for the structural elements in soil-pile-structure interaction analyses. However, soils exhibit highly nonlinear behavior even under low strains, and the main uncertainty in the analyses arises from the modeling approach taking this nonlinearity into account. The 3D method discretizes the soil domain (Figure 3.1b). In the numerical model, finer elements are used in the vicinity of the pile, whereas the coarser mesh can be employed near the boundaries. The dynamic input motion is defined at the bottom boundary of the model. Since the major component of the earthquake is in the horizontal direction, the lateral boundaries should allow for absorption of the lateral movement to prevent the waves from reflecting into the model.

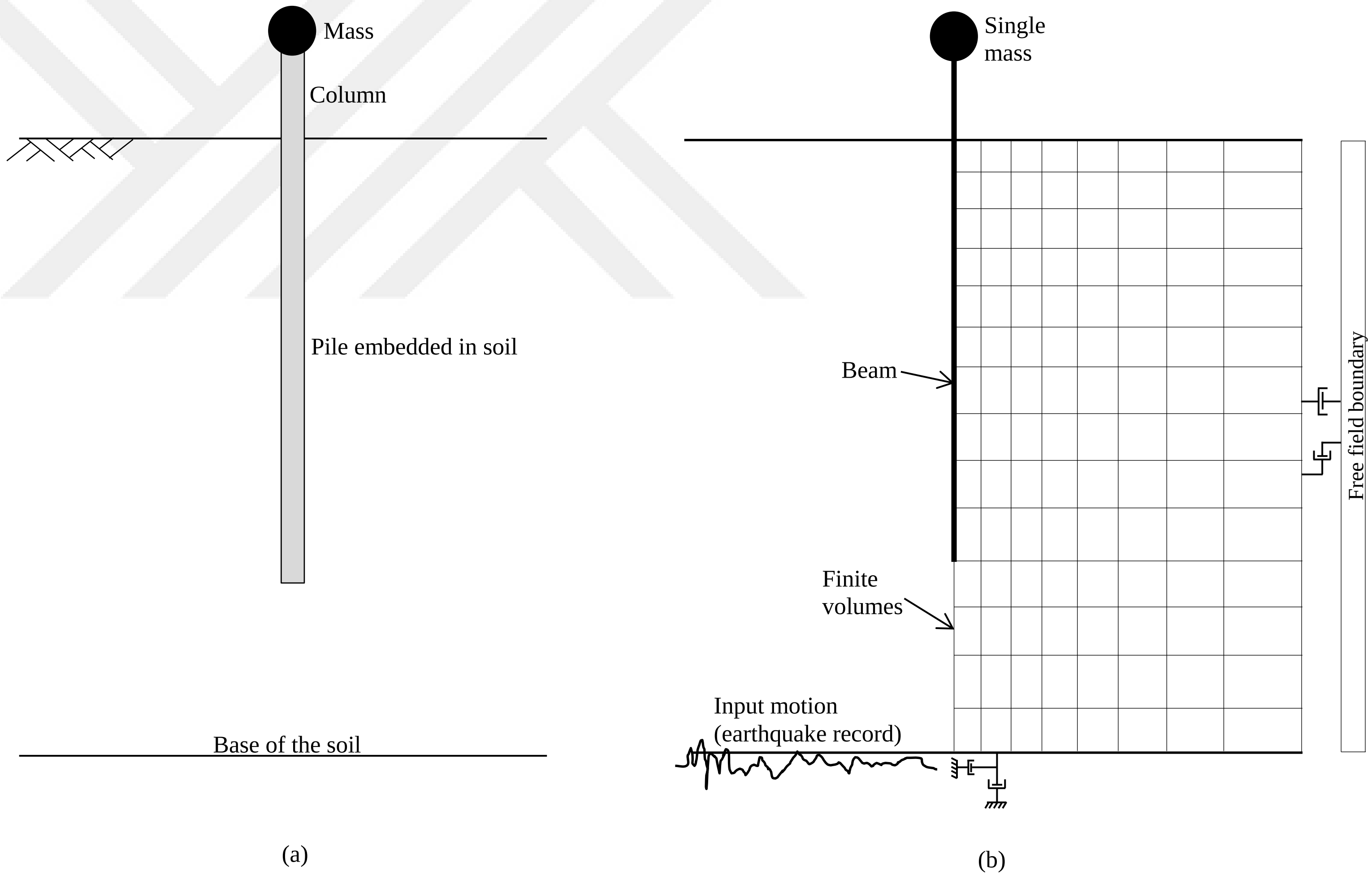

Figure 3.1 : The soil-pile-structure interaction problem: (a) Idealization of the problem, (b) Mathematical model with the boundary conditions.

3.1.1 Numerical model

In this study, the three-dimensional (3D) analyses were performed in FLAC3D, a numerical analysis program that solves the dynamic equation of motion using the finite difference method. The procedure to create a numerical model in the program includes the generation of the model geometry (grid generation), defining the initial and boundary conditions, assigning the constitutive material model to the elements, applying the input motion, and finally, analyzing the model. These steps of numerical model generation are explained below.

The first step in the numerical model generation is to create the model geometry using suitable elements. Next, the structural elements can be modeled using the beam elements. Beams are two noded elements, and each node has three translational and three rotational degrees of freedom, as shown in Figure 3.2.

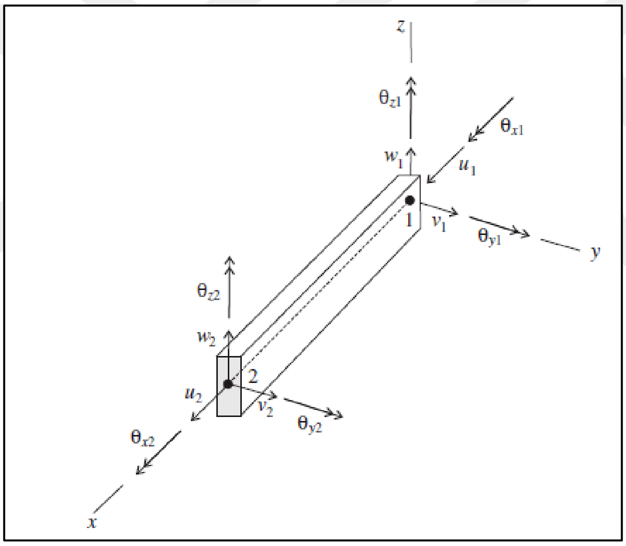

Figure 3.2 : Degrees of freedom of the beam elements in FLAC^{3D}.

The superstructure is modeled as a single-degree-of-freedom system (SDOF), which consists of a mass representing the structure connected to the soil utilizing a beam element representing the column of the SDOF system. The natural angular frequency of a single degree of freedom system is calculated using equation 3.1:

$$\omega = \sqrt{\frac{k}{m}} \tag{3.1}$$

where *m* is the structure's mass, and k is the stiffness of the single-column model.

The stiffness of a column is calculated by equation 3.2 if the bottom end is fixed and the top end is free:

$$k = \frac{3EI}{h^3} \tag{3.2}$$

where the *EI* is the flexural rigidity of the column and *h* is the column height.

The soil domain in 3D analyses is created using the volume elements. The grid generation in FLAC^{3D} is similar to the mesh generation in the finite element method. Several elements are available in FLAC^{3D} for 3D solids. The most commonly used ones are brick, cylinder, and radial cylinder elements, which create the soil domain and the piles with circular cross-sections. The gridpoints (or nodal points in finite element terminology) for these elements are shown in Figure 3.3.

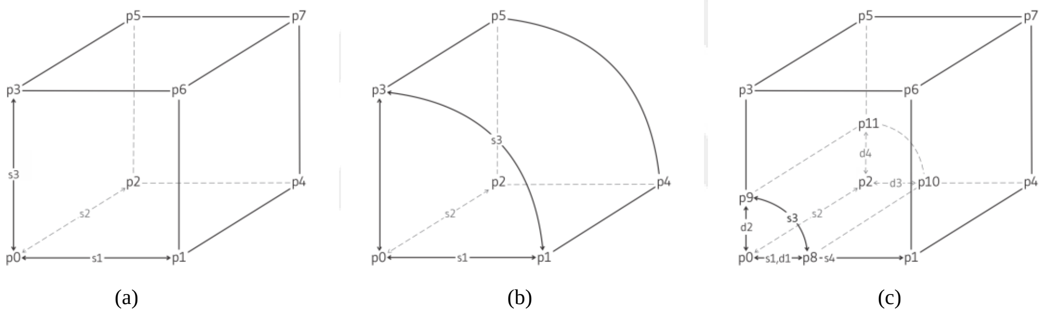

Figure 3.3 : Solid elements used in FLAC^{3D}: (a) Brick, (b) Cylinder, (c) Radial cylinder.

The grid of the soil domain can be generated using the brick, cylinder, and radial cylinder elements for solid pile-soil interaction analyses. However, the size of these volume elements might affect the solution of the analysis. Therefore, finer grids allow higher sensitivity in the analysis, making the resulting solution more precise. Especially the high-stress regions must be modeled with finer zones to capture the response better. However, the solution time is higher as the number of elements used in the model increase.

The pile-soil interaction problem consists of a cylinder (pile) and radially graded mesh (soil domain). The vicinity of the cylinder must be modeled with a finer grid than the soil domain since the stresses around the pile are higher. The zone size near the lateral boundaries could be increased to obtain an effective solution. The change of zone size of consecutive elements is controlled with the zone aspect ratio command. The accuracy of the analysis is better as the zone aspect ratio is close to unity. However, different zone sizes are inevitably used in pile-soil interaction problems. The change of zone size should be as gradual as possible for a better solution. Usually, a sensitivity analysis is required to determine the number of elements used in the numerical model.

The wave transmission criteria determine the zone sizes in a model subjected to dynamic loading. The seismic excitation is applied to 3D models at the bottom boundary. The created grid must be fine enough to allow wave propagation through the soil domain accurately. According to Kuhlemeyer and Lysmer (1973), the minimum zone size in the direction of wave propagation should be equal to or less than one-tenth to one-eighth of the wavelength:

$$\Delta l = \frac{\lambda}{10} \tag{3.3}$$

The wavelength in equation 3.3 is calculated using the shear wave velocity of the soil and the highest frequency component of the input motion as follows:

$$\lambda = \frac{V_s}{f_{max}} \tag{3.4}$$

Equation 3.4 shows that as the soil modulus decreases or the frequency of the input motion increases, the associated wavelength will be smaller, thus the zone size. Therefore, finer zone sizes are required near the ground surface since the soil modulus is not significant under the low confining pressure.

3.1.2 Soil constitutive model

The soil-pile interaction analyses are carried out in this study to determine the relationship between pile displacements and soil resistance. The forces are related to the stresses in the discretized domain through the equation of motion by equilibrium. Compatibility provides the relation between the strains and displacements. The equilibrium and compatibility relations depend on the geometry of the problem, independent of the material's mechanical behavior. The mechanical behavior of a material is defined by the stress-strain relation, which is achieved thorough the constitutive models. Therefore, the second stage in generating a numerical model is to select a proper constitutive model for soil behavior. The schematic view of the equations of a boundary value problem is shown in Figure 3.4, according to Puzrin (2012)

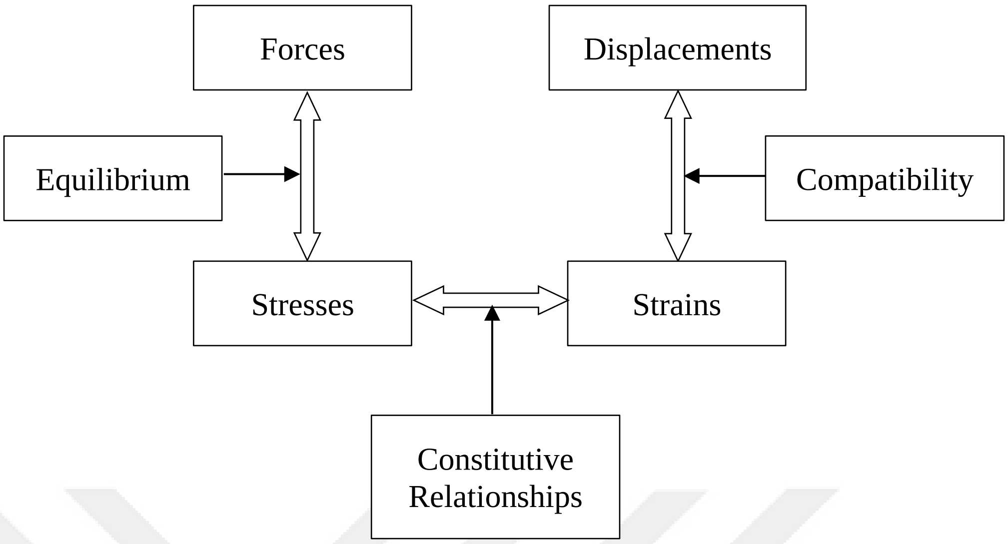

Figure 3.4 : The relations in the boundary value problem (Puzrin, 2012).

3.1.2.1 Hardin & Drnevich model

Shear stress-strain relation is defined in the following form according to Hardin and Drnevich (1972):

$$\tau = \frac{G_{max}\gamma}{1 + \frac{\gamma}{\gamma_{ref}}} \tag{3.5}$$

Hardin and Drnevich (1972) model requires the initial soil modulus for small-strain behavior. Several suggestions or correlations are available for the initial shear modulus in the literature (Hardin & Black, 1966; Iyisan, 1996; Wair et al., 2012). In this study, the small strain shear moduli, G_{max} equation suggested by Seed and Idriss (1970) was employed, which depends on the relative density of sand and the confining pressure:

$$G_{max} = 21.7\ (K_2)_{max}\ p_a \left(\frac{\sigma'_m}{p_a}\right)^{0.5} \tag{3.6}$$

where $(K_2)_{max}$ is a modulus parameter that depends on the relative density of sand, p_a is atmospheric pressure, σ'_m is the mean effective stress.

The effective confining pressure can be calculated using equation 3.7.

$$\sigma'_m = \frac{\sigma'_v + 2\sigma'_h}{3} \tag{3.7}$$

In the above equation, σ'_h is the horizontal effective stress, calculated by multiplying the vertical effective stress, σ'_v, with the lateral earth pressure coefficient, K_o. Seed and Idriss (1970) suggested the following equation to express the $(K_2)_{max}$ as a function of relative density D_r:

$$(K_2)_{max} = 3.5\ (D_R)^{2/3} \tag{3.8}$$

where D_r is the relative density.

The nonlinear behavior of soil is represented by equation 3.5, which is based on the hyperbolic model of Kondner (1963). The relation is linear for very small strain levels ($\gamma \leq 10^{-5}$ %). The shear stress-strain relation of cohesionless soils includes the initial modulus for the very small strain stages of loading and the modulus at large strain. The initial shear modulus can be calculated using equation 3.6. The nonlinear behavior is considered with the normalized modulus reduction (or degradation) curves. The reduction of initial shear modulus with increasing shear strain is formulized as follows:

$$\frac{G}{G_{max}} = \frac{1}{1 + \gamma_{ref}} \tag{3.9}$$

Many researchers have studied the nonlinear behavior of cohesionless soils under cyclic loads, and reduction curves have been suggested (Darendeli, 2001; Ishibashi & Zhang, 1993; Seed & Idriss, 1970). The curves suggested by Seed and Idriss (1970) have been implemented by several researchers (Boulanger et al., 1999; Finn, 2005; Kwon & Yoo, 2020; Thavaraj et al., 2010). In this study, effective stress-dependent curves of Darendeli (2001) were employed to consider the variation with depth better. The shear modulus reduction equation in Darendeli (2001) is given in equation 3.10.

$$\frac{G}{G_{max}} = \frac{1}{1 + \left(\frac{\gamma}{\gamma_{ref}}\right)^{0.919}} \tag{3.10}$$

The reference strain in equation 3.10 depends on the effective confining stress. Darendeli (2001) formulized the reference strain of cohesionless soils depending on the confining stress as:

$$\gamma_r = 0.0352 \left[\frac{\sigma'_m}{p_a}\right]^{0.3483} \tag{3.11}$$

Equation 3.11 yields the modulus reduction curves for various confining stress levels. Figure 3.5 shows the curves for 10 kPa, 25 kPa, and 100 kPa levels. These modulus reduction curves allow the model to consider the nonlinear soil behavior, but the ultimate strength is not defined explicitly.

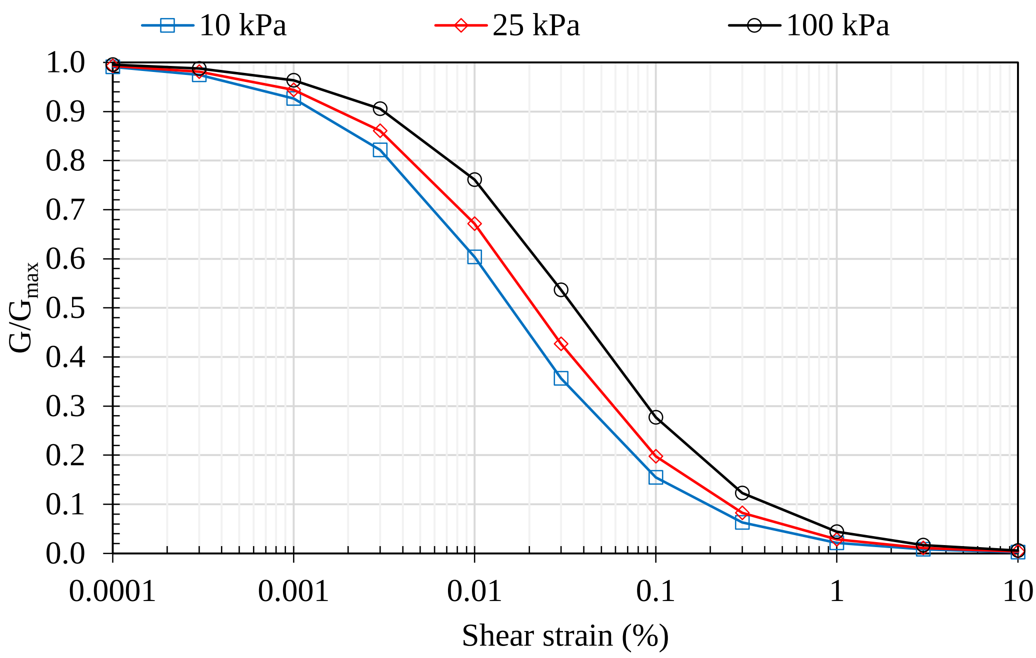

Figure 3.5 : Modulus reduction curves of Darendeli (2001).

The initial modulus and the modulus reduction curves define the soil behavior under monotonic loading. However, the model should include the unloading/reloading rule for time-dependent dynamic (cyclic or transient) loading. Figure 3.6 depicts the soil behavior in the hyperbolic model for the initial loading-unloading-reloading cycle. The Masing (1926) rule is implemented for the unloading/reloading behavior, which assumes that the subsequent unloading/reloading behavior is enlarged by a factor of 2, as shown in Figure 3.6.

$$\frac{\tau - \tau_a}{2} = f\left(\frac{\gamma - \gamma_a}{2}\right) \tag{3.12}$$

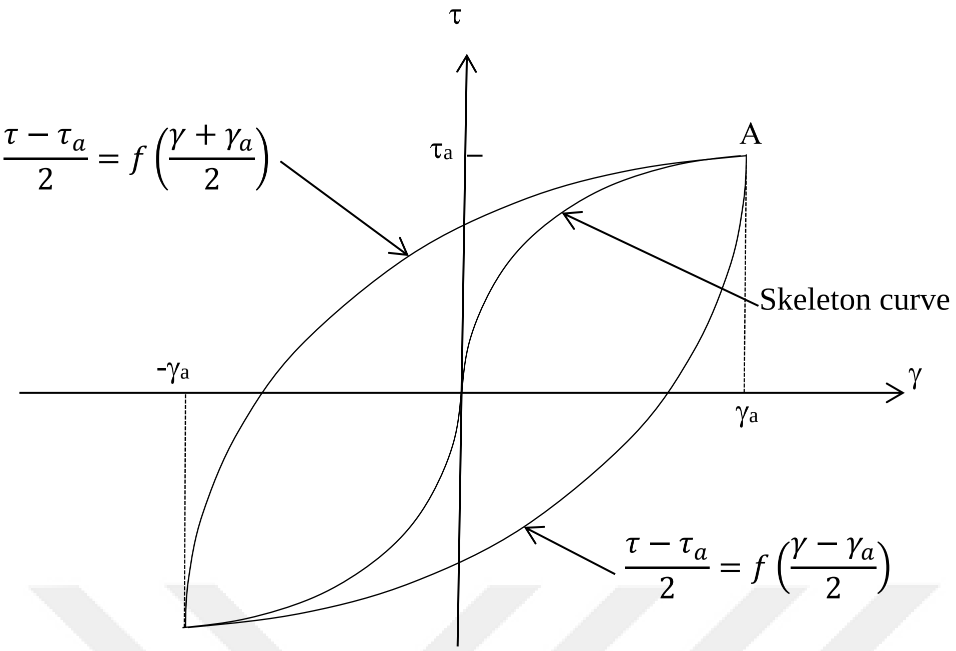

Figure 3.6 : Shear stress-strain relation with unloading/reloading rule according to Masing (1926).

The definition of hysteretic damping is the ratio of the energy dissipated in one cycle to the maximum stored energy. The damping ratio for the stress-strain loops shown in Figure 2.6 can be calculated using equation 3.13 in the hyperbolic model.

$$D_{\text{masing}} = \frac{2}{\pi}\left\{2\frac{1+\frac{\gamma_c}{\gamma_{ref}}}{\left(\frac{\gamma_c}{\gamma_{ref}}\right)^2}\left[\frac{\gamma_c}{\gamma_{ref}} - \ln(1+\frac{\gamma_c}{\gamma_{ref}})\right] - 1\right\} \tag{3.13}$$

The hysteretic damping command in FLAC^{3D} was utilized for the soil domain in the model. The reference strain values were assigned to each zone by considering the initial effective stress (total stress approach). However, the maximum shear strain was on the order of 0.1%-0.3% in the study performed by Darendeli (2001), which could not involve the large strain (>1%) behavior. In comparison, the study of Seed and Idriss (1970) showed that the G/G_{max} value for modulus degradation curves at 3% shear strain varies between 0.03 and 0.05. Therefore, a cut-off for G/G_{max} is required to represent the large strain behavior in the modulus degradation accurately. Since the experimental study presented by Darendeli (2001) does not include the large strain data (≥1%), 0.05 was assumed for minimum G/G_{max} considering the Seed and Idriss (1970) curves. Thus, a minimum cut-off value of 0.05 was applied in this thesis for the modulus reduction ratio to prevent further increase of damping beyond a certain shear strain.

3.1.2.2 Mohr-Coulomb model with hysteretic damping

The most commonly used constitutive relationship in soil mechanics is the Mohr-Coulomb, and the yield function in the model is defined as:

$$\tau_f = c + \sigma_n \phi \tag{3.14}$$

In plasticity theory, the total strain is decomposed into elastic and plastic components ($\varepsilon=\varepsilon^e+\varepsilon^p$). Therefore, the initial state of the numerical model must be in elastic equilibrium. The soil element is subjected to the stress increment, and the resulting strains are evaluated assuming the elastic behavior. Once the stress reaches the ultimate value in the stress space according to the yield criteria, the deformations are no longer elastic, and irreversible (plastic) deformations occur. The stresses cause reversible strains at the elastic region, but further stress increments cause plastic deformations. The flow rule controls the stress increment due to the plastic strain, and it is defined in Mohr-Coulomb as:

$$f_s = -\sigma_1 + \sigma_3 N_\phi - 2c\sqrt{N_\phi} \tag{3.15}$$

where N_ϕ is given:

$$N_\phi = \frac{1 + sin\phi}{1 - sin\phi} \tag{3.16}$$

If the stress state yields f_s=0 condition, the material is subjected to plastic deformations. The yield envelope of the Mohr-Coulomb model is shown in Figure 3.7 in 3-dimensional stress space.

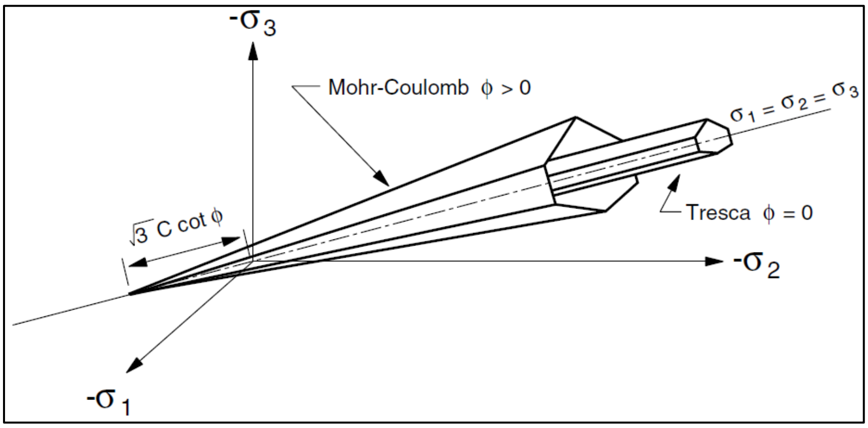

Figure 3.7 : Mohr-Coulomb model in 3-dimensional stress space.

In the theory of plasticity, the strain is decomposed into elastic and plastic parts, as in equation 3.17:

$$d\varepsilon = d\varepsilon^e + d\varepsilon^p \tag{3.17}$$

The stress-stain equation is written as:

$$d\sigma = (d\varepsilon - d\varepsilon^p) \tag{3.18}$$

The plastic part of the strain is defined as:

$$d\varepsilon^p = d\lambda \frac{\partial g}{\partial \sigma} \tag{3.19}$$

where $d\lambda$ is a constant and g is the potential function. A constitutive model is associated if the potential function is equal to the flow rule (f=g case). Otherwise, the model is nonassociated for $f \neq g$. The Mohr-Coulomb model in FLAC^{3D} is nonassociated since the potential function is described as:

$$g_s = -\sigma_1 + \sigma_3 N_\psi \tag{3.20}$$

where ψ is, the dilation angle and N_ψ is defined as:

$$N_\psi = \frac{1 + sin\psi}{1 - sin\psi} \tag{3.21}$$

In the classical theory of Mohr-Coulomb, the model is elastic-perfectly plastic, in which the behavior is linear in the elastic stage. However, the Mohr-Coulomb model in FLAC^{3D} allows us to consider the nonlinearity in the small strain levels by including the hysteretic damping approach. Therefore, the model is called Mohr-Coulomb with the hysteretic damping approach. Furthermore, the model is an extension of the hyperbolic model of Hardin & Drnevich, which does not include a certain failure criterion.

The nonlinear behavior of soil is considered through the modulus degradation curves in the Hardin&Drnevich model, and the ultimate strength is not defined explicitly. The Mohr-Coulomb model with the hysteretic damping approach overcomes the mentioned problem. The reference strain concept defines the nonlinear soil behavior, and the yield function limits the ultimate stress that can be sustained.

3.1.2.3 HS-Small model

In this study, the HS-Small model was used for soil behavior in the static analysis of the soil-pile interaction problem, developed by Benz (2007), and verified using the laboratory test results and a case study. The HS-Small model includes the original features of the plastic hardening (PH) model, which can simulate shear and volumetric hardening. The PH model was introduced by Schanz et al. (2019) within the framework of hardening plasticity extending the original non-linear elastic model of Duncan and Chang (1970). Benz (2007) developed the original model to account for the very small strain stiffness. The original hyperbolic stress-strain relation in the Hardening model is shown in Figure 3.8. The HS-Small model adopts the failure hypothesis of Matsuoka&Nakai and Drucker-Prager's potential function for flow rule (Figure 3.9). The input parameters for the model include the friction angle (ϕ) and the dilation angle (ψ). The ratio of q_f/q_a is defined as R_f in the model and can generally be taken as 0.9 for cohesionless soils.

The soil nonlinearity in the HS-Small model is achieved using the stiffness parameters; E_0, E_{ur}, and E_{50}, for very small strain stiffness, unloading-reloading stiffness, and secant stiffness corresponding to 50% of the ultimate strength, respectively. The strain-dependent behavior shown in Figure 3.8 can be constructed in q-ε space by equation 3.22 using E_{50}.

$$\varepsilon_i = \frac{q_a q}{E_{50}(q_a - q)} \tag{3.22}$$

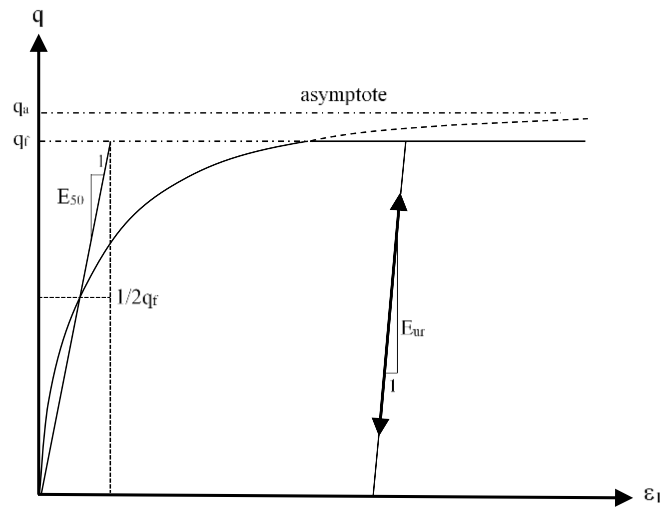

Figure 3.8 : Hyperbolic stress-strain curve in q-ε space in HS-Small model.

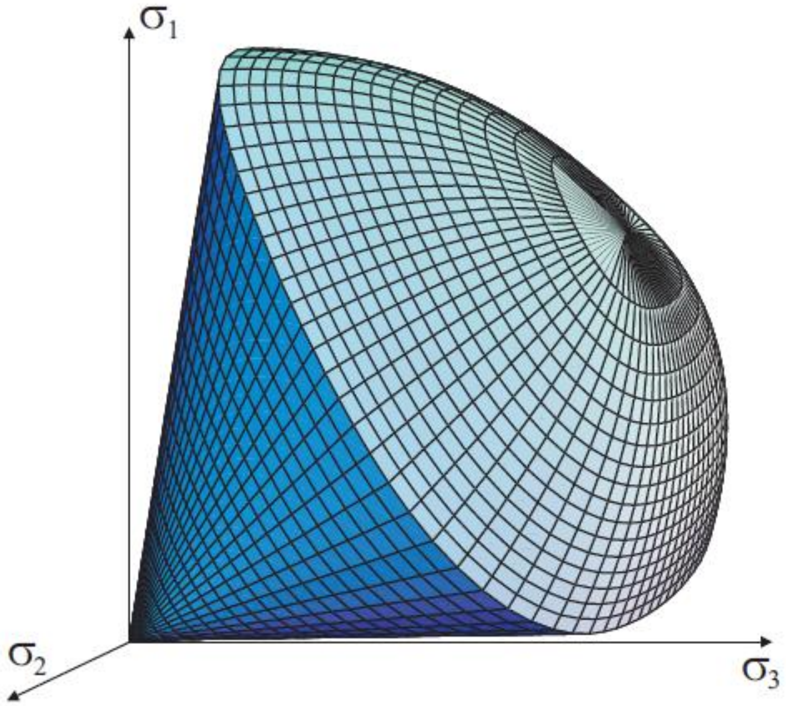

Figure 3.9 : Yield surfaces of Matsuoka&Nakai in 3D stress space (Benz, 2007).

Another essential feature of the HS-Small model is that it allows the stress-dependent soil moduli with the power law. Once the initial stress state is created, the soil stiffness is obtained by equation 3.23.

$$E_{50} = E_{50}^{ref}\left(\frac{c\ cot\phi - \sigma_3}{c\ cot\phi + p_{ref}}\right)^m \tag{3.23}$$

The stress dependency "m" power is generally 0.5-0.7 for cohesionless soils. The parameter E_{50} can be either determined by a triaxial compression test in the laboratory or, in the lack of a laboratory test, it can be estimated by selecting a proper ratio for the E_{ur}/E_{50} depending on the degree of nonlinearity. Compared to the plastic hardening model, the HS-Small includes two additional parameters: Small-strain modulus E_0 and reference strain $\gamma_{0.7}$. In this study, the small strain stiffness (E_0) was calculated using the maximum shear modulus equation suggested by Seed and Idriss (1970).

The rough estimation for unloading/reloading stiffness is 1/3 of E_0, while the E_{50} is about 1/3 to 1/4 of E_{ur}. E_0 can be estimated using the maximum shear modulus according to equation 3.24.

$$E_0 = G_{max}\, 2\,(1 + v) \tag{3.24}$$

$\gamma_{0.7}$ is the reference strain, which can be written as:

$$\gamma_{0.7} = (1 - 0.722)\frac{\tau_f}{G_0} \tag{3.25}$$

where τ_f is the shear strength, and G_0 is the small-strain shear modulus. The stiffness reduction curve is obtained using the reference strain HS-Small model. Figure 3.10 shows a typical stiffness degradation curve and various strain levels for the geotechnical structures.

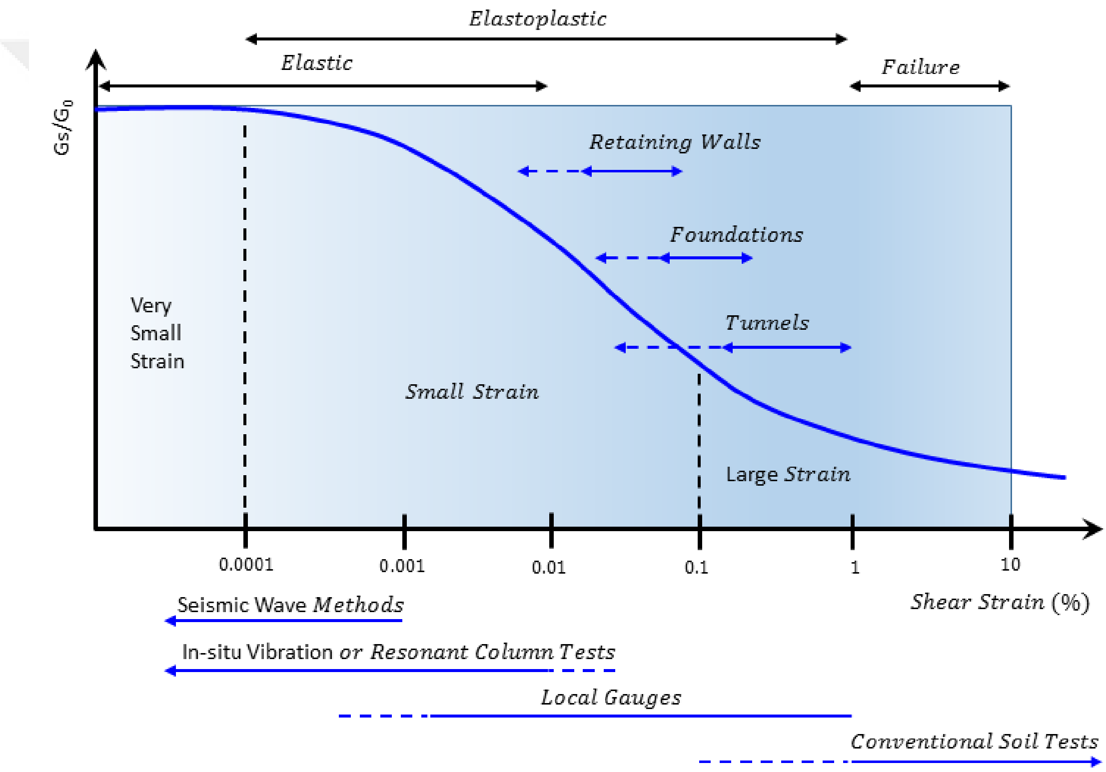

Figure 3.10 : Stiffness modulus degradation curve and typical strain ranges (Modified from Atkinson and Sallfors 1991 and Ishihara 1996).

3.1.3 Initial and boundary conditions

The mathematical model of the soil-pile-structure interaction problem is defined with differential equations. The finite volumes discretize the domain, and the stress-strain behavior is assigned to the materials in the model. The solution of the differential equations requires the definition of boundary conditions.

A numerical model of a geotechnical engineering problem must include a stage to create the initial stress state for the geostatic conditions. First, the model must be in equilibrium statically under vertical and horizontal stresses. Next, the initial stress state should be created since the constitutive model includes stress-dependent soil properties. Finally, the bottom and the lateral boundaries should be fully fixed in this stage. The fixity condition is provided by predefining the velocities (or displacements) in the gridpoints at the boundaries. After the boundary conditions are defined for the initial stage, the model is solved to create the initial stress conditions.

Seismic soil-structure interaction problems include the dynamic input motion mostly applied at the bottom boundary. However, the fixed boundaries do not allow the dynamic waves to travel outwards, and reflection takes place. Therefore, viscous boundaries should be used in the boundaries to absorb the waves. The viscous boundaries developed by Lysmer and Kuhlemeyer (1969) are employed in FLAC^{3D}. The lateral boundaries of the model should also prevent wave reflection. The free-field option in the program absorbs the energy through the sides of the model to accurately represent the wave propagation. The viscous dashpots are placed between the main grid and the free-field boundaries to simulate the quiet boundary condition.

3.1.4 Selection of input motion

The input motions of the seismic soil-structure interaction analysis are the real earthquake records. In addition, the databases provide the acceleration time histories of the earthquake records. After initializing the model with the geostatic conditions, the dynamic input motion can be applied to the model's base. When the bottom boundary is fixed, the acceleration (or velocity) records can be directly applied as a prescribed displacement to the model. The incoming earthquake motion vertically propagates through the bedrock and reaches the surface, and the acceleration time histories are usually recorded at the rock outcrop. According to the site response analysis theory, the amplitude of the earthquake motion recorded on the rock outcrop is double the incoming motion, as shown in Figure 3.11 (Bardet et al., 2000). However, the recorded outcrop motion differs from the motion at the top of the rock. Therefore, the outcrop record should not be directly applied to the base of the 3D numerical models.

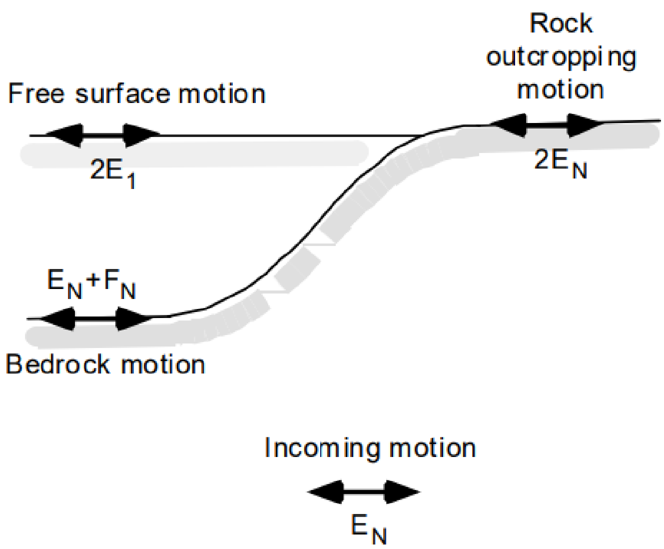

Figure 3.11 : Terminology for the motions in seismic site response analysis.

The stiffness contrast between the bedrock and overlying soil affects the motion at the bottom of the soil profile. Suppose the stiffness of the soil just above the bedrock is significantly lower than the bedrock stiffness. In that case, the incoming motion is doubled in amplitude at the top of the rock (bedrock motion) and becomes similar to the rock outcrop motion. Therefore, the rock outcropping motion can only be used directly on the top of the rock if there is a high stiffness contrast between the soil and the bedrock. If the bottom of the soil profile includes a layer at which the shear wave velocity is close to the bedrock, then the bedrock motion becomes very similar to the incoming motion.

A simple hypothetical problem is introduced in Figure 3.12 to compare input motions. Figure 3.12a shows a high stiffness contrast between the bedrock and the soil layer, whereas the contrast is low in Figure 3.12b.

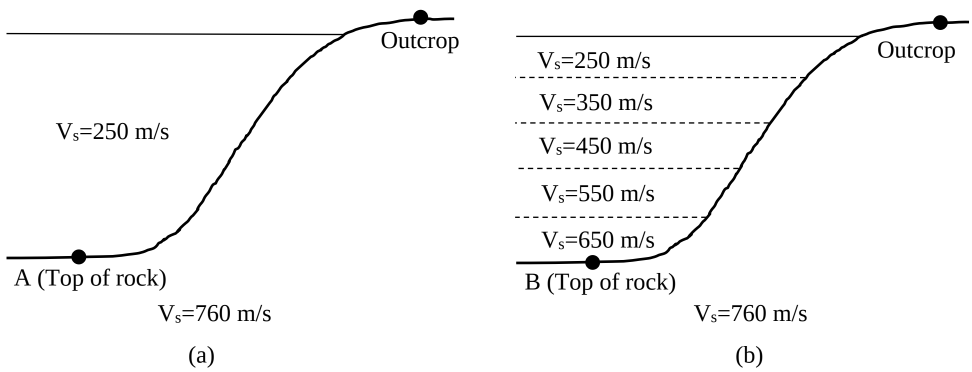

Figure 3.12 : Hypothetical example for the input motion: (a) High stiffness contrast, (b) Low stiffness contrast between the bedrock and the soil.

Two site response analyses were performed in Deepsoil to compare the top of rock motions. The target motion is the record of the Kocaeli earthquake (Figure 3.13). The shear wave velocity of the elastic halfspace is 760 m/s.

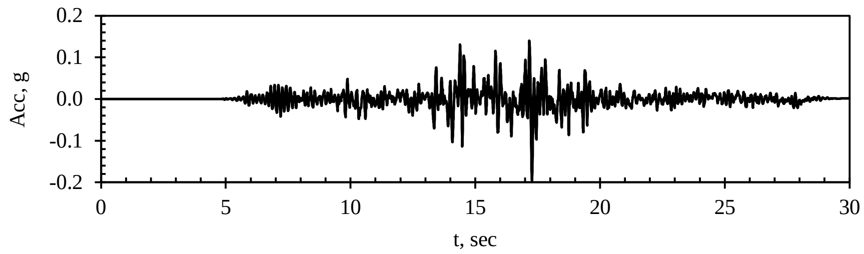

Figure 3.13 : The Kocaeli earthquake record in Deepsoil.

The input motion in Figure 3.13 is applied as outcrop motion, and the results at the top of the rock are compared with the input motion (Figure 3.14). The top of rock motion in the first profile (A) is very similar to the input (outcrop) motion. However, in the second profile, the top of rock motion (B) is approximately ½ of the input motion.

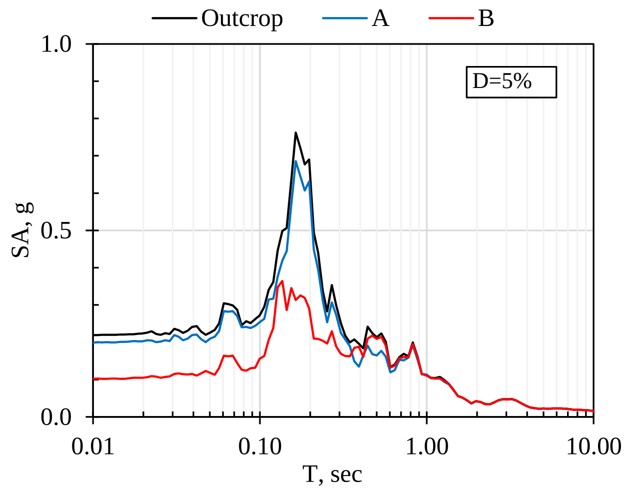

Figure 3.14 : Comparison of the top of rock motions in the hypothetical problem.

The above example concludes that two approaches can be followed to determine the motion used in 3D models. The first method is to create a 1D model and obtain the top of rock motion in the profile using the rock outcropping motion. The second approach is to extend the 3D model and define a bedrock layer beneath the soil profile to apply the incoming motion, which is ½ of the rock outcropping motion, to the bedrock base.

3.2 Beam on Nonlinear Winkler Foundation (BNWF) Method

The soil-pile-structure interaction problem is mostly analyzed using the beam on nonlinear Winkler foundation (BNWF) method. In this method, the nonlinear soil behavior is represented by the springs attached to the pile at the specified depths. The lateral load-deflection relation represents the near-field behavior of the soil-pile interface. Fully dynamic (seismic) soil-pile-structure interaction analysis can be performed using the BNWF method in two steps. In the first step, the free-field site response analysis is performed to obtain the soil displacement-time histories at the selected depths. Then, a fully nonlinear analysis is performed by applying the soil displacements to the springs. The fully dynamic analysis method of BNWF for the soil-pile-structure interaction problem is summarized in Figure 3.15.

3.2.1 Site response analysis

The first step of the BNWF approach for dynamic soil-pile-structure interaction analysis is to determine the free-field soil displacement-time histories by site response analysis. In this first step, the nonlinear soil response analysis is performed either by equivalent linear or fully nonlinear analysis methods. Shear modulus reduction and damping curves are implemented in the equivalent linear method; however, the approach is unsuitable for seismic events resulting in large shear strains (for γ>0.2 %). Frequency domain analysis is preferred for equivalent linear analysis since the method is linear, and the nonlinearity is considered via an iterative approach. However, fully nonlinear analysis is required in the time domain to capture the true nonlinear soil behavior at large strains accurately. The main uncertainty in the nonlinear analysis is the soil model, which should properly consider the loading-unloading-reloading behavior.

Hardin&Drnevich model can be used in the fully nonlinear analysis with the Masing rule for unloading/reloading behavior. However, as shown in Section 3.1.2, the main drawback of this model is the high damping ratio at large strains. Many researchers have investigated the high damping problem, and several suggestions are proposed to improve the model's performance. In this study, the method proposed by Groholski et al. (2016) was used in 1D site response analysis, which was implemented in Deepsoil.

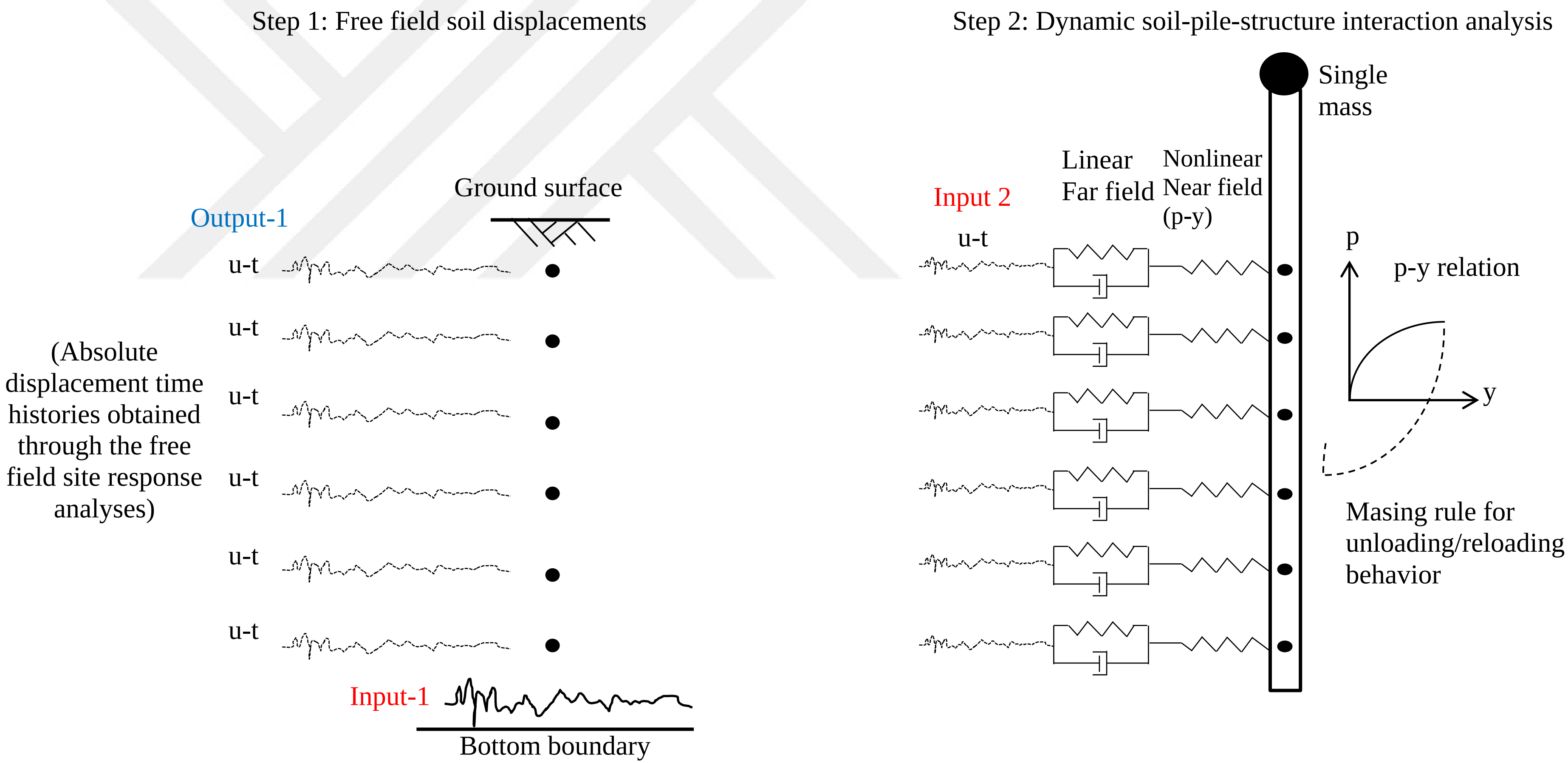

Figure 3.15 : Dynamic analysis with BNWF method: (a) Site response analysis, (b) Dynamic analysis.

3.2.2 Fully dynamic analysis of the soil-pile-structure system

In the second step of the dynamic BNWF method, the numerical model of the soil-pile-structure system is created. The beam and the structure are modeled using the beam elements, and the soil reaction to the lateral load is represented by nonlinear springs. The nonlinear spring can reproduce the hysteretic damping through the unloading/reloading rule. The system should include a dashpot to simulate the radiation damping in the fully dynamic time-history analysis.

The effect of several arrangements of the spring-dashpot systems on the soil-pile-structure interaction analysis has been investigated by Nogami et al. (1992) and Wang et al. (1998). They concluded that the near-field element could represent the hysteretic behavior, and the linear far-field element should be placed in series to simulate the radiation damping. A similar approach was followed in this study. The far-field element represents the radiation damping with the dashpot coefficient suggested by Gazetas and Dobry (1984), which is given in equation 3.26.

$$\frac{c_r}{4r\rho_s V_s} = \left\{1 + \left[\frac{3.4}{\pi(1-\upsilon)}\right]^{5/4}\right\} {a_0}^{-1/4} \tag{3.26}$$

where V_s is the shear wave velocity, r is the radius of the pile, and a_0 is the dimensionless frequency factor=2π.f.r/V_s where the parameter f can be taken as the dominant frequency of the earthquake record. The spring stiffness of the linear far-field element can be estimated from the initial section of the p-y curve, according to Wang et al. (1998). However, in this study, a very high stiffness value was assigned to minimize the increase of flexibility due to the arrangement of the spring-dashpot system, placed in series with the near-field element.

The p-y curves represent the nonlinear behavior in the near-field element. In the time-domain analysis, hysteretic damping is considered by the unloading/reloading rule. Therefore, the soil behavior in BNWF is simulated using the near-field and far-field elements, which should represent the soil behavior under lateral loading.

The BNWF model is analyzed by applying the displacement time histories obtained in the first step to the fixed end of the far-field elements, as shown in Figure 3.15. The Newmark method is used in the direct integration scheme for the time-domain analysis. In this approach, a direct analysis of the soil-pile-structure system can be performed.

3.2.3 Static nonlinear (pushover) analysis of the soil-pile-structure system

The soil-pile-structure system response under dynamic loading can be predicted by the static nonlinear (pushover) analysis. In this approach, the model is reduced to substructures to analyze the kinematic and inertial interaction separately. The superposition is conducted to obtain the overall system response.

The kinematic interaction analysis is performed to obtain the internal forces and pile displacements due to the soil displacement. Then, the maximum value of time histories of the free-field soil displacements is applied to the fixed end of the p-y curves. The maximum displacements are applied in a single step instead of using the dynamic time histories. The loading is static in this approach. However, nonlinear analysis is required as the soil springs (p-y curves) are not linear.

The inertial interaction analysis is conducted to simulate the behavior under the loading caused by the acceleration of the superstructure. First, however, the superstructure acceleration should be estimated to calculate the inertial load. The code-based spectrum, or the site-specific spectra, can predict the superstructure response based on the natural period. Then, the superstructure mass is multiplied by acceleration. Finally, the calculated load is applied to the piles in this approach. If the linear superstructure behavior is expected, the nonlinear p-y curves can be employed directly. The reduction coefficient (R) can be used to consider the nonlinear behavior of the superstructure. The response obtained by the linear analysis is reduced by applying the R parameter. However, only the initial stiffness of the p-y curves should be used in this case. The details of the method is given in Alver et al. (2021)

Since linear analyses are carried out in the static nonlinear (pushover) approach, the superposition technique can obtain the total internal forces and the displacements. Therefore, the method is suitable for small to moderate shaking intensities. This approach cannot determine the superstructure response, but it is predicted using code-based or site-specific spectra. Besides, the kinematic and inertial interaction analyses are carried out separately. The method is summarized in Figure 3.16. Although the method has some drawbacks, it is still employed by engineers in practice due to its simplicity. However, fully dynamic analysis (3.1.2) is required for systems subject to high nonlinearity under earthquake loading. In addition to the piles subject to dynamic loading, the method is widely used for onshore and offshore structures.

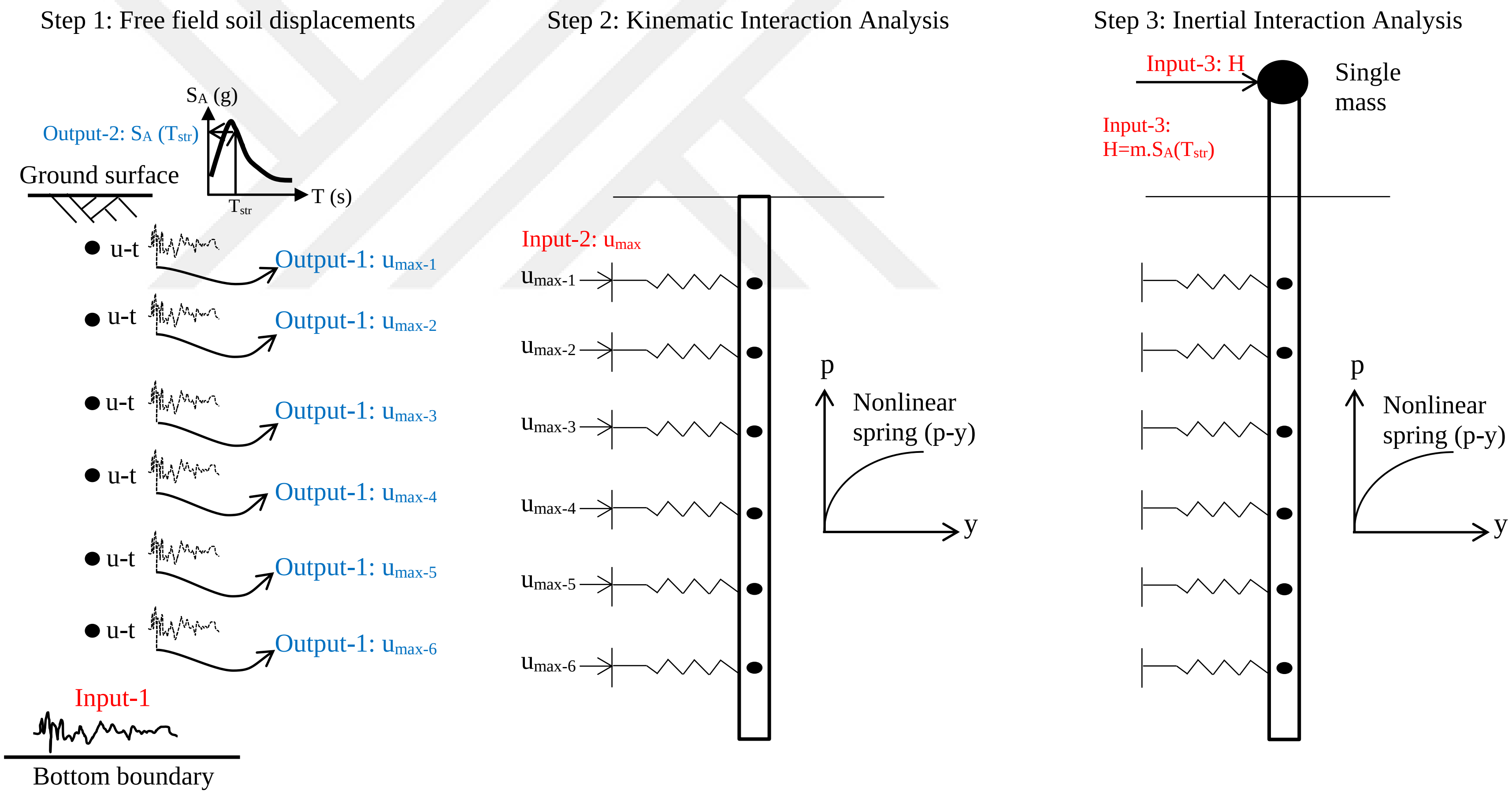

Figure 3.16 : Nonlinear static (pushover) analysis in BNWF method: (a) Site response analysis, (b) Kinematic interaction analysis, (c) Inertial interaction analysis

4. NUMERICAL MODELLING of LATERALLY LOADED PILE PROBLEM: STATIC PILE HEAD LOADING

Historically, the load-displacement behavior of piles embedded in soils has been predicted by the stress-strain relation (Bouzid et al., 2013; Lombardi et al., 2017; Scott, 1981; Terzaghi, 1955). Several researchers have suggested direct correlations (Bransby, 1999; Randolph & Houlsby, 1984; Zhang & Andersen, 2017) for piles in clays using the rigid disc analogy. However, the problem has not been clearly understood for piles in sands since the shear strength of sands is not constant but depends upon the effective confining stress, which increases with depth. The first suggestion for the *p-y* relation under static loads in sands was made by Terzaghi (1955). Based on the full-scale field test performed on Mustang Island (Cox et al., 1974), a piecewise non-linear relation was proposed by Reese et al. (1974). Murchison and O'Neill (1984) suggested a hyperbolic tangent function, and API (2007) adopted this form. Pender (1993) proposed an equation based on the finite element analysis results. Thieken et al. (2015) developed new equations for *p-y* curves in sands based on the finite element analysis results. The hyperbolic stress-strain curve of Kondner (1963) was implemented by Georgiadis et al. (1992) for p-y curves to capture the experimentally obtained p-y curves.

This thesis investigates the laterally loaded pile problem in $FLAC^{3D}$ numerically (Itasca Consulting Group, 2019) using the hardening model with small-strain stiffness (HS-Small Model). The parametric analyses were performed on the verified numerical model to show the effect of soil and pile properties on the static *p-y* curves. The selected parameters were the pile diameter and flexural stiffness, relative density of soil, and degree of soil nonlinearity. The modified hyperbolic model was proposed to characterize the p-y curves better. The proposed model includes the initial stiffness, the ultimate soil resistance, and two additional parameters for the degree of nonlinearity, the last of which allows the *p-y* curves to be efficient from very small to large displacement ranges.

4.1 Verification Analyses

The full-scale field test, carried out on Mustang Island in Texas-Austin, was selected to verify the model created in FLAC^{3D} (Itasca Consulting Group, 2019). The soil profile consists of a medium-dense sand layer from the ground surface down to 5 m depth, followed by a dense sand layer, as shown in Figure 4.1 (Dodds, 2005; Dodds & Martin, 2007).

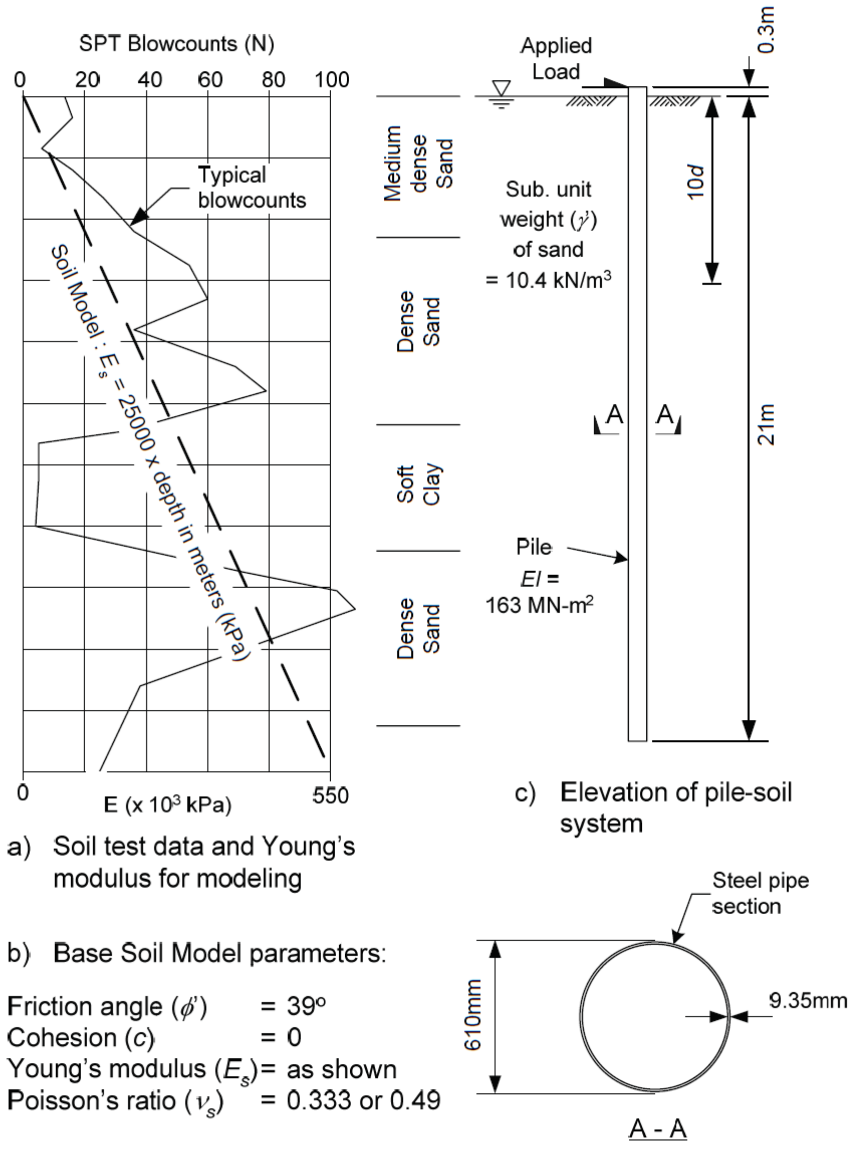

Figure 4.1 : Mustang Island Test details (Dodds & Martin, 2007).

The groundwater table was on the surface, and the submerged unit weight of the sand was 10.4 kN/m^3. The internal friction angle was determined as 39^o by Reese et al. (1974). A steel pipe pile having 61 cm diameter and 21 m length was tested in the field. The thickness of the pipe section was 9.35 mm, corresponding to the flexural stiffness of 163 MN.m^2.

The HS-Small model parameters selected for the verification problem are given in Table 4.1. The friction angle was taken as given (Reese et al., 1974), and the dilation angle was assumed zero, considering the existence of a medium-dense layer near the surface. Small-strain modulus was estimated by the elastic relation, $E_0=2G_0\,(1+v)$. The ratios E_0/E_{ur} and E_{ur}/E_{50} were anticipated as 2.5 and 4, respectively.

Table 4.1 : The selected soil parameters of the sand for Mustang Island in the HS-Small Model.

Parameter	Value	Parameter	Value
Friction angle, ϕ' (°)	39	$E_{0,ref}$ (MPa)	387
Dilation angle, ψ (°)	0	$E_{ur,\,ref}$ (MPa)	155
γ_{sat} (kN/m^3)	20.4	$E_{50,ref}=E_{oed,ref}$ (MPa)	39
Pressure reference (kPa)	100	m	0.5
R_f	0.9	Reference strain, $\gamma_{0.7}$ (%)	$(1-0.722)\dfrac{\tau_f}{G_0}$

The 3-dimensional geometry of the numerical model was created in FLAC^{3D} (Itasca Consulting Group, 2019). The pile geometry was generated with a cylinder, and radially graded brick elements were used for simulating the soil around the pile. The radial grid enables the finer elements to be placed near the pile, and gradually coarser mesh could be built as it approaches the model boundary. The model dimensions were 24 m x 12 m x 21 m, making the distance from the pile center to the model boundary 20 times the pile diameter (20*D*). The side and bottom boundaries were fixed in the normal and vertical directions. The created numerical model, including the pile, the soil, and the interface elements, is shown in Figure 4.2.

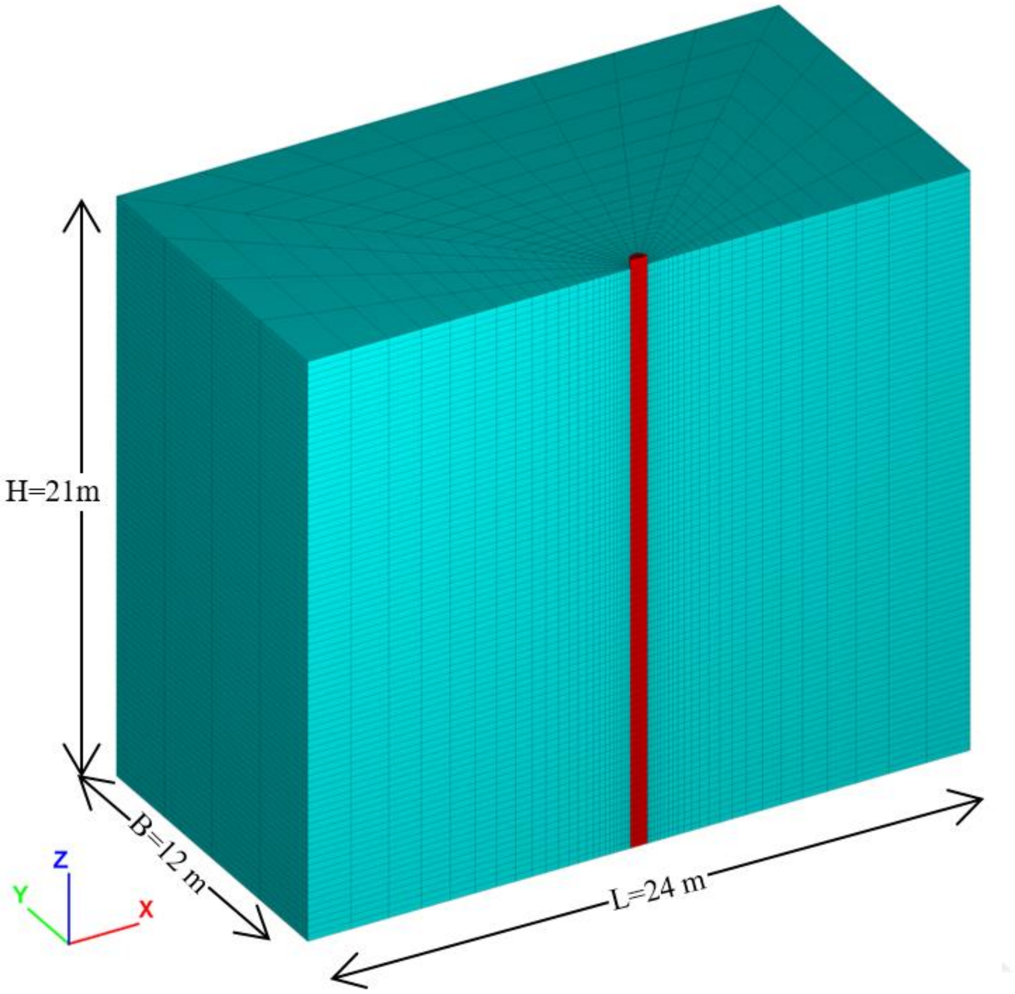

Figure 4.2 : The numerical model created for Mustang Island Field Test.

The numerical analyses aimed to derive load-displacement (*p-y*) curves. An interface was inserted between the cylindrical pile and the surrounding soil to obtain the stresses on the interface. The equivalent stiffness parameter in the normal and shear direction (k_n and k_s) for an interface is given in equation 4.1:

$$k_n = k_s = max\left[\frac{\left(K + \frac{4}{3}G\right)}{\Delta z_{min}}\right] \tag{4.1}$$

where K and G are the bulk and shear moduli, respectively, and Δz_{min} is the minimum width of the adjoining zone in the normal direction. The rule of thumb is to set the interface stiffness as ten times the equivalent stiffness according to the FLAC^{3D} Manual (Itasca Consulting Group, 2019). Therefore, sensitivity analyses were conducted with ten times the equivalent stiffness, equivalent stiffness, and 10 % of the equivalent stiffness. Figure 4.3 shows the effect of interface stiffness on the p-y curves.

The results revealed that the obtained p-y curves did not differ significantly. Consequently, the depth-dependent stiffness was assigned ten times the equivalent stiffness for the interface as the soil modulus increased with depth.

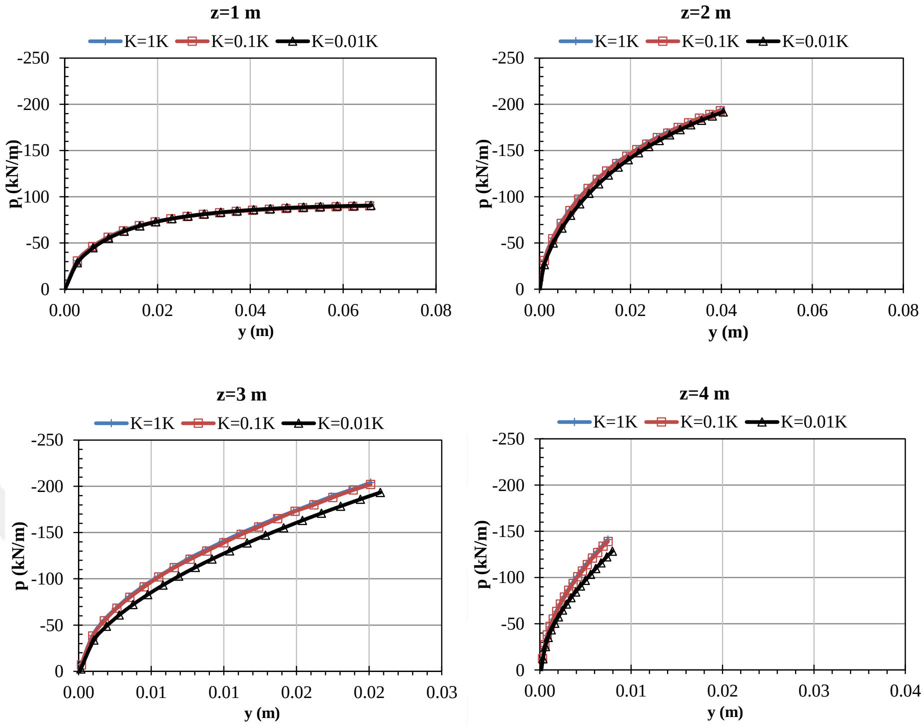

Figure 4.3 : The effect of interface stiffness on the p-y curves.

Pile resistance to lateral loading was obtained using the normal and the shear stresses at the gridpoints of the pile-soil interface. The stresses were multiplied by the 'gridpoints' characteristic area, and the total force was calculated via built-in code. Finally, the resulting force was divided by the tributary length, the distance between the nodes in the vertical direction, to find the load resistance (*p*) in force/distance units. Pile displacement was the lateral pile displacement of the center gridpoint. The Mohr-Coulomb criterion was valid for the interface, which allows the slip and separation based on the applied shear stresses.

A constant velocity of $4x10^{-8}$ m/s was given to the top of the pile in 10^7 steps, reaching the pile head displacement of about 400 mm. The program's pile-head load outputs were taken using the built-in fish function. The pile-head load vs. ground line displacement obtained from the 3D numerical analyses was compared with Reese et al. (1974). Figure 4.4 shows the comparison, and the close results, particularly at the small displacements, confirm that the selected soil parameters reflect the field conditions with reasonable accuracy.

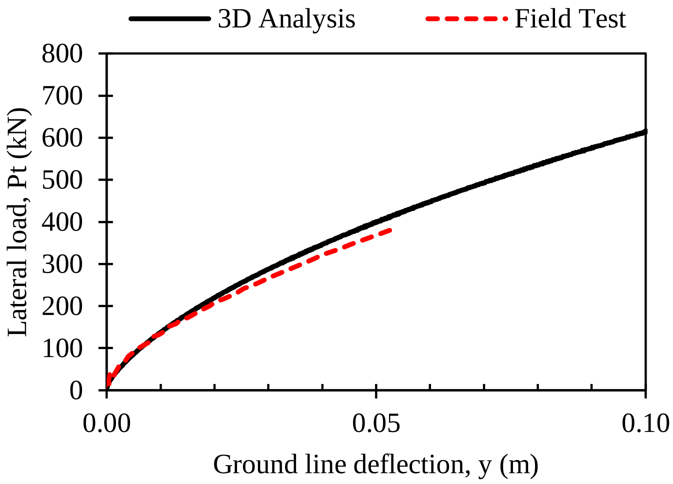

Figure 4.4 : Applied lateral load vs. ground line deflection results: Mustang Island and numerical analysis results.

The non-linear load resistance vs. deflection (*p*-*y*) curves at the selected depths were obtained numerically. The results of *p*-*y* curves were compared with the ones obtained using the equations by Reese et al. (1974) and API (2007), as shown in Figure 4.5 and Figure 4.6. The results showed that the ultimate resistance of soil (p_u) at 0.5 m depth was quite close to those of Reese et al. (1974). However, p_u values in the numerical analyses were higher at greater depths.

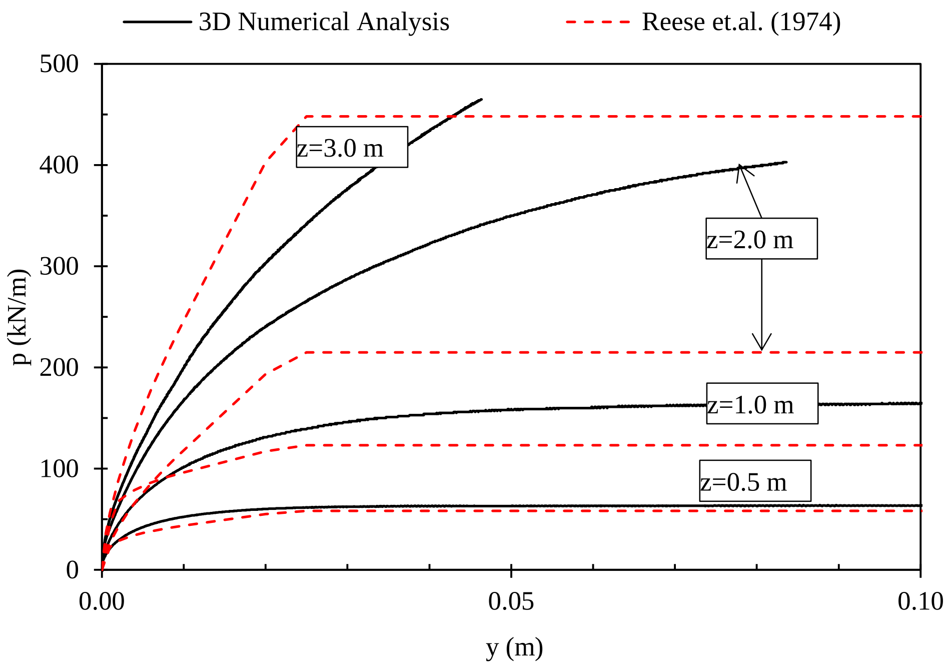

Figure 4.5 : Comparison of *p*-*y* curves obtained through 3D numerical analyses with Reese et al. (1974).

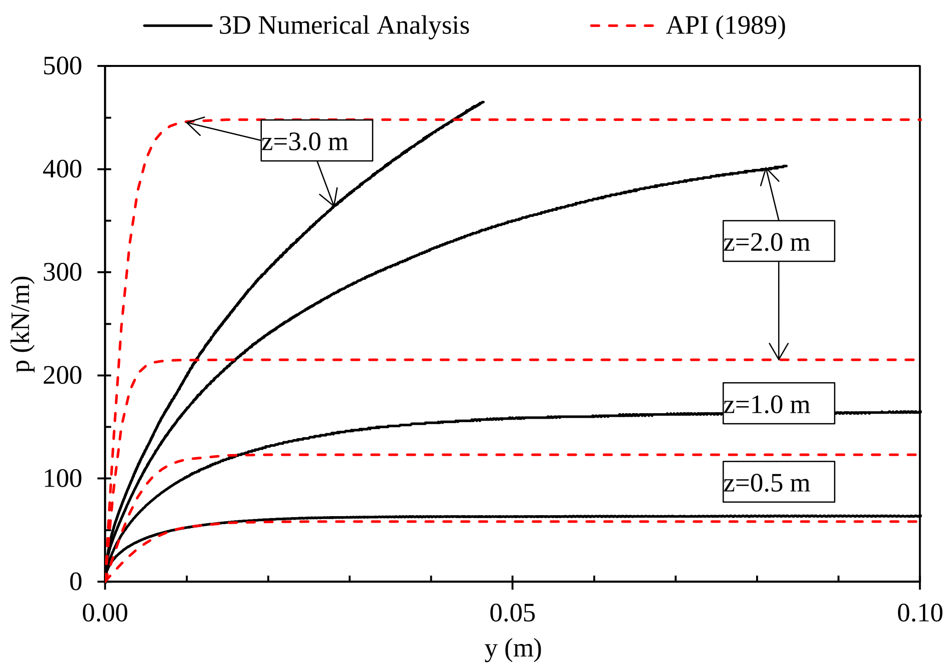

Figure 4.6 : Comparison of *p-y* curves obtained through 3D numerical analyses with API.

4.2 Parametric Analyses

This study aims to characterize the *p-y* curves in small to large displacement ranges. For this purpose, a numerical model was created, similar to the verification model. The model consisted of the solid circular pile, the surrounding soil, and the interface to obtain the lateral resistance applied by the soil. Only half of the problem was modeled due to the symmetry, and the dimensions were 20D, 10D, and 2L in the x, y, and z directions, where D and L were the pile diameter and the pile length, respectively. A constant velocity was applied to the pile head so that the ultimate resistance could mobilize at depth.

The parametric analyses were performed to show the effect of the relative density of soil, pile flexural rigidity, pile diameter, degree of nonlinearity (E_0/E_{50}) of soil, and power of stress dependency (m) on the *p-y* curves. The selected parameters are given in Table 4.2, where the bold values are the baseline analysis of a solid circular pile with D=0.65 m, EI=263 MN.m^2, D_R= 55%, E_0/E_{50}=10, and m=0.5. The young modulus of the pile material (E) was 30 GPa in the baseline analysis. The effect of flexural rigidity was investigated for three different moduli of elasticity of the pile material, keeping the pile diameter (D=0.65 m) and soil properties constant. In the analyses, the ratio E_{ur}/E_{50}=4 was kept constant. The analyses were performed for the flexible piles with lengths of 8 m, 12 m, and 19 m for diameters of 0.65 m, 1.00 m, and 1.60 m, respectively (*L/D*=12). The effect of the slenderness ratio was beyond the scope of this thesis.

Table 4.2 : The parameters used in the parametric static analysis of the single pile.

	The Variables		
Flexural Rigidity, EI (MN.m^2)	26.3	**263**	2630
Pile Diameter, D (m)	**0.65**	1.0	1.60
Relative Density, D_R (%)	30	**55**	80
Degree of Nonlinearity, E_0/E_{50}	5	**10**	20
Power of stress dependency, m	**0.5**	0.7	

4.2.1 Effect of pile flexural stiffness

The effect of flexural stiffness (*EI*) on the *p-y* curves has been investigated in the literature (Ashour & Norris, 2000; Fan & Long, 2005; Wang et al., 2020). In this study, three *EI* values were selected to study the *EI* effect on the *p-y* curves. In Figure 4.7, the *p-y* curves at four depths show a slight increase in the ultimate soil resistance as the pile modulus reduces. Figure 4.8 shows the *p-y* curves with the vertical axis normalized to the ultimate soil resistance at three depths. Apart from the pile flexibility, the normalized *p-y* curves reveal the depth effect. The ultimate displacement at the maximum soil resistance increases as the confining stress increases. This behavior is consistent with the soil behavior in that the increase in the confining stress causes the soil strength to be reached at relatively higher strains. Therefore, greater ultimate soil resistances obtained in the flexible pile can be attributed to the change in stress distribution around the pile. Figure 4.9 shows the comparison of the displacement fields for the flexible (*E*=3 GPa) and rigid (*E* =300 GPa) piles, having the same length (*L* =12 m), where the rigid pile causes higher lateral displacements in deeper regions. It is noted in this study that the maximum lateral soil resistances are lower as the pile flexural stiffness increases. However, the difference is insignificant for elastic moduli greater than *E*=30 GPa, which corresponds to the flexural stiffness of concrete piles commonly used in practice.

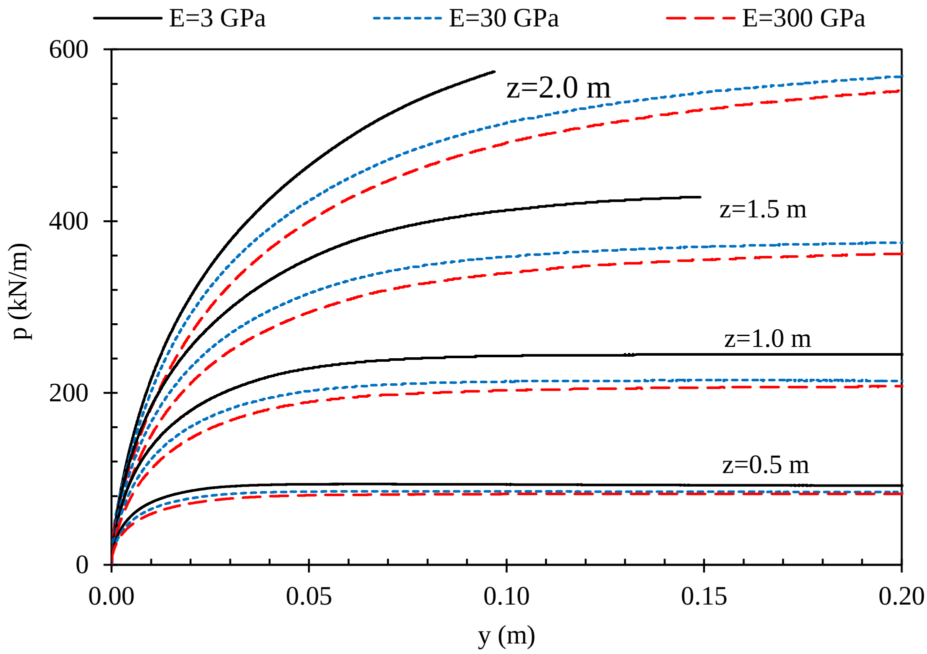

Figure 4.7 : Effect of the pile flexural rigidity on the *p-y* curves.

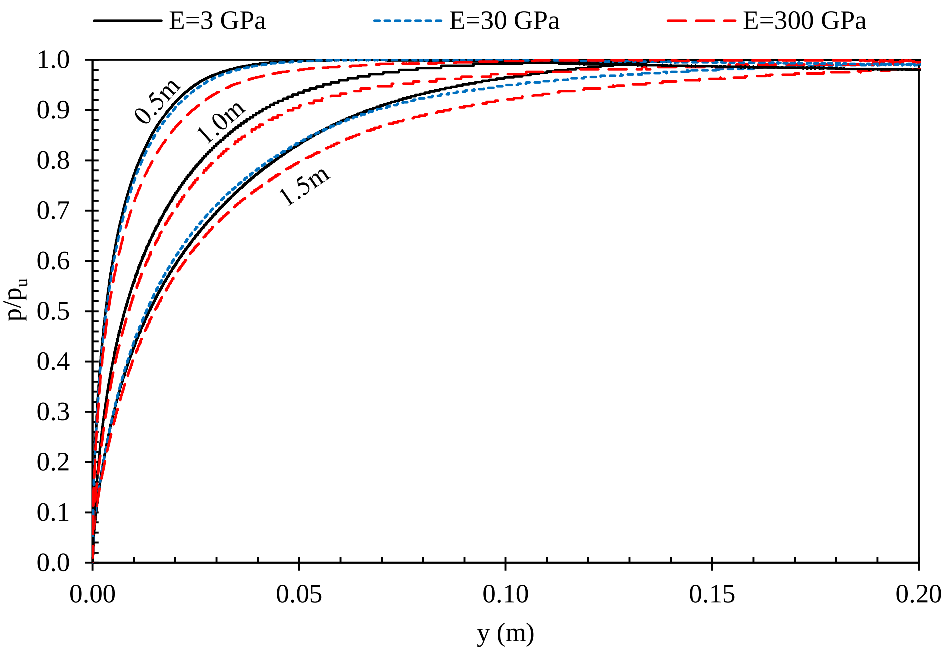

Figure 4.8 : Effect of the pile flexural rigidity on the normalized static *p-y* curves.

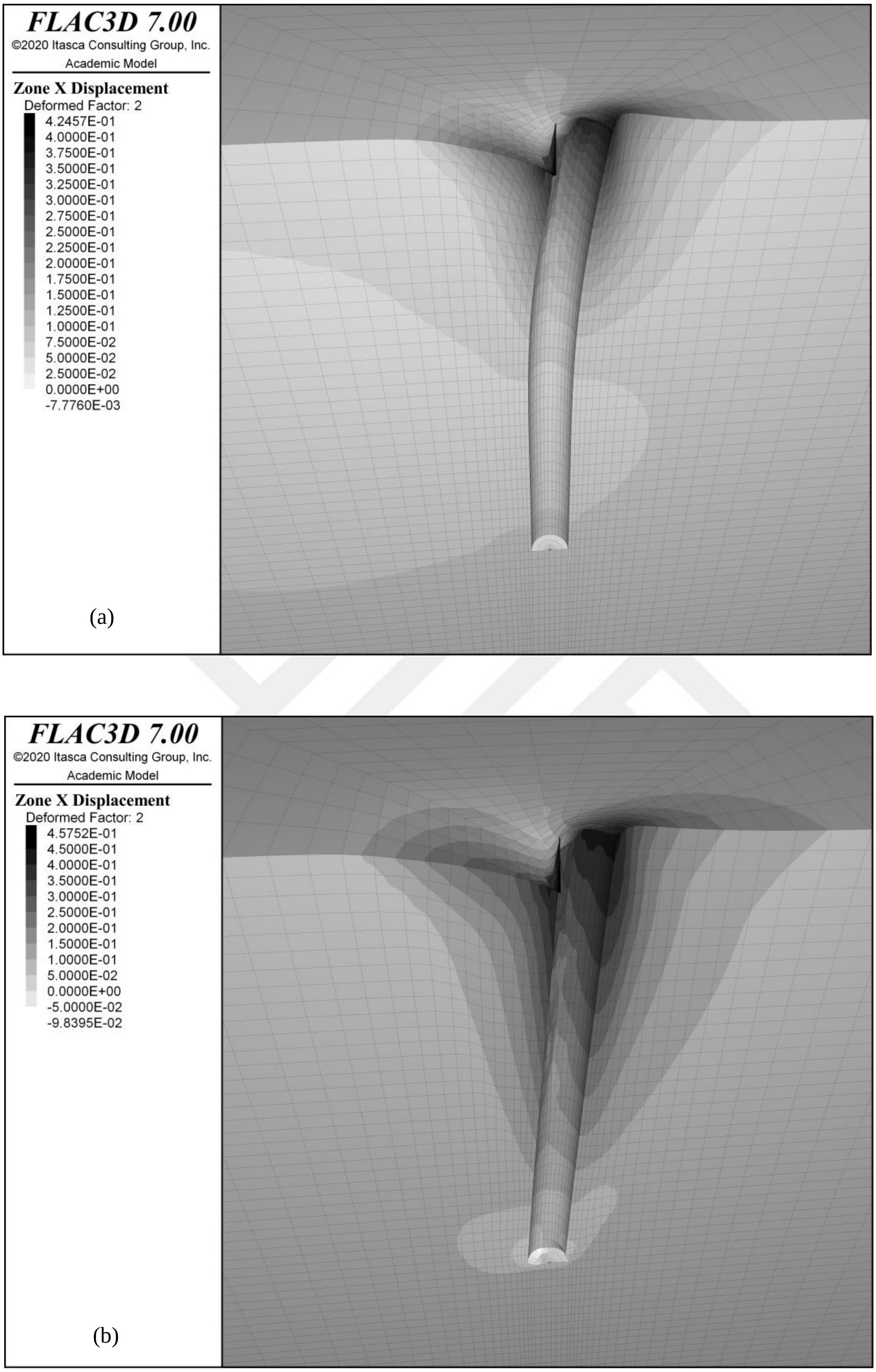

Figure 4.9 : Soil displacement contours under the laterally loaded: (a) flexible pile, (b) rigid pile.

4.2.2 Effect of pile diameter

The effect of pile diameter on the *p-y* curves under static pile-head loading was investigated for various pile diameters: *D*=0.65 m, *D*=1.0 m, and *D*=1.6 m. The parametric analysis results shown in Figure 4.10 indicate the diameter's effect on the ultimate lateral resistance (p_u). Besides, normalized p-y curves were plotted in Figure 4.11, where the vertical axis is normalized by p_u. Although the curves verify the slight influence of diameter on the initial stiffness, the ultimate resistance (p_u) is more sensitive to the pile diameter.

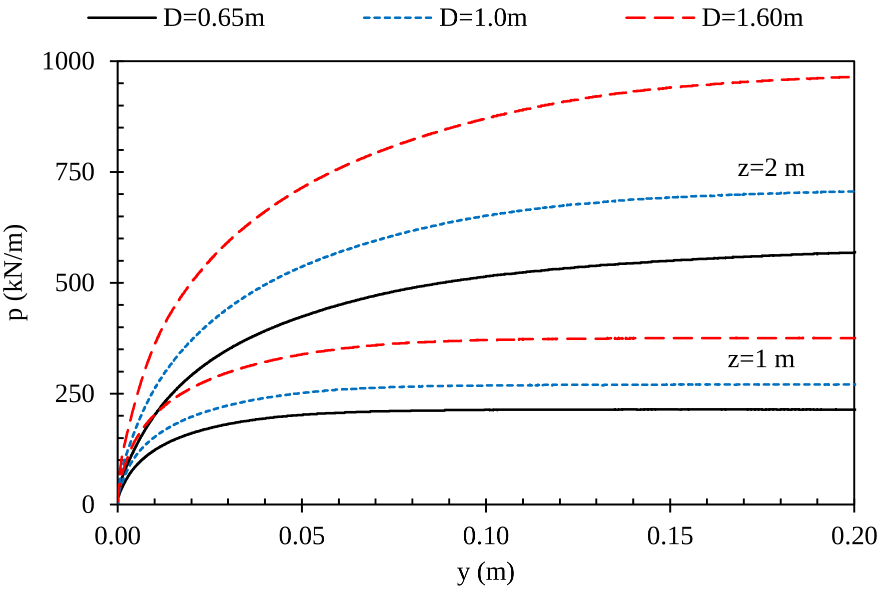

Figure 4.10 : Effect of pile diameter on the static *p-y* curves.

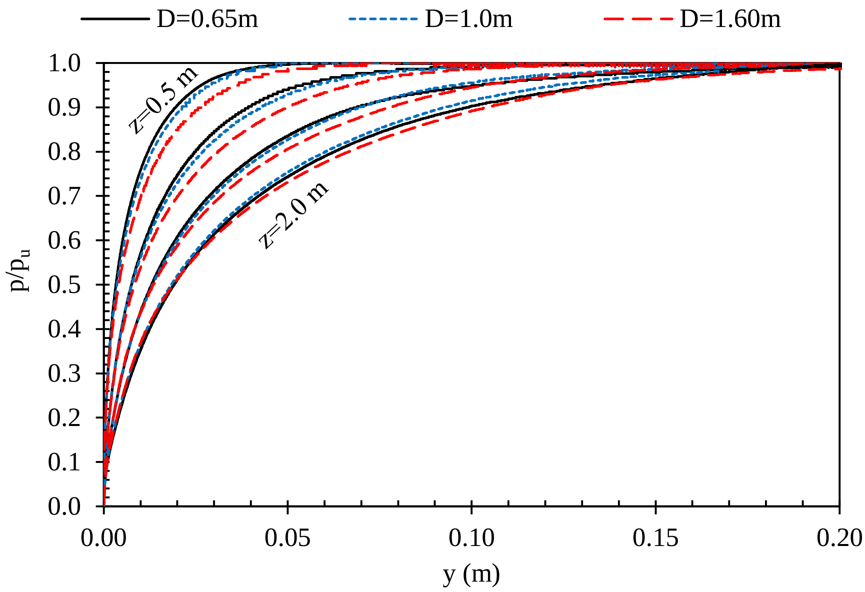

Figure 4.11 : Effect of pile diameter on the normalized static *p-y* curves.

4.2.3 Effect of relative density of soil (D_R)

This study investigated the effect of relative density to characterize the *p-y* curves. The selected relative densities were 30%, 55%, and 80%, representing the loose, medium-dense, and dense sand, respectively. Equations 4 and 5 were utilized for the small strain modulus, and the internal angle of friction values were 32°, 36°, and 40°. Figure 4.12 and Figure 4.13 show the *p-y* and the normalized p-y curves (p/p_u) for various relative densities at certain depths. According to the results, the effect of D_R on the ultimate soil resistance is much more pronounced, while Figure 4.13 indicates the slight influence of the initial soil modulus.

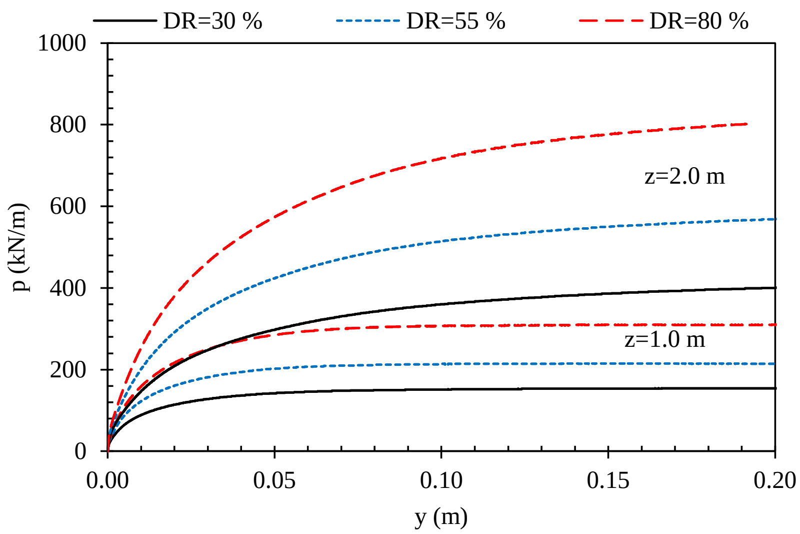

Figure 4.12 : Effect of soil relative density on the static *p-y* curves.

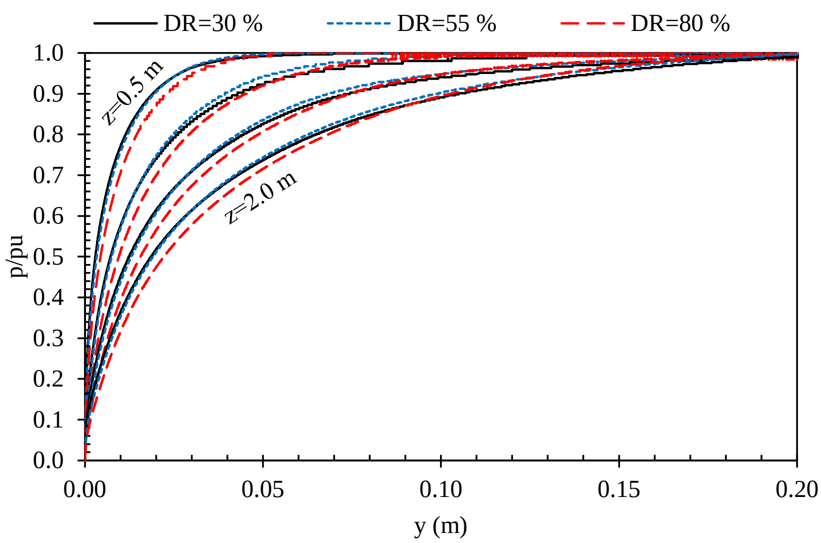

Figure 4.13 : Effect of soil relative density on the normalized static *p-y* curves.

4.2.4 Effect of degree of soil nonlinearity (E_0/E_{50})

The effect of the degree of soil nonlinearity on the laterally loaded piles was investigated with three E_0/E_{ur} values of 1.25, 2.5, and 5, keeping the E_0 constant. Since the selected unloading/reloading modulus ratio to the secant stiffness was assumed E_{ur}/E_{50}=4, E_0/E_{50} equals 5, 10, and 20, respectively. The *p-y* curves for different soil nonlinearities are shown in Figure 4.14. As the ratio of initial stiffness to secant stiffness increases, the degree of soil nonlinearity also increases. As a result, the displacement at which the ultimate soil resistance is mobilized has increased significantly, as shown in Figure 4.15.

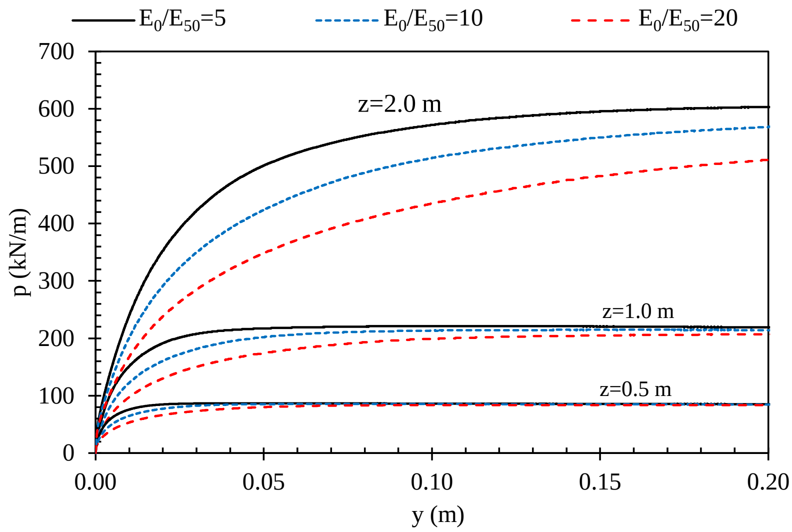

Figure 4.14 : Effect of degree of soil nonlinearity on the p-y curves.

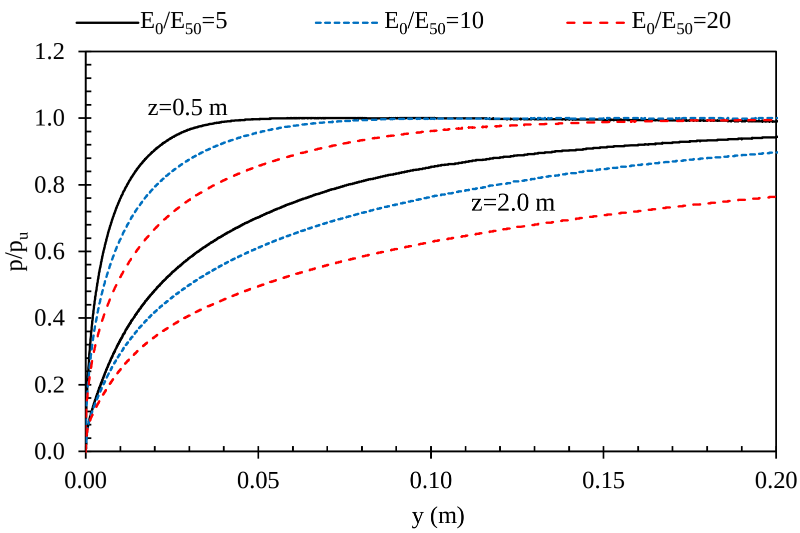

Figure 4.15 : Effect of degree of soil nonlinearity on the normalized *p-y* curves.

4.2.5 Effect of power of stress dependency (m)

The effect of the power of stress dependency (*m*) in equation 3.6 on the laterally loaded piles was investigated with the most common two values for cohesionless soils: 0.5 and 0.7. Figure 4.16 and Figure 4.17 show the resulting *p*-*y* curves at the selected depths. The higher parameter "m" values cause the soil modulus to be lower at shallow depths. Therefore, the lower soil resistances in the case of *m*=0.7 is that the soil modulus is lower at shallow depths.

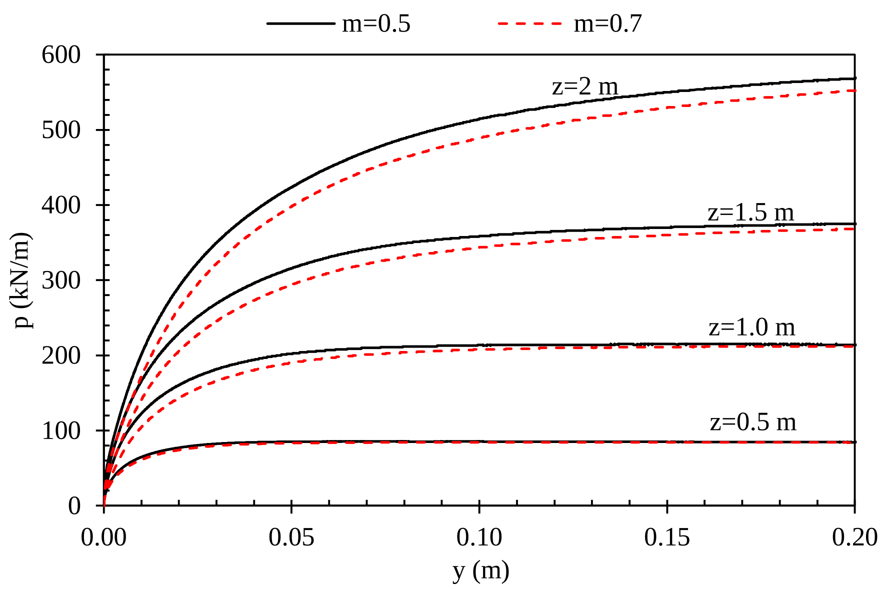

Figure 4.16 : Effect of power of stress dependency on the p-y curves.

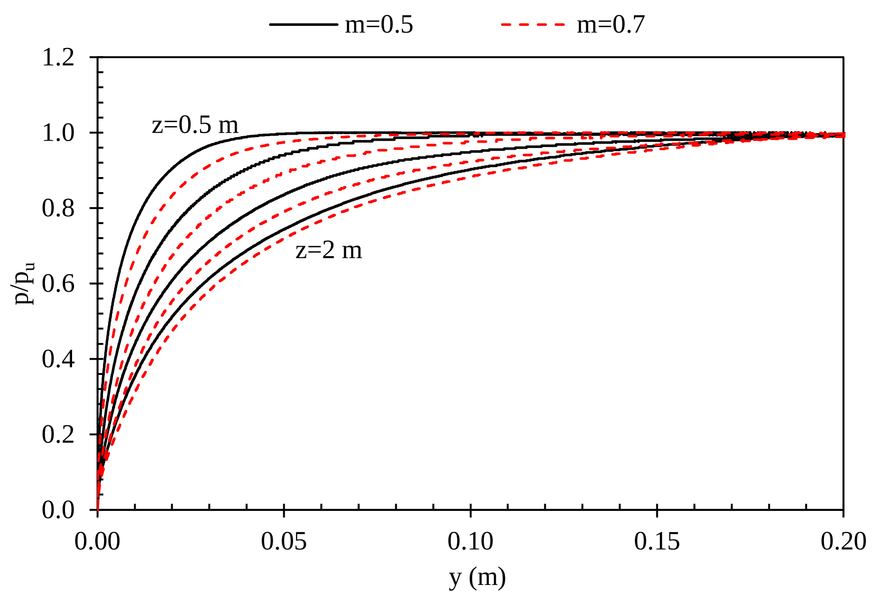

Figure 4.17 : Effect of power of stress dependency on the normalized *p*-*y* curves.

4.3 Comparison of the Ultimate Soil Resistance with the Past Studies

The parametric analysis results performed in this study have shown that the ultimate soil resistance does not linearly increase with diameter, which is consistent with the theory given by Reese et al. (1974). The theoretical value for the maximum soil resistance was multiplied by a coefficient (A) in Reese et al. (1974) since the field test measurements gave higher resistances at shallow depths. The numerical analysis results for the same field test showed that the ultimate soil resistances at shallow depths were very close, but for greater depths, the agreement was poor, and the ultimate resistances were higher in the analyses. The higher soil resistances at greater depths were observed in centrifuge tests by Barton et al. (1983), and the modified equation of Broms (1964) was suggested for greater depths by . Recent studies also confirm higher soil resistance at greater depths in the centrifuge tests (Lu et al., 2021). L. Zhang et al. (2005) proposed a relation for piles in cohesionless soils considering the side shear friction and passive frontal resistance. Varun (2010) suggested further increasing the ultimate lateral resistance based on finite element analyses. Thieken et al. (2015) performed finite element analyses with the HS-Small model (in Plaxis 3D), and the ultimate resistance in DIN 4085 was adopted.

The ultimate soil resistance obtained in this study was higher at shallow depths when compared with the DIN 4085 and Reese et al. (1974) estimations. However, the results complied with DIN 4085 at greater depths where Reese et al. (1974) considerably underestimated the p_u.

The effect of relative density was investigated in this study to characterize the p-y curves, which require the initial stiffness (K_{py}) and ultimate soil resistance (p_u). The selected relative densities were 30%, 55%, and 80%, representing the loose, medium-dense, and dense sand, respectively. The small strain modulus was assigned to the soil domain based on equation 3.6, and the internal angle of friction values were 32^o, 36^{o,} and 40^o for the relative densities of 30%, 55%, and 80%, respectively. The variation of ultimate lateral resistances with depth obtained in the numerical analyses were compared with those obtained using the p_u relations in the literature in Figure 4.18. The maximum depth in the figure is limited to 2.5D to capture better the small variations at shallow depths where the pile response is mostly governed. The ultimate soil resistances obtained in the numerical analyses were higher than those obtained using the literature, except the DIN 4085, which was relatively close to the values in this study, especially for greater depths (for z>1D). A similar agreement was shown in the finite element analysis results published by Thieken et al. (2015). However, DIN 4085 yields lower ultimate lateral soil resistances (p_u) at depths less than one pile diameter (for z<1D) than those obtained in this study, while the p_u at these shallow depths is closer to the findings obtained using equations of Reese et al. (1974).

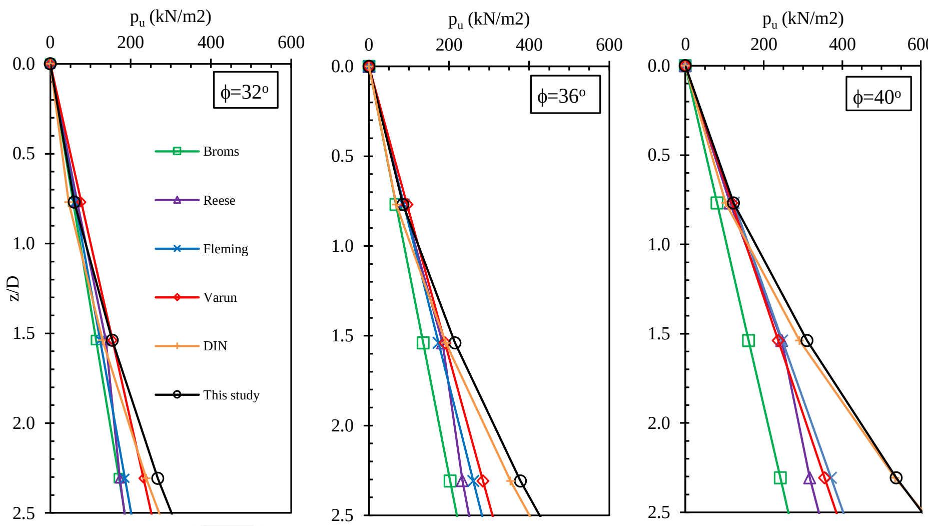

Figure 4.18 : The variation of p_u in this study compared with the literature's relations for various friction angles.

The verification analysis showed that the ultimate resistances obtained at the shallow depths in this study agreed well with the results published by Reese et al. (1974) for the field tests on Mustang Island. However, the maximum soil resistances at greater depths were higher in the numerical analysis results. The effect of pile diameter on the ultimate soil resistance and the shape of p-y curves under static pile-head loading was investigated for various pile diameters: D=0.65 m, D=1.0 m, and D=1.6 m. The parametric analysis showed that the pile diameter significantly affects the ultimate lateral resistance (p_u). Although the curves verify the slight effect of diameter on the initial stiffness, the ultimate resistance (p_u) is much more sensitive to the pile diameter. Besides, compared with the past studies, the variation of p_u vs. depth for different pile diameters are presented in Figure 4.19. The numerical analysis results showed that the p_u was close to Reese et al. (1974) at shallow depths (z<1D) and close to DIN 4085 at greater depths (z>1D). Besides, the variation of ultimate soil resistance does not linearly increase with the depth and the diameter. As a result, the effect of pile diameter on the obtained p-y curves have two aspects; the initial stiffness and the ultimate lateral resistance.

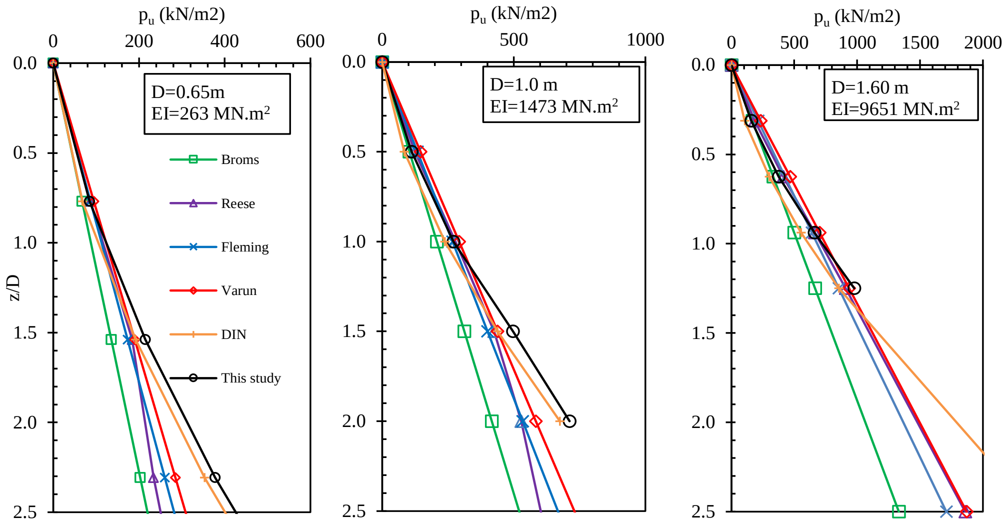

Figure 4.19 : The variation of p_u in this study and the relations in the literature for various pile diameters.

5. NUMERICAL MODELLING of LATERALLY LOADED PILE PROBLEM: DYNAMIC LOADING

This chapter presents the dynamic *p-y* curves obtained in the FLAC^{3D}. Two centrifuge tests from the literature were simulated numerically by the 3-dimensional analyses, and the results of the verification analysis were presented. The parametric studies were carried out to show the effect of soil and pile properties on the cyclic *p-y* curves. The total-stress approach considered the soil nonlinearity using the small-strain shear modulus and modulus degradation curves.

5.1 The Method

The main purpose of this thesis is to investigate the pile-soil interaction considering the soil nonlinearity under cyclic loads. Numerical analyses were performed in FLAC^{3D} using the Mohr-Coulomb model with the hysteretic damping approach, which allows adapting the nonlinear stress-strain relation based on the modulus degradation curves up to the failure stress. In addition, the nonassociated flow rule for shear failure was employed.

In general, the nonlinear stress-strain behavior of soils under dynamic loading can be considered by shear modulus reduction (G/G_{max}) curves. In this study, the small-strain shear modulus of soil (G_{max}) was determined by Seed and Idriss (1970) using equation 3.6. Then, the bulk modulus was calculated by elastic theory using the shear modulus and Poisson's ratio. The Poisson's ratio (ν) was assumed to be 0.45 and 0.30 for saturated and dry sands, respectively.

The hysteretic damping approach was utilized for the nonlinear behavior of soil. FLAC^{3D} requires a functional form for the modulus degradation curves to ensure continuity. The program could invoke the curves using several functions, and the sigmoidal-3 model was preferred in this study. The function in the program is given in equation 5.1, and the parameters for Darendeli (2001) curves are shown in Table 5.1.

$$M_s = \frac{a}{1 + exp(-\frac{L - x_o}{b})} \tag{5.1}$$

Table 5.1 : The coefficients of the sigmoidal-3 function for Darendeli (2001) curves for sands.

L	a	b	x_o
Log(γ)	1	-0.4726	$-1.45 + 0.15\, ln(\frac{\sigma'_m}{p_a})$

The modulus degradation relations were invoked to represent the hysteretic damping behavior of soils. A very low value of Rayleigh damping (0.5 %) at the center frequency of 3 Hz was applied to remove the high-frequency component at very low strains. The small amount of Rayleigh damping applied to the soil domain prevents low-level noise without affecting the response.

5.2 Verification Analyses

Two well-known centrifuge tests (Gohl, 1991; Wilson, 1998) were used to verify the dynamic numerical analyses. The laminar soil container used in Wilson's study is shown in Figure 5.1. An aluminum pipe section was employed for the pile. The diameter and the length of the highly instrumented single pile were 0.67 m and 16.7 m, respectively. A 49 Mg mass placed on the pile created a single-degree-of-freedom system. The free height of the single pile was 3.8 m. The soil in which the piles were embedded was the saturated Nevada sand placed at two different relative densities. The thicknesses of these layers were 9.4 m and 11.3 m, and the relative densities were 55% and 80%, respectively.

The soil container and the setup of the centrifuge test of Gohl (1991) are shown in Figure 5.2. The soil container was a rigid box filled with dry Nevada sand with a relative density of D_R=40%. A steel pipe section was employed for the pile with a diameter of 0.57 m in the study of Gohl (1991). The single mass was placed on top of the pile extending to 2.0 m from the ground surface.

The friction angles for medium-dense and dense sand were selected as 36° and 40° for soil layers in Wilson (1998). The friction angle was 34° for the sand in Gohl (1991). The soil parameters selected for the verification analyses are given in Table 5.2.

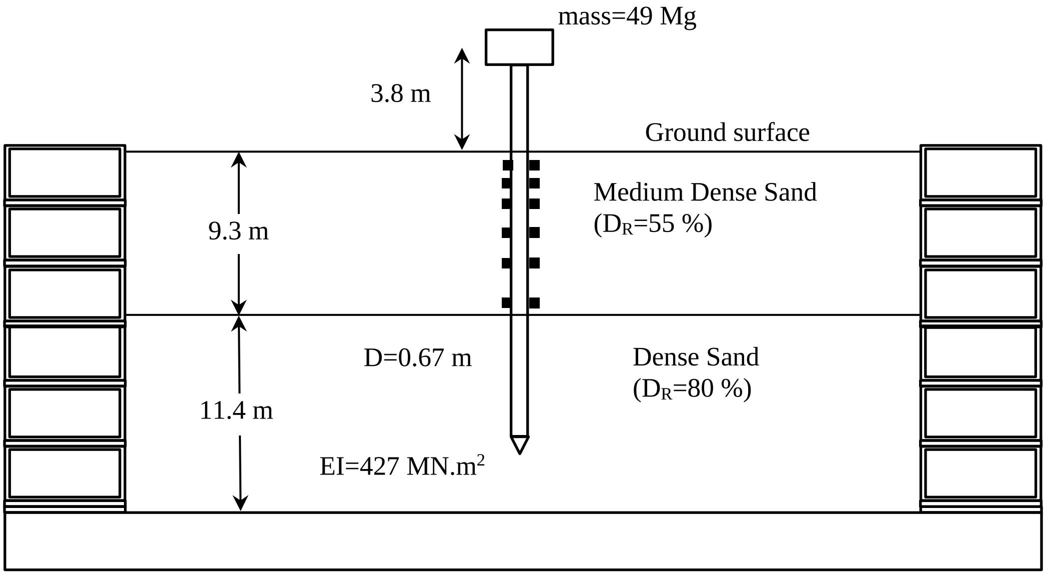

Figure 5.1 : Laminar soil container used in the centrifuge tests of Wilson (1998).

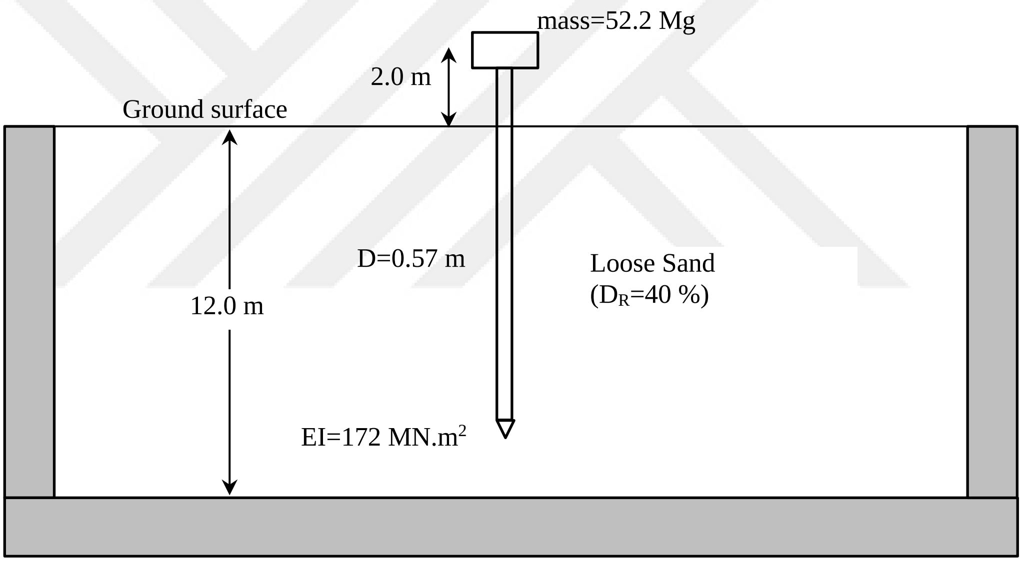

Figure 5.2 : Rigid soil container used in the centrifuge tests of Gohl (1991).

5.2.1 Numerical model

The numerical model was created for the verification analyses (Figure 5.3). The prototype dimensions were 20 m x 51 m x 20 m in Wilson (1998) and 16 m x 10 m x 12 m in Gohl (1991). The zones in the plan view were kept as uniform as possible. The limit value for the zone size (Δl) in the vertical direction is one-tenth to one-eighth of the wavelength of the input wave motion ($\Delta l < \lambda /8$), as suggested by Kuhlemeyer and Lysmer (1973). The wavelength is estimated by the shear wave velocity ratio to the records' maximum frequency component ($\lambda = V_s/f_{max}$). A maximum frequency component of 15 Hz was taken for f_{max} for the earthquake records used in the verification analyses. Shear wave velocity varies with depth and has been as low as 95 m/s near the ground surface. Therefore, the minimum wavelength was estimated as $\lambda \cong 6.3$ m. Although the minimum zone size of 0.8 m ($\Delta l < \lambda/8$) could be anticipated in the vertical direction to ensure the wave transmission, the finer mesh was employed near the ground surface ($\Delta l = 0.33$ m in Wilson (1998) and $\Delta l = 0.25$ m in Gohl (1991)) based on the suggestion of Di Laora and Rovithis (2015). The coarser mesh was used at greater depths ($\Delta l = 0.75$ m in Wilson (1998) and $\Delta l = 0.5$ m in Gohl (1991) for $z > 3$ m). The bottom boundary of the numerical models was fixed. The lateral boundaries in Gohl (1991) were also fixed as a rigid box was used in the test. In the case of Wilson (1998), free-field boundaries were employed to prevent the reflection of waves since the container in the tests was a flexible shear beam container.

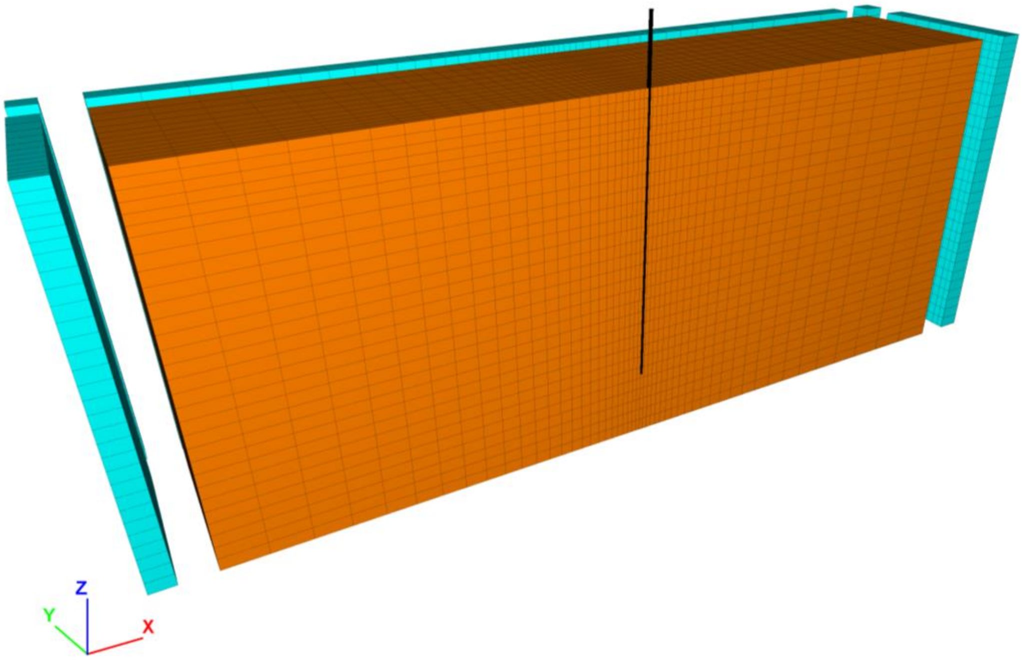

Figure 5.3 : The numerical model created for the verification analyses.

The initial shear modulus and the reference strain values were applied to each zone by considering the initial effective stress level (total stress approach). The shear modulus reduction factor (G/G_{max}) at the very large strain (>1%) might be very low. Besides, Masing's rule was employed for unloading/reloading behavior, which may cause the damping ratio to be unrealistically high. The free-field soil displacement might be overdamped due to the lower shear strength resulting from the low confining pressure, particularly at shallow depths.

Therefore, the minimum modulus reduction value was set to 0.05, and a small cohesion value (10 kPa) was assigned in the verification analyses to overcome the mentioned problem. The calibration process of the damping ratio was studied in detail by the author in separate papers (O. Alver & E. Eseller-Bayat, 2022; O. Alver & E. E. Eseller-Bayat, 2022).

Table 5.2 : The soil parameters used in the verification analyses.

	Wilson, 1998		Gohl, 1991
Layer	**Layer 1**	**Layer 2**	**Single Layer**
Effective unit weight, γ' (kN/m3)	9.5	9.9	15.1
Relative density (%)	55	80	40
Friction angle, ϕ' (°)	36	40	34
Dilation angle ψ (°)	4	8	2
Cohesion, c (kPa)	10	10	10
Poisson's ratio, ν	0.45	0.45	0.30

Although the piles and the structure are 3-dimensional, they were modeled with the beam elements for simplicity. The structural elements (beam) were connected to the surrounding soil rigidly, where the pile displacement is the same as the soil deformation. Several researchers adopted the rigid connection approach (Finn, 2005; Finn & Fujita, 2002; Rahmani et al., 2018). Since the problem is a laterally loaded pile model under dynamic loading, the key property affecting the response is the flexural stiffness of the pile and the superstructure. Therefore, the superstructure properties summarized in Table 5.3 were assigned to the beam elements used in the numerical analyses.

Table 5.3 : The superstructure properties in the verification analyses.

Structure (Wilson, 1998)				Structure (Gohl, 1991)			
Flexural Stiffness, EI (MN.m^2)	Height (m)	Mass (Mg)	T_{fixed} (s)	Flexural Stiffness, EI (MN.m^2)	Height (m)	Mass (Mg)	T_{fixed} (s)
427	3.8	49	0.3	172	2.0	52.2	0.3

5.2.2 Input motions

Two earthquake records were used in Wilson (1998): 1989 Loma Prieta (Santa Cruz Station) Event K and Event N. The centrifuge laboratory of UC Davis provides the acceleration time history of the input motions for these records. The Santa Cruz records (Event K and Event N), in which the maximum acceleration (a_{max}) scaled to 0.11 g, were used in this study. These motions were selected to eliminate the liquefaction behavior since the resulting pore water pressures in the medium-dense sand layer were too low to consider. The motion used in the centrifuge test of Gohl (1991) was provided by Dr. Amin Rahmani and Dr. Mahdi Taiebat (personal communication). Baseline correction was applied to the records to remove the displacement offset. The acceleration-time histories of the input motions after the baseline corrections are shown in Figure 5.4.

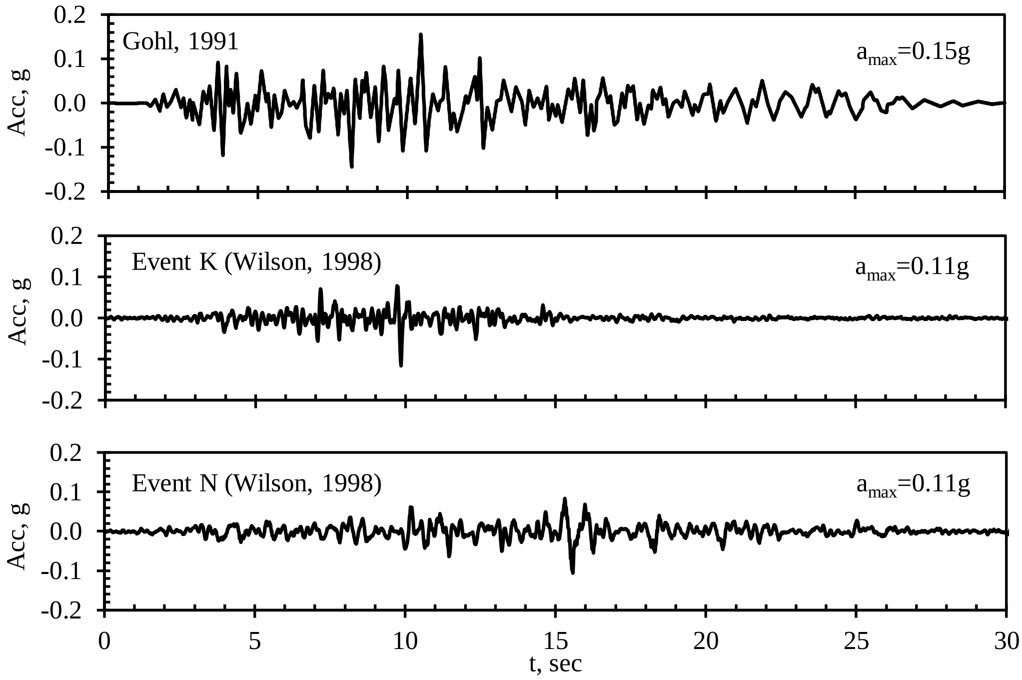

Figure 5.4 : Input motions used in the numerical analyses: a) Gohl (1991), b) Event K (Wilson, 1998), c) Event N (Wilson, 1998).

5.2.3 Verification analyses results

The results obtained from the numerical verification analyses were compared with the centrifuge test results. Figure 5.5 compares acceleration response spectra for the superstructure in Gohl (1991). Figure 5.6 and Figure 5.7 show the acceleration response spectra of the superstructure for Event K and Event N, respectively (Wilson, 1998). According to the comparisons, the spectral accelerations of the superstructure response were slightly higher at low periods (T<0.8-1.0 s) and reasonably close to the measurements by Gohl (1991) and Event K (Wilson, 1998) at higher periods. In contrast, the spectral accelerations in the numerical analysis for Event N were lower than those in the centrifuge test.

The maximum bending moments obtained from the numerical analyses are compared with the centrifuge test results in Figure 5.8, Figure 5.9, and Figure 5.10. The bending moment outputs agreed well with the centrifuge test results by Gohl (1991) and Event

K (Wilson, 1998). However, the bending moments in the numerical analysis for Event N were lower than those in the centrifuge test. The lower response in the numerical analyses for Event N can be attributed to higher damping ratios due to Masing's rule for unloading/reloading behavior. However, the overall behavior was reasonably captured by the numerical analyses.

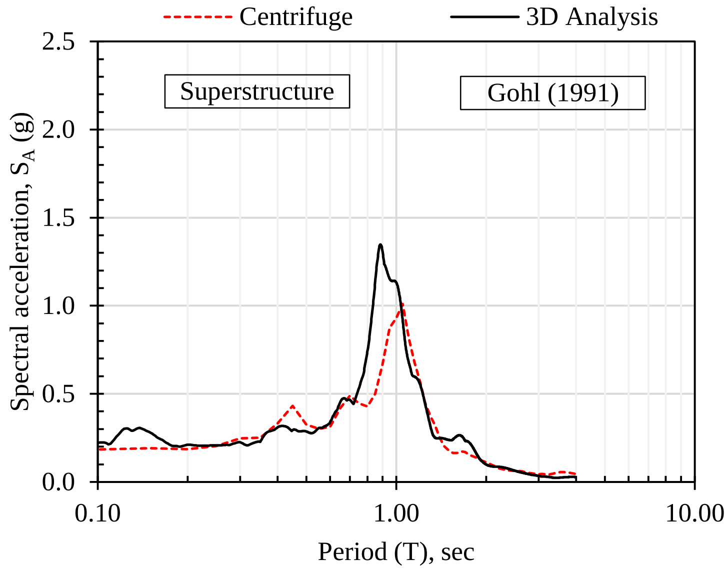

Figure 5.5 : Acceleration response spectra of the superstructure in Gohl (1991).

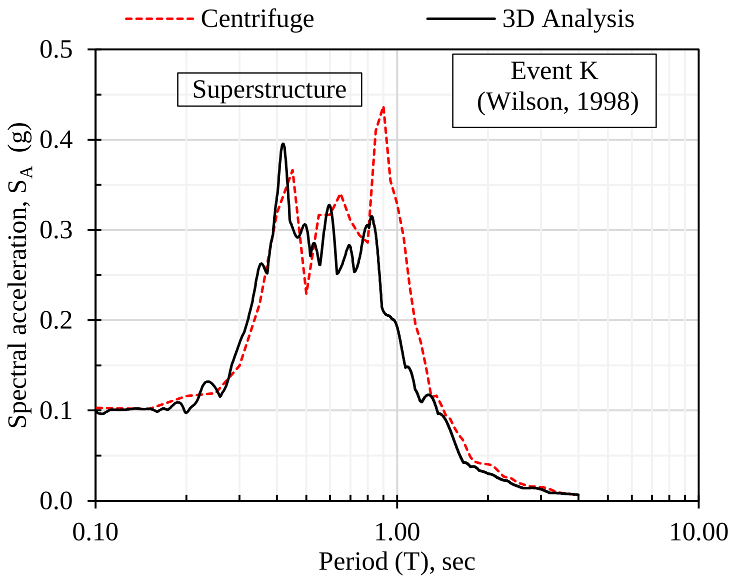

Figure 5.6 : Acceleration response spectra of the superstructure in Event K (Wilson, 1998).

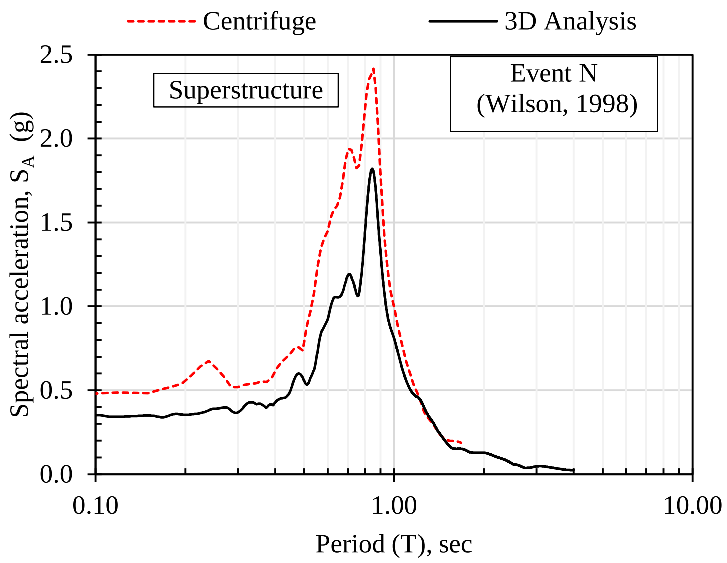

Figure 5.7 : Acceleration response spectra of the superstructure in Event N (Wilson, 1998).

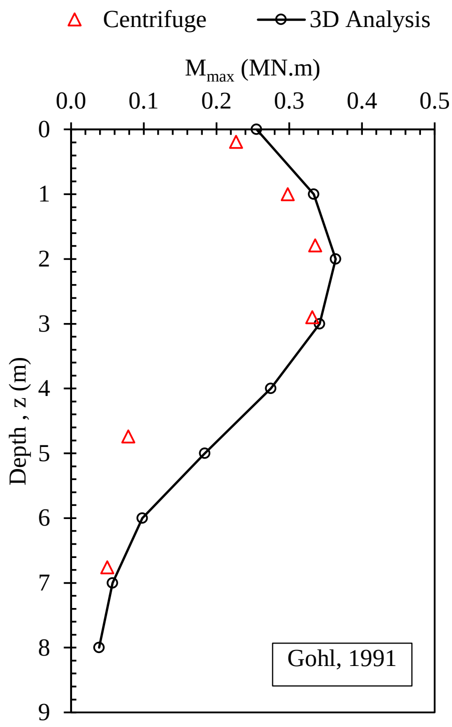

Figure 5.8 : Maximum bending moment variations with depth in Gohl (1991).

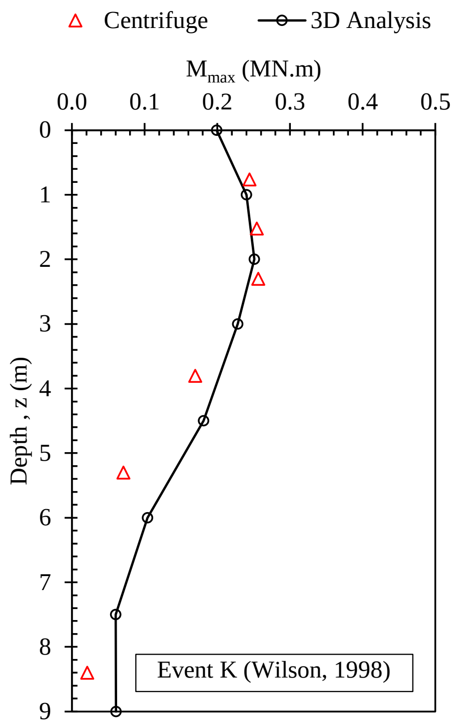

Figure 5.9 : Maximum bending moment variations with depth in Event K (Wilson, 1998).

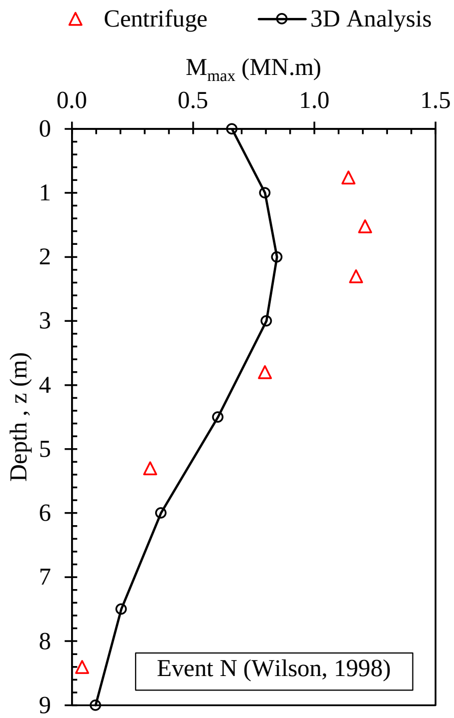

Figure 5.10 : Maximum bending moment variations with depth in Event N (Wilson, 1998).

5.3 Parametric Analyses

Dynamic soil-pile interaction analyses were carried out to show the effect of soil and pile properties on the cyclic *p-y* curves, and the results were presented in this section. The numerical model includes the solid circular pile, the surrounding soil, and the interface. Only half of the problem was modeled due to symmetry. The model dimensions were 20*D* and 10*D* in the *x* and *y* directions, where *D* and *L* are the pile diameter and length, respectively. The vertical height of the model was 5 m longer than the pile length. The numerical model created for the parametric analyses is shown in Figure 5.11.

Similar to the non-linear behavior of soils, non-linear *p-y* curves can be obtained depending on several parameters: The soil nonlinearity, the pile diameter, the small-strain shear modulus, and the friction angle, which are the key parameters for the pile-soil interaction behavior (Hussein & El Naggar, 2022). The pile diameter and the relative density of the soil govern the initial soil-pile modulus (K_{py}) and ultimate soil resistance (p_u), in which the very small displacement and the large displacement region of the *p-y* curves can be obtained.

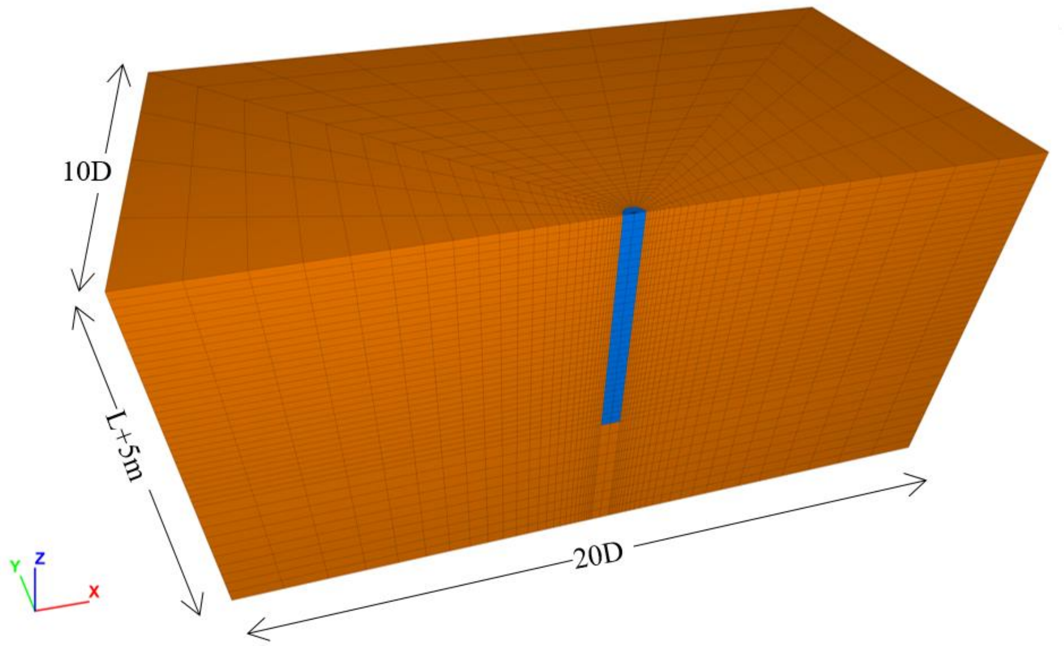

Figure 5.11 : The 3D single pile model created for parametric analyses.

Various pile diameters and soil relative densities were used to investigate the effect on the K_{py} and p_u. The behavior under small to moderate displacement levels is controlled by the soil nonlinearity that mostly depends on the employed modulus degradation curves. As the nonlinearity of soils is the function of effective confining stress in cohesionless soils, various curves for soil nonlinearity were implemented in the analyses. The parameters for the parametric analyses are shown in Table 5.4, where the bold ones represent the default values in the analysis. The pile lengths (*L*) were 8 m, 12 m, and 19 m for pile diameters (*D*) of 0.65 m, 1.0 m, and 1.6 m, respectively, to keep the slenderness ratio constant (*L=12D*).

Table 5.4 : The parameters used in the numerical analyses.

	The Variables		
Unit weight of soil γ (kN/m^3)	18	18	18
Friction angle, ϕ' (^{o})	32	**36**	40
Pile Diameter, D (m)	**0.65**	1.0	1.60
Relative Density, D_R (%)	30	**55**	80
Degree of Nonlinearity (Darendeli (2001) curves for the given confining pressures, kPa)	10	25	100

Solid volumes modeled the soil and the pile in the parametric analyses. Elastic properties of concrete were assigned to the pile element. The cyclic lateral velocity was applied to the pile all along. The lateral displacement history was obtained directly at the center gridpoint of the pile. However, an interface must be placed between the pile and the surrounding soil to obtain lateral soil resistance. The interface allows deriving the stresses applied by the soil to the pile due to cyclic motion. The normal and the shear stresses occur at the gridpoints of the interface. The lateral force was calculated by multiplying the stresses with the characteristic area of each gridpoint. The sum of the forces at the gridpoints in a cross-section yields the total resistance at that depth. The soil resistance (*p*) was calculated in units of force/distance by dividing the force by the characteristic length. This procedure to obtain the lateral resistance (*p* axis of the *p-y* curves) was achieved using the built-in fish function in $FLAC^{3D}$.

The interface property for the normal and shear components (k_n and k_s) were determined based on the constraint modulus as in equation 4.1. The depth-dependent stiffness was assigned ten times the equivalent stiffness through the pile. The Mohr-Coulomb criterion was valid for the interface, which allows the slip and separation based on the applied shear stresses.

5.3.1 Input motion

The parametric analyses were conducted by applying the cyclic motion through the pile. The displacement history applied to the pile is shown in Figure 5.12. Gradually increasing amplitude allowed obtaining both small and large displacement behavior. The frequency of the input motion was 0.5 *Hz* which is low enough to minimize the effect of the radiation damping, which can be considered separately using the approach suggested by Gazetas and Dobry (1984).

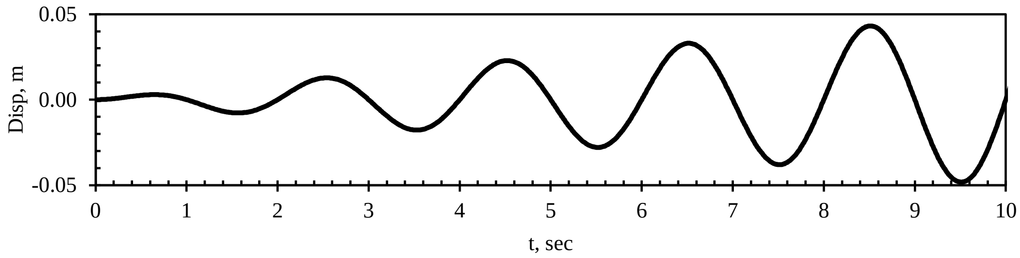

Figure 5.12 : The input motion applied to the pile in the parametric analyses.

The parametric analyses' results, described earlier, were presented in this section. Time histories of the pile displacement and the ultimate soil resistance were obtained. The effect of pile diameter, the relative density of soil, and the degree of soil nonlinearity was discussed.

5.3.2 Effect of pile diameter

The effect of pile diameter on the cyclic *p-y* curves was investigated for three diameters: 0.65 m, 1.0 m, and 1.6 m. Soil resistance (p) and pile displacement (y) histories for D=0.65 m and D_R=55% are given down to 4 m depth in Figure 5.13. The *p-y* curves obtained at 1 m and 2 m depths are shown in Figure 5.14 and Figure 5.15. According to the analysis results, the effect of pile diameter was observed on two important characteristics of dynamic *p-y* curve outputs: The initial soil-pile stiffness (K_{py}) and ultimate soil resistance (p_u). However, the impact on the ultimate soil resistance is much more significant than the effect on the initial modulus. Experimental (Lee et al., 2019; Rollins et al., 2005; Yoo et al., 2013) and numerical (Choi et al., 2016; McGann et al., 2011) studies have shown that the API (2007) underestimates the ultimate soil resistance under cyclic loading. The numerical analysis results obtained in this thesis have also confirmed that the ultimate soil resistance was greater than the suggestions of past studies.

Figure 5.13 shows the variation of the pile displacement and soil resistance with time for D=0.65 m and D_R=55 %. Pile displacement is the same for all depths for a given soil and pile properties. However, the soil resistance increases with depth. The results for various pile diameters, relative densities, and soil nonlinearities are presented in Appendix B.

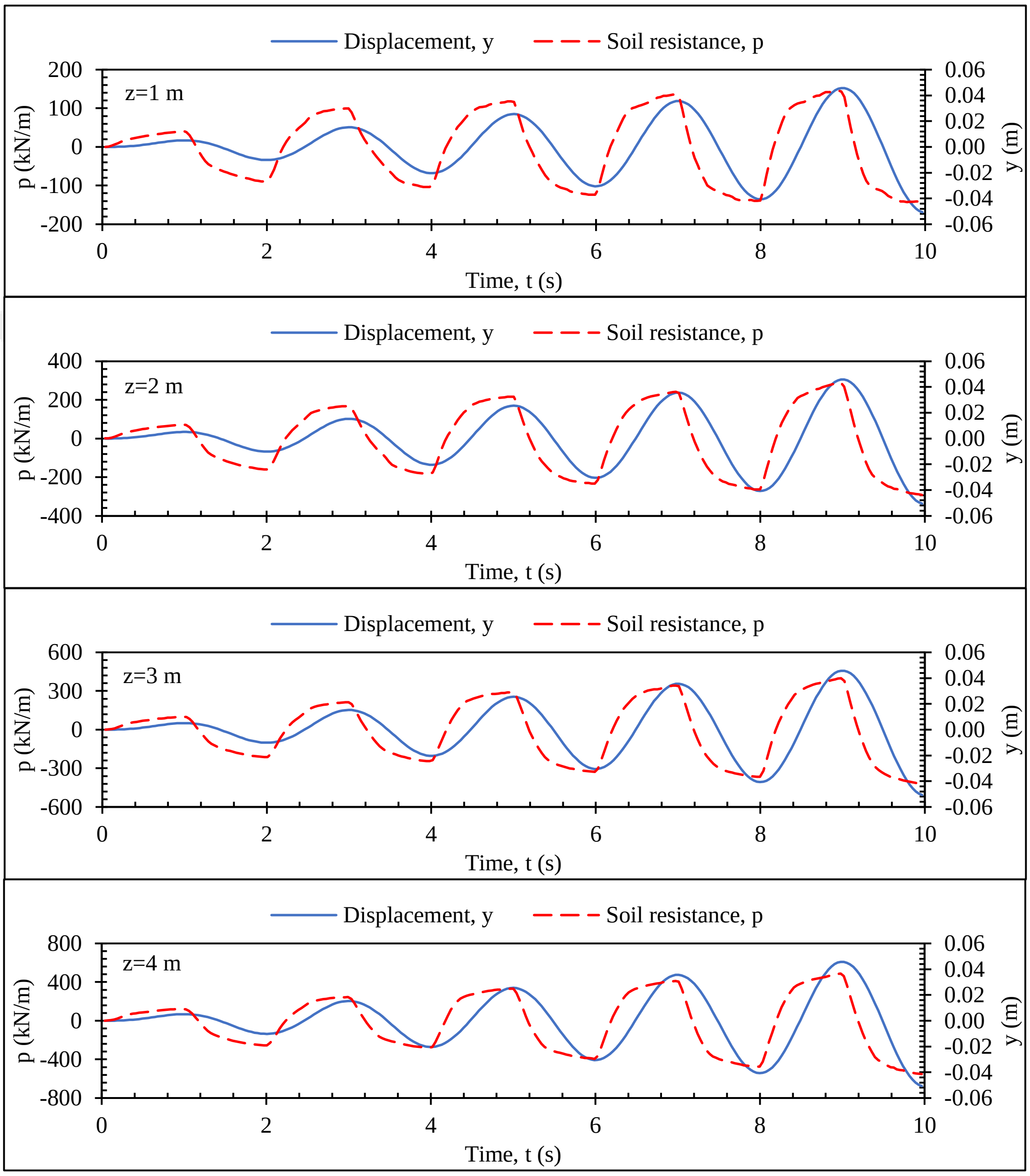

Figure 5.13 : The pile displacement and soil resistance time histories for D=0.65 m, D_R=55 %.

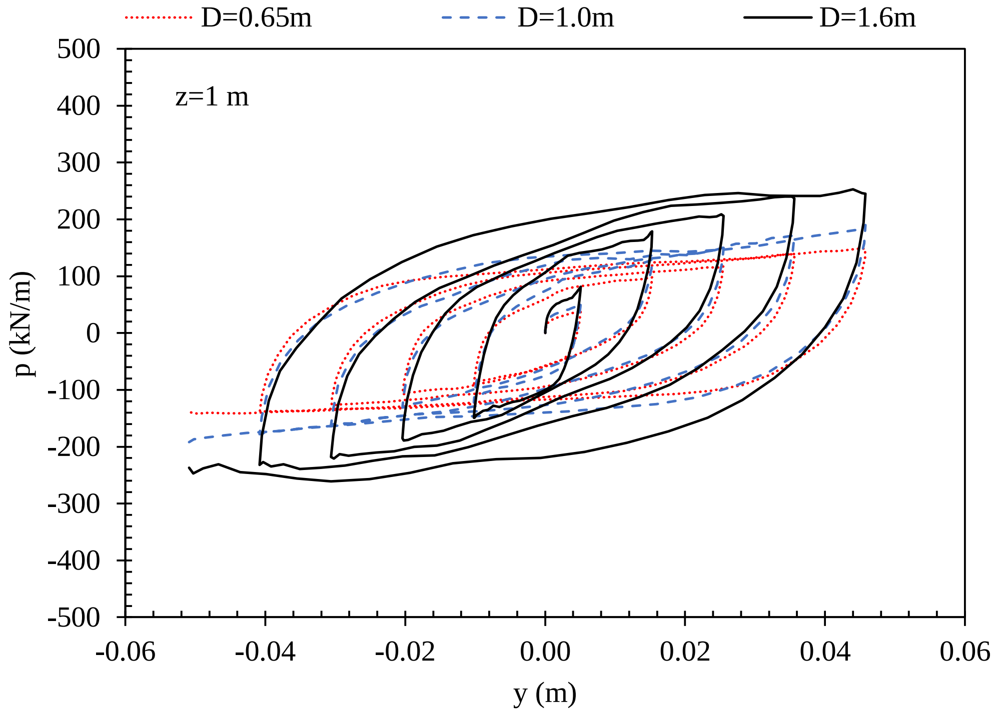

Figure 5.14 : The dynamic p-y curves (hysteretic loops) for D=0.65 m, D=1.0 m, and D=1.6 m at z=1 m.

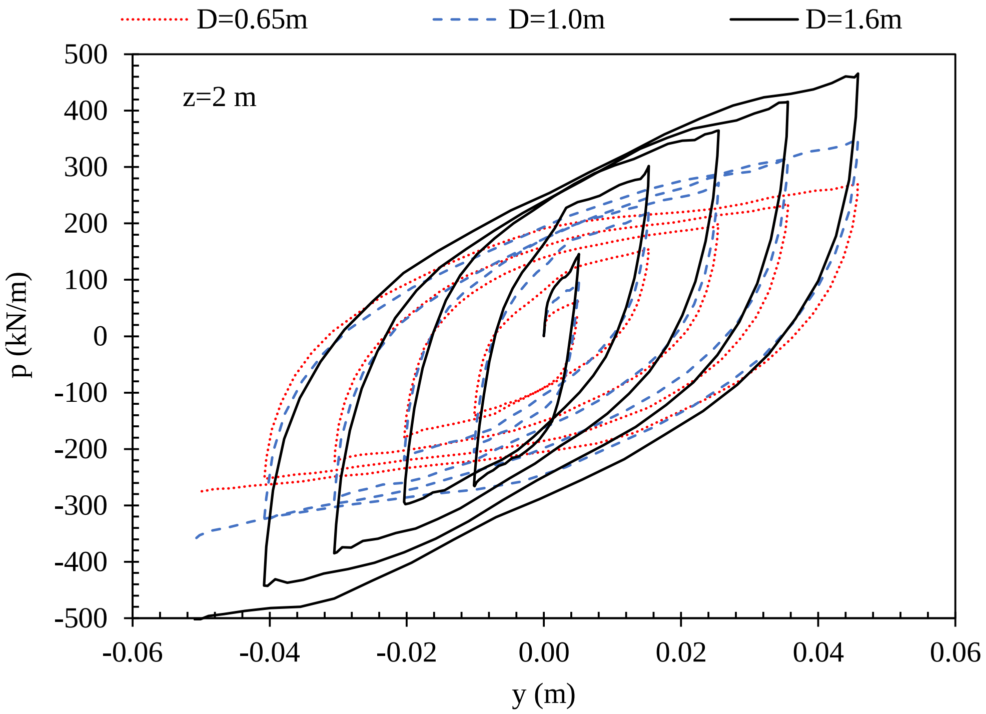

Figure 5.15 : The dynamic p-y curves (hysteretic loops) for D=0.65 m, D=1.0 m, and D=1.6 m at z=2 m.

5.3.3 Effect of relative density

Dynamic *p-y* curves under the cyclic lateral load were investigated for the selected relative densities of 30%, 55%, and 80%, representing the loose, medium-dense, and dense sand, respectively. The small strain shear modulus was calculated by equation 3.6 according to the given relative densities. The internal angle of friction (ϕ) was determined to be 32º, 36º, and 40º, with D_R being 30%, 55%, and 80%, respectively. Figure 5.16 and Figure 5.17 show the *p-y* hysteretic curves at 1 m and 2 m depths for the given relative densities. According to the results, larger *p-y* curves were achieved as the relative density of soil increased. The main reason for having greater soil resistance is the increase in the internal angle of friction, which can be characterized by the ultimate soil resistance (p_u). Another impact of the relative density on the dynamic *p-y* curves was the increase in the initial soil-pile stiffness (K_{py}). These results confirm that the dynamic *p-y* curves can be characterized by the initial soil-pile stiffness (K_{py}) and ultimate soil resistance (p_u) at very small and large displacement levels.

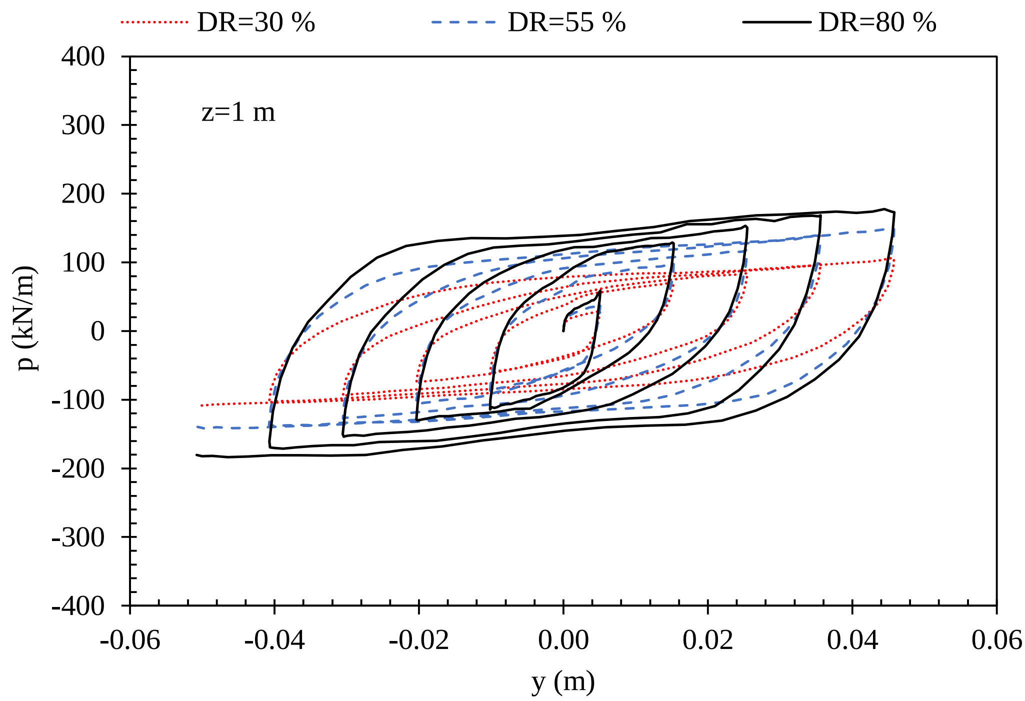

Figure 5.16 : The effect of relative density on the dynamic *p-y* curves at *z*= 1 m.

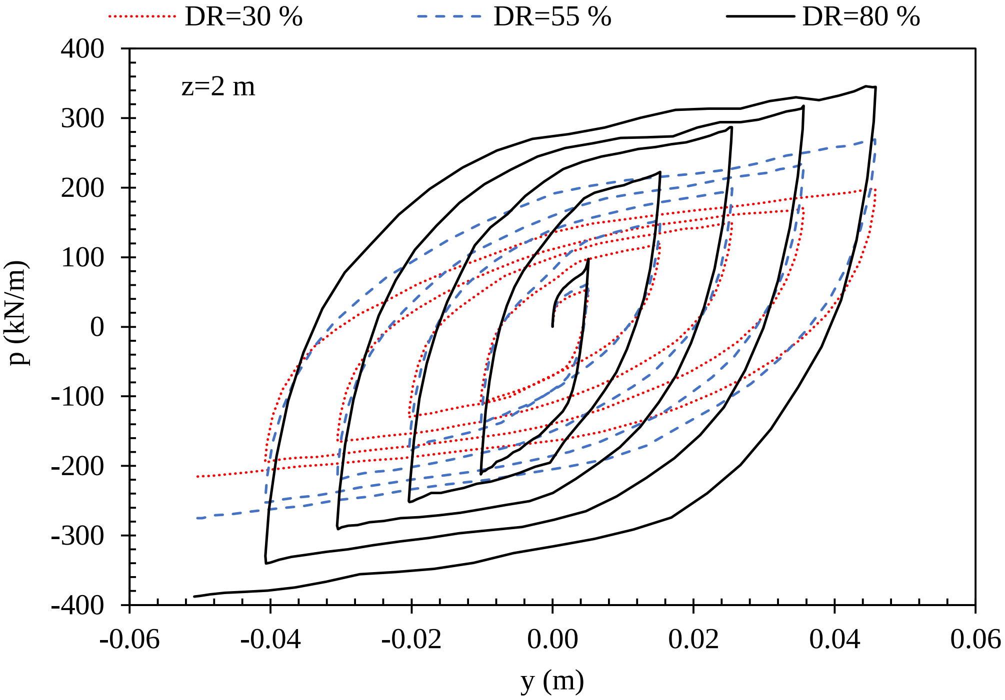

Figure 5.17 : The effect of relative density on the dynamic *p-y* curves at *z*=2 m.

5.3.4 Effect of soil nonlinearity

The soil behavior under cyclic loading has been investigated by many researchers so far. As was shown in the verification analyses, soil nonlinearity can be considered by modulus degradation curves. The most widely used relations for cohesionless soils were suggested by Seed and Idriss (1970). However, Ishibashi and Zhang (1993), Darendeli (2001), and J. Zhang et al. (2005) have shown that the nonlinear behavior of cohesionless soils has been mostly affected by confining pressure. In this study, the effect of soil nonlinearity on the cyclic *p-y* curves was investigated with three confining stress levels being 10 kPa, 25 kPa, and 100 kPa using the curves of Darendeli (2001), where the reference strains correspond to γ_r=0.0158%, γ_r=0.0217%, and γ_r=0.0352%, respectively. The dynamic load (Figure 5.12) was applied through the pile, and the *p-y* curves were obtained at the selected depths, as shown in Figure 5.18 and Figure 5.19. According to the results, as the confining stress reduces, the soil nonlinearity causes the backbone of the *p-y* curves to have smaller soil resistances at a specified displacement (increasing nonlinearity). This finding confirms the influence of confining stress on the soil nonlinearity, hence on the dynamic *p-y* curves.

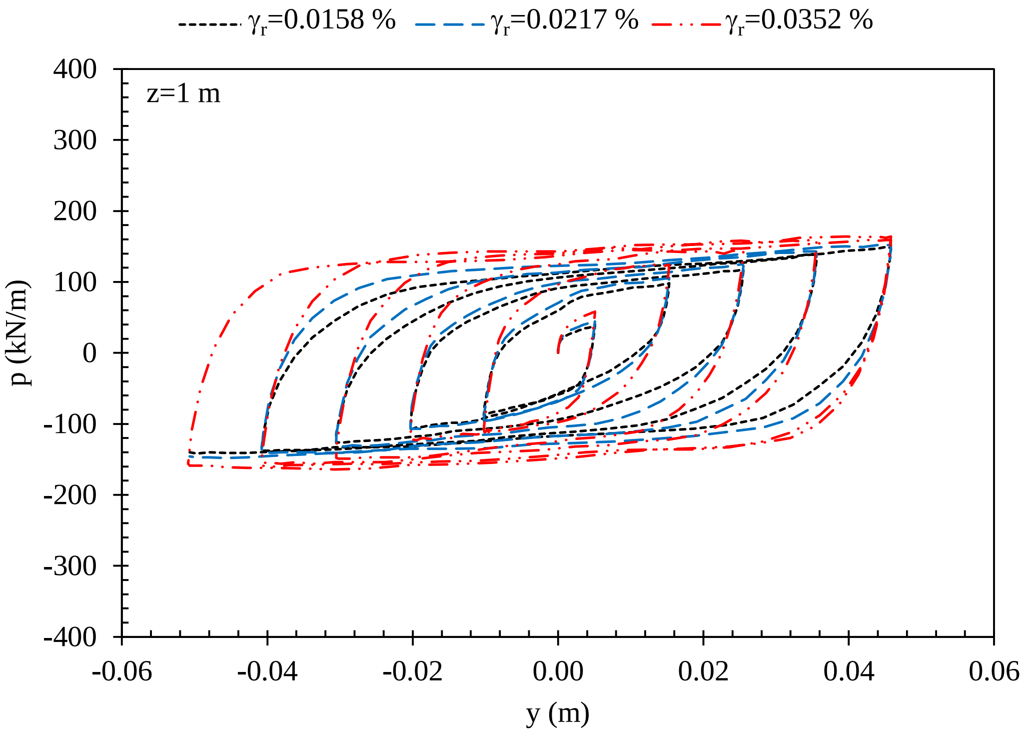

Figure 5.18 : Effect of soil nonlinearity on the cyclic *p-y* curves at z= 1 m.

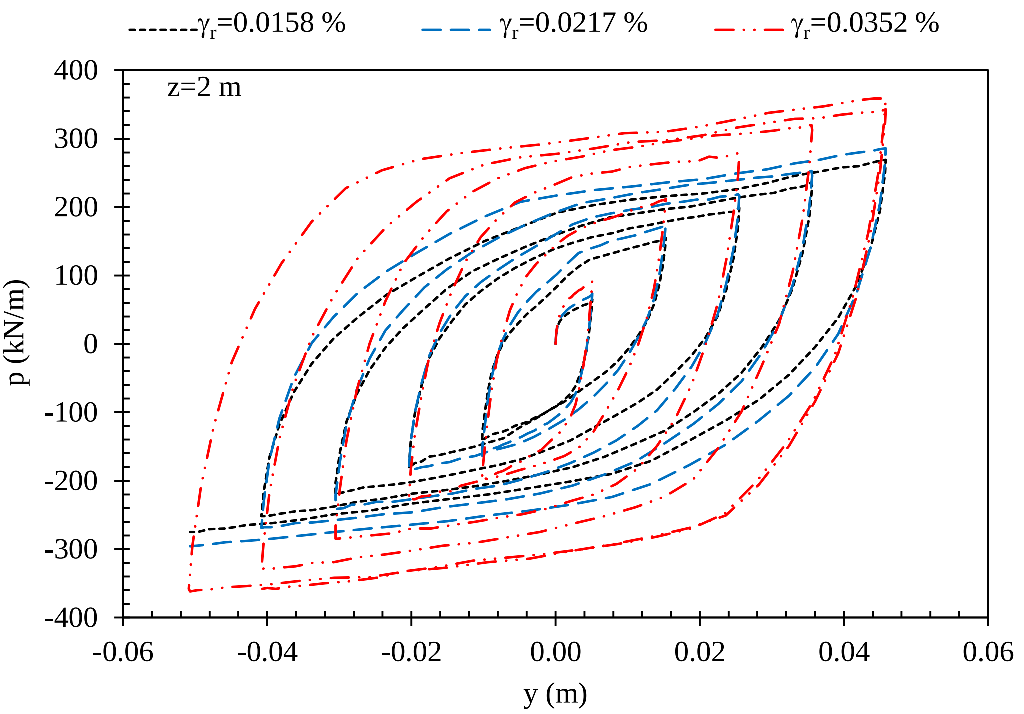

Figure 5.19 : Effect of soil nonlinearity on the cyclic *p-y* curves at z=2 m.

6. PROPOSED MODELS for STATIC and DYNAMIC p-y CURVES

The main aim of this thesis is to characterize the static and dynamic *p-y* curves based on the validated numerical analyses. The numerically derived p-y curves under static loading have been presented in Chapter 4. Similarly, dynamic p-y curves were obtained based on the numerical analyses in Chapter 5. In this chapter, the mathematical models were proposed to represent the static and dynamic p-y curves.

6.1 p-y Curves Under Static Loading

Several researchers have used the hyperbolic model after Georgiadis et al. (Georgiadis et al., 1992) to construct the *p-y* curves. The original model has two parameters: 1) the initial modulus and 2) the ultimate resistance. A similar approach was used in this thesis, but the modified hyperbolic model of Matasovic and Vucetic (Matasović & Vucetic, 1993) was implemented with the two additional parameters. In this model, the curves were characterized by the initial stiffness (K_{py}), the ultimate resistance (p_u), and the degree of nonlinearity parameters (β and s), as shown in equation 6.1.

$$p = \frac{K_{py}\, y}{1 + \beta\left(\frac{y}{y_{ref}}\right)^{s}} \tag{6.1}$$

In the above equation, K_{py} represents the initial pile-soil stiffness, and y_{ref} is the threshold displacement at which the behavior is linear. The normalized *p-y* curves show the two sources of nonlinearity: 1) the soil modulus (E_{50}) and 2) the confining stress (or depth). As the soil modulus (E_{50}) reduces, the pile-soil stiffness decreases, and more non-linear behavior is observed. A similar effect was shown for the depth in Figure 4.8, Figure 4.11, Figure 4.13, and Figure 4.15. Lower normalized resistances at a constant displacement indicated that a larger displacement was required to reach the same ultimate resistance. This behavior can be considered using the concept of reference displacement, which is the ratio of ultimate resistance to initial pile-soil stiffness ($y_{ref}=p_u/K_{py}$).

6.1.1 Ultimate lateral resistance (p_u)

The parametric analysis results showed that the ultimate soil resistance does not linearly increase with diameter, which is consistent with the theory given by Reese et al.(Reese et al., 1974). The numerical analysis results at shallow depths were consistent with the mentioned study, but the agreement was poor for greater depths, and the ultimate resistances were higher in the analyses. The higher soil resistances at greater depths were observed in centrifuge tests (Barton et al., 1983; Lu et al., 2021), and modified equations have been suggested (Fleming et al., 2008; Thieken et al., 2015; Varun, 2010; L. Zhang et al., 2005). The ultimate soil resistances obtained in the numerical analyses were higher than those obtained using the literature (Broms, 1964; Fleming et al., 2008; Reese et al., 1974). In contrast, the DIN 4085 (DIN, 2011) was relatively close to the values in this thesis, especially for greater depths (for $z>1D$). A similar agreement was shown in the finite element analysis results published by Thieken et al. (2015). However, DIN 4085 (DIN, 2011) yields lower ultimate lateral soil resistances (p_u) at depths less than one pile diameter (for $z<1D$) than those obtained in this study. The p_u at these shallow depths is closer to the findings obtained using the equations of Reese et al. (Reese et al., 1974). Equation 6.2 was proposed for the ultimate lateral resistance p_u based on the numerical analysis carried out in this thesis. The proposed equation is similar to Fleming et al. (2008), however, the z/D term is included in the equation so that the nonlinear variation with depth and diameter is provided.

$$\frac{p_u}{D\sigma_{v0}'{K_p}^2} = \mathrm{a} + \mathrm{b} * \left(\frac{z}{D}\right)^c \tag{6.2}$$

The Matlab curve fitting tool was used to determine the parameters of equation 6.2. The nonlinear least squares method was selected for the fitting procedure. For this purpose, the variation of normalized soil ultimate resistance with normalized depth (z/D) was plotted as shown in Figure 6.1. The model parameters were determined as; a=0.591, b=0.449, and c=0.824 based on the fitting process.

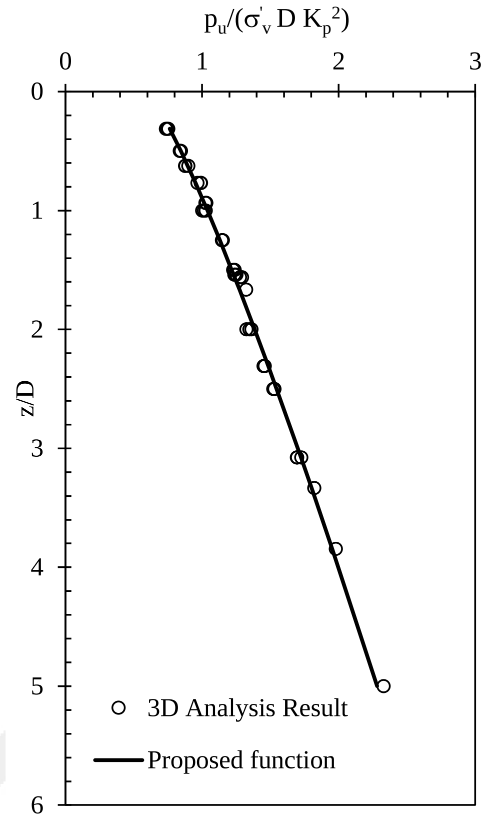

Figure 6.1 : The variation of ultimate soil resistance with normalized depth under lateral load (pile head loading).

6.1.2 Initial pile-soil stiffness (K_{py})

The suggestions made by several researchers for initial pile-soil modulus vary from 0.48E_0/D to 2.3E_0/D (Medjitna & Amar Bouzid, 2019; Scott, 1981; Sørensen et al., 2010), which linearly proportional to soil modulus. The numerical analysis results obtained in this thesis have revealed that the soil-pile stiffness is not linearly varying with depth and pile diameter. Figure 6.2 shows the normalized p-y curves for different pile diameters when $K_{py}=E_0$. According to Figure 6.2, the pile-soil stiffness should be greater as the diameter increases. This result indicates that the pile diameter should be included in the soil-pile stiffness equation.

Apart from the pile diameter effect, the results have shown that K_{py} is greater than E_0 at shallow depths and less than E_0 at greater depths. Normalized p-y curves were plotted in Figure 6.3 to show the effect of depth (z) for a given pile diameter (D=1.0 m). Therefore, a non-linear increase in soil-pile stiffness should be provided to accurately reflect the depth effect and pile diameter.

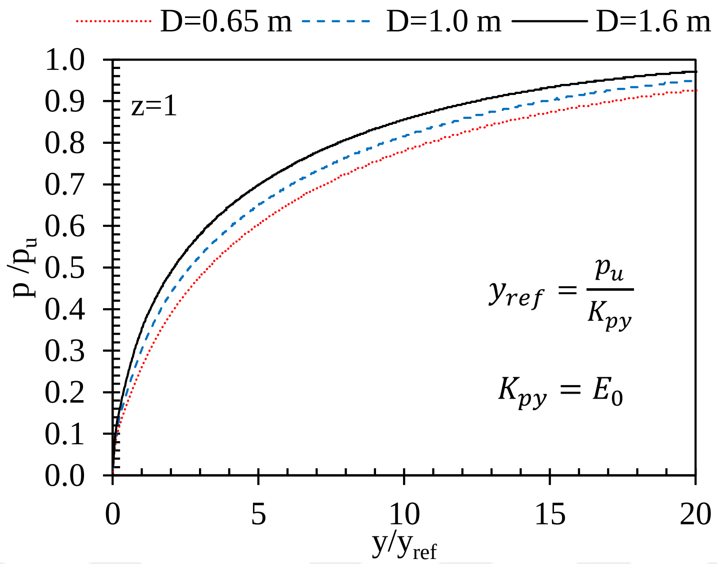

Figure 6.2 : Normalized p-y curves at z=1 m for different pile diameters when $K_{py}=E_0$.

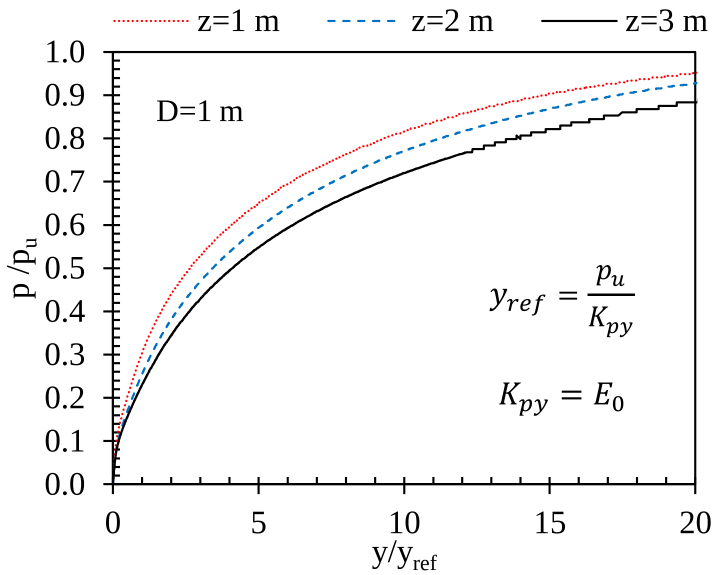

Figure 6.3 : Normalized p-y curves for D=1 m at different depths when $K_{py}=E_0$.

In this thesis, equation 6.3 is proposed for pile-soil stiffness, K_{py}:

$$K_{py} = E_0 * \left(\frac{D}{z}\right)^{\alpha} \tag{6.3}$$

where E_0 is the small strain soil modulus, D is the pile diameter, z is the depth, and α *the* parameter represents the nonlinear variation with the depth and pile diameter.

The effect of α values on the normalized p-y curves has been investigated. The best fit is obtained when α =0.4. This value provides almost identical normalized p-y curves for different pile diameters and depths. Figure 6.4 and Figure 6.5 show the normalized p-y curves using the proposed equation of pile-soil stiffness for various pile diameters and depths, respectively.

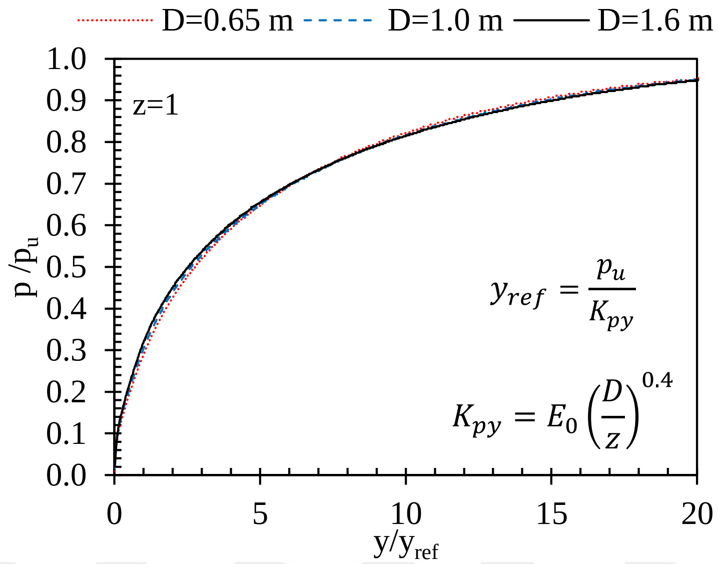

Figure 6.4 : Normalized p-y curves at z=1 m for different pile diameters using the proposed soil-pile stiffness equation.

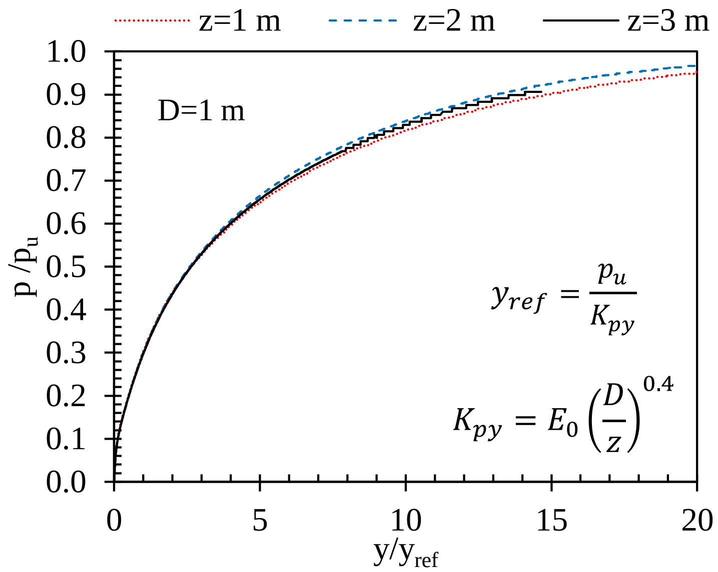

Figure 6.5 : Normalized p-y curves for D=1 m at different depths using the proposed soil-pile stiffness equation.

Equation 6.3 allows K_{py} to vary with depth not as sharply as in E_0. This fact ensures that the nonlinearity of *p-y* curves is greater than the soil nonlinearity. *D/z* term causes the K_{py} to increase to a certain extent as the depth increases. The power α in the equation limits the increase of K_{py} with depth and prevents the sharp increase. A similar result was presented by Gerolymos and Gazetas (2006) for the translational stiffness of caisson foundations. Therefore, Equation 6.3 provides the K_{py} increase slightly with depth, causing the reference displacement (y_{ref}) to be mainly controlled by the ultimate soil resistance.

6.1.3 Degree of nonlinearity (β and s)

Atkinson (2000) stated that the peak stress and degree of nonlinearity, including the initial stiffness and stiffness degradation, should characterize soil behavior. A similar concern can be followed for the characterization of the *p-y* curves. The proposed equations for ultimate lateral resistance (p_u) and initial stiffness (K_{py}) predict the response of the piles at large and very small displacements. Furthermore, the piles' small to moderate displacement behavior can be controlled by the nonlinearity parameters: β and *s*. The power s controls the slope after the first yield, and a constant value of 0.7 is proposed in this study to fit the analysis results. Table 6.1 shows the β values for the parameters analyzed in this study. The variation of β with the degree of nonlinearity value (E_0/E_{50}) is given in Figure 6.6.

Table 6.1 : Degree of nonlinearity parameters.

E_0/E_{50}	5	10	20
β	1.8	2.3	2.85
s	0.7	0.7	0.7

Equation 6.4 is proposed in this thesis for the degree of nonlinearity of β depending on the E_0/E_{50}.

$$\beta = \left(\frac{E_0}{E_{50}}\right)^{0.35} \tag{6.4}$$

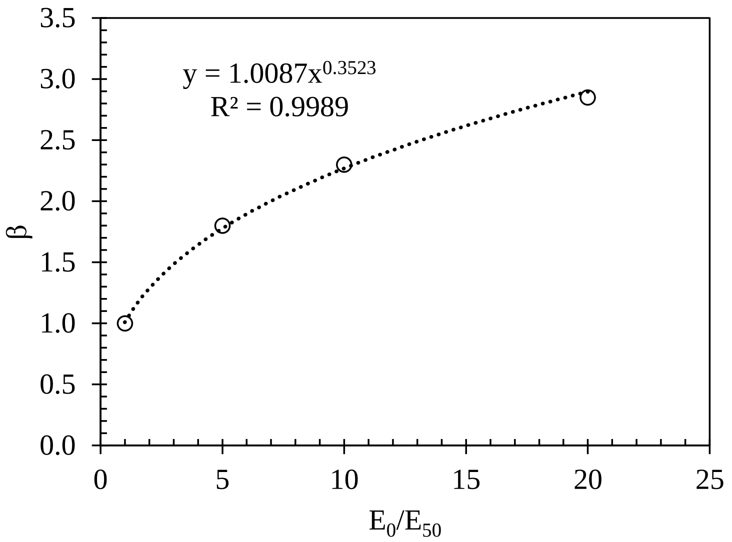

Figure 6.6 : Variation of β parameter with E_0/E_{50}.

The proposed model for the static p-y curves is summarized in Figure 6.7. The model's main advantage is the ability to consider the degree of soil nonlinearity. Besides, simple yet efficient equations were suggested for the ultimate soil resistance (p_u), and the pile-soil modulus (K_{py}). The model parameters represent the soil resistances from very small to large displacements. The proposed equations can be used to analyze the piles subject to static lateral loads. Even the pseudo-static (or nonlinear static-pushover) earthquake analysis can be performed.

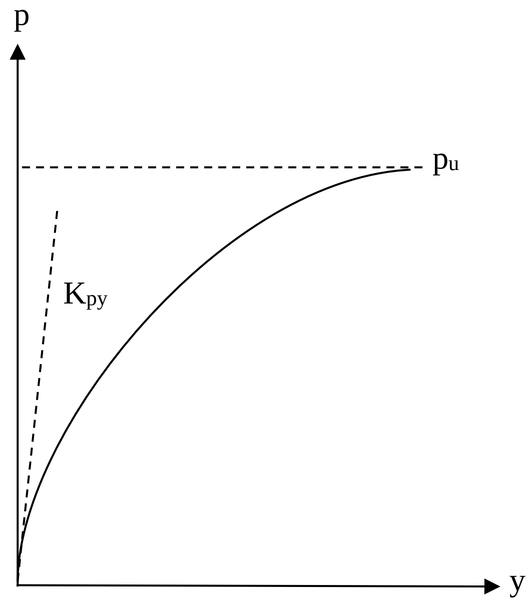

$$p = \frac{K_{py}\, y}{1 + \beta\left(\frac{y}{y_{ref}}\right)^{s}}$$

$$y_{ref} = \frac{p_u}{K_{py}}$$

$$\frac{p_u}{\sigma_{v0}' D {K_p}^2} = 0.59 + 0.45\left(\frac{z}{D}\right)^{0.82}$$

$$K_{py} = E_0 * \left(\frac{D}{z}\right)^{0.4}$$

$$\beta = \left(\frac{E_0}{E_{50}}\right)^{0.35}$$

Figure 6.7 : The proposed model for static p-y curves in sands.

6.1.4 Accuracy of the proposed model

The accuracy of the proposed static *p-y* curves can be shown by comparing the 1D model outputs with the 3D numerical analysis results. To better quantify the difference, the accuracy metric concept was used, which was defined by Burd et al. (2020) and Taborda et al. (2020) as in Equation 6.5.

$$\eta = \frac{A_{ref} - A_{diff}}{A_{ref}} \tag{6.5}$$

where the A_{ref} is the area below the reference curve, the curve obtained from the numerical analyses, and A_{diff} is the dashed area bounded by the difference between the reference curve (numerical analysis results here) and the model curve (predicted values by the proposed static *p-y* model). The definition of the areas is shown in Figure 6.8. The metric was used separately for small and large displacement ranges to assess the predictions more accurately.

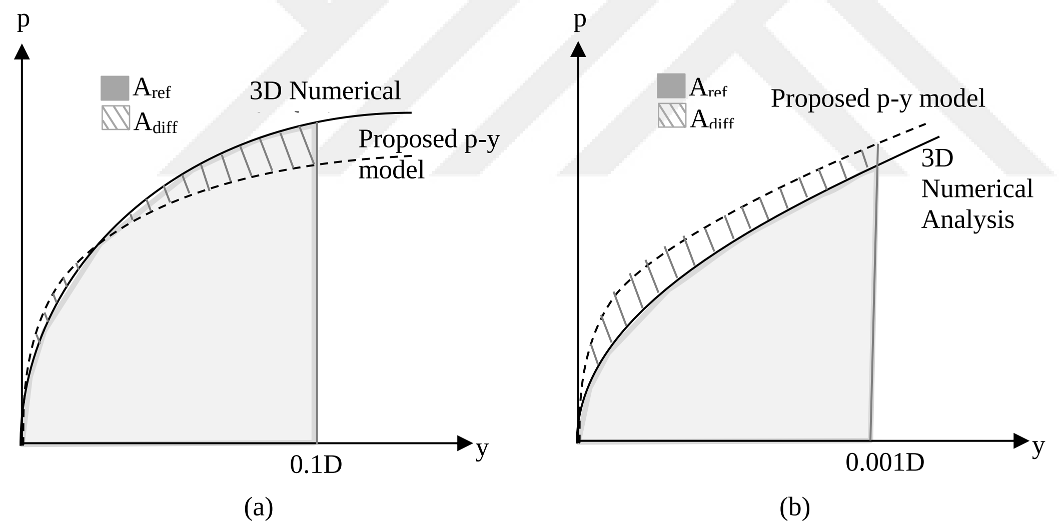

Figure 6.8 : Graphical definition of the accuracy metric: (a) large displacement; (b) small displacement range.

Figure 6.9, Figure 6.10, and Figure 6.11 compare the 3D analysis and the proposed static *p-y* models up to 10 cm (large displacement range). The vertical axis is normalized by p_u so that the curves are independent of the pile diameters and soil relative densities.

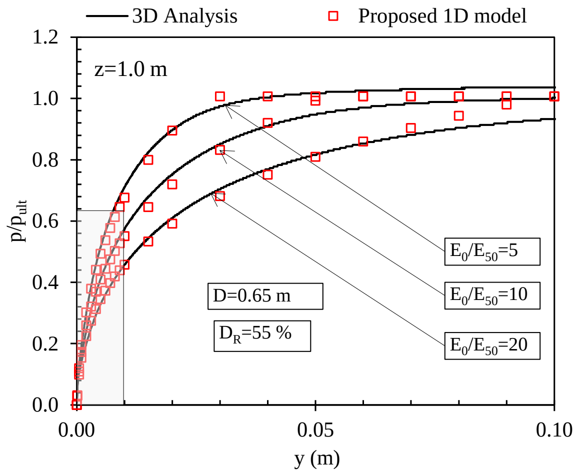

Figure 6.9 : Comparison of the *p-y* obtained in 3D analysis with the proposed model outputs for large displacement range (at z=1 m depth).

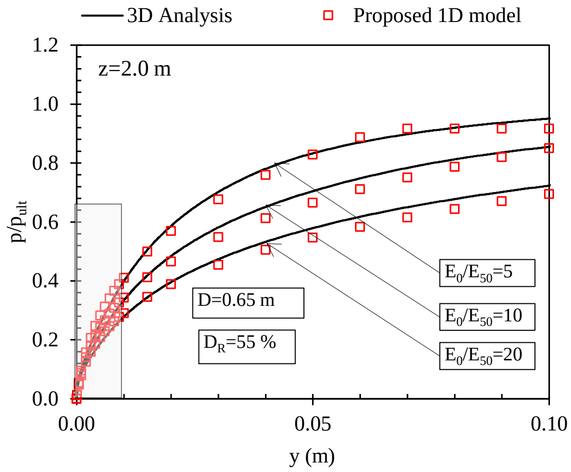

Figure 6.10 : Comparison of the *p-y* obtained in 3D analysis with the proposed model outputs for large displacement range (at z=2 m depth).

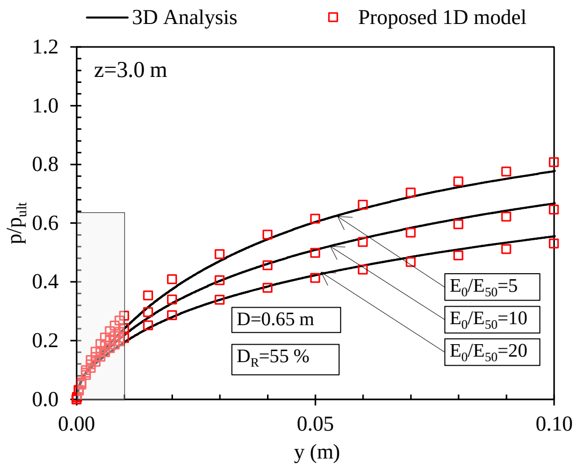

Figure 6.11 : Comparison of the *p-y* obtained in 3D analysis with the proposed model outputs for large displacement range (at z=3 m depth).

The accuracy metric (η) concept (Eq. 6.6) was used to show the difference between the 3D numerical analysis and the proposed model. Figure 6.12, Figure 6.13, and Figure 6.14 present the η values down to 3 m depth for the full displacement range for various soil nonlinearities. Accordingly, the η value is approximately 0.94-0.98, concluding a good agreement between the proposed *p-y* model outputs and those in 3D analysis results.

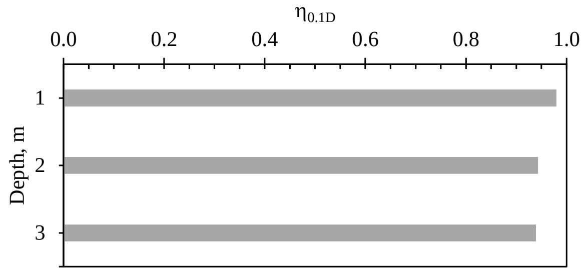

Figure 6.12 : Accuracy metric for large displacement range for E_0/E_{50}=5.

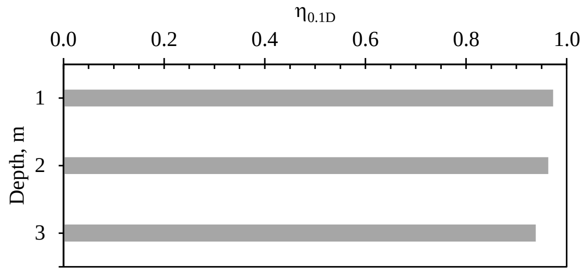

Figure 6.13 : Accuracy metric for large displacement range for E_0/E_{50}=10.

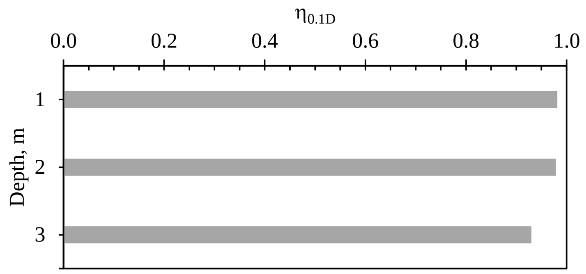

Figure 6.14 : Accuracy metric for large displacement range for E_0/E_{50}=20.

Figure 6.15, Figure 6.16, and Figure 6.17 compare the 3D analysis and the proposed static *p-y* models up to 1 cm (small displacement range). Again, the vertical axis is normalized by p_u so that the curves are independent of the pile diameters and soil relative densities.

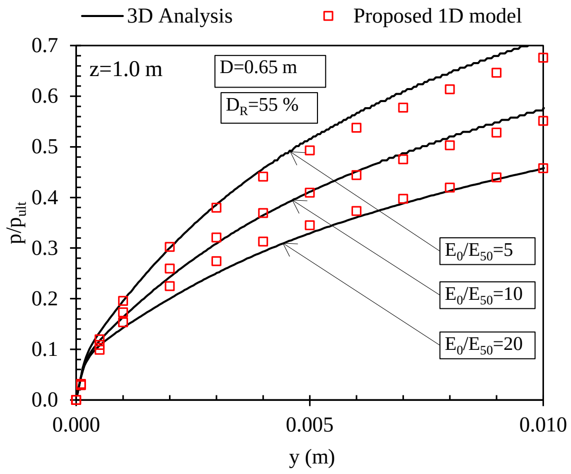

Figure 6.15 : 3D analysis results with the proposed 1D model for small displacement range (at z=1 m depth).

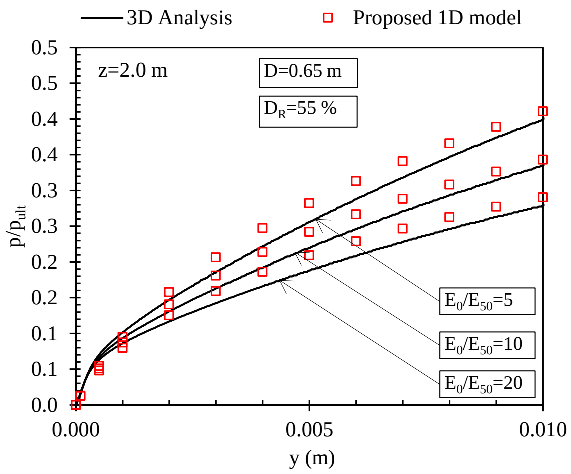

Figure 6.16 : 3D analysis results with the proposed 1D model for small displacement range (at z=2 m depth).

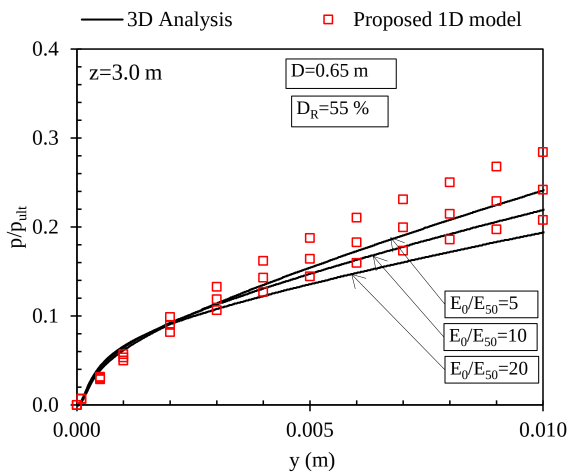

Figure 6.17 : 3D analysis results with the proposed 1D model for small displacement range (at z=3 m depth).

The accuracy metric (η) was applied to show the difference for the small displacement range. Figure 6.18, Figure 6.19, and Figure 6.20 present the η values down to 3 m depth for the small displacement range. The η value is around 0.72-0.80 for E_0/E_{50}=5 (low soil nonlinearity), while it is as low as 0.65 at 3 m depth for E_0/E_{50}=20.

In general, the predicted values by the proposed model agreed well with the *p-y* values obtained through 3D numerical analysis results. However, the proposed model is not as close to 3D analysis in the small displacement range as in the large displacement range. Especially the difference becomes more pronounced for greater depths, and future studies must focus on improving the behavior for small displacement ranges.

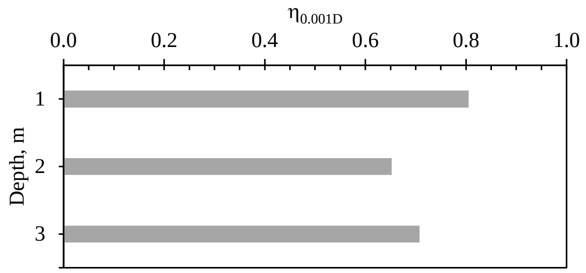

Figure 6.18 : Accuracy metric for small displacement range for E_0/E_{50}=5.

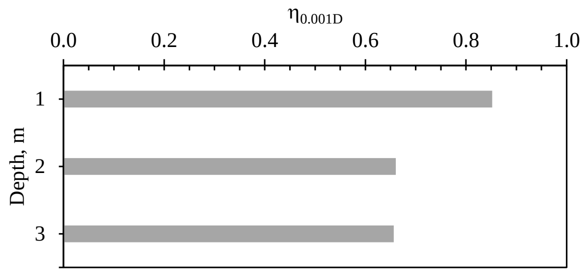

Figure 6.19 : Accuracy metric for small displacement range for E_0/E_{50}=10.

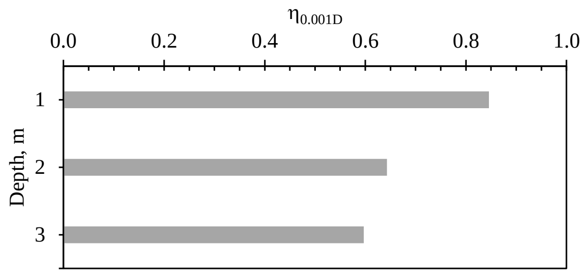

Figure 6.20 : Accuracy metric for small displacement range for E_0/E_{50}=20.

6.1.5 Validation of the proposed model

A validation study was performed by comparing the results obtained using the proposed *p-y* curves with the field and laboratory measurements for the laterally loaded pile tests in the literature (Georgiadis et al., 1992; Reese et al., 1974). The sketch of a typical laterally loaded pile problem is shown in Figure 6.21a, together with the finite element model created in structural analysis software (Figure 6.21b).

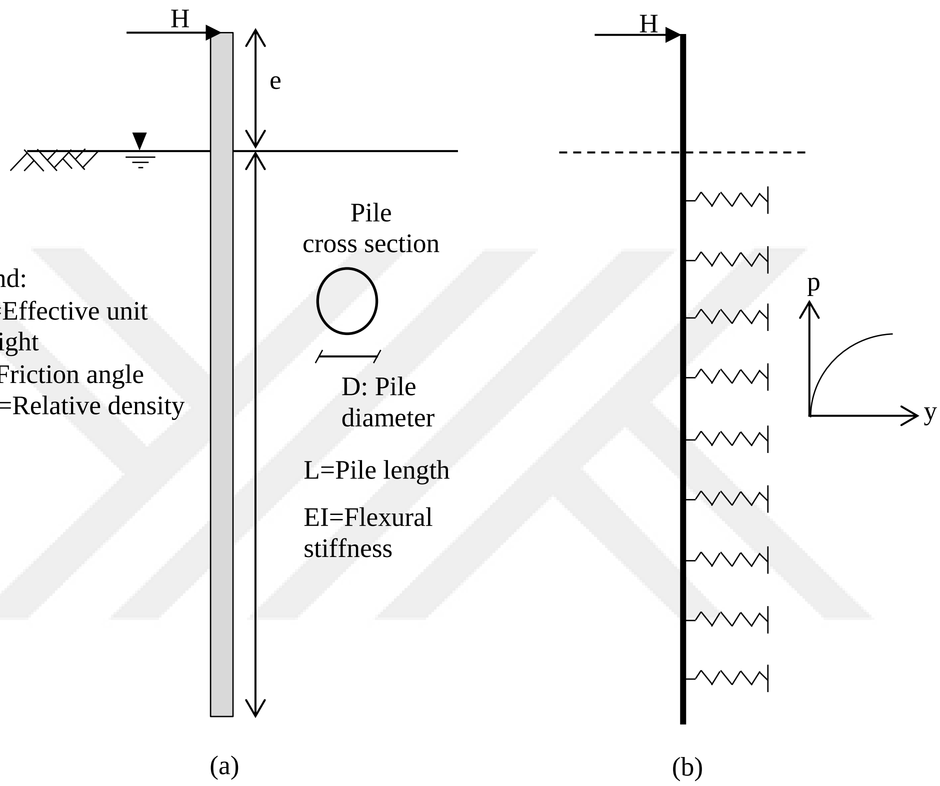

Figure 6.21 : (a) Sketch of a typical laterally loaded pile problem (b) Finite element model.

A beam element was used for the pile, and the soil reaction was represented by nonlinear links (*p-y* curves) placed at 0.5 m intervals along the pile. In the *p-y* curve formulation, equation 3.6 were used for the small strain modulus of soil. Equation 6.2 and Equation 6.3 have been implemented for p_u and K_{py}, while the nonlinearity parameter s=0.7. Although the degree of nonlinearity depends on the relative density of cohesionless soils, a constant value was adopted for the nonlinearity parameter (β=2.3). Table 6.2 presents the soil and pile properties with the loading condition.

Table 6.2 : The pile load tests used for the validation of the proposed model.

		Soil Properties			Pile Properties			Load	
Reference	Test	γ' (kN/m^3)	D_R (%)	ϕ (°)	D (m)	L (m)	EI (MN.m^2)	H (kN)	e (m)
Reese et al. (1974)	Field	10.4	90	39	0.61	21	163	210	0.305
Georgiadis et al. (1992)	Centrifuge	16.3	60	36	1.224	9	2495	1304	1.25

The differential equation for the laterally loaded pile problem is given in the equation. 6.6.

$$\frac{d^2}{dz^2}\left(E_p I_p \frac{d^2 y}{dz^2}\right) - k_h y - W = 0 \tag{6.6}$$

where EI is the flexural stiffness, z is the depth along the pile axis, W is the lateral load distributed along the pile, k_h is the secant stiffness, and y is the pile deflection.

The geometry of the soil-pile interaction problem was created, and the pile and soil (*p-y* curve) properties were assigned accordingly based on the data in Table 6.2. Link elements were used for the interface with the multilinear plastic option. The lateral load was applied to the pile head, and the analyses were performed in SAP2000 (CSI, 2016) to solve equation 6.7. As the soil resistance-pile displacement relation is achieved using p-y curves, a nonlinear analysis is required for the solution. The Newton-Raphson method was used in SAP2000 for the iteration in nonlinear analysis. The maximum iteration in each step was 40, and the convergence tolerance was set to 1e-4.

The bending moments obtained along the pile were compared with the measurements from the tests in Figure 6.22. According to the results, the bending moments along the pile were reasonably close to the measured bending moments. The bending moments were also computed using the *p-y* curves by API (2007) and presented in Figure 6.22 for comparison. The maximum bending moments (M_{max}) predicted by the proposed model and API (2007) were similar. However, bending moments along the pile at deeper levels estimated by API (2007) were generally underpredicted compared to the test results and those estimated by the proposed model. Hence, the proposed model better represents the response at deeper levels.

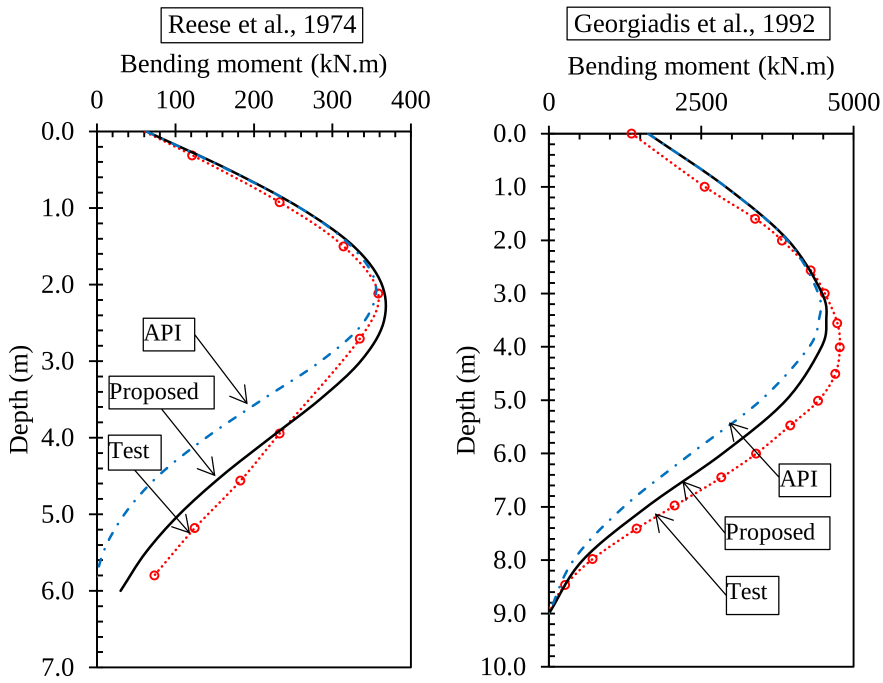

Figure 6.22 : Bending moment variation in the validation analyses with the field tests.

Furthermore, the pile head load-deflection curves obtained by the numerical analyses were compared with the test results (Figure 6.23 and Figure 6.24). In general, the load-deflection curves predicted by the proposed model agreed with the test results. However, the deflections obtained by API (2007) curves were significantly underpredicted, especially when compared with the measurements of centrifuge tests by Georgiadis et al. (1992), where the applied load was relatively higher. The stated result confirms the shortcoming of the high initial stiffness of API (2007), which was already stated in past studies. The proposed static p-y curves significantly improve the predicted deflections, particularly at larger loads.

Although the pile displacements were not predicted accurately by API in Georgiadis et al. (1992), a reasonably close result was obtained for the maximum bending moment. The selected p-y curves influence the displacements directly, but the bending moments may not be sensitive to the pile displacements for pile head loading. However, a performance-based design methodology has been adopted recently, which requires the assessment of the pile and the structural displacements. The proposed model better predicts the displacements that might be important, especially for piles subjected to high lateral loads and/or embedded in loose to medium-dense cohesionless soils.

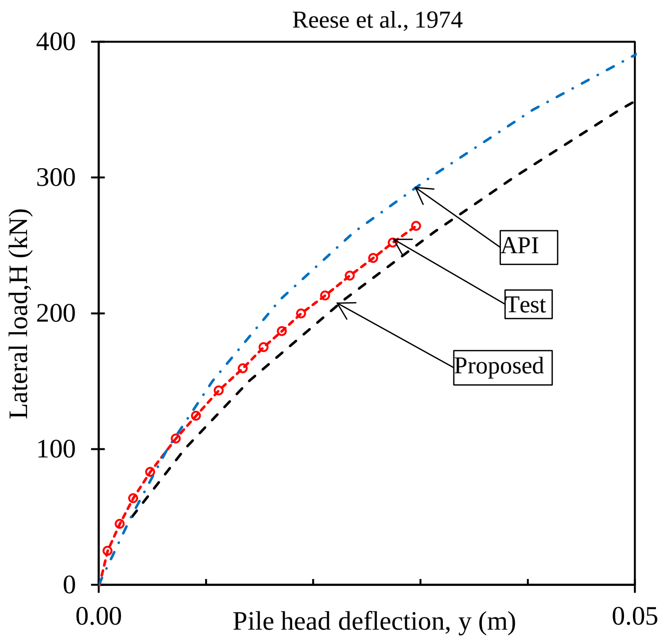

Figure 6.23 : Lateral load-deflection curves obtained through the 1D analyses and test results for the field test given Reese et al. (1992).

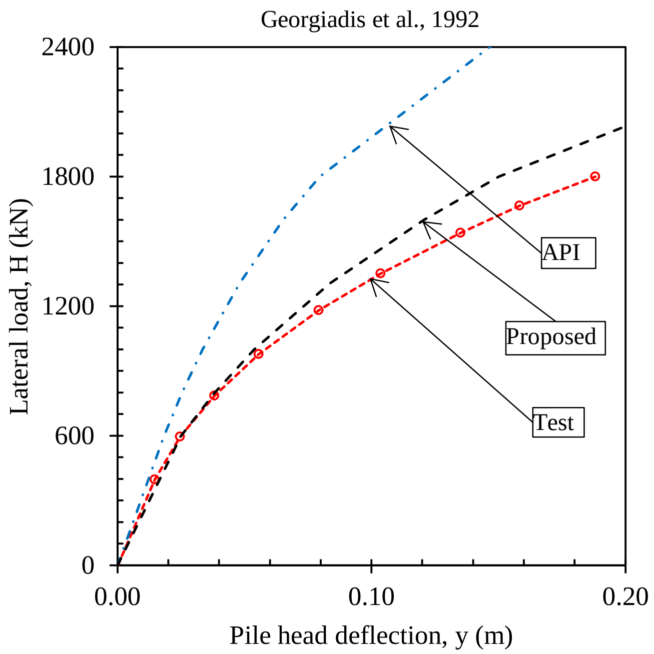

Figure 6.24 : Lateral load-deflection curves obtained through the 1D analyses and test results for the centrifuge test given in Georgiadis et al. (1992).

6.2 p-y Curves Under Dynamic Loading

The numerical analysis have shown that the dynamic *p-y* curves in cohesionless soils have three significant characteristics: Initial stiffness, ultimate lateral resistance, and degree of nonlinearity. The backbone curve and the unloading/reloading rule represent the behavior of soils under dynamic loading. A similar approach can be applied to dynamic *p-y* curves. The backbone curve formulation was proposed in this thesis, and Masing's rule was adopted for unloading/reloading behavior.

Three models have been widely used for nonlinear soil behavior: Ramberg&Osgood, Hyperbolic, and Bouc-Wen model. Researchers have used Ramberg&Osgood (1943) model for modeling the soil behavior under dynamic loads. However, since the stress-based approach is adopted, the model is not sensitive to the initial modulus (Gohl, 1991). The most used method in soil dynamics for nonlinear soil behavior is the Hardin-Drnevich (1972) model, extending Kondner's (1963) model to the dynamic loading case. It requires two parameters: Initial stiffness and ultimate resistance. The model was further developed to consider the soil nonlinearity more realistically, and the modified Kondner&Zelasko (MKZ) model was proposed by Matasovic (1993) by including two additional curve fitting parameters (β and s). More recently, Bouc-Wen (Bouc, 1971; Wen, 1976) model has been used to characterize the soil behavior under dynamic loading (Gerolymos & Gazetas, 2005). Several researchers adopted the approaches mentioned above for nonlinear soil behavior to dynamic p-y curves, which are summarized in Table 6.3.

The Bouc-Wen model is used in this thesis to construct the backbone of dynamic *p-y* curves. The model requires the initial stiffness (K_{py}), the ultimate resistance (p_u), and the degree of nonlinearity parameter (n). The proposed equations for these parameters are given in the following sections.

The accuracy of the proposed model is shown by comparing the results with the 3-dimensional analysis outputs. Furthermore, the validity of the proposed model was demonstrated by implementing the proposed curves in the simulation of centrifuge tests. Besides, additional numerical analyses are carried out in FLAC^{3D} with the selected earthquake records, and the soil-pile-structure interaction analyses are compared with the proposed model and API results.

Table 6.3 : The models used in the literature for dynamic p-y curves.

Model	Ramberg&Osgood	Hyperbolic model	Bouc-Wen model
p-y form	$p = \dfrac{k_h\, y}{1 + a\left(\dfrac{p}{p_u}\right)^{r-1}}$	$p = \dfrac{y}{\dfrac{1}{k_{ini}} + \dfrac{y}{p_u}}$	$p = \alpha K_{py} y + (1-\alpha) p_u \xi$ $d\xi = \left(A - \lvert\xi\rvert^n (b + g\, sgn\,(dy\,\xi))\right) \dfrac{dy}{y_{ref}}$ $d\xi = (A - \lvert\xi\rvert^n) \dfrac{dy}{y_{ref}}\ for\ monotonic\ loading$
Definitions	α and r are the constants	k_{ini}= initial stiffness p_u: lateral load capacity	k_{ini}= initial stiffness p_u: lateral load capacity ξ: degradation function
Used by	Desai and Kuppusamy (1980); Gohl, (1991)	Georgiadis,(1992); Lim and Jeong, (2018)	Gerolymos,(2006); Varun,(2010); Varun et al. (2013)

6.2.1 Initial pile-soil stiffness

The initial pile-soil stiffness represents the small displacement behavior of the soil-pile interface. Since the HS-Small model is used for the static p-y curves, which employs the small-strain stiffness, the equation proposed for the static p-y curves can also be used for initial pile-soil stiffness for dynamic p-y curves.

6.2.2 Ultimate soil resistance

Most of the studies about dynamic *p-y* curves have adopted the API relation for ultimate soil resistance (p_u). Fleming et al. (2008) proposed a simple equation (higher at shallow depths), where $D\sigma'_{v0}$ normalized the ultimate resistance. However, p_u was linearly dependent on the depth in Fleming et al. (2008), contradicting the findings in this study. Furthermore, it was recognized in this thesis that the p_u is not linearly dependent on the pile diameter (*D*) as well. The nonlinear variation complies with the theoretical results given by Reese et al. (1974). Therefore, Fleming's (2008) suggestion is modified in this study, and equation 6.7 is proposed to consider the depth and pile diameter better.

$$\frac{p_u}{D\sigma_{v0}' {K_p}^{1.5}} = \mathrm{a} + \mathrm{b} * \left(\frac{z}{D}\right)^c \tag{6.7}$$

Equation 6.8 includes the normalized depth (*z/D*) in the power of passive earth pressure coefficient K_p, which provides the nonlinear variation with depth and diameter. The Matlab Curve fitting tool was employed to determine the model parameters and fitting procedure yields: a=1, b=0.639, and c=0.815. The comparison of the data obtained through 3D analysis with the proposed equation is given in Figure 6.25. It should be stated that the loading condition is a key factor affecting the ultimate resistance. The proposed equation was derived from the numerical analyses where the pile was subjected to rigid lateral movement. However, pile head loading might provide higher resistances than the rigid pile movement since the passive resistance is generated at the back of the pile in the pile head loading. Furthermore, as the dynamic (earthquake) loadings cause both inertial and kinematic effects on the pile, the p_u values obtained by the rigid pile movement could be more accurate than the ones obtained from pile head loading.

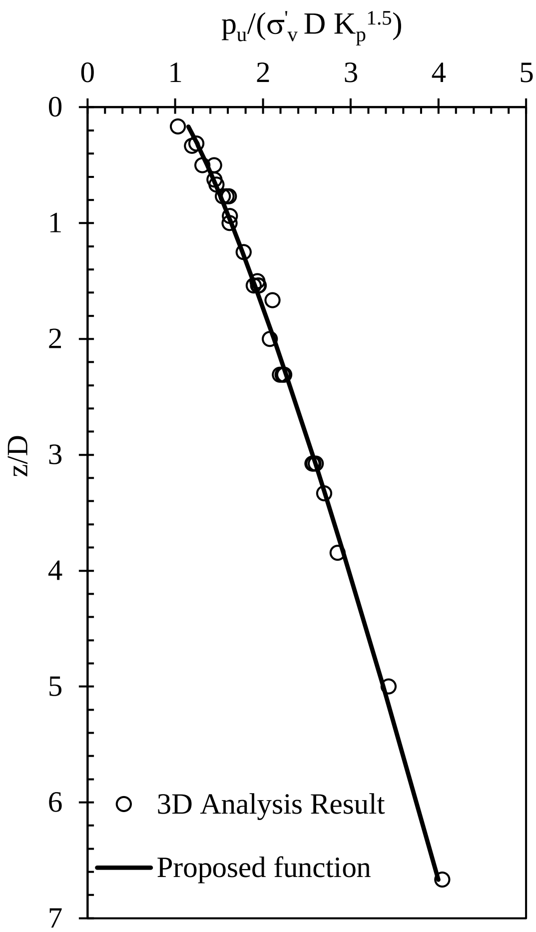

Figure 6.25 : The variation of ultimate soil resistance with normalized depth under lateral load (dynamic pile loading).

6.2.3 Degree of nonlinearity

Dynamic *p-y* curves can be defined with the backbone curve and loading/unloading rule. The initial pile-soil stiffness (K_{py}) and the ultimate soil resistance (p_u) are the key parameters to represent the very small and the large displacement behavior, respectively. Besides, the backbone curve formulation should include the degree of nonlinearity for moderate displacement levels.

This study used Wen (1976) model to describe the nonlinear dynamic *p-y* curves. Equation 6.8 defines the nonlinear relation as follows:

$$p = \alpha K_{py} y + (1-\alpha) p_u \zeta \tag{6.8}$$

where the parameter α is the post-yielding ratio.

The degradation parameter ζ in equation 6.8 describes the nonlinear relation, and Equation 6.9 is suggested by Wen (1976) for ζ in a differential form. The parameter n in the equation controls the degree of nonlinearity. The parameters β and γ govern the unloading/reloading behavior, where $\beta=\gamma=0.5$ corresponds to the Masing (1926) criteria.

$$d\zeta = \left(A - |\zeta|^n (\beta + \gamma \; sgn \; (dy \; \zeta))\right) \frac{dy}{y_{ref}} \tag{6.9}$$

In this study, the best fit to the numerical analysis results is obtained with α=0, while the parameter n depends on the confining stress (Equation 6.10).

$$n = 0.12 \left(\frac{\sigma'_m}{p_a}\right)^{0.34} \tag{6.10}$$

Equation 6.11 can be rewritten using the relation between the confining stress and reference strain (using equation 3.11). Therefore, the degree of nonlinearity parameter can be written in terms of the reference strain of soil (Equation 6.11). The schematic view of the proposed model is given in Figure 6.26.

$$n = 3.14 {\gamma_r}^{0.97} \tag{6.11}$$

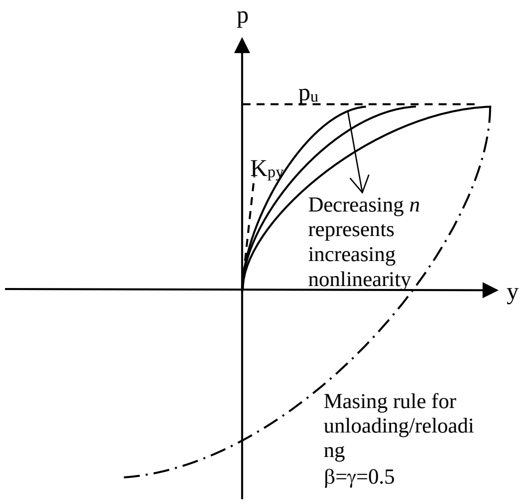

$$p = p_u \zeta$$

$$d\zeta = \left(A - |\zeta|^n(\beta + \gamma\, sgn\,(dy\,\zeta))\right)\frac{dy}{y_{ref}}$$

$$y_{ref} = \frac{p_u}{K_{py}}$$

$$\frac{p_u}{\sigma_{v0}' D K_p^{1.5}} = 1 + 0.639\left(\frac{z}{D}\right)^{0.815}$$

$$K_{py} = E_0 * \left(\frac{D}{z}\right)^{0.4}$$

$$n = 3.14{\gamma_r}^{0.97}\ (\gamma_r\ in\ \%)$$

$$\beta = \gamma = 0.5\ (\text{Masing's rule})$$

Figure 6.26 : The proposed model for dynamic p-y curves in cohesionless soils.

6.2.4 Accuracy of the proposed model

The backbone curves of the proposed model for *D*=0.65 m D_R=55% were given in Figure 6.27, Figure 6.28, and Figure 6.29, together with the p-y curves obtained in the 3D numerical analyses. According to the figures, the backbone curves are quite close to the dynamic *p-y* curves obtained by the 3D numerical models.

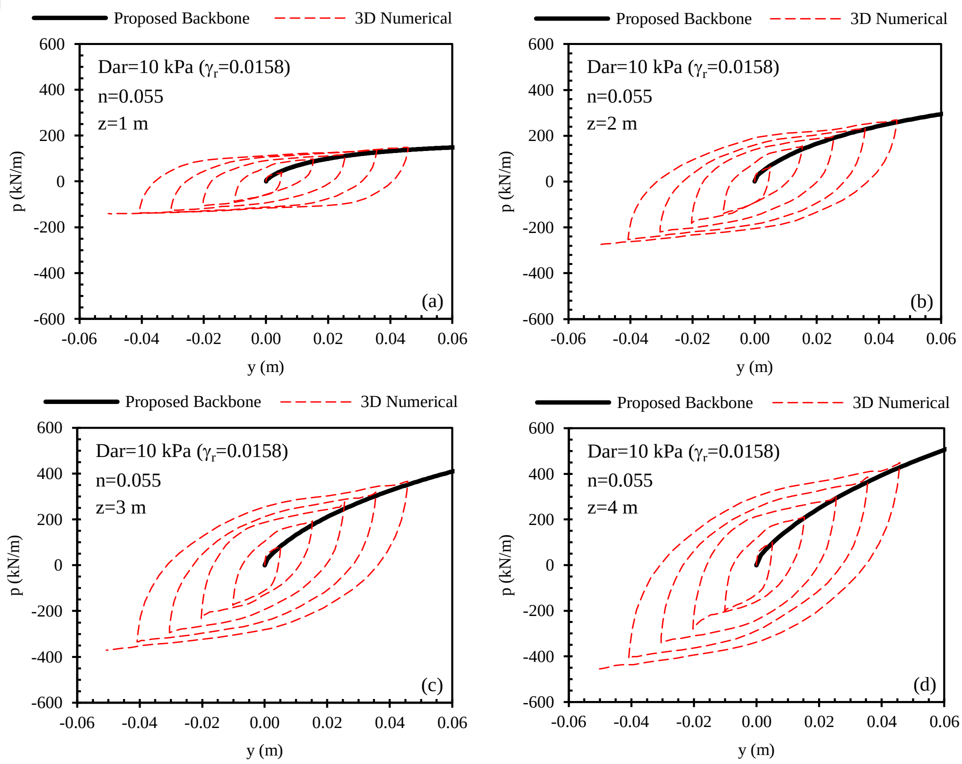

Figure 6.27 : Comparison of the proposed p-y curves and 3D numerical analyses results for D=0.65 m, D_R=55 %, and γ_r=0.0158 %.

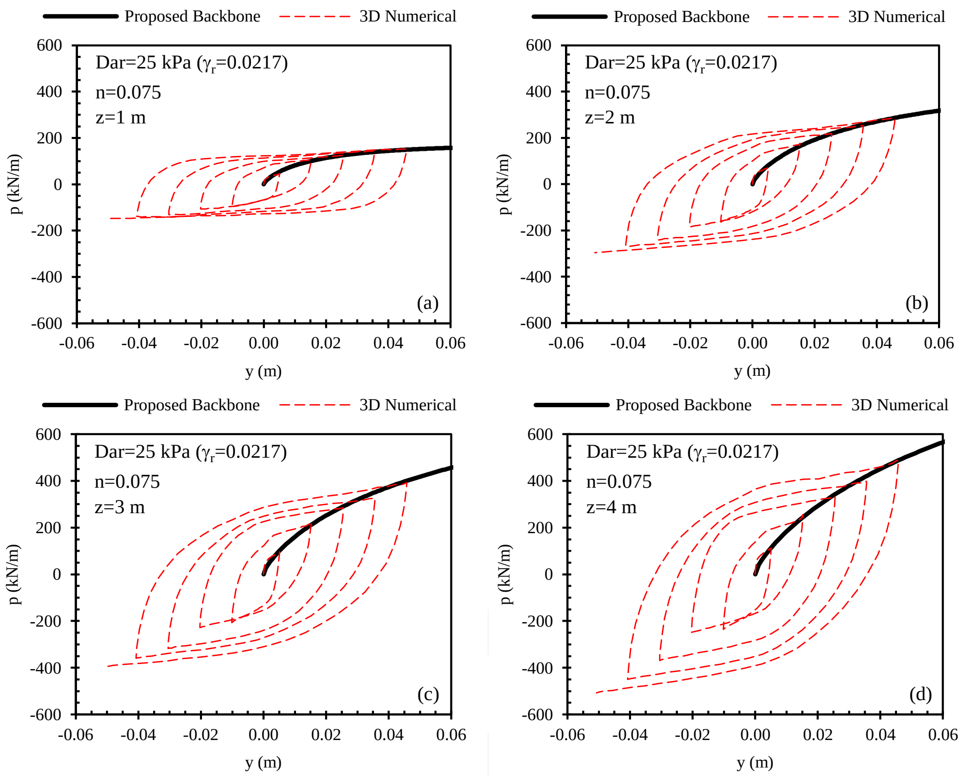

Figure 6.28 : Comparison of the proposed p-y curves and 3D numerical analyses results for D=0.65 m, D_R=55 %, and γ_r=0.0217 %.

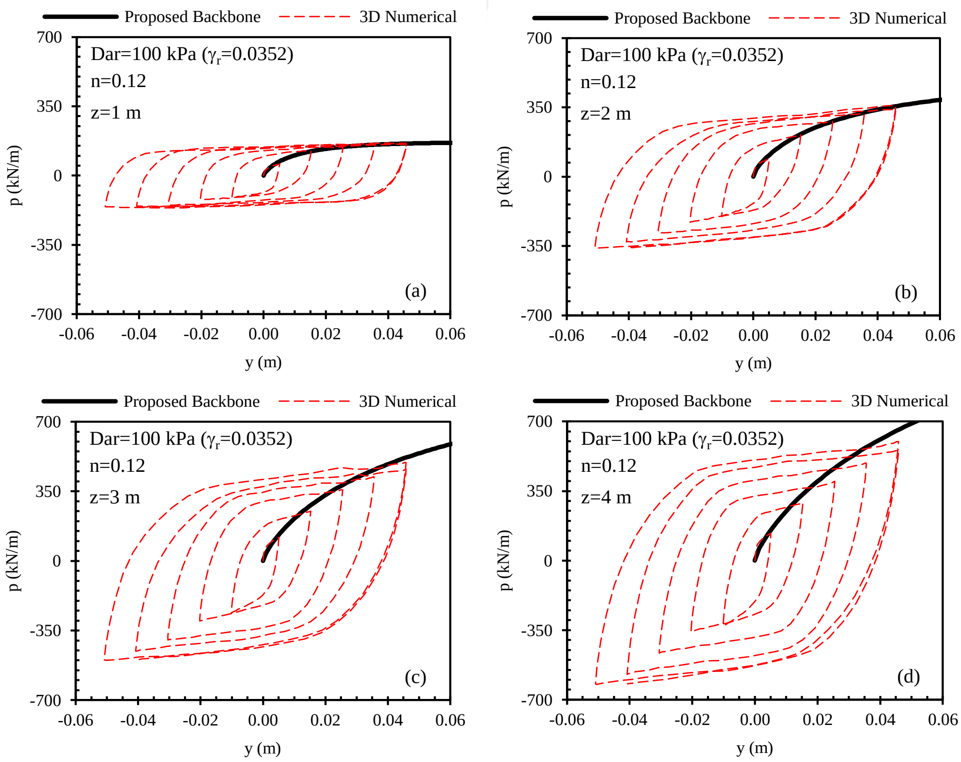

Figure 6.29 : Comparison of the proposed p-y curves and 3D numerical analyses results for D=0.65 m, D_R=55 %, and γ_r=0.0352 %.

The curves obtained with the proposed model are plotted in Figure 6.30 together with the API (n=2) for comparison. The curves in Figure 6.27, Figure 6.28, Figure 6.29 were obtained using the fourth-order Runge-Kutta approach since a numerical method is required for the solution.

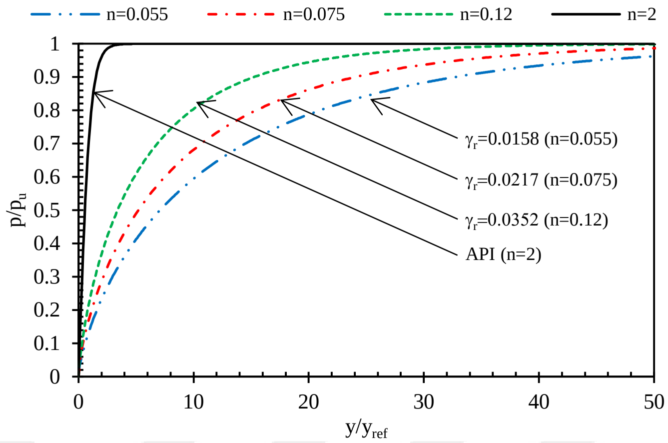

Figure 6.30 : The proposed p-y curves (p/p_u vs. y/y_{ref}) for various confining stresses compared to API.

6.2.5 Validation of the proposed model

The validation analyses for the proposed model were performed using the BNWF method (Boulanger et al., 1999). The first validation includes comparing the analysis with the centrifuge test results in the verification analyses. Besides, a new soil-single pile-structure model was created in FLAC^{3D}, and the dynamic analyses were performed under six different earthquake records.

6.2.5.1 Comparison with the centrifuge tests

The single pile models presented by Gohl (1991) and Wilson (1998) were created in the structural analysis software SAP2000 (2016). The dynamic loading in the BNWF method is the time histories of soil displacements obtained through 1D site response analyses (Step 1). First, a structural beam element was used for the single pile. Next, the soil pile interface, including the far-field and near-field elements, was created. Then, the near-field part of the interface was modeled using the nonlinear link elements with the hysteretic Wen model. Next, the far-field elements were modeled using a linear spring-dashpot link. Finally, a fully dynamic analysis was performed by applying the free field displacements to the interface elements. The schematic view of the BNWF method is shown in Figure 6.31.

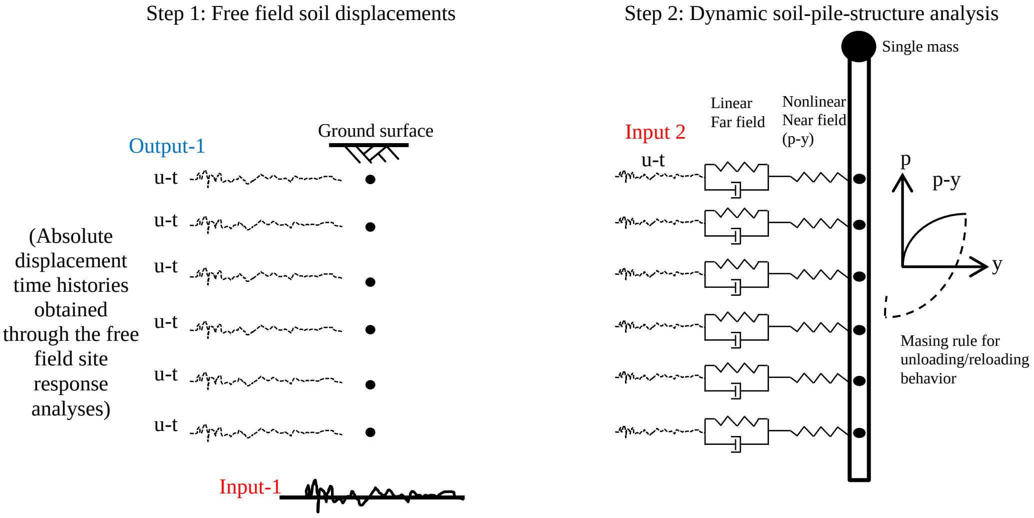

Figure 6.31 : The schematic view of the beam on nonlinear Winkler foundation method (BNWF) for pile analysis.

The dynamic backbone of *p-y* curves obtained from the numerical analyses was implemented for the near-field in validation analyses. The model has three parameters: Initial stiffness (K_{py}), ultimate resistance (p_u), and degree of nonlinearity (n). The default values for unloading/reloading parameters (β and γ) were 0.5 in Wen's model, which corresponds to Masing's criteria. API (2007) method was also employed for the near-field elements for comparison. The radiation-damping model of Gazetas and Dobry (1984) was adopted for the linear far-field element (Equation 6.12). A very high stiffness value (10^7 kN/m) was assigned to the linear (far-field) element not to increase the flexibility of the system since the radiation damping element was placed in series with the near-field (p-y) element as suggested by Wang et al. (1998).

$$\frac{c_r}{4B\rho_s V_s} = \left\{1 + \left[\frac{3.4}{\pi(1-\upsilon)}\right]^{5/4}\right\} {a_0}^{-1/4} \tag{6.12}$$

In equation 6.12, V_s is the shear wave velocity, B is the radius of the pile, and a_0 is the dimensionless frequency factor=$2\pi fB/V_s$, where f can be taken as the dominant frequency of the earthquake record.

The General Quadratic/Hyperbolic (GQ/H) model (Groholski et al., 2016) was employed in DeepSoil (2017) for free field soil displacements, as the displacement time histories of centrifuge tests were accurately captured. Figure 6.32, Figure 6.33, and Figure 6.34 show the acceleration response spectra of the motions at the ground surface obtained by 1D analyses, comparing with those in the centrifuge tests of Gohl (1991) and Wilson (1998).

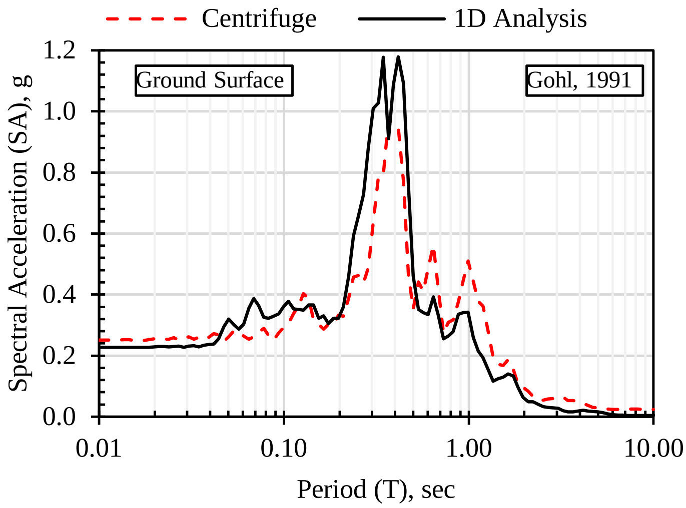

Figure 6.32 : Acceleration response spectra at the ground surface obtained from the 1D site response analyses for Gohl (1991).

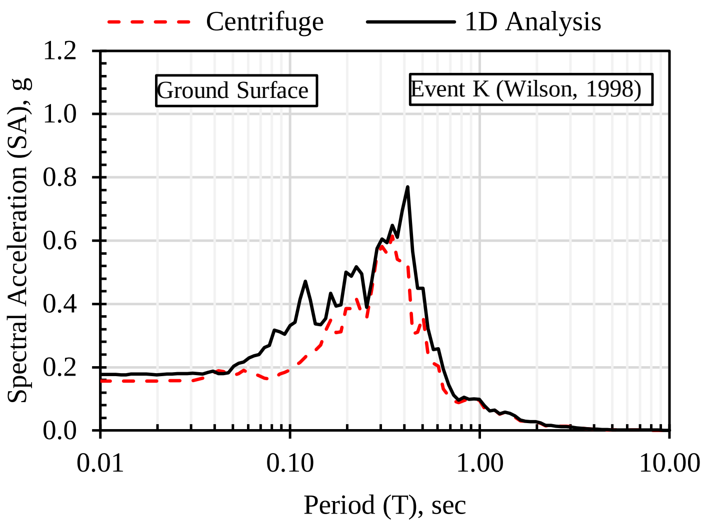

Figure 6.33 : Acceleration response spectra at the ground surface obtained from the 1D site response analyses for Event K (Wilson, 1998).

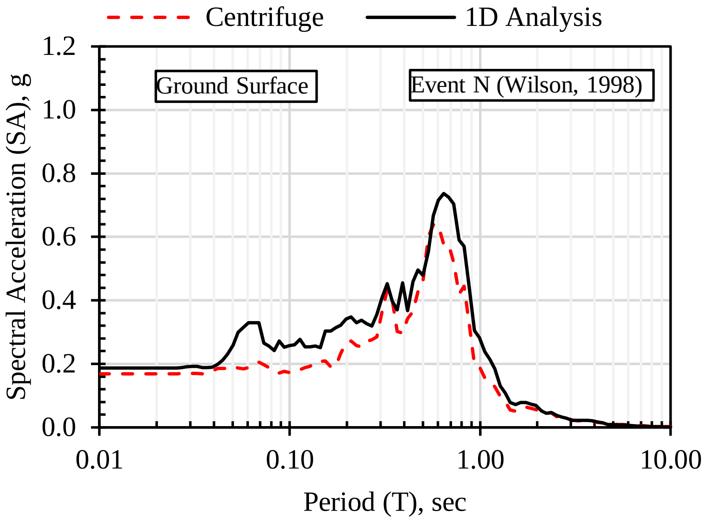

Figure 6.34 : Acceleration response spectra at the ground surface obtained from the 1D site response analyses for Event N (Wilson, 1998).

Absolute displacements from the 1D analyses were applied to the fixed end of the links, and nonlinear time history analyses were performed. The Newmark method was used for the direct integration, and the time integration parameters were γ=0.6 and β=0.3025 to provide the numerical damping as suggested by Boulanger et al. (1999). The result of the superstructure accelerations obtained in the numerical analysis was compared with the centrifuge test results by the acceleration response spectrum (ARS) in Figure 6.35, Figure 6.36, and Figure 6.37 for Gohl (1991), Event K and Event N, respectively. The figures show that the peak superstructure accelerations were close to the centrifuge test results. However, the spectral accelerations were somewhat overestimated at the low-period (T<0.8-1.0 s) region in Gohl (1991) and Event K (Wilson, 1998).

On the other hand, the accuracy for spectral accelerations was high in Event N (Wilson, 1998) for both the API (2007) and the proposed model. In this stage, the major component of the BNWF analyses was the free-field soil displacements obtained through the 1D site response analyses. The accuracy in the superstructure accelerations (especially for Event N) can be attributed to the well-estimated displacement time histories obtained in the site response analyses. Therefore, the superstructure acceleration results can be promising, especially given the complex loading sequence in the centrifuge tests.

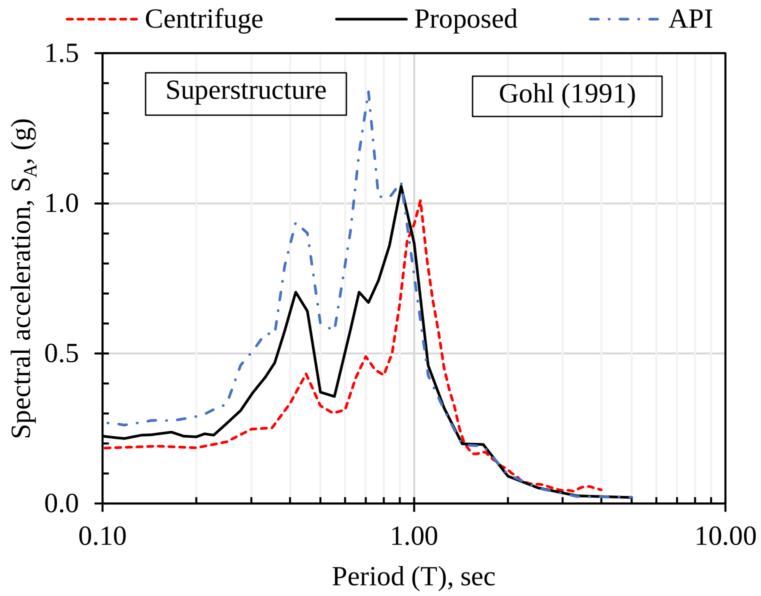

Figure 6.35 : ARS of the superstructure obtained through the BNWF method and centrifuge test results for Gohl (1991).

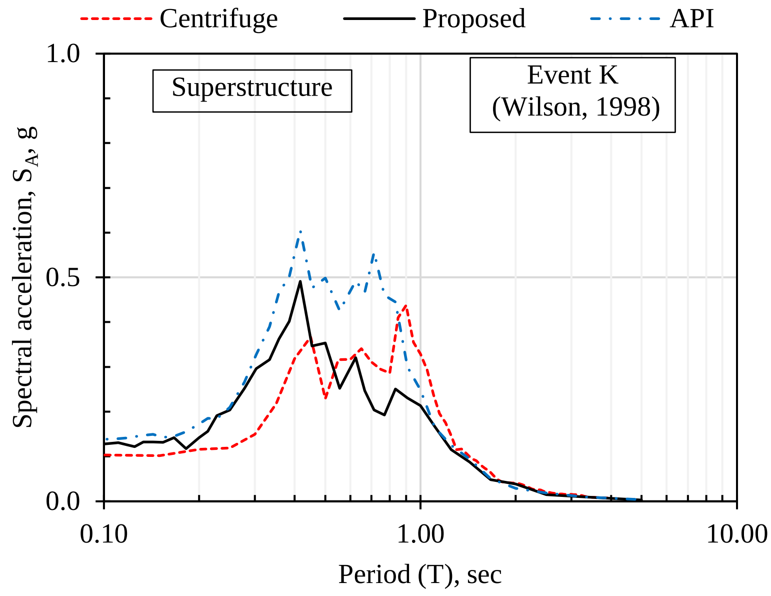

Figure 6.36 : ARS of the superstructure obtained through the BNWF method and centrifuge test results for Event K (Wilson, 1998).

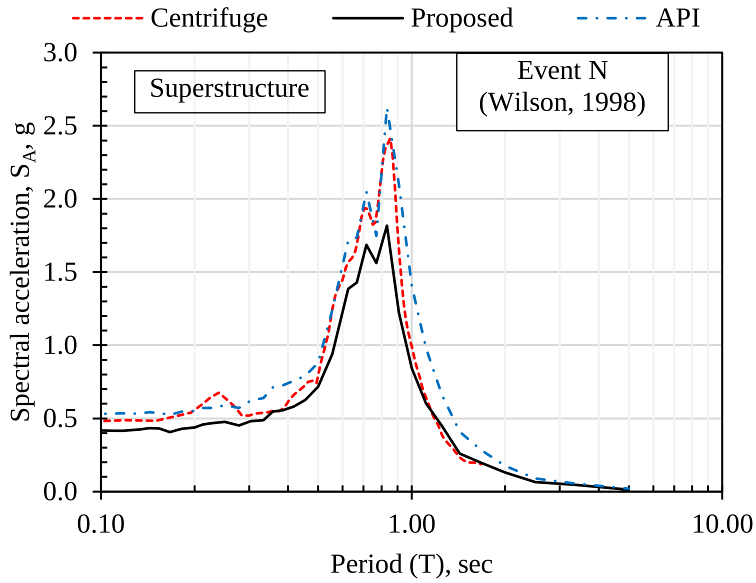

Figure 6.37 : ARS of the superstructure obtained through the BNWF method and centrifuge test results for Event N (Wilson, 1998).

The results for the variation of the maximum bending moment with depth are given in Figure 6.38. Since the maximum bending moments are directly related to the superstructure acceleration, the numerical analysis results with the proposed model were quite close to the centrifuge test results. The bending moments obtained from the numerical analyses were slightly higher than the centrifuge test results both for the proposed model and the API in Event K, where the demand was low. However, the API (2007) overestimated the bending moments in Gohl (1991) and Event N (Wilson, 1998). To sum up, the suggestion of API (2007) yields higher bending moments than the centrifuge tests for all records, particularly at higher demands.

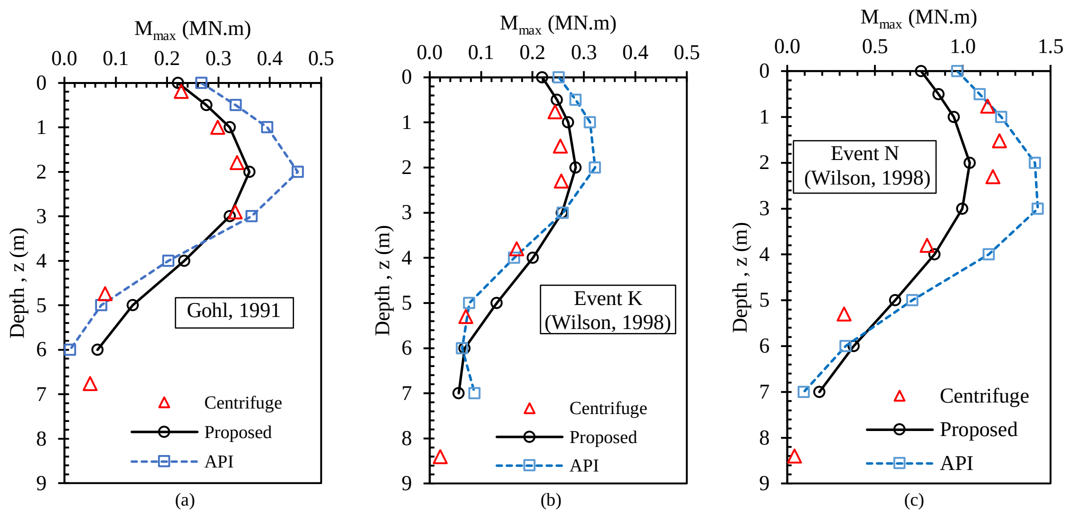

Figure 6.38 : Maximum bending moments obtained through the BNWF method and centrifuge test results.

Recent studies have shown that the Bouc-Wen model can be used effectively for dynamic *p-y* curves. This study shows that the normalized backbone is not a unique curve but varies with depth due to soil nonlinearity. The degree of nonlinearity parameter *n* for the dynamic *p-y* curves was related to the soil nonlinearity by the reference strain, and closer agreement to the centrifuge tests was achieved. However, the model parameters should be improved in future studies, as the estimated curve with the proposed parameters provides slightly lower responses than the numerical analysis results in the small displacement region.

6.2.5.2 Comparison with the 3D analyses

A new single pile-soil-structure model was created and analyzed in $FLAC^{3D}$ using the additional earthquake records. The numerical model consists of a single layer of dry cohesionless soil where D_R=55%. The unit weight of the soil was 18 kN/m^3. The friction angle and dilation angle values were 36° and 4°, respectively. The model dimensions were 20x20x30 in x, y, and z directions. The soil properties used in the verification analyses are given in Table 6.4. The bottom boundary of the model was fixed, and the lateral sides were free-field to prevent wave reflection from the model boundaries to the model.

Table 6.4 : The soil properties used in the 3D model of validation analyses.

Parameter	Value
Effective unit weight, γ' (kN/m3)	18
Relative density (%)	55
Friction angle, ϕ' (°)	36
Dilation angle ψ (°)	4
Poisson's ratio, ν	0.30

The diameter of the single pile was 0.65 m in the analyses, and the elastic modulus of concrete (E=30 GPa) was set to the pile. The pile length was 12 m, setting the slenderness ratio L/D=18 (flexible pile). A single-degree-of-freedom system was created with a column having the same properties as the pile. A 40-tonne mass was placed at the top of the 5 m high column. The fixed base natural period of the single degree of freedom system was approximately 0.5 s. The parameters for the pile and the structure used in the numerical analyses are given Table 6.5.

Table 6.5 : Pile and superstructure properties used in the numerical analyses.

Pile		Structure					
Diameter (m)	Length (m)	E (MN/m^2)	I (m^4)	Mass (Mg)	Flexural Stiffness, EI ($MN.m^2$)	H (m)	T_{fixed} (s)
0.65	16	30 000	0.00876	40	263	5.0	0.5

The earthquake records were selected from the PEER (2005) and AFAD (2022) databases, with corresponding parameters given in Table 6.6. The stations where the average shear wave velocity ($V_{s,30}$) values were minimum of 650 m/s (almost engineering bedrock) were selected so that the input motions could be directly applied to the bottom of the model. The original records were linearly scaled by the given factors (SF) such that the peak ground accelerations were around 0.15g without changing the frequency content. The acceleration time histories of the selected motions are shown in Figure 6.39.

Table 6.6 : The earthquake records used in the soil-pile-structure interaction analyses.

	Earthquake	PEER/ AFAD Code	Year	M_w	Station	Fault	R_{rup} (km)	$(V_s)_{30}$ (m/s)	Pga (g)	SF
EQ-1	Tabas, Iran	RSN143	1978	7.35	Tabas	Reverse	2	766	0.14	0.17
EQ-2	Irpinia, Italy-01	RSN285	1980	6.90	Bagnoli Irpinio	Normal	8	650	0.13	1.0
EQ-3	Taiwan SMART1(45)	RSN572	1986	7.30	SMART1 E02	Reverse	51	672	0.14	1.0
EQ-4	Loma Prieta	RSN769	1989	6.93	Gilroy Array #6	Reverse Oblique	18.3	663	0.13	1.0
EQ-5	Northridge-01	RSN1091	1994	6.69	Vasquez Rocks Park	Reverse	24	996	0.15	1.0
EQ-6	Kobe, Japan	RSN1108	1995	6.9	Kobe University	Strike slip	0.9	1043	0.15	0.56
EQ-7	Kocaeli, Turkey	RSN1161	1999	7.6	Gebze	Strike slip	10.9	792	0.15	0.58
EQ-8	Chi-Chi, Taiwan	RSN1206	1992	7.62	CHY042	Reverse Oblique	28	665	0.15	1.5
EQ-9	Duzce, Turkey	RSN1613	1999	7.14	Lamont 1060	Strike Slip	26	782	0.16	3.0
EQ-10	Elazig, Turkey	A4404	2020	6.8	Pütürge, Malatya	Strike Slip	25	1380	0.15	0.625
EQ-11	Samos, Greece	A3514	2020	6.6	Bayraklı, İzmir	Normal	77	836	0.15	2.63

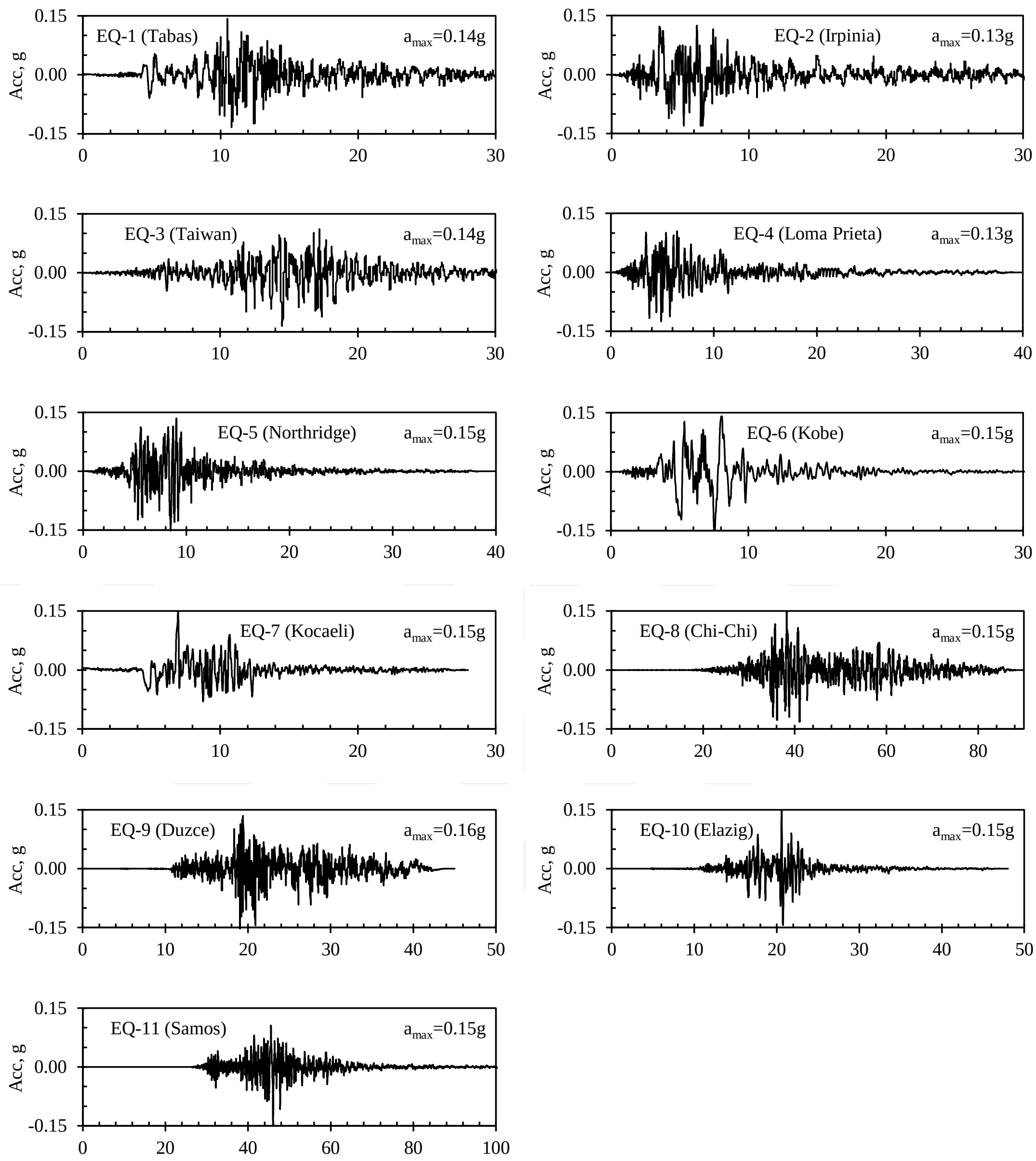

Figure 6.39 : The input motions of the selected earthquakes for the validation analyses.

Numerical analyses were performed with the earthquake records given in Figure 6.39 to validate the proposed 1D model by comparing the results with the 3D analyses. In addition, the acceleration response spectra (ARS) for the superstructure and maximum bending moments along the pile were compared. A comparison of the acceleration response spectra, including the input motions (I.M.), is given in Figure 6.40. The results of the suggested method are close to the 3D analysis except for the Kobe Earthquake (EQ-6). However, the API yields significantly higher acceleration demands than the 3D analysis for all earthquake records.

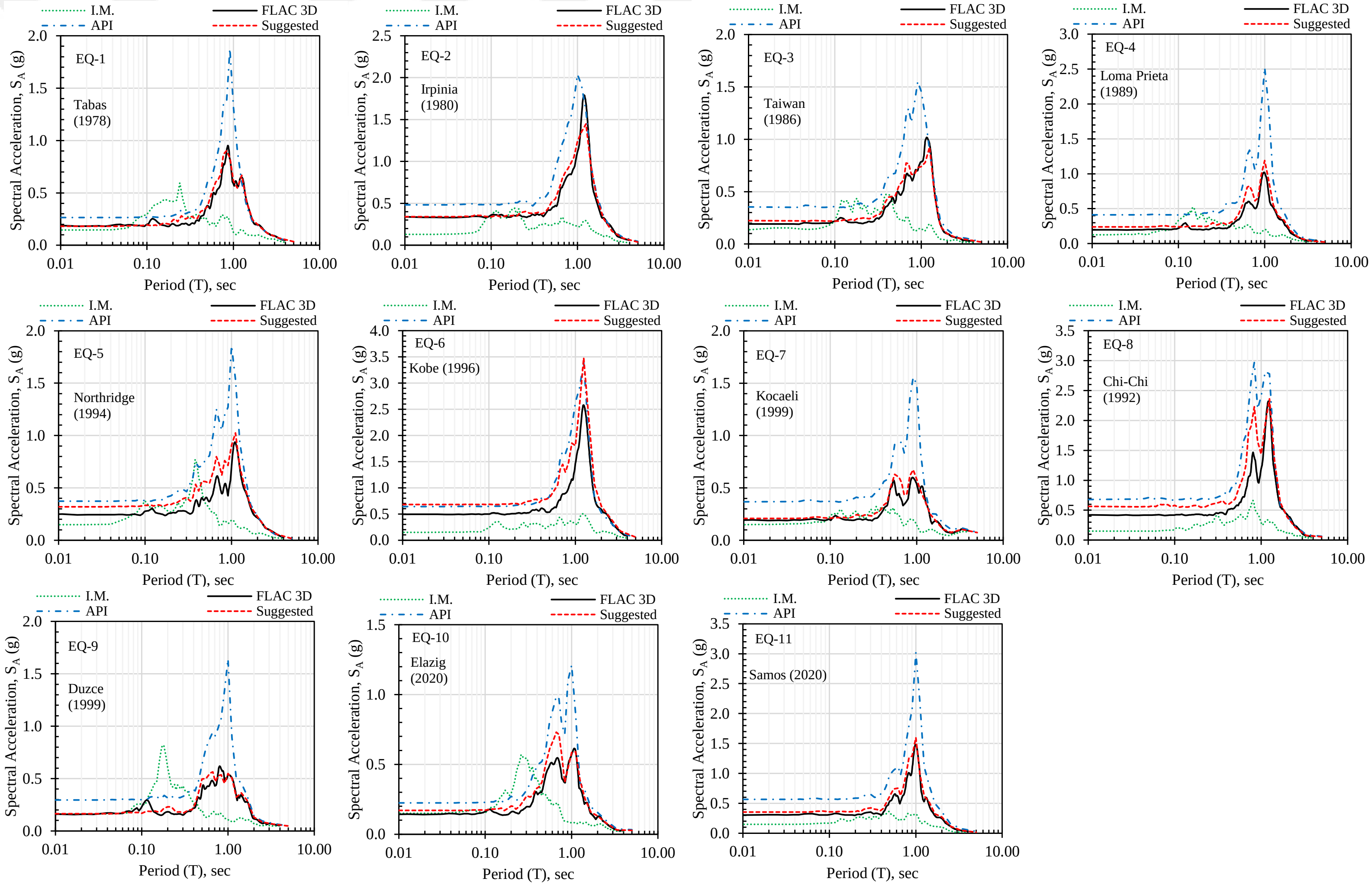

Figure 6.40 : Acceleration response spectra comparison of 3D analysis results with the proposed method and API.

According to Figure 6.40, the superstructure acceleration is higher in EQ-6 and EQ-8. Spectral acceleration of the superstructure reaches its maximum at T≈1.0 sec, which is the period of the soil-pile-structure system. The acceleration response spectra (ARS) of the selected earthquake records (Figure 6.41) have shown that spectral accelerations are maximum at T≈1.0 sec in EQ-6 and EQ-8. The reason for obtaining greater acceleration demand in these earthquakes is that the system period is close to the peak spectral acceleration of the input motions (Soil-Structure interaction effect). The result has shown that the structure response highly depends on the soil-pile-structure system period and the frequency content of the input motion.

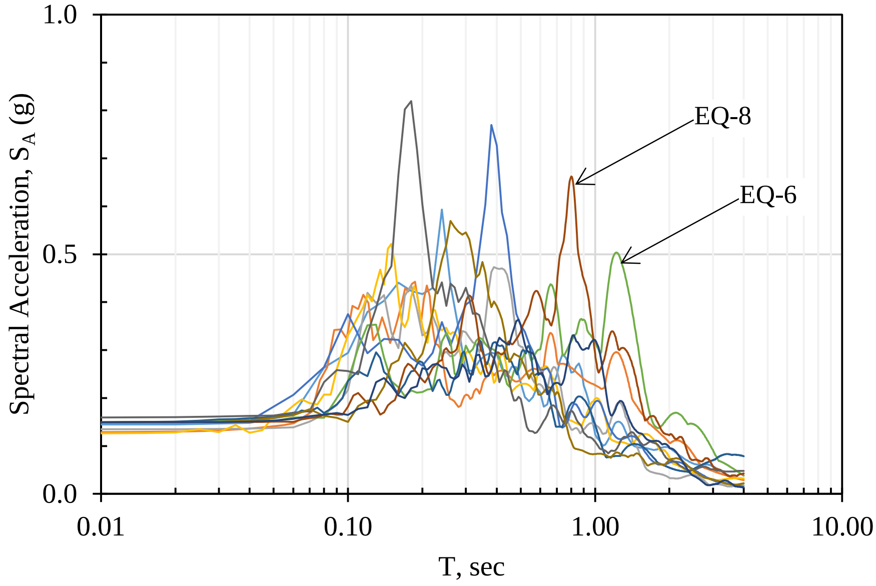

Figure 6.41 : Acceleration response spectra of the selected earthquake records.

The bending moment comparison along the pile is given in Figure 6.42. Similar to the acceleration response spectra, the suggested method results in considerably close bending moments to the 3D analysis except for the EQ-6 (Kobe Earthquake). The magnitude of the bending moments is directly related to the acceleration of the superstructure. Therefore, the maximum bending moment of the selected earthquake records occurred in EQ-6, where the superstructure acceleration is maximum. The API results in significantly higher acceleration demands in the superstructure for all records, hence higher bending moments in a pile. In conclusion, the suggested method considerably increases the performance of the beam on the nonlinear Winkler foundation method, giving closer responses to the 3D numerical analysis.

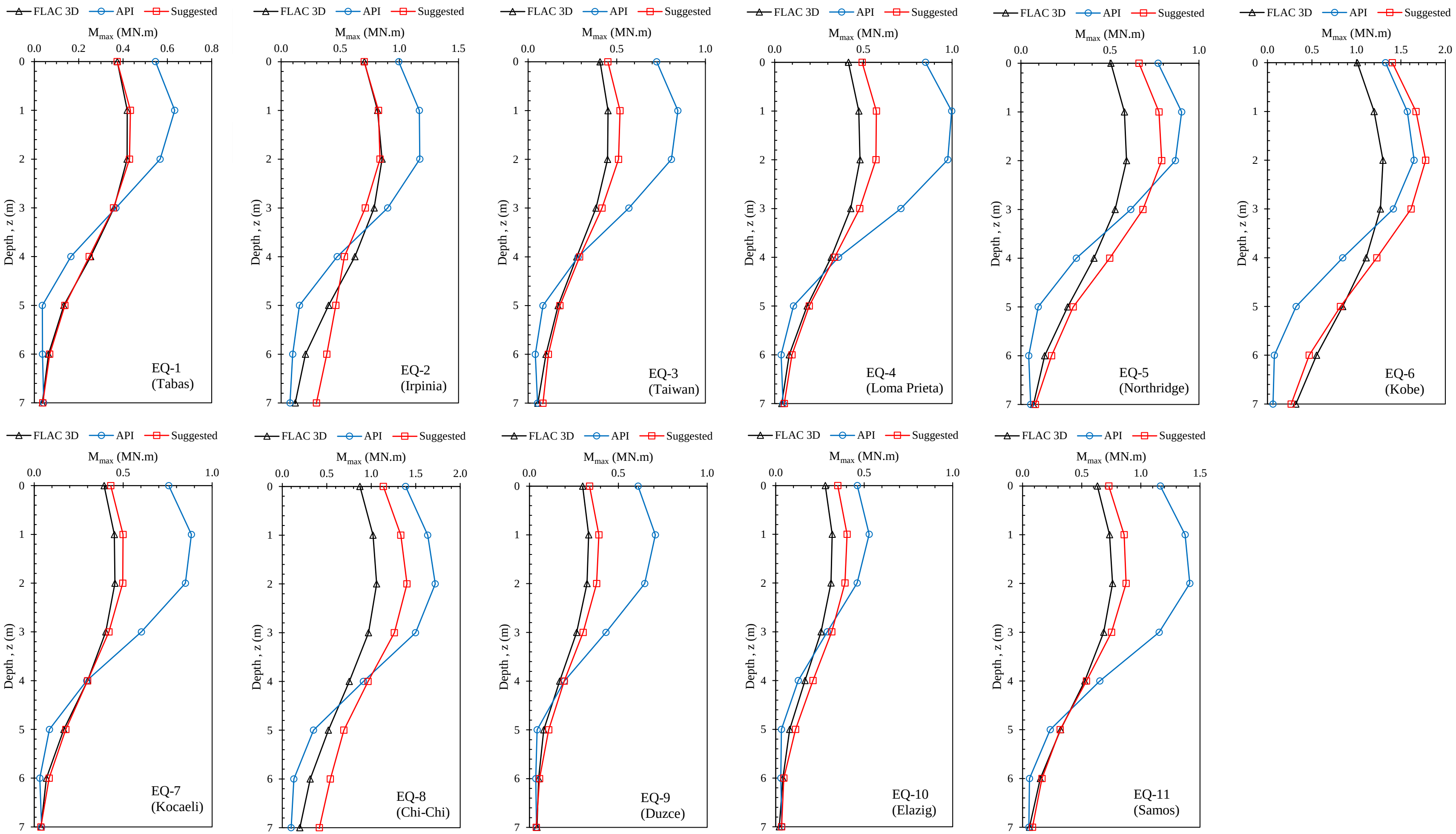

Figure 6.42 : The bending moment comparison of 3D analysis results with the proposed method and API.

7. CONCLUSIONS

In this thesis, 3-dimensional nonlinear analyses were carried out to investigate the load resistance-deflection relationship for piles in cohesionless soils. The main contribution of the study is the enhancement of the p-y curves used in static and dynamic soil-pile-structure interaction analyses. For this purpose, 3D numerical models were created for static and dynamic analyses and verified by the field and laboratory tests in the literature. Parametrical analyses were performed, and the p-y curves were obtained under static and cyclic (dynamic) loading. Mathematical models were proposed for static and dynamic p-y curves.

7.1 Research Findings

The laterally loaded pile behavior under lateral loads was investigated by numerical analyses in FLAC^{3D} (Itasca Consulting Group, 2019). The pile was modeled as a linear elastic material in the numerical analyses, and the HS-Small model represented the soil nonlinearity. The numerical model was verified by a well-known field test (Reese et al., 1974), and the parametric analyses were conducted to show the effect of the pile flexural stiffness, the pile diameter, the relative density of soil, and the soil nonlinearity on the static *p-y* curves. Based on the numerical analysis results and the measurements from the field test data, an enhanced static lateral load-deflection (*p-y*) model was proposed. According to the proposed model, the static p-y curves can be characterized by the initial pile-soil stiffness (K_{py}), ultimate lateral resistance (p_u), and nonlinearity parameters (β and s). In addition, the small strain modulus of soil (E_0) was included in the K_{py} formulation so that the small displacement behavior was considered accurately. The modified model overcomes the drawbacks of the single stiffness models by incorporating the degree of nonlinearity parameters, which allows controlling the stiffness reduction for small to moderate displacements.

The accuracy of the proposed static *p-y* model was shown by comparing the model predictions with the 3D numerical analysis results. Besides, field and centrifuge tests were selected from the literature (Georgiadis et al., 1992; Reese et al., 1974) for validation purposes. The laterally loaded pile problem was analyzed using the proposed static *p-y* curves, and reasonably good agreement was obtained in the bending moments along the pile. The proposed model better captured the bending moments at deep levels than the API (2007) method. In addition, the load-deflection behavior predicted by the proposed model generally agreed with the test results.

On the other hand, the deflections obtained by API (2007) were significantly underpredicted, especially at the larger lateral loads. Hence, the proposed static *p-y* model better represents the response of the laterally loaded piles in cohesionless soils. Overall, the proposed static *p-y* model has significantly enhanced the efficiency of the Winkler spring approach by taking the soil nonlinearity and stiffness reduction into account more elaborately.

A model for dynamic *p-y* curves was then proposed that considers the initial stiffness (K_{py}), ultimate resistance (p_u), and degree of nonlinearity. First, a numerical pile-soil-structure model was created in FLAC^{3D} and verified by two centrifuge tests published in the literature. Verification analyses have shown that soil nonlinearity can be considered using the modulus degradation curves. The parametric analyses were then conducted to investigate the effect of the pile diameter, the relative density of soil, and the soil nonlinearity on the dynamic *p-y* curves. Based on the parametric analyses, a mathematical model was proposed for the dynamic p-y curves for cohesionless soils. The proposed model was validated through the beam on nonlinear Winkler foundation (*BNWF*) approach, which is mostly used in analyzing and designing piles subject to lateral loading. Based on the parametric analyses, pile diameter has a more dominant effect on the ultimate resistance (p_u).

In contrast, the relative density of soil governs both the initial stiffness (K_{py}) and the ultimate resistance (p_u). The soil nonlinearity has a crucial effect on the degree of nonlinearity of the dynamic *p-y* curves. All these parameter influences on the dynamic *p-y* curves were carefully studied and integrated into a mathematical model.

The proposed model characterizes the backbone of dynamic *p-y* curves based on the three leading parameters (initial stiffness K_{py}, ultimate resistance p_u, and degree of nonlinearity n). The Bouc-Wen mathematical formulation best fitted the dynamic *p-y* curves obtained through the parametric analyses. The initial pile-soil stiffness (K_{py}) and the ultimate resistance (p_u) represent very small and large displacement behavior, respectively. Therefore, an equation was proposed for K_{py} using the small-strain stiffness of soil (E_0). A simple yet efficient equation was proposed for ultimate soil resistance (p_u), nonlinearly varying with depth and pile diameter. The numerical analyses showed that the *p-y* curve nonlinearity depends on the modulus reduction curves, which is the function of effective confining stress in cohesionless soils. In the model, the degree of nonlinearity parameter (*n*) was directly related to the reference strain γ_r, which is a soil parameter, and a function of effective stress. Therefore, the degree of nonlinearity parameter *n* mostly governs the behavior for small to moderate displacements.

The validation analyses were performed for the centrifuge tests published in the literature. As the earthquake records used in the centrifuge tests were limited, a new numerical model was created in FLAC^{3D}, and additional analyses were carried out with the selected records. The 3D analysis results were compared with the BNWF analyses. The validation analysis results have demonstrated that the proposed dynamic *p-y* curves could reasonably estimate the pile and structure response. The promising results make the proposed equations highly practical, considering the complexity of modeling the soil-pile interaction problem. The advantage of the proposed model is the ability to create hysteretic *p-y* curves that could involve the soil nonlinearity effect. Since the nonlinear soil behavior is represented by the reference strain (γ_r), which can be determined by laboratory tests, the incorporation of the γ_r into dynamic *p-y* formulation allows us to consider the true soil-pile interaction behavior under dynamic loading. Although the model was proposed for cohesionless soils using the modulus degradation curves, it can be extended to any soil provided that the reference strain is accurately determined. Overall, the proposed model for dynamic *p-y* curves can consider the dynamic soil properties (G_{max} and γ_{ref}) that significantly affect the nonlinear *p-y* behavior.

7.2 Recommendations for Future Studies

This thesis focused on the single pile behavior under lateral loading. However, piles are constructed as a group in practice to withstand external loads. Therefore, the group pile behavior must be considered in future research studies.

The numerical analyses have shown that the pile and structure response highly depend on the free-field soil displacements obtained by the site response analysis. This study used the Mohr-Coulomb model with a hysteretic damping approach and General Quadratic and Hyperbolic Model (GQ/H) for 3D and 1D analyses, respectively. In the Mohr-Coulomb model, the Masing rule was employed for unloading/reloading behavior which is known to cause overprediction in the damping ratios under large strains. More elaborate 3D models are available in the literature, but the model parameters are quite complex and require more effort for parameter calibration. Therefore, future studies must be carried out to develop less complicated models for engineers to be used in 3D analyses. On the other hand, soil response under earthquake loading can be determined quite efficiently in free-field site response analyses with 1D models. Besides, employing non-masing rules is relatively simple in 1D analyses.

This thesis investigated pile behavior under lateral load using the total stress approach by modulus degradation curves. Therefore, the proposed methods could be applied to dry and saturated soils. However, saturated sand might liquefy during a seismic event. Thus, 3D and 1D soil models must be improved to capture the true behavior of liquefied soils better. Besides, the cohesionless soils are usually partially saturated in the field. Hence, the effect of saturation degree and liquefaction must be considered separately.

In this study, the earthquake loading was given in the horizontal direction. However, earthquakes induce the movement in 3-dimension simultaneously. Therefore, future studies must consider the bi-directional movement and the vertical component of the motion, which might significantly impact the regions where the fault is close.

REFERENCES

AFAD. (2022). *Türkiye İvme Veri Tabanı ve Analiz Sistemi*. https://tadas.afad.gov.tr/map

Allotey, N., & El Naggar, M. H. (2008). A numerical study into lateral cyclic nonlinear soil–pile response. *Canadian Geotechnical Journal*, *45* (9), 1268-1281. https://doi.org/10.1139/T08-050

Alver, O., & Eseller-Bayat, E. (2022). *The Effect of Soil Damping on the Soil-Pile-Structure Interaction Analyses in Liquefiable and Non-liquefiable Soils*. Conference on Performance-based Design in Earthquake Geotechnical Engineering (Beijing 2022). PBD-IV 2022. Geotechnical, Geological and Earthquake Engineering, vol 52. Springer, Cham. https://doi.org/10.1007/978-3-031-11898-2_83

Alver, O., & Eseller-Bayat, E. E. (2022). Effect of Soil Damping on the Soil–Pile–Structure Interaction Analyses in Cohesionless Soils. *Applied Sciences*, *12* (18), 9002. https://doi.org/10.3390/app12189002

Alver, O., Sezen, A., & Eseller-Bayat, E. (2021). Geotechnical Design with Respect to TBDY-2018: Liquefaction and Soil-Pile-Structure Interaction Analyses. *TEKNIK DERGI*, *32* (5), 11197-11225. https://doi.org/10.18400/tekderg.744891

American Petroleum Institute (API). (2007). *Recommended practice for planning, designing, and constructing fixed offshore platforms*. American Petroleum Institute. API RP2A-WSD, 21th Edition, Washington, D. C.

Ashour, M., & Norris, G. (2000). Modeling lateral soil-pile response based on soil-pile interaction. *Journal of Geotechnical and Geoenvironmental Engineering*, *126* (5), 420-428.

Atkinson, J. (2000). Non-linear soil stiffness in routine design. *Géotechnique*, *50* (5), 487-508. https://doi.org/10.1680/geot.2000.50.5.487

Augustesen, A. H., Brødbæk, K., Møller, M., Sørensen, S. P. H., Ibsen, L. B., Pedersen, T. S., & Andersen, L. (2009). *Numerical modelling of large-diameter steel piles at Horns Rev* Proceedings of the Twelfth International Conference on Civil, Structural and Environmental Engineering Computing.

Baguelin, F., Frank, R., & Said, Y. (1977). Theoretical study of lateral reaction mechanism of piles. *Géotechnique*, *27* (3), 405-434. https://doi.org/10.1680/geot.1977.27.3.405

Banerjee, P., & Davies, T. (1978). The behaviour of axially and laterally loaded single piles embedded in nonhomogeneous soils. *Géotechnique, 28* (3), 309-326. https://doi.org/10.1680/geot.1978.28.3.309

Bardet, J., Ichii, K., & Lin, C. (2000). *EERA: a computer program for equivalent-linear earthquake site response analyses of layered soil deposits*. University of Southern California, Department of Civil Engineering.

Barton, Y., Finn, W., Parry, R., & Towhata, I. (1983). *Lateral pile response and py curves from centrifuge tests*. Proc., 15th Annual Offshore Technology Conf., Houston, Paper 4502, 503–508.

Benz, T. (2007). *Small-Strain Stiffness of Soils and its Numerical Consequences* [Dissertationsschrift, Universität Stuttgart]. Germany.

Bouc, R. (1971). A mathematical model for hysteresis. *Acta Acustica united with Acustica*, *24* (1), 16-25.

Boulanger, R. W., Curras, C. J., Kutter, B. L., Wilson, D. W., & Abghari, A. (1999). Seismic soil-pile-structure interaction experiments and analyses. *Journal of Geotechnical and Geoenvironmental Engineering, 125*(9),750-759. doi:10.1061/(ASCE)1090-0241(1999)125:9(750)

Bouzid, A. D. (2021). Analytical Quantification of Ultimate Resistance for Sand Flowing Horizontally around Monopile: New p-y Curve Formulation. *International Journal of Geomechanics, 21* (3). doi:10.1061/(ASCE)GM.1943-5622.0001927

Bouzid, D., Bhattacharya, S., & Dash, S. (2013). Winkler Springs (p-y curves) for pile design from stress-strain of soils: FE assessment of scaling coefficients using the Mobilized Strength Design concept. *Geomechanics & engineering*, *5* (5), 379-399. https://doi.org/10.12989/gae.2013.5.5.379

Bransby, M. (1999). Selection of p–y curves for the design of single laterally loaded piles. *International Journal for numerical and analytical methods in geomechanics*, *23* (15), 1909-1926. https://doi.org/10.1002/(SICI)1096-9853(19991225)23:15<1909::AID-NAG26>3.0.CO;2-L

Broms, B. B. (1964). Lateral resistance of piles in cohesionless soils. *Journal of the Soil Mechanics and Foundations Division, 90* (3), 123-156. https://doi.org/10.1061/JSFEAQ.0000614

Brown, D. A., O'Neill, M., Hoit, M., McVay, M., El Naggar, M., & Chakraborty, S. (2001). *Static and dynamic lateral loading of pile groups*. National Cooperative Highway Research Program. In NCHRP Report 461, Washington, D.C: Transportation Research Board, National Academy Press.

Brown, D. A., & Shie, C.-F. (1991). Some numerical experiments with a three dimensional finite element model of a laterally loaded pile. *Computers and Geotechnics, 12* (2), 149-162. https://doi.org/10.1016/0266-352X(91)90004-Y

Burd, H. J., Taborda, D. M., Zdravković, L., Abadie, C. N., Byrne, B. W., Houlsby, G. T., Gavin, K. G., Igoe, D. J., Jardine, R. J., & Martin, C. M. (2020). PISA design model for monopiles for offshore wind turbines: application to a marine sand. *Géotechnique*, *70* (11), 1048-1066. https://doi.org/10.1680/jgeot.18.P.277

Choi, J. I., Kim, M. M., & Brandenberg, S. J. (2016). Cyclic p-y Plasticity Model Applied to Pile Foundations in Sand *Journal of Geotechnical and Geoenvironmental Engineering, 142* (6), 08216001. doi:10.1061/(ASCE)GT.1943-5606.0001261

Correia, A. A., & Pecker, A. (2021). Nonlinear pile-head macro-element for the seismic analysis of structures on flexible piles. *Bulletin of Earthquake Engineering, 19* (4), 1815-1849. https://doi.org/10.1007/s10518-020-01034-4

Cox, W. R., Reese, L. C., & Grubbs, B. R. (1974). *Field testing of laterally loaded piles in sand.* Offshore Technology Conference, Houston, TX, paper no. 2080.

CSI. (2016). *SAP2000 Integrated Software for Structural Analysis and Design*. In *Version 18.2*. Structural Analysis Program, Computers and Structures, Inc., California, Berkeley, USA, 2016

Darendeli, M. B. (2001). *Development of a new family of normalized modulus reduction and material damping curves* [Ph.D. Dissertation, The university of Texas at Austin].

Desai, C., & Kuppusamy, T. (1980). Application of a numerical procedure for laterally loaded structures. In *Numerical methods in offshore piling* (pp. 93-99). Thomas Telford Publishing.

Deutsches Institut für Normung (DIN). (2011). *DIN 4085:2011-05: Subsoil – Calculation of earth-pressure*. https://www.beuth.de/en/standard/din-4085/139496465

Di Laora, R., & Rovithis, E. (2015). Kinematic bending of fixed-head piles in nonhomogeneous soil. *Journal of Geotechnical and Geoenvironmental Engineering*, *141* (4), 04014126.

Dodds, A. (2005). *A numerical study of pile behavior in large pile groups under lateral loading*. University of Southern California.

Dodds, A. M., & Martin, G. R. (2007). *Modeling pile behavior in large pile groups under lateral loading* (MCEER-07-0004).

Duncan, J. M., & Chang, C.-Y. (1970). Nonlinear analysis of stress and strain in soils. *Journal of the Soil Mechanics and Foundations Division*, *96* (5), 1629-1653. https://doi.org/10.1061/JSFEAQ.0001458

El Naggar, M., & Novak, M. (1996). Nonlinear analysis for dynamic lateral pile response. *Soil Dynamics and Earthquake Engineering*, *15* (4), 233-244. https://doi.org/10.1016/0267-7261(95)00049-6

Fan, C.-C., & Long, J. H. (2005). Assessment of existing methods for predicting soil response of laterally loaded piles in sand. *Computers and Geotechnics*, *32* (4), 274-289. https://doi.org/10.1016/j.compgeo.2005.02.004

Finn, W. (2005). A study of piles during earthquakes: issues of design and analysis. *Bulletin of Earthquake Engineering*, *3* (2), 141-234. https://doi.org/10.1007/s10518-005-1241-3

Finn, W., & Fujita, N. (2002). Piles in liquefiable soils: seismic analysis and design issues. *Soil Dynamics and Earthquake Engineering*, *22* (9-12), 731-742. https://doi.org/10.1016/S0267-7261(02)00094-5

Fleming, K., Weltman, A., Randolph, M., & Elson, K. (2008). *Piling engineering*. CRC press. https://doi.org/10.1201/b22272

Gazetas, G., & Dobry, R. (1984). Horizontal response of piles in layered soils. *Journal of Geotechnical Engineering*, *110* (1), 20-40. doi:10.1061/(ASCE)0733-9410(1984)110:1(20)

Georgiadis, M., Anagnostopoulos, C., & Saflekou, S. (1992). Centrifugal testing of laterally loaded piles in sand. *Canadian Geotechnical Journal*, *29* (2), 208-216. https://doi.org/10.1139/t92-024

Gerolymos, N., Escoffier, S., Gazetas, G., & Garnier, J. (2009). Numerical modeling of centrifuge cyclic lateral pile load experiments. *Earthquake Engineering and Engineering Vibration*, *8* (1), 61-76. https://doi.org/10.1007/s11803-009-9005-8

Gerolymos, N., & Gazetas, G. (2005). Constitutive model for 1-D cyclic soil behaviour applied to seismic analysis of layered deposits. *Soils and foundations*, *45* (3), 147-159. https://doi.org/10.3208/sandf.45.3_147

Gerolymos, N., & Gazetas, G. (2006). Development of Winkler model for static and dynamic response of caisson foundations with soil and interface nonlinearities. *Soil Dynamics and Earthquake Engineering*, *26* (5), 363-376. https://doi.org/10.1016/j.soildyn.2005.12.002

Giannakos, S., Gerolymos, N., & Gazetas, G. (2012). Cyclic lateral response of piles in dry sand: Finite element modeling and validation. *Computers and Geotechnics*, *44*, 116-131. https://doi.org/10.1016/j.compgeo.2012.03.013

Gohl, W. B. (1991). *Response of pile foundations to simulated earthquake loading: experimental and analytical results volume I* [Ph.D. Dissertation, University of British Columbia].

Groholski, D. R., Hashash, Y. M., Kim, B., Musgrove, M., Harmon, J., & Stewart, J. P. (2016). Simplified model for small-strain nonlinearity and strength in 1D seismic site response analysis. *Journal of Geotechnical and Geoenvironmental Engineering*, *142* (9), 04016042. doi:10.1061/(ASCE)GT.1943-5606.0001496

Hardin, B. O., & Black, W. L. (1966). Sand stiffness under various triaxial stresses. *Journal of the Soil Mechanics and Foundations Division*, *92* (2), 27-42.

Hardin, B. O., & Drnevich, V. P. (1972). Shear modulus and damping in soils: measurement and parameter effects (terzaghi leture). *Journal of the Soil Mechanics and Foundations Division*, *98* (6), 603-624.

Hashash YMA, M. M., Harmon J, et al (2017). *DEEPSOIL User manual*. In (Version 7.0)

Hussein, A. F., & El Naggar, M. H. (2022). Seismic behaviour of piles in non-liquefiable and liquefiable soil. *Bulletin of Earthquake Engineering*, *20* (1), 77-111. https://doi.org/10.1007/s10518-021-01244-4

Ishibashi, I., & Zhang, X. (1993). Unified dynamic shear moduli and damping ratios of sand and clay. *Soils and foundations*, *33* (1), 182-191. https://doi.org/10.3208/sandf1972.33.182

Ishihara, K. (2021). Evaluation of soil properties for use in earthquake response analysis. In *Geomechanical modelling in engineering practice* (pp. 241-275). Routledge.

Itasca Consulting Group, I. (2019). *FLAC3D — Fast Lagrangian Analysis of Continua in Three-Dimensions*. In *Ver. 7.0*

Iyisan, R. (1996). Correlations between shear wave velocity and in-situ penetration test results. *TEKNIK DERGI* (7), 371-374.

Kagawa, T., & Kraft, L. M. (1980). Lateral load-deflection relationships of piles subjected to dynamic loadings. *Soils and foundations*, *20* (4), 19-36.

Kondner, R. L. (1963). *A hyperbolic stress-strain formulation for sands* Proc. 2 nd Pan Am. Conf. on Soil Mech. and Found. Eng., Brazil, 1963.

Kuhlemeyer, R. L. (1979). Static and dynamic laterally loaded floating piles. *Journal of the Geotechnical Engineering Division*, *105* (2), 289-304. https://doi.org/10.1061/AJGEB6.0000771

Kuhlemeyer, R. L., & Lysmer, J. (1973). Finite element method accuracy for wave propagation problems. *Journal of the Soil Mechanics and Foundations Division*, *99* (5), 421-427.

Kwon, S. Y., & Yoo, M. (2020). Study on the dynamic soil-pile-structure interactive behavior in liquefiable sand by 3D numerical simulation. *Applied Sciences, 10* (8), 2723. https://doi.org/10.3390/app10082723

Lee, M., Bae, K.-T., Lee, I.-W., & Yoo, M. (2019). Cyclic py curves of monopiles in dense dry sand using centrifuge model tests. *Applied Sciences, 9* (8), 1641. https://doi.org/10.3390/app9081641

Lim, H., & Jeong, S. (2018). Simplified p-y curves under dynamic loading in dry sand. *Soil Dynamics and Earthquake Engineering, 113,* 101-111. https://doi.org/10.1016/j.soildyn.2018.05.017

Lombardi, D., Dash, S. R., Bhattacharya, S., Ibraim, E., Muir Wood, D., & Taylor, C. (2017). Construction of simplified design p–y curves for liquefied soils. *Géotechnique, 67* (3), 216-227. https://doi.org/10.1680/jgeot.15.P.116

Lu, W., Kaynia, A. M., & Zhang, G. (2021). Centrifuge study of p–y curves for vertical–horizontal static loading of piles in sand. *International Journal of Physical Modelling in Geotechnics*, *21* (6), 275-294. https://doi.org/10.1680/jphmg.19.00030

Lysmer, J., & Kuhlemeyer, R. L. (1969). Finite dynamic model for infinite media. *Journal of the Engineering Mechanics Division*, *95* (4), 859-877.

Makris, N., & Gazetas, G. (1992). Dynamic pile-soil-pile interaction. Part II: Lateral and seismic response. *Earthquake engineering & structural dynamics*, *21* (2), 145-162. https://doi.org/10.1002/eqe.4290210204

Masing, G. (1926). *Eigenspannungen und Verfestigung beim Messing [Fundamental stresses and strengthening with brass]* International Congress of Applied Mechanics, 2d, Zurich.

Matasović, N., & Vucetic, M. (1993). Cyclic characterization of liquefiable sands. *Journal of Geotechnical Engineering, 119* (11), 1805-1822. doi:10.1061/(ASCE)0733-9410(1993)119:11(1805)

McGann, C. R., Arduino, P., & Mackenzie-Helnwein, P. (2011). Applicability of conventional p-y relations to the analysis of piles in laterally spreading soil. *Journal of Geotechnical and Geoenvironmental Engineering*, *137* (6), 557-567. doi:10.1061/(ASCE)GT.1943-5606.0000468

Medjitna, L., & Amar Bouzid, D. (2019). A numerical procedure to correlate the subgrade reaction coefficient with soil stiffness properties for laterally loaded piles using the FSAFEM. *International Journal of Geotechnical Engineering, 13* (5), 458-473. https://doi.org/10.1080/19386362.2017.1365475

Murchison, J. M., & O'Neill, M. W. (1984). *Evaluation of p-y relationships in cohesionless soils.* Proceedings of the ASCE symposium on analysis and design of pile foundations, San Francisco, pp. 174 – 191.

Murphy, G., Igoe, D., Doherty, P., & Gavin, K. (2018). 3D FEM approach for laterally loaded monopile design. *Computers and Geotechnics*, *100*, 76-83. https://doi.org/10.1016/j.compgeo.2018.03.013

Naggar, M. H. E., & Bentley, K. J. (2000). Dynamic analysis for laterally loaded piles and dynamic p-y curves. *Canadian Geotechnical Journal*, *37* (6), 1166-1183.

Nguyen, B. N., Tran, N. X., Han, J.-T., & Kim, S.-R. (2018). Evaluation of the dynamic p–y loops of pile-supported structures on sloping ground. *Bulletin of Earthquake Engineering*, *16* (12), 5821-5842. https://doi.org/10.1007/s10518-018-0428-3

Nist, G. (2012). *Soil–structure interaction for building structures*. National Institute of Standards and Technology, US Department of Commerce.

Nogami, T., Otani, J., Konagai, K., & Chen, H.-L. (1992). Nonlinear soil-pile interaction model for dynamic lateral motion. *Journal of Geotechnical Engineering*, *118* (1), 89-106. doi:10.1061/(ASCE)0733-9410(1992)118:1(89)

Papadopoulou, M. C., & Comodromos, E. M. (2014). Explicit extension of the p–y method to pile groups in sandy soils. *Acta Geotechnica*, *9* (3), 485-497. https://doi.org/10.1007/s11440-013-0274-z

PEER. (2005). *Strong Motion Database on Line*. Pacific Earthquake Engineering Research Center. Retrieved 12.01.2022 from https://peer.berkeley.edu/peer-strong-ground-motion-databases

Pender, M. (1993). Aseismic pile foundation design analysis. *Bulletin of the New Zealand Society for Earthquake Engineering*, *26* (1), 49-160. https://doi.org/10.5459/bnzsee.26.1.49-160

Poulos, H. G. (1971). Behavior of laterally loaded piles: I-single piles. *Journal of the Soil Mechanics and Foundations Division*, *97* (5), 711-731. https://doi.org/10.1061/JSFEAQ.0001592

Puzrin, A. (2012). *Constitutive modelling in geomechanics: introduction*. Springer Science & Business Media.

Rahmani, A., Taiebat, M., Finn, W. L., & Ventura, C. E. (2018). Evaluation of p-y springs for nonlinear static and seismic soil-pile interaction analysis under lateral loading. *Soil Dynamics and Earthquake Engineering*, *115*, 438-447. https://doi.org/10.1016/j.soildyn.2018.07.049

Ramberg, W., & Osgood, W. R. (1943). *Description of stress-strain curves by three parameters*. Technical Note No. 902, National Advisory Committee for Aeronautics, Washington, D.C., USA.

Randolph, M. F. (1981). The response of flexible piles to lateral loading. *Géotechnique*, *31* (2), 247-259. https://doi.org/10.1680/geot.1981.31.2.247

Randolph, M. F., & Houlsby, G. (1984). The limiting pressure on a circular pile loaded laterally in cohesive soil. *Géotechnique*, *34* (4), 613-623. https://doi.org/10.1680/geot.1984.34.4.613

Reese, L. C., Cox, W. R., & Koop, F. D. (1974). *Analysis of laterally loaded piles in sand.* Offshore Technology Conference, Houston, Texas. https://doi.org/10.4043/2080-MS

Reese, L. C., & Van Impe, W. F. (2000). *Single piles and pile groups under lateral loading*. CRC press. https://doi.org/10.1201/b17499

Rollins, K. M., Lane, J. D., & Gerber, T. M. (2005). Measured and computed lateral response of a pile group in sand. *Journal of Geotechnical and Geoenvironmental Engineering*, *131*(1), 103-114. doi:10.1061/(ASCE)1090-0241(2005)131:1(103)

Rovithis, E., Kirtas, E., & Pitilakis, K. (2009). Experimental p-y loops for estimating seismic soil-pile interaction. *Bulletin of Earthquake Engineering*, *7* (3), 719-736. https://doi.org/10.1007/s10518-009-9116-7

Schanz, T., Vermeer, P., & Bonnier, P. G. (2019). The hardening soil model: formulation and verification. In *Beyond 2000 in computational geotechnics* (pp. 281-296). Routledge.

Scott, R. F. (1981). *Foundation analysis*. Prentice-Hall.

Seed, H. B., & Idriss, I. M. (1970). *Soil moduli and damping factors for dynamic response analysis* (EERC 70-10).

Sørensen, S. P. H. (2012). *Soil-structure interaction for nonslender, large-diameter offshore monopiles* [Ph.D. Dissertation, Aalborg University].

Sørensen, S. P. H., Ibsen, L. B., & Augustesen, A. H. (2010). Effects of diameter on initial stiffness of p-y curves for large-diameter piles in sand. *Numerical Methods in Geotechnical Engineering*, 907-912.

Taborda, D. M., Zdravković, L., Potts, D. M., Burd, H. J., Byrne, B. W., Gavin, K. G., Houlsby, G. T., Jardine, R. J., Liu, T., & Martin, C. M. (2020). Finite-element modelling of laterally loaded piles in a dense marine sand at Dunkirk. *Géotechnique*, *70* (11), 1014-1029. https://doi.org/10.1680/jgeot.18.PISA.006

Terzaghi, K. (1955). Evalution of conefficients of subgrade reaction. *Géotechnique*, *5* (4), 297-326. https://doi.org/10.1680/geot.1955.5.4.297

Thavaraj, T., Liam Finn, W., & Wu, G. (2010). Seismic response analysis of pile foundations. *Geotechnical and Geological Engineering*, *28* (3), 275-286. https://doi.org/10.1007/s10706-010-9311-y

Thieken, K., Achmus, M., & Lemke, K. (2015). A new static p-y approach for piles with arbitrary dimensions in sand. *geotechnik*, *38* (4), 267-288. https://doi.org/10.1002/gete.201400036

Varun. (2010). *A non-linear dynamic macroelement for soil structure interaction analyses of piles in liquefiable sites* [Ph.D. Dissertation, Georgia Institute of Technology].

Varun, Assimaki, D., & Shafieezadeh, A. (2013). Soil-pile-structure interaction simulations in liquefiable soils via dynamic macroelements: Formulation and validation. *Soil Dynamics and Earthquake Engineering*, *47* (Suppl 1), 92-107. https://doi.org/10.1016/j.soildyn.2012.03.008

Vesić, A. B. (1961). Bending of Beams Resting on Isotropic Elastic Solid. *Journal of the Engineering Mechanics Division*, *87* (2), 35-53. https://doi.org/doi:10.1061/JMCEA3.0000212

Wair, B. R., DeJong, J. T., & Shantz, T. (2012). *Guidelines for estimation of shear wave velocity profiles*. Pacific Earthquake Engineering Research Center.

Wang, H., Lehane, B., Bransby, M., Wang, L., & Hong, Y. (2022). Field and numerical study of the lateral response of rigid piles in sand. *Acta Geotechnica*, 1-12. https://doi.org/10.1007/s11440-022-01532-6

Wang, H., Wang, L., Hong, Y., He, B., & Zhu, R. (2020). Quantifying the influence of pile diameter on the load transfer curves of laterally loaded monopile in sand. *Applied Ocean Research*, *101*, 102196. https://doi.org/10.1016/j.apor.2020.102196

Wang, S., Kutter, B. L., Chacko, M. J., Wilson, D. W., Boulanger, R. W., & Abghari, A. (1998). Nonlinear seismic soil-pile structure interaction. *Earthquake spectra*, *14* (2), 377-396. https://doi.org/10.1193/1.1586006

Wen, Y.-K. (1976). Method for random vibration of hysteretic systems. *Journal of the Engineering Mechanics Division*, *102* (2), 249-263.

Wilson, D. W. (1998). *Soil-pile-superstructure interaction in liquefying sand and soft clay* [Ph.D. Dissertation, University of California at Davis].

Yang, E.-K., Choi, J.-I., Kwon, S.-Y., & Kim, M.-M. (2011). Development of dynamic py backbone curves for a single pile in dense sand by 1g shaking table tests. *KSCE Journal of Civil Engineering*, *15* (5), 813-821.

Yoo, M.-T., Choi, J.-I., Han, J.-T., & Kim, M.-M. (2013). Dynamic p-y curves for dry sand from centrifuge tests. *Journal of Earthquake Engineering*, *17* (7), 1082-1102. https://doi.org/10.1080/13632469.2013.801377

Zhang, J., Andrus, R. D., & Juang, C. H. (2005). Normalized shear modulus and material damping ratio relationships. Journal of Geotechnical and Geoenvironmental Engineering, 131(4), 453-464. do:10.1061/(ASCE)1090-0241(2005)131:4(453)

Zhang, L., Silva, F., & Grismala, R. (2005). Ultimate lateral resistance to piles in cohesionless soils. Journal of Geotechnical and Geoenvironmental Engineering, 131(1), 78-83. doi:10.1061/(ASCE)1090-0241(2005)131:4(453)

Zhang, Y., & Andersen, K. H. (2017). Scaling of lateral pile p-y response in clay from laboratory stress-strain curves. *Marine Structures*, *53*, 124-135. https://doi.org/10.1016/j.marstruc.2017.02.002

Zhou, H., Liu, H., Ding, X., & Kong, G. (2020). A p–y curve model for laterally loaded XCC pile in soft clay. *Acta Geotechnica*, *15* (11), 3229-3242. https://doi.org/10.1007/s11440-020-00944-6

APPENDICES

APPENDIX A: Acceleration-time histories obtained in the verification analyses

APPENDIX B: Soil resistance and pile displacement-time histories in the parametric analysis

APPENDIX C: Acceleration-time histories obtained in the validation analyses with the centrifuge test results

APPENDIX D: Pile head bending moment-time histories obtained in the validation analyses with the selected earthquake test results

APPENDIX A: Acceleration-time histories obtained in the verification analyses

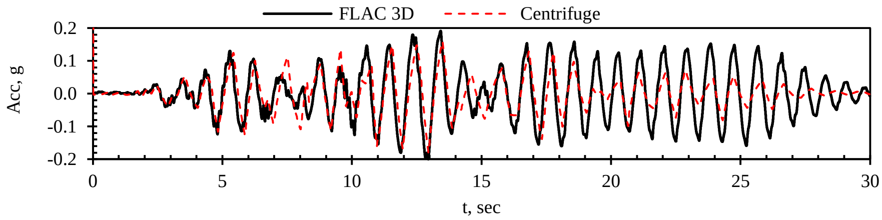

Figure A.1 : Acceleration time history of the superstructure obtained in 3D numerical analysis compared with the test results (Gohl, 1991).

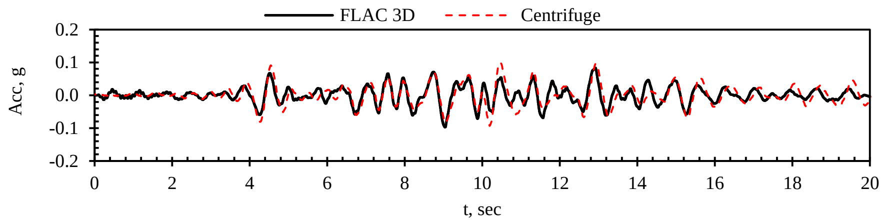

Figure A.2 : Acceleration time history of the superstructure obtained in 3D numerical analysis compared with the test results (Event K).

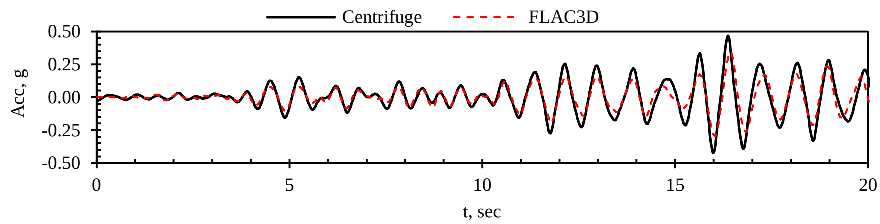

Figure A.3 : Acceleration time history of the superstructure obtained in 3D numerical analysis compared with the test results (Event N).

APPENDIX B: Soil resistance and pile displacement-time histories in the parametric analysis

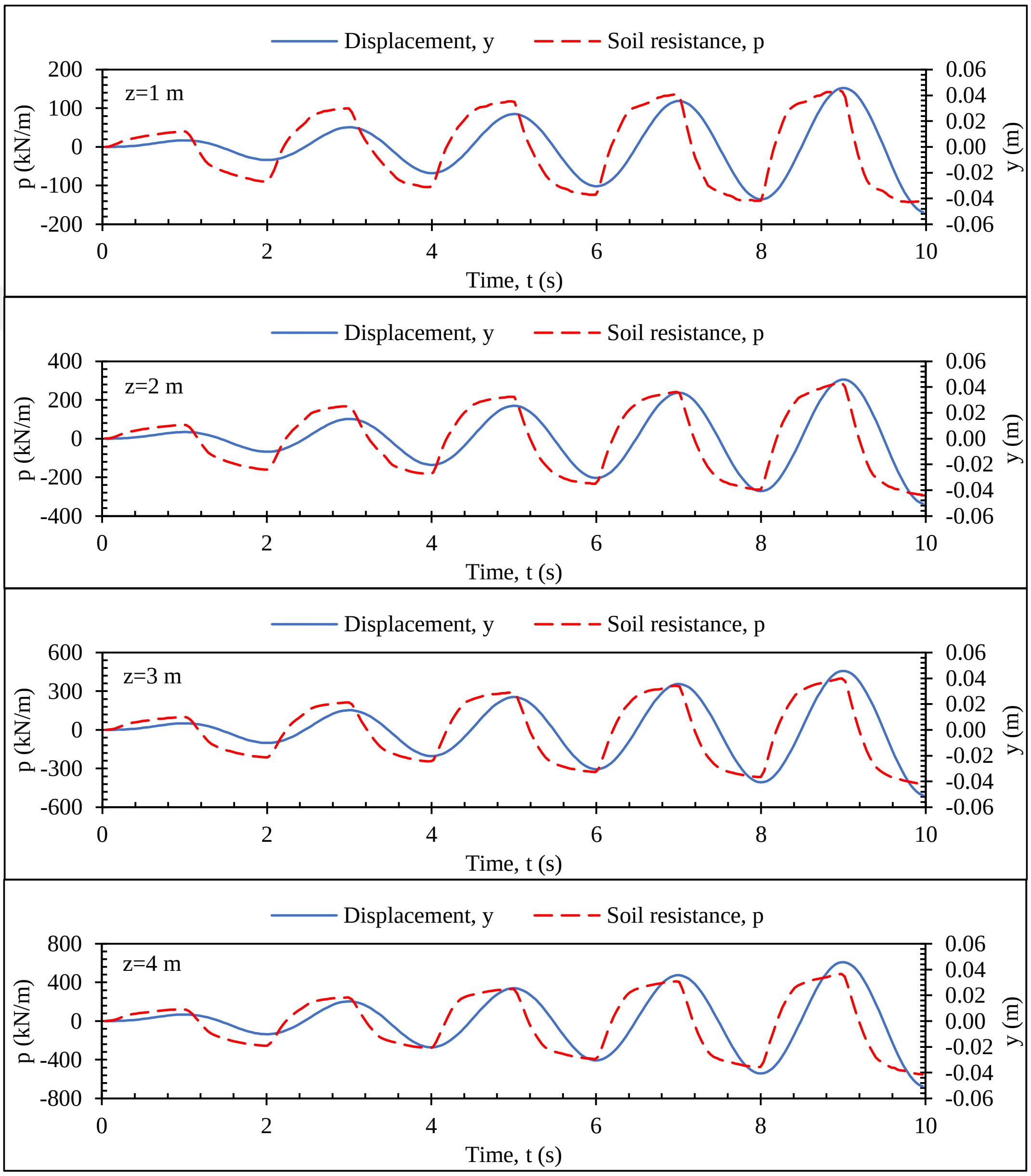

Figure B.1 : The pile displacement and soil resistance time histories for D=0.65 m, D_R=55 %.

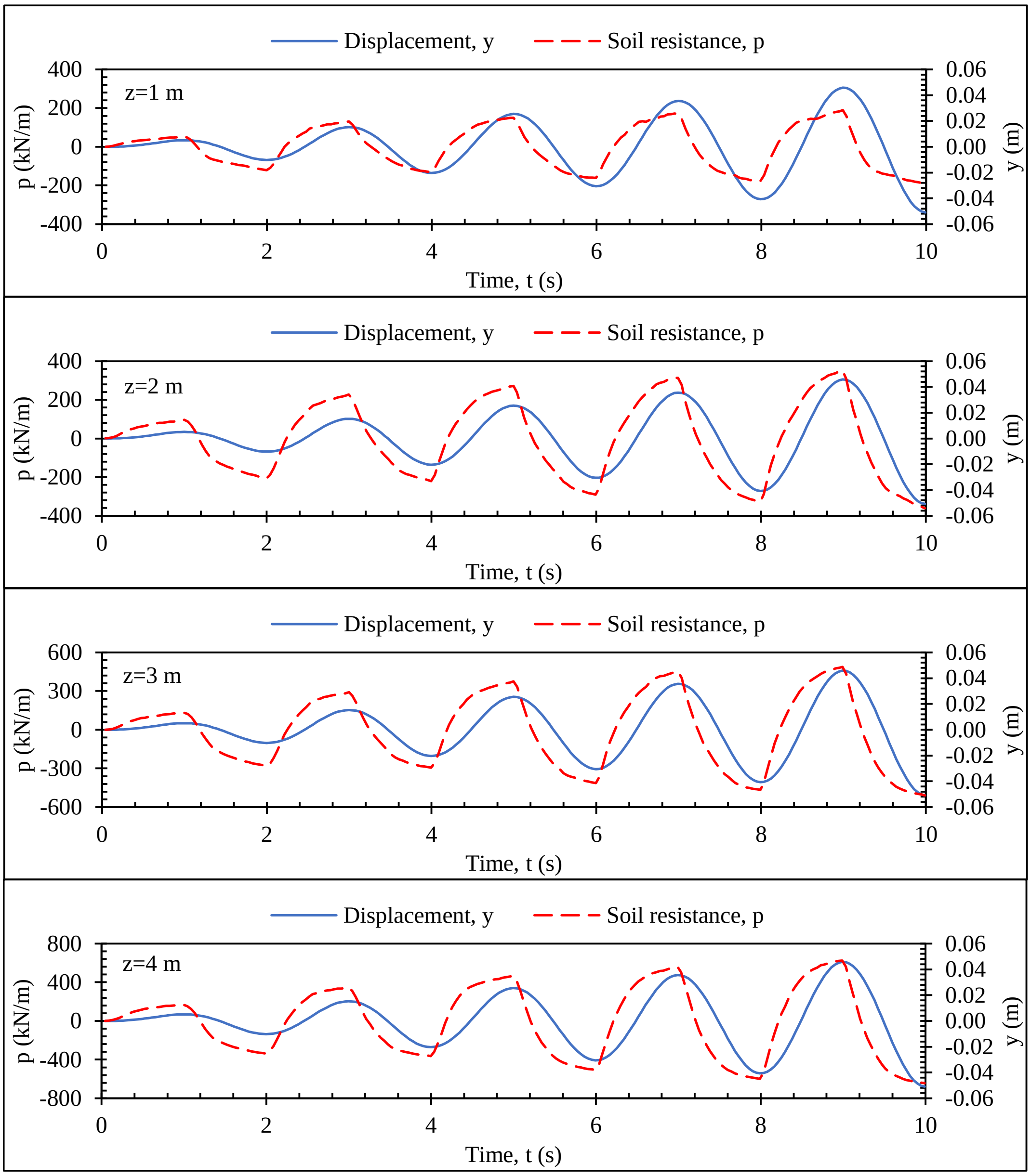

Figure B.2 : The pile displacement and soil resistance time histories for D=1.0 m, D_R=55 %.

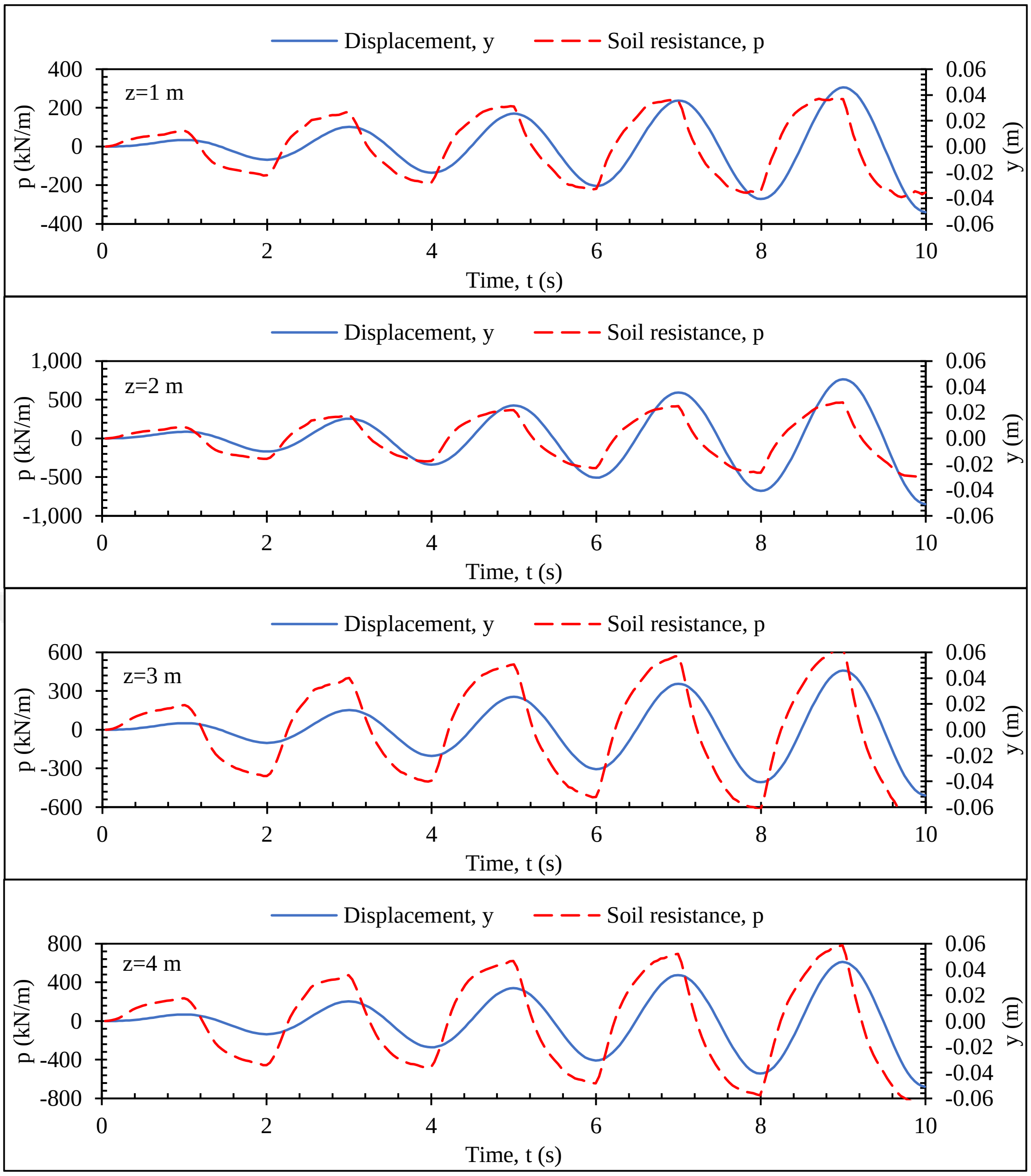

Figure B.3 : The pile displacement and soil resistance time histories for D=1.6 m, D_R=55 %.

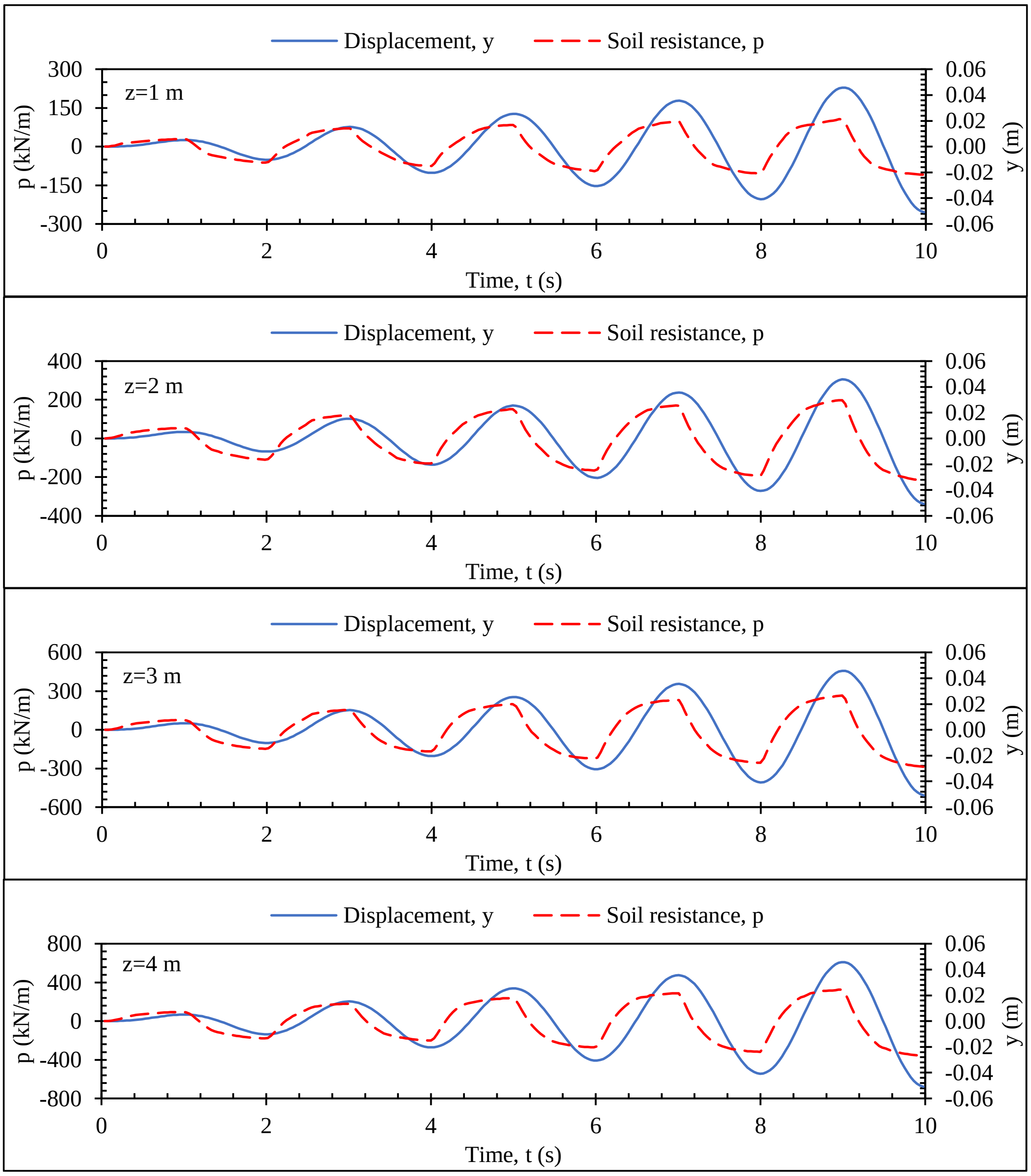

Figure B.4 : The pile displacement and soil resistance time histories for D=0.65 m, D_R=30 %.

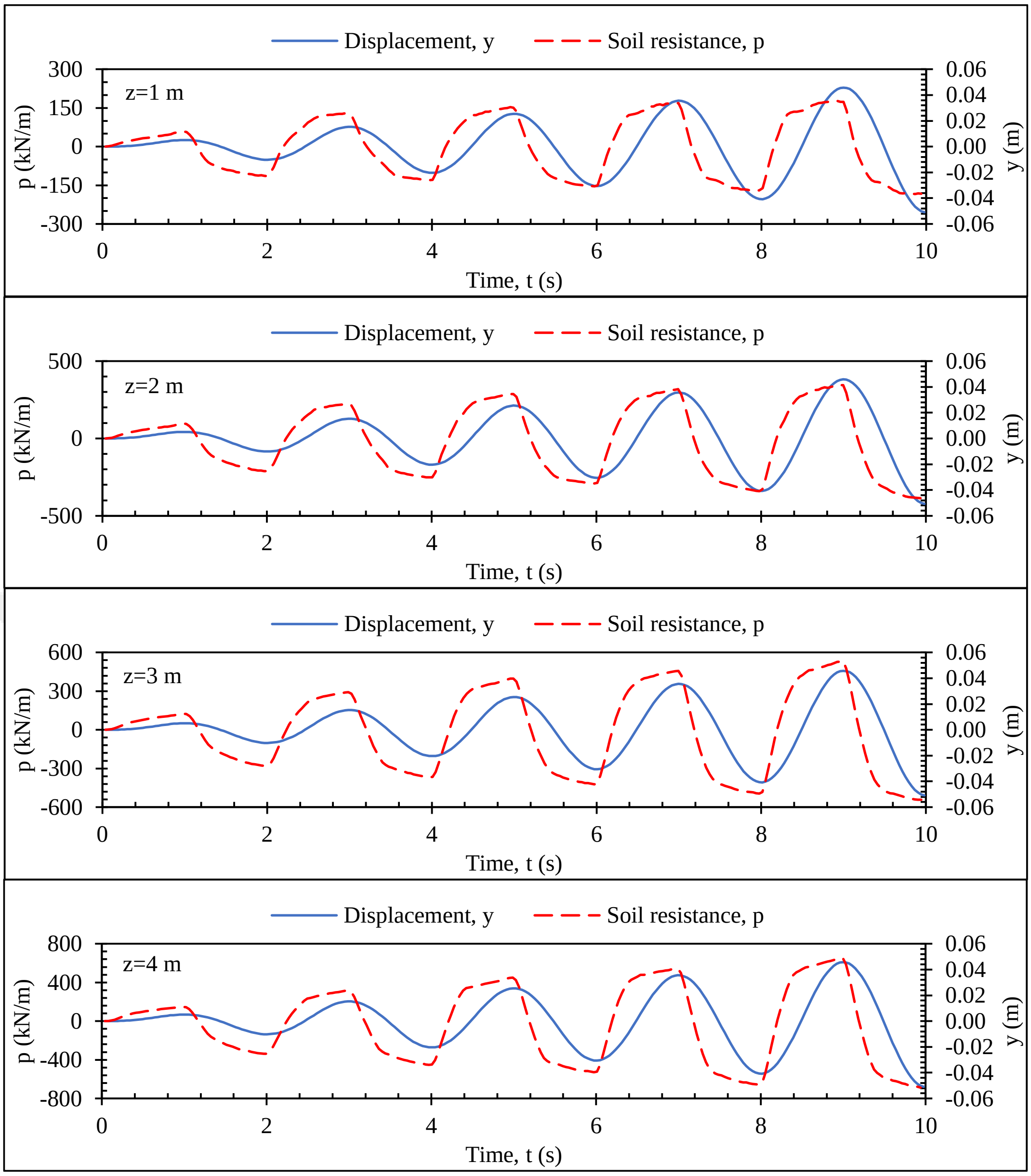

Figure B.5 : The pile displacement and soil resistance time histories for D=0.65 m, D_R=80 %.

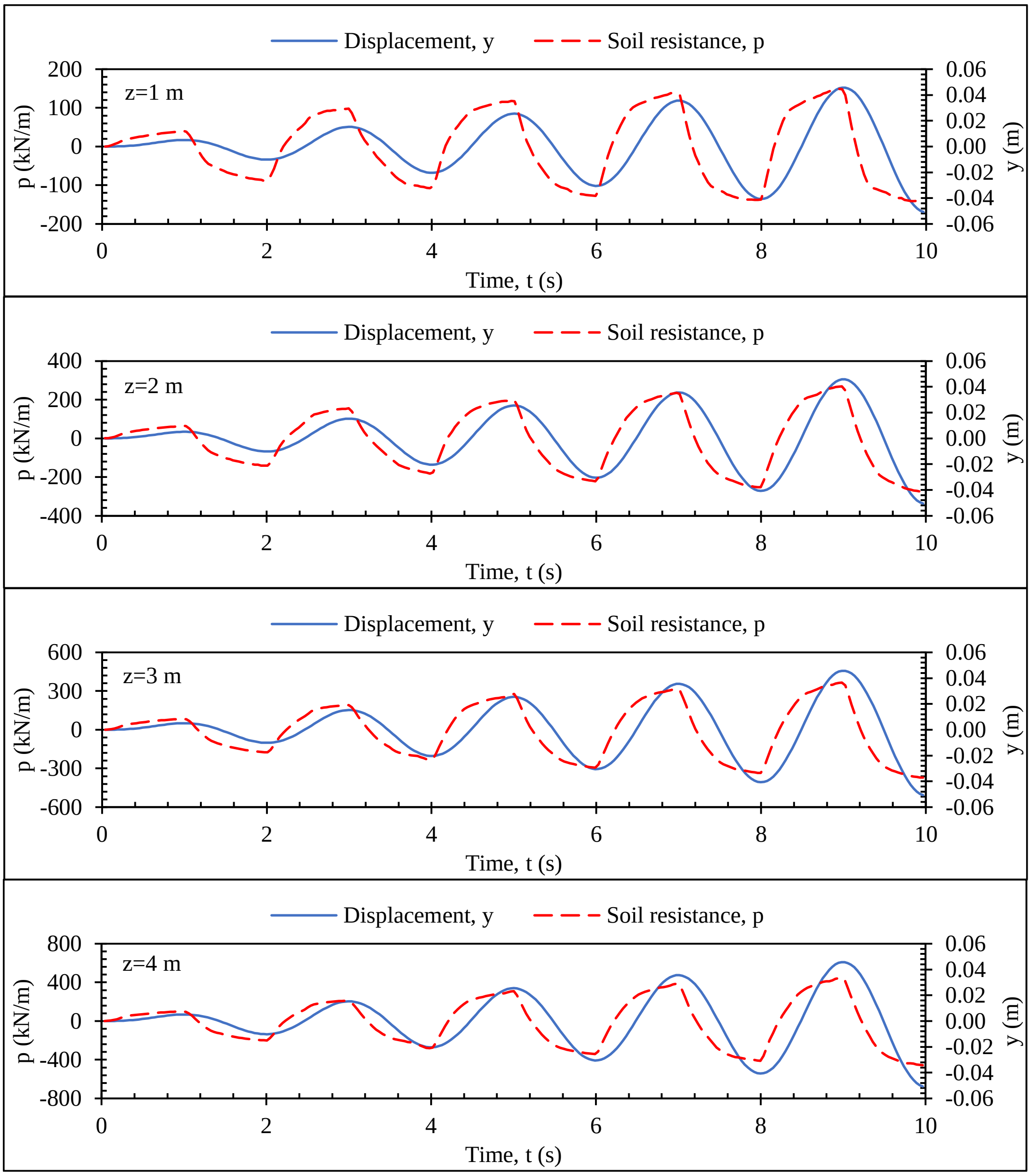

Figure B.6 : The pile displacement and soil resistance time histories for D=0.65 m, D_R=55 %, γ_r=0.0158 %.

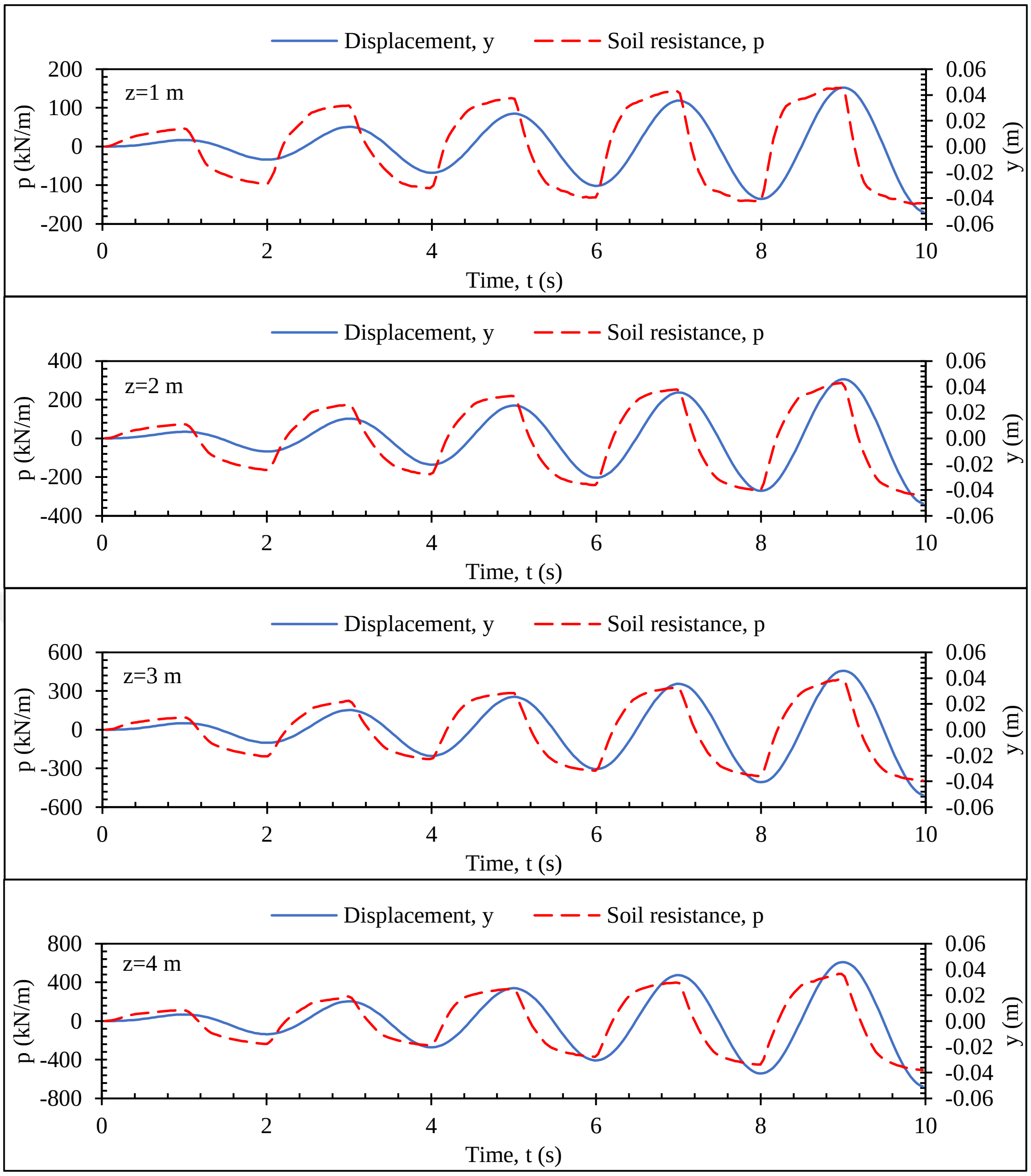

Figure B.7 : The pile displacement and soil resistance time histories for D=0.65 m, D_R=55 %, γ_r=0.0217 %.

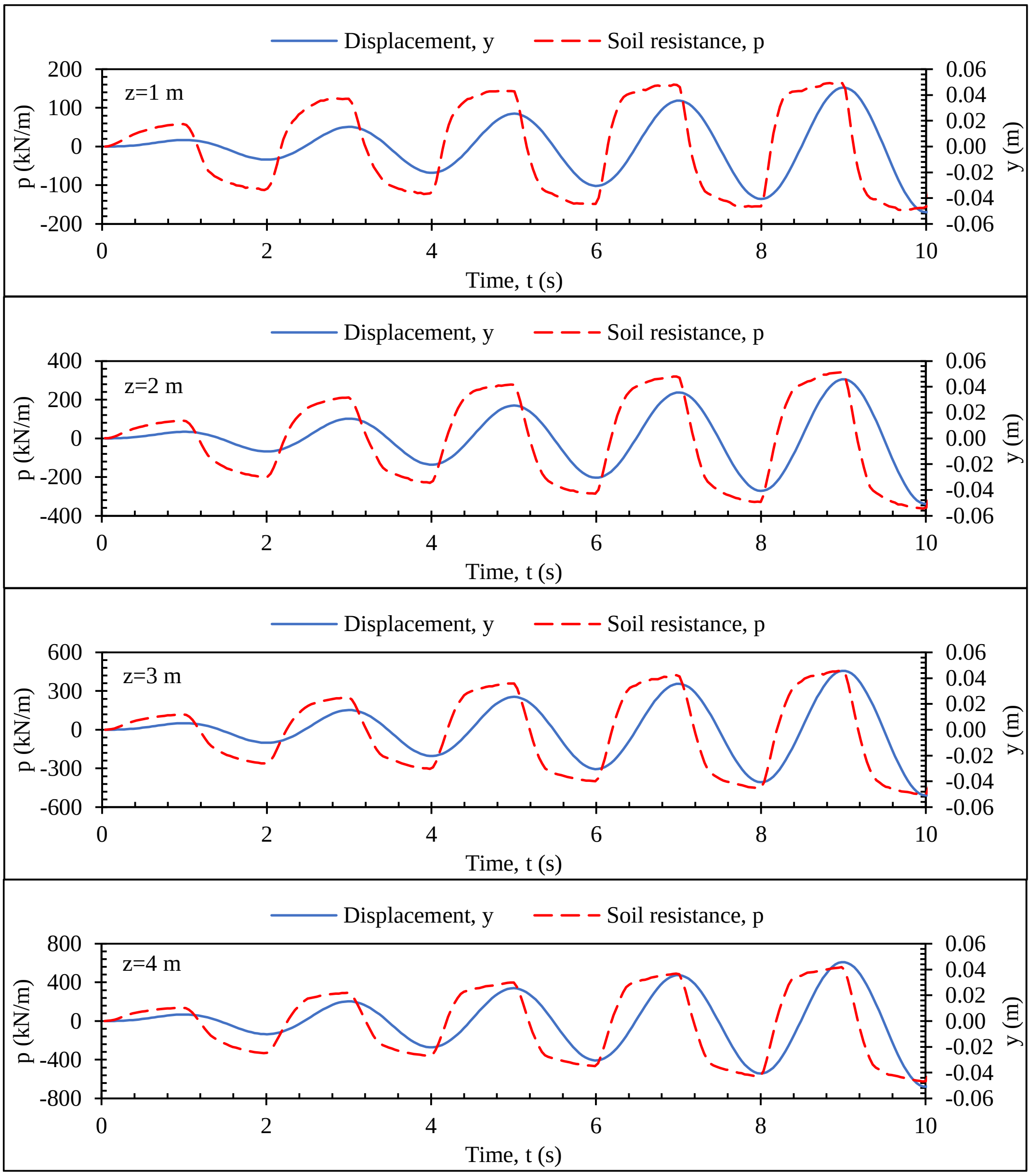

Figure B.8 : The pile displacement and soil resistance time histories for D=0.65 m, D_R=55 %, γ_r=0.0352 %.

APPENDIX C: Acceleration-time histories obtained in the validation analyses with the centrifuge test results

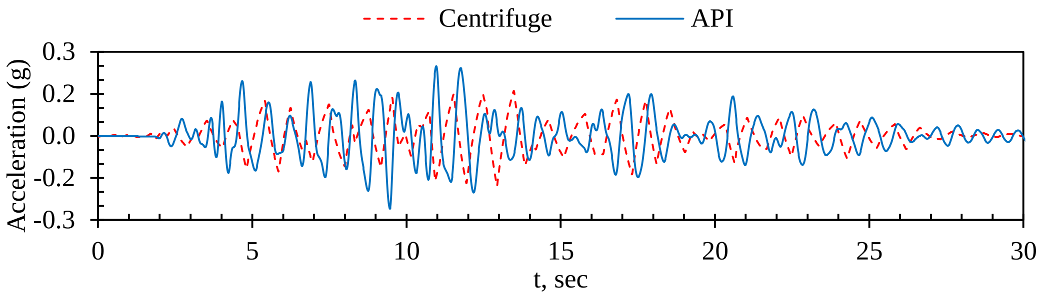

Figure C.1 : Comparison of the superstructure acceleration obtained in the centrifuge test and API for Event Gohl.

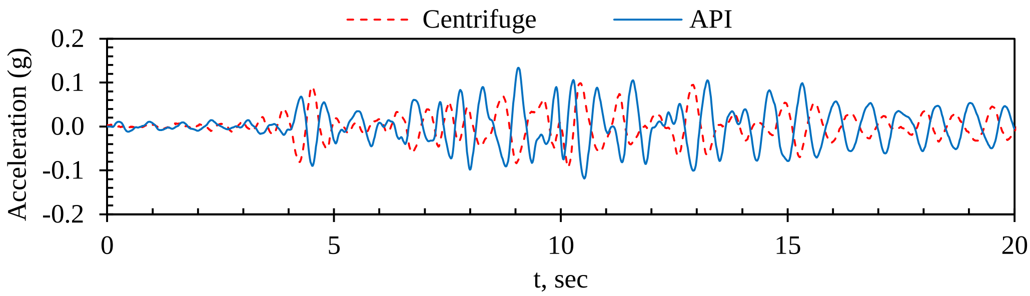

Figure C.2 : Comparison of the superstructure acceleration obtained in the centrifuge test and API for Event K.

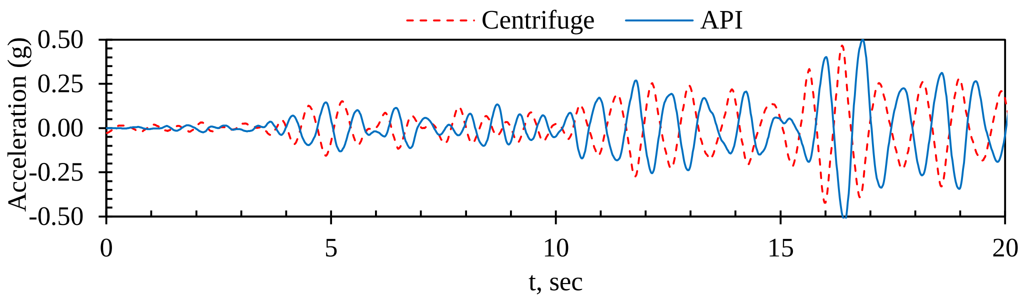

Figure C.3 : Comparison of the superstructure acceleration obtained in the centrifuge test and API for Event N.

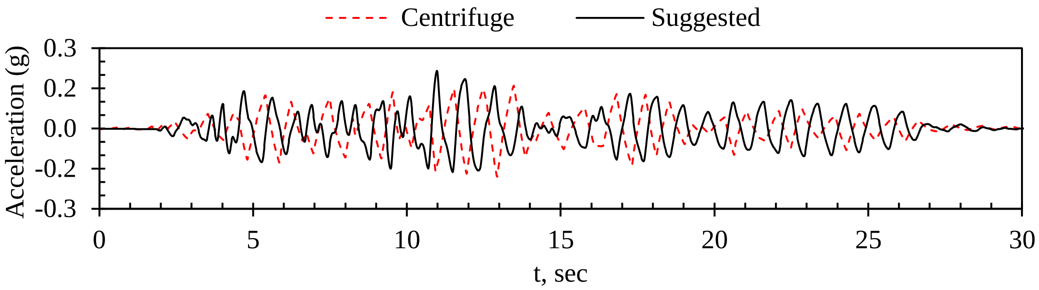

Figure C.4 : Comparison of the superstructure acceleration obtained in the centrifuge test and suggested model for Event Gohl.

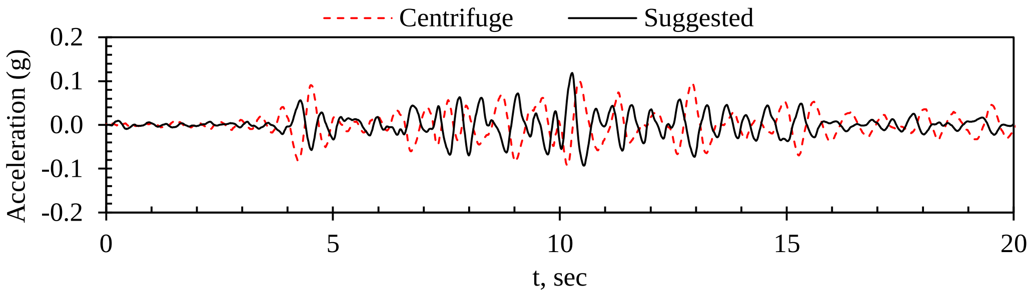

Figure C.5 : Comparison of the superstructure acceleration obtained in the centrifuge test and suggested model for Event K.

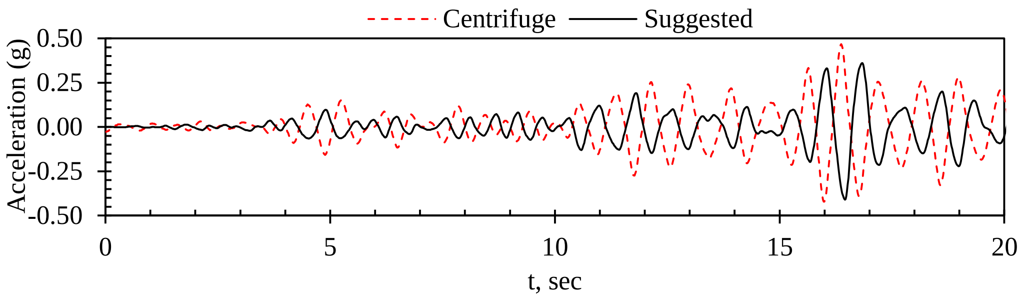

Figure C.6 : Comparison of the superstructure acceleration obtained in the centrifuge test and suggested model for Event N

APPENDIX D: Pile head bending moment-time histories obtained in the validation analyses with the selected earthquake test results

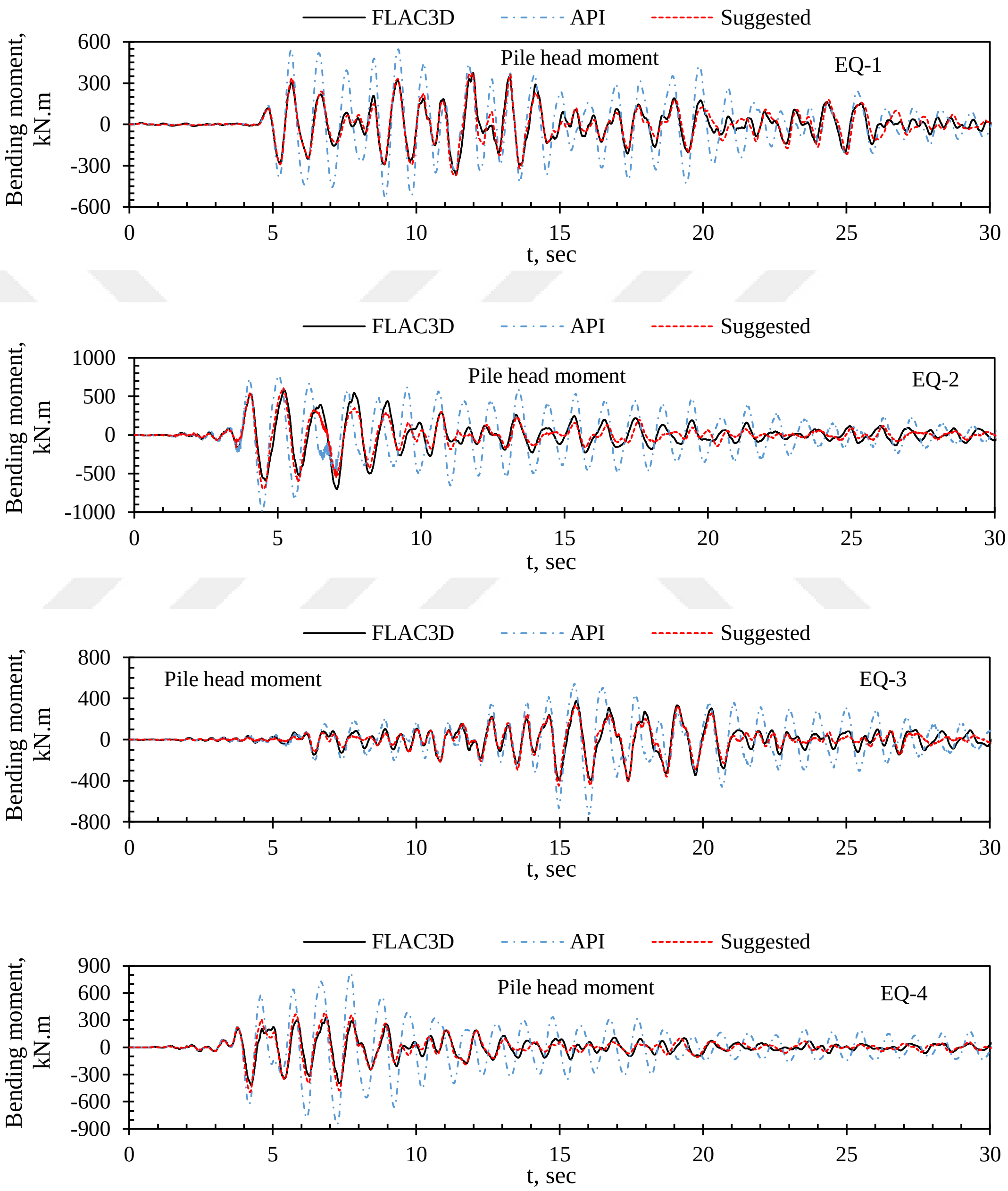

Figure D.1 : Comparison of the 3-dimensional dynamic analysis with the proposed method and API (Set-1).

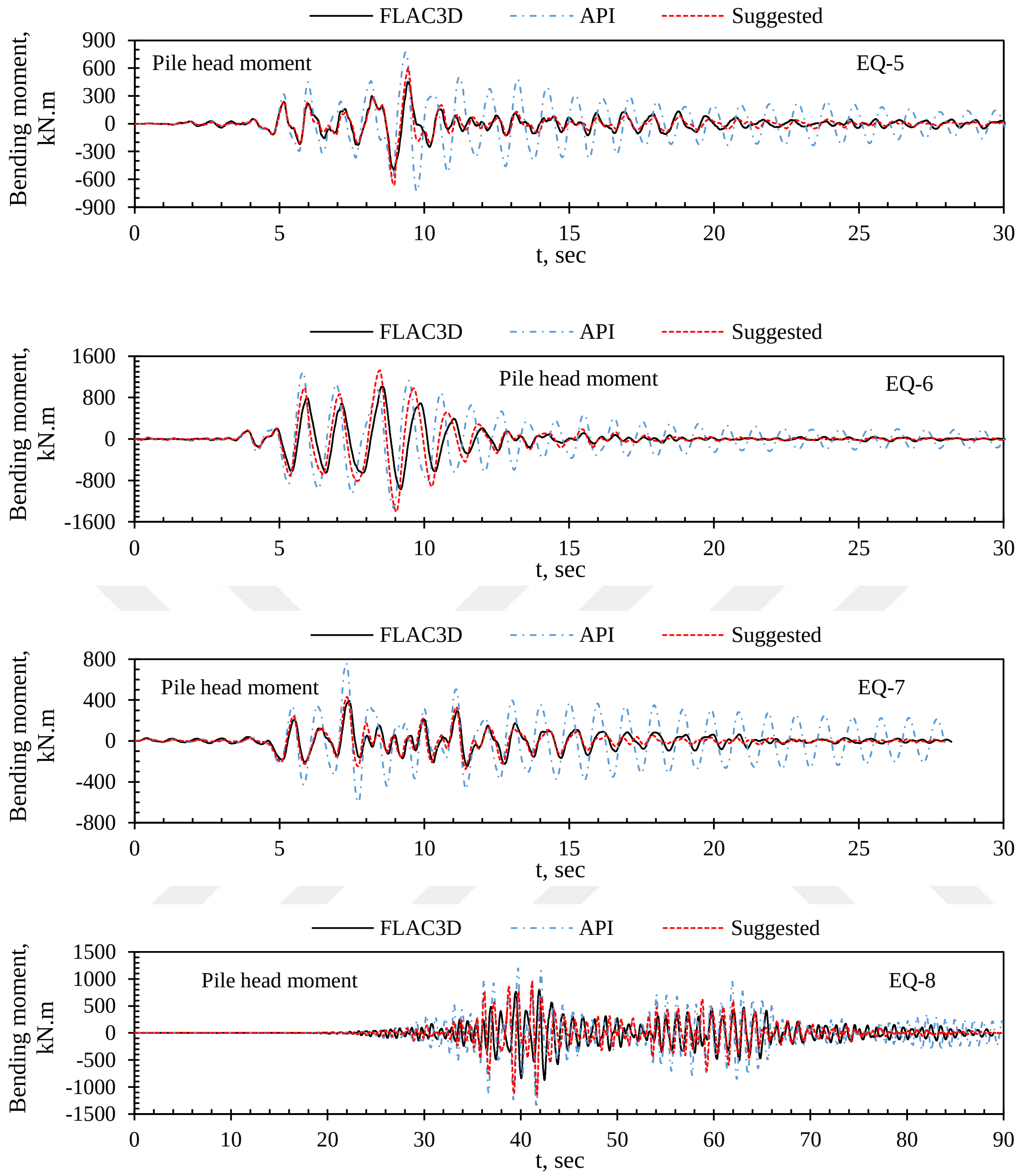

Figure D.2 : Comparison of the 3-dimensional dynamic analysis with the proposed method and API (Set-2).

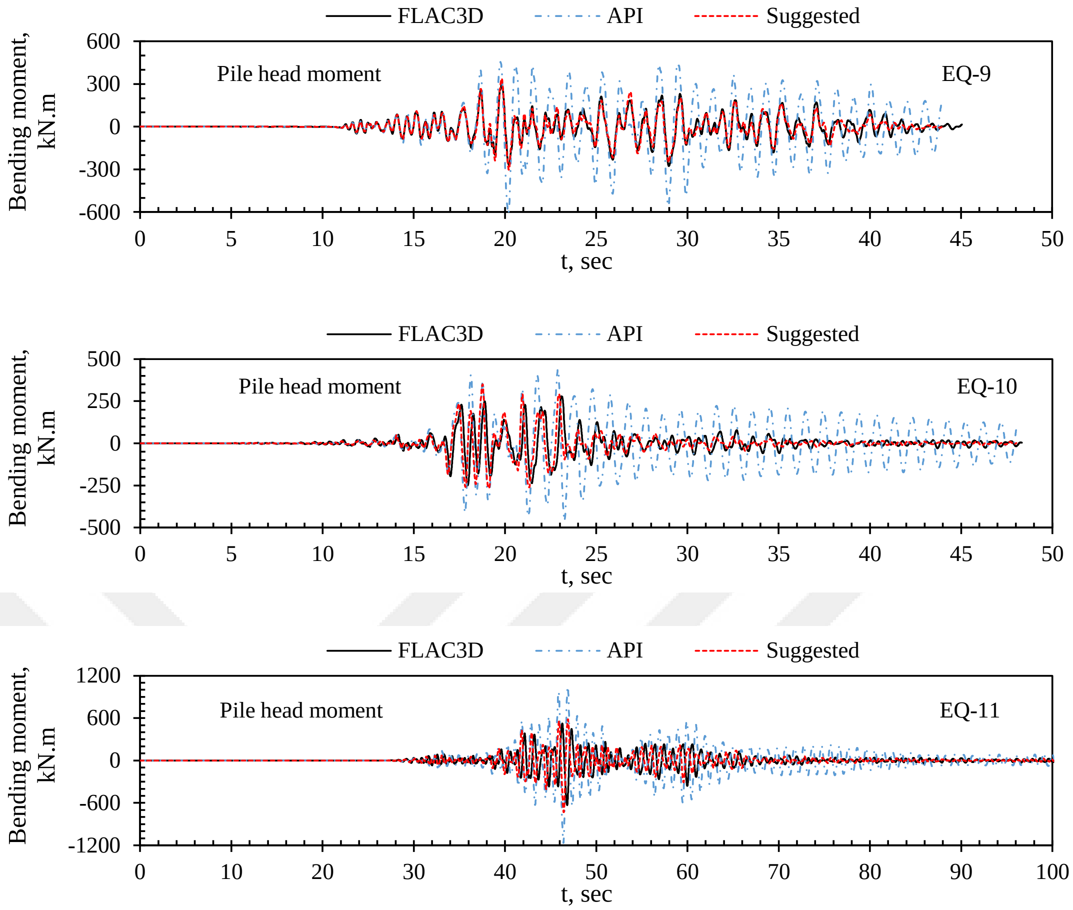

Figure D.3 : Comparison of the 3-dimensional dynamic analysis with the proposed method and API (Set-3).

CURRICULUM VITAE

Name Surname : Ozan ALVER

EDUCATION :

- **B.Sc.** : 2013, Dokuz Eylül University, Engineering Faculty, Department of Civil Engineering
- **M.Sc.** : 2015, Dokuz Eylül University, The Graduate School of Natural and Applied Sciences, Geotechnical Engineering Program

PROFESSIONAL EXPERIENCE AND REWARDS:

- 2018-2022 Research Assistant at Istanbul Technical University
- 2018-2021 Project Researcher: General Research Project (GAP): Investigation of the Nonlinear Behavior of Piles Embedded in Sands under Earthquake Excitation using the Soil-Pile-Structure Interaction Software. Project No: MGA-2018-41122
- 2019-2022 Research Scholar: TUBITAK 1001 Project: Development of Lateral Load Resistance-Deflection Curves for Piles in Sands under Earthquake Excitation. Project No: 119M624
- 2017 Visiting Researcher: Program on Resilience Engineering for Energy and Urban Systems at Tokyo Institute of Technology, Japan.

PUBLICATIONS, PRESENTATIONS AND PATENTS ON THE THESIS:

- **Alver, O.,** & Eseller-Bayat, E. E. (2022). A Dynamıc p-y Model For Piles Embedded in Cohesionless Soils. *Bulletin of Earthquake Engineering*. (Submitted-Under review).

- **Alver, O.,** & Eseller-Bayat, E. E. (2022). Effect of Soil Damping on the Soil–Pile–Structure Interaction Analyses in Cohesionless Soils. *Applied Sciences*, *12* (18), 9002. https://doi.org/10.3390/app12189002

- **Alver, O.,** Eseller-Bayat, E.E. (2022). "The Effect of Soil Damping on the Soil-Pile-Structure Interaction Analyses in Liquefiable and Non-liquefiable Soils". In: Wang, L., Zhang, JM., Wang, R. (eds) Proceedings of the 4th International Conference on Performance Based Design in Earthquake Geotechnical Engineering (Beijing 2022). PBD-IV 2022. Geotechnical, Geological and Earthquake Engineering, vol 52. Springer, Cham. **https://doi.org/10.1007/978-3-031-11898-2_83**

- **Alver, O.,** Sezen, A., & Eseller-Bayat, E. (2021). Geotechnical Design with Respect to TBDY-2018: Liquefaction and Soil-Pile-Structure Interaction Analyses. *TEKNIK DERGI*, *32* (5), 11197-11225. https://doi.org/10.18400/tekderg.744891
- **Alver, O.,** Eseller-Bayat, E.E. (2021). "Comparison of Equivalent Linear and Fully Nonlinear Methods in Soil-Pile-Structure Interaction Analyses". 6th International Conference on Earthquake Engineering and Seismology, Gebze-Turkey.
- Eseller-Bayat, E., Bagheri, O., **Alver, O.,** & Gunduz, M.S. (2021). Geliştirilmiş Geçirimsiz Saydam Laminer Zemin Konteyneri. Patent Submission to Turkish Patent and Trademark Office with the reference no: 1490P193.

OTHER PUBLICATIONS, PRESENTATIONS AND PATENTS:

- Deniz, O., Eseller-Bayat, E.E., **Alver, O.** (2021). "TBDY 2018'e göre Anakaya Derinliğinin Serbest Saha Analizine Etkisi ve Tasarım Spektrumlarıyla Karşılaştırılması", 9. Türkiye Deprem Mühendisliği Konferansı (2021), İstanbul, Turkey.
- Ayraçma, B.B., Teymür, B., **Alver, O.** (2019). "Rigid inclusions as a foundation support system in soft clay", 1st Mediterranean Young Geotechnical Engineers Conference, Muğla-Turkey.
- Erginag, U., Ozden, G., **Alver, O.** (2019). "A Study on Kinematic Interaction of a Piled Foundation", 3rd International Soil-Structure Interaction Symposium, İzmir-Turkey.
- **Alver, O.,** Ozden, G. (2016). "Settlement Based Optimization of Piled Rafts", Proceedings of the 16. (2016) National Soil Mechanics and Geotechnical Engineering Conference, Erzurum, Turkey (in Turkish).
- Erginag, U.C., Ozden, G., **Alver, O** (2016). "A Case Study for Investigation of Soil-Deep Foundation Kinematic Interaction Analysis Using Finite Difference Method", Proceedings of the 16. (2016) National Soil Mechanics and Geotechnical Engineering Conference, Erzurum, Turkey (in Turkish).
- **Alver, O.,** Ozden, G. (2015). Tabakalı Zeminlerde Kazıklı Radye Temellerin Optimum Tasarımı. Dokuz Eylül Üniversitesi Mühendislik Fakültesi Fen ve Mühendislik Dergisi, 17(49), 13-26.